PhD Thesis

Université de Limoges

École Doctorale Gay Lussac - Sciences pour l'Environnement (ED 523)

LCSN EA1069

Submitted for the degree of

Doctor of the University of Limoges

Discipline / Speciality: Applied Chemistry / Natural Substances Chemistry

Presented and defended by

Olivier Rezazgui

On December 18, 2015

Towards a bio-inspired photoherbicide: Synthesis and studies of fluorescent tagged or water-soluble porphyrins, from solution to plant cells

Thesis supervised by Dr. Stephanie Leroy-Lhez and Dr. Patrick Trouillas

JURY:

Referees

M. Frederic Fages, Pr, CINaM UMR CNRS 7325, Université Aix-Marseille

M. Mathieu Linares, Dr, IFM, Linköping University

Examiners

M. Johannes Gierschner, Dr, IMDEA Nanosciencia, Universitario de Cantoblanco

M. Mathias Senge, Pr, SFI-Tetrapyrrole Laboratory, Trinity College of Dublin

Mme. Rachida Zerrouki, Pr, LCSN, Université de Limoges

Mme. Catherine Riou, MCF-HDR, LCSN, Université de Limoges

Mme. Stephanie Leroy-Lhez, MCF-HDR, LCSN, Université de Limoges

M. Patrick Trouillas, MCF-HDR, INSERM UMR-850, Université de Limoges

"La théorie, c'est quand on sait tout et que rien ne fonctionne.
La pratique, c'est quand tout fonctionne et que personne ne sait pourquoi.
Ici, nous avons réuni théorie et pratique: Rien ne fonctionne... et personne ne sait pourquoi !"

Albert Einstein

"*I have not failed. I've just found 10,000 ways that won't work*".

Thomas A. Edison

Acknowledgments / Remerciements

Avant tout, je tiens à remercier le Professeur Vincent SOL de m'avoir accueilli au sein du Laboratoire de Chimie des Substances Naturelles, et ainsi d'avoir pu mener à bien ce projet. J'espère avoir renvoyé une bonne image du laboratoire au cours des congrès auxquels j'ai eu la chance de participer, ainsi que durant les conseils d'Ecole Doctorale 523 comme de l'Institut GEIST.

A mes deux directeurs de thèse, sans qui rien de tout ça n'aurait pu avoir lieu. Tout d'abord, je tiens à exprimer mes plus sincères remerciements au Docteur Stéphanie LEROY-LHEZ, ma deuxième maman pendant 3 ans. Merci de m'avoir fait confiance pour mener ce projet à bien, de m'avoir donné la chance d'aller présenter mes travaux dans d'autres pays, et surtout de m'avoir supporté. Merci au Docteur Patrick TROUILLAS de m'avoir fait une place au sein de son équipe, pour son humour en toutes circonstances (un Apple ne tombe jamais en panne hein ?…), et sa confiance. Stéphanie, Patrick, il n'y a pas de mots assez forts pour vous exprimer toute ma gratitude. J'ai eu la chance d'évoluer tant professionnellement que personnellement à vos côtés, et j'en suis fier. Merci pour votre rigueur scientifique, vos conseils, pour avoir toujours répondu présents malgré mon pessimisme naturel et les aléas du quotidien, mais aussi pour vos remarques pertinentes et avoir cru en moi … Bref merci d'avoir été vous!

La recherche scientifique est avant tout un partenariat entre différents domaines, ce que cette thèse reflète parfaitement. Merci Au Docteur Catherine RIOU, pour sa bonne humeur et sa nomenclature pour le moins originale (habemus PAPam) ; et au Docteur Claude CALLISTE spécialiste de la RPE, toujours disponible pour des questions. Et enfin merci au Docteur Yves CHAMPAVIER, « Monsieur RMN » de son petit nom ; un grand merci pour ton aide pour les analyses de spectre et les discussions pas toujours scientifiques qu'on a pu avoir.

Je suis très honoré de la présence au titre de rapporteur du professeur Frederic FAGES et du professeur associé Mathieu LINARES. Je les remercie d'avoir accepté de juger ce travail.

I also express my thanks to Professor Mathias SENGE for agreeing to come and examine this work. Doctor Johannes GIERSCHNER, it would have been inconceivable to me that you will not be present. It is a great honor to have you in my jury.

J'en viens au Professeur Rachida ZERROUKI. La formation entamée sous vos ordres en Master 2 voit son aboutissement. Je vous avais dit à l'époque que j'apprécierais vous compter parmi mon jury le jour de ma soutenance…Me voilà exaucé ! Vous avez toujours répondu présente pour moi, et c'est un honneur que de vous avoir comme examinatrice.

Une énorme dédicace à toi Evelyne, pour tout ce que tu m'as apporté. Ta bonne humeur, tes conseils scientifiques, ton self-control face à nos blagues foireuses avec Florent, ton astuce « image »

qui m'a plus que dépanné, et tout tes petits trucs en plus qui facilitent la vie. Merci à toi, aujourd'hui affublée du sobriquet « maman » suite à un malheureux lapsus de ma part… Et en même temps c'est précisément ce que tu as été et seras toujours pour nous!

Je pense bien entendu à mes collègues au sein du laboratoire. Amandine, entre deux épilations de tes sapins tu m'auras entrainé dans un tas de lieux incroyables (Canada, Suède, Grande-Bretagne) ou inhospitaliers (Dordogne). Pour reprendre un dicton de biologiste, tu gères la fougère. Dédé, notre envoyée (très spéciale) à l'ED. Tu m'auras réconcilié avec l'administration française, avec tes jeux de mots, ta bonne humeur contagieuse, et ton sourire Colgate ! Florent, mon regret aura été de ne pas t'avoir rencontré avant. On aura bien rigolé tous les deux, ton absence de système immunitaire décent et ton rituel du matin vont me manquer! Blowkiss firegun mec! Petit crochet par le Grese : Francky, oh mignonnette, ne change rien t'es un type génial. Pitou qui arriverait presque à trouver des qualités au rosé de Verneuil! A Jihane, hostie de câlice de saint-sacrament, ton accent canadien me manque déjà. Et bien sûr à mon BRO-disciple Gabin (où devrais-je dire Gabinet), avec qui j'ai partagé les joies et douleurs de la mise en forme du manuscrit et l'addiction au Kofola.

Merci pour tout ce que vous m'avez apporté, humainement, scientifiquement et professionnellement : Idelette, Aurélie, Romain, Amandine, Jean-Jean, Mac, Shihong, Tom, Olivier, Claire, Amaury, Manon, Salim, Zineb, Nicolas mais aussi aux expatriés de pharmacie Benjamin, Tahani, Michal, Chloé, et le meilleur pour la fin notre président TRG Cédric. Pensée spéciale pour Mohammad et Guillaume, qui reprennent le flambeau des porphyrines anioniques. Bon courage à vous pour la suite !

Une pensée particulière va à Benj, PH, PAF et Flo; 4 mecs extraordinaires à leur manière qui ont fait de mon Master 2 un moment inoubliable et qui encore aujourd'hui répondent présents.

Merci pour tout à mes stagiaires. A Léa et Goran, mes toutes premières victimes ; vous n'avez jamais voulu le croire mais j'étais mort de trouille. Vous avez été géniaux, et pardon si jamais vous avez dû essuyer les plâtres. Quand à toi Léa, je retire une certaine fierté de t'avoir convertie au côté obscur de la chimie. Chloé, Ludo que le pouvoir de la laitue soit avec vous! Denis, Rémy, Laurie à quand la thèse ?

Bien évidemment, je remercie l'ensemble du laboratoire. Mention spéciale à Fredo ma coloc de bureau ; toujours à l'écoute, souriante et grande prêtresse de la quiche lorraine. Merci à Sylvie, aux Vincent, à Dorothée, Michèle, Nicolas, Gäelle, Cricri et tous les autres! Et à Odette, bien souvent oubliée mais sans qui notre cadre de travail se dégraderait.

Manu, Flo, Damien, Etienne et Geoffrey. Je vais faire bref car sinon c'est un autre manuscrit qu'il me faudrait pour résumer notre amitié. Vous avez tous subi mon caractère de cochon, partagé mes moments de joie et de peine depuis plus de 9 ans. Aujourd'hui chacun a évolué, certains se sont mariés, et pourtant nous sommes toujours liés par cette même amitié débutée sur les bancs de la fac. Alors cette

thèse c'est un peu la vôtre, car sans vous je n'écrirais pas ces lignes. Je suis fier de vous compter parmi mes proches. Merci également à mes amis hors du laboratoire: les Corréziens (Gui, Cookie, Juju, Marc, Pipette, Cesco….), les vieux de la vieille (Floflo, Jerem, Romain, Julien, Gaëtan…) et mes amis en général.

A Sophie et Elodie, qui telles deux étoiles ont illuminé ma vie. Sophie, on s'était promis que l'un de nous serait docteur... Je la tiens pour nous deux. Elodie, ton arrivée dans ma vie a été soudaine, malheureusement tu en es partie de la même façon. Je sais que de là-haut vous continuez de veiller sur moi. « Tu n'es plus là où tu étais, mais tu es partout là où je suis », Victor Hugo.

Je tenais à terminer ces remerciements par les personnes les plus importantes de toutes à mes yeux, mes parents. Maman, Papa, vous avez toujours cru en moi et m'avez offert les moyens de réaliser ce rêve. Sans l'éducation que j'ai reçue et votre amour, jamais je n'aurais pu aller aussi loin. Merci également à ma famille, qui a toujours été derrière moi. Je vous aime.

Droits d’auteurs

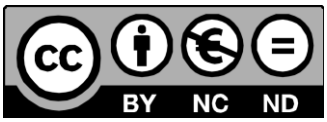

Table of contents

List of abbreviations

$^1O_2$	Singlet oxygen
2,4,5-T	2,4,5-trichlorophenoxyacetic acid
2,4-D	2,4-dichlorophenoxyacetic acid
A	Absorbance
ACoA	Acetyl Coenzyme A
ALA	δ-aminolevulinic acid
ALS	Acetolactate synthase
ATP	Adenosine Triphosphate
Bn	Benzen
Bu	Butyl
CI	Configuration Interaction
CSS	Charge-Separated State
CT	Charge Transfer
d	Doublet (^{1}H NMR)
DBU	1,8-diazabicycloundec-7-ene
DCM	Dichloromethane
dd	Double doublet (^{1}H NMR)
DDQ	2,3-Dichloro-5,6-dicyano-1,4-benzoquinone
DFT	Density Functional Theory
DHP	Dihydropteroate synthase
DMA	9,10-dimethylanthracene
DMAE	N,N-dimethylaminoethanol
DMF	Dimethylformamide
DMSO	Dimethylsulfoxide
DNA	Deoxyribonucleic acid
DNOC	4,6-dinitro-o-cresol
DNP	Dinitrophenols
DSSC	Dye-Sensitized Solar Cells
dt	Double triplet (^{1}H NMR)
e	Molar absorption coefficient
E	Energy
Em	Emission
EPSP	5-enolpyruvoylshikimate-3-phosphate synthase
equiv.	Equivalent
ES	Excited State
ET	Energy Transfer
Exc	Excitation
Fr	Front report
FRET	Förster Resonance Energy Transfer
fwdh	Full Width at Half Maximum
GCSD	General Commission for Sustainable Development
GMO	Genetically Modified Organism
h	Hour

HF	Hartree-Fock
HOMO	Highest Occupied Molecular Orbital
HPLC	High Performance Liquid Chromatography
HRAC	Herbicide Resistance Action Committee
HRMS	High Resolution Mass Spectra
IAA	Indoleacetic Acid
IC	Internal Conversion
ICT	Intramolecular Charge Transfer
IR	Infra-Red
ISC	Intersystem Crossing
ISE	Ion Selective Electrode
IUPAC	International Union of Pure and Applied Chemistry
J	Coupling constant
λ	Wavelenght
LCAO	Loinear Combination of Atomic Orbitals
LCD	Liquid Crystal Display
LMCT	Ligand to Metal Charge Transfer
LUMO	Lowest Unoccupied Molecular Orbital
M	Molar
m/z	Mass to charge ratio
MALDI	Matrix-Assisted Laser Desorption/Ionization
MD	Molecular Dynamics
min	Minute
MLCT	Metal to Ligand Charge Transfer
MM	Molecular Mechanics
MO	Molecular Orbital
Mp	Melting point
MW	Microwaves
n	Refracting index
NADP	Nicotinamide Adenine Dinucleotide Phosphate
nm	Nanometer
NMR	Nuclear Magnetic Resonance
ns	Nanoseconds
$O_2^{\cdot -}$	Superoxide
OD	Optic Density
OFET	Organic Field Effect Transistor
OLED	Organic Light Emitting Diode
OPV	Organic PhotoVoltaic
PACT	Photodynamic Antimicrobial Chemo-Therapy
PCM	Polarizable Continuum Model
PDT	Photodynamic Therapy
PET	Photo-induced Energy Transfer
PET/CT	Positron Emission Tomography / Computed Tomography
ppm	Parts Per Million

PPO	Protoporphyronogen oxidase
PS	Photosensitizer
PS I/II	Photosystem I and II
p-TSH	ρ-toluenesulfonhydrazide
QM	Quantum Mechanics
quint	Quintuplet (^{1}H NMR)
RET	Resonance Energy Transfer
RNA	Ribonucleic acid
ROS	Reactive oxygen species
s	Singlet (^{1}H NMR)
S_0	Ground state
S_n	Excited state
STO	Slater-Type Orbitals
t	Triplet (^{1}H NMR)
tBu	Tertiary Butyl
TBY-2	Tobacco Bright Yellow-2
TCDD	2,3,7,8-tetradichlorodibenzo-p-dioxin
TD	Time-Dependent
TEOA	Triethyl-orthoacetate
TFA	Trifluoroacetic acid
THF	Tetrahydofuran
TLC	Thin Layer Chromatography
TMS	Tetramethylsilane
TOF	Time of Flight
TPP	Tetraphenylporphyrin
UV-Vis	UV-Visible
VR	Vibrational Relaxation
W	Watt
WHO	World Health Organization
wt	Mass fraction
Φ_f	Fluorescence quantum yield
Φ_Δ	Singlet oxygen production quantum yield

Introduction

Herbicides are molecules bearing numerous different structures and exhibiting different mechanisms of action, however they all kill plants with more or less selectivity. Since the 50s, the market of herbicides has constantly increased. This is attributed to the explosion of food demand, which is related to the relative World geostability, increase of living standards, and greater demography. Accordingly, the use of pesticides, especially herbicides, has dramatically increased. However, several drawbacks have emerged over the last decades and several products were banned. To agree with increased needs and current legislation, much efforts have been made to search and develop new herbicidal substances. Henceforth, new herbicides need to be harmless to human health, but also easily degradable by soil and micro-organisms. Therefore, their by-products must be inert to prevent any risk of environmental pollution.

Having such requirements in mind, tetrapyrrolic macrocycles have appeared as a promising alternative to regular herbicides. Indeed, porphyrins and their analogues (*e.g.* chlorines) are a family of colored compounds naturally present in living organisms (both in animals and plants). There are involved in a wide range of biological processes including photosynthesis, oxygen transport, and protein synthesis. They have been extensively studied and a particular attention has been paid to the development of new synthetic strategies to yield new derivatives with well controlled properties and at a relatively low cost. Porphyrins exhibit a number of fascinating properties, which allow targeting a wide range of applications such as in energy, environmental or medicinal domains. In the latter case, their capacity to produce reactive oxygen species (ROS) after light irradiation has allowed development of new medical techniques as photodynamic therapy (PDT) and photodynamic antimicrobial chemotherapy (PACT). In both cases, tetrapyrrolic macrocycles are used for their capacity to destroy microorganisms as human cells (*e.g.* cancer therapy) or bacteria.

Borrowing the knowledge acquired from the numerous studies performed on mammal cells, the present work suggests using porphyrins on plant cells. Being natural compounds, we suggest the development of new photo-activable bio-inspired herbicides. This work has emerged from the collaboration between chemists (theoretician as organist) and biologists.

Chapter 1 draws up state of the art on tetrapyrollic macrocycles, namely history and recent advances on their synthesis; photophysical properties; and applications. In the same section, herbicides are described from their mechanisms of action to their respective advantages and disadvantages; tetrapyrrolic macrocycle description is revisited in terms of their potential use as photoherbicides.

Chapter 2 evaluates efficiency of porphyrins as potential herbicides. For such biological purpose, water-soluble compounds, namely commercial as synthesized charged porphyrins (Figure 1), were studied for their physicochemical properties, in water as well as in plant cell growth medium. Their biological activities on plant cells (*in vitro* assays) were measured. Nature and numbers of charged functions were modulated to identify the best performing compound. Due to their use in biological environment, a special attention was paid to their purity degree.

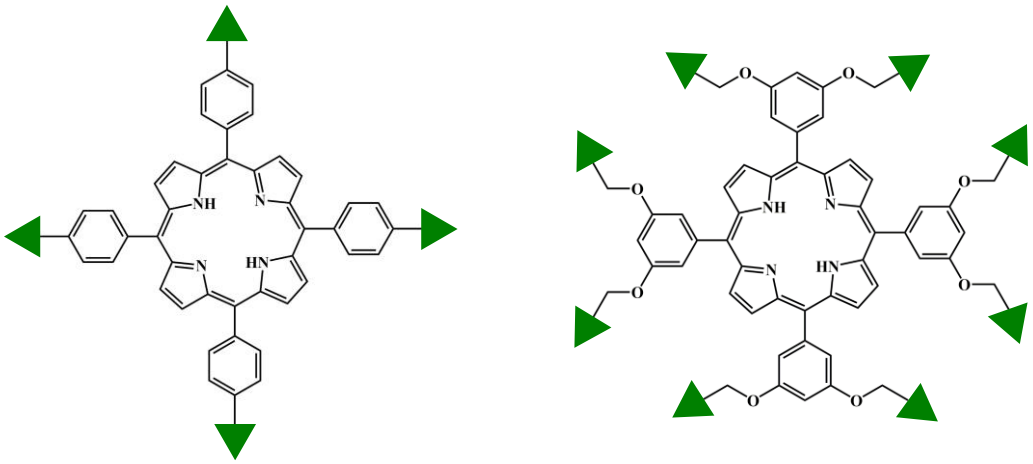

Figure 1: General structure of anionic porphyrins. Green triangles represent the anionic

A better understanding of mechanisms of action involved in cell death has appeared mandatory to enhance biological activities (Chapter 3). In that purpose tracking the new herbicides in plant and plant cells is required. Tagged porphyrins with a fluorophore has appeared an elegant and efficient choice. Based on molecular modeling study, a series of adequate dyads containing porphyrin and a fluorescent tag were selected, mainly according to the choice of the linker (Figure 2). Then, synthesis of the new dyads was achieved and the related photophysical properties.

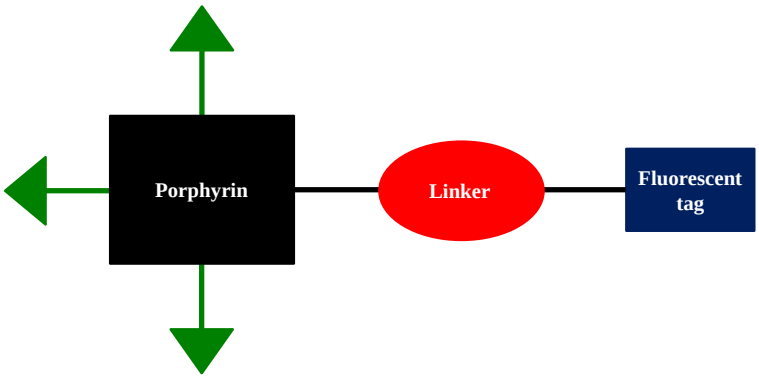

Figure 2: General structure of synthesized dyads. Green triangles represent water-soluble functions.

State of the art

I. PORPHYRINS AND THEIR DERIVATIVES

1. Introduction

1.1. A brief history

In the tetrapyrrollic macrocycles' family, porphyrins and their derivatives (chlorins, bacterio- and *iso*bacterio-chlorins …) (Figure 3) are unquestionably the most studied.[1]

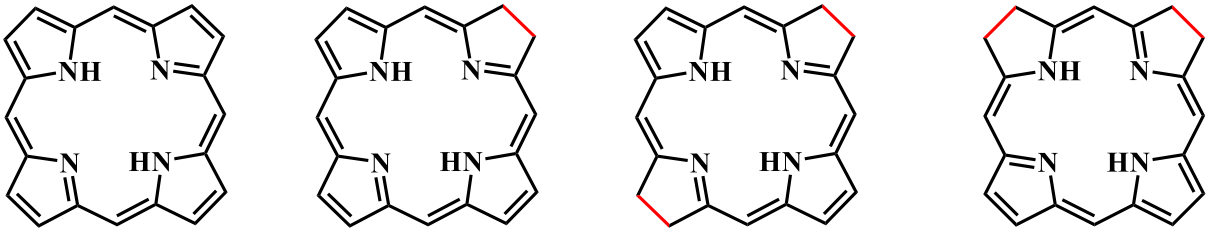

Figure 3: Chemical structure of tetrapyrrolic macrocycles and number of electron implied in aromaticity. From left to right: porphyrin, chlorin, bacteriochlorin and isobacteriochlorin.

Naturally present in *Fauna* and *Flora*, these pigments are crucial for a wide range of biological functions including oxygen transport in animals thanks to heme[2] and hematoporphyrin,[3] (Figure 4A) photosynthesis thanks to chlorophylls,[4] brain and nervous system thanks to vitamin B12 or cobalamin[5] (Figure 4B). Due to their particular optical properties, these compounds are a class of photosensitive molecules of interest.

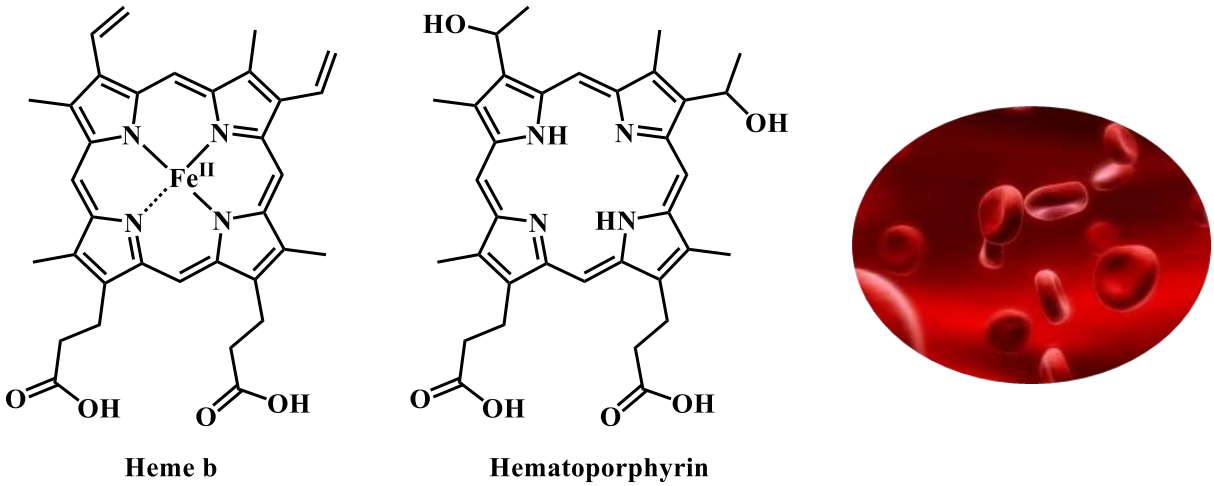

Figure 4A: Examples of porphyrins in nature: *heme b* and *hematoporphyrin*.

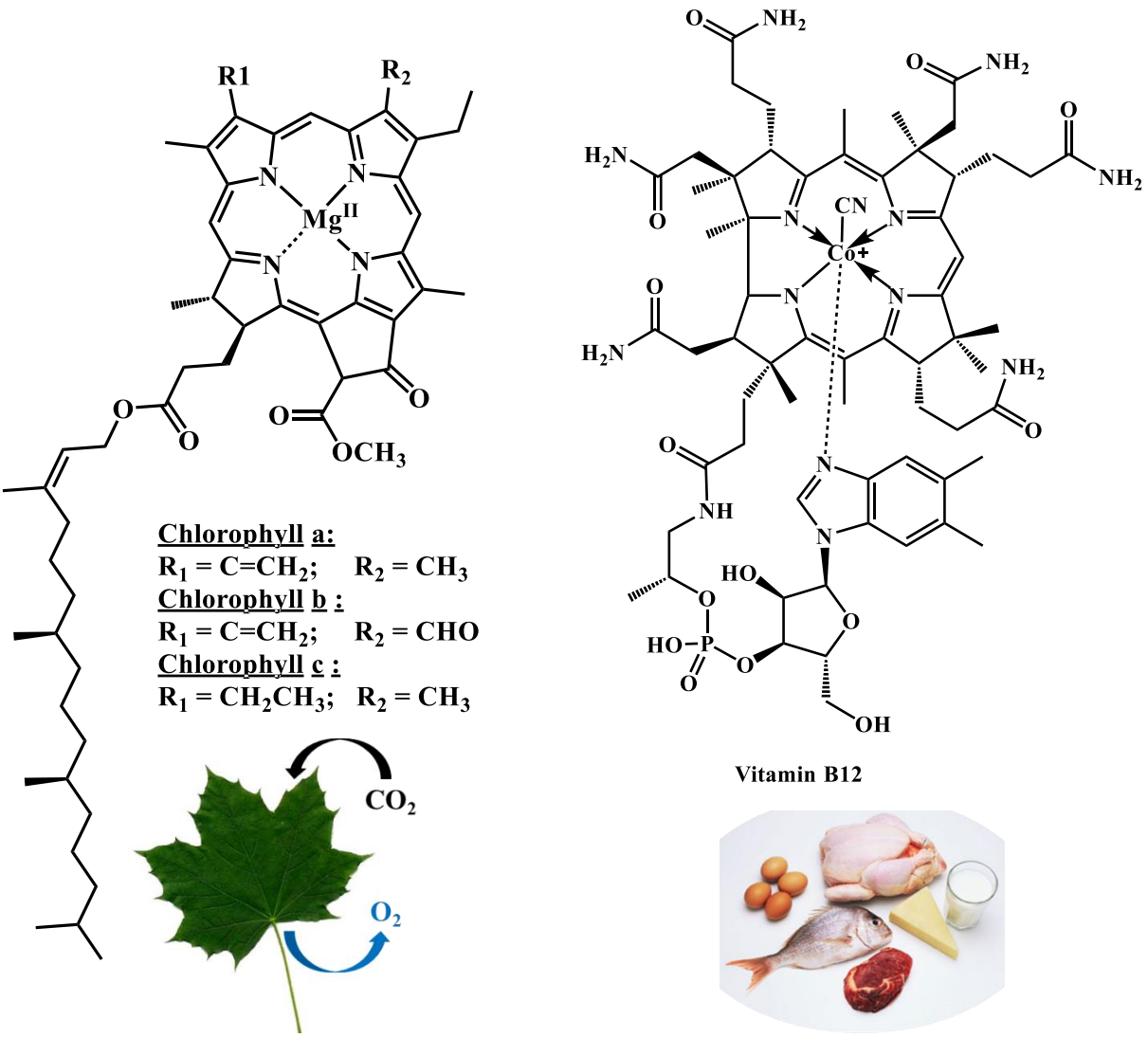

Figure 2B: Examples of porphyrins in nature: c*hlorophyll* and *vitamin B12*.

The etymology of the name "*porphyrin*" originates in ancient Greece and reflects their special feature. It comes from the Greek *porphyra* (or the Latin *porphurá*) as referring to the deep purple or violet color of many of these compounds. Due to this vivid color and their biological relevance in nature, porphyrins were named the "pigments of life".[6]

Ever since the first isolation of a porphyrin from blood, namely the hematoporphyrin (originally named *cruentine*) by J. L. W. Thudichun in 1867,[7,8] this unique *tetra*-pyrrol-macrocycle and its derivatives have attracted much interest in the scientific community. In 1955, a pioneer conference on porphyrins was born as founded by the "Ciba Foundation symposium on porphyrin biosynthesis and metabolism".[9] Since that time, the number of publications on porphyrin chemistry has dramatically increased (Figure 5). A dedicated scientific journal was founded, namely the *Journal of Porphyrins and Phthalocyanines (JPP)*

in 1997, and *The Society of Porphyrins and Phthalocyanines (SPP)* was created in 2000, which exemplified the great impact of this research topic.

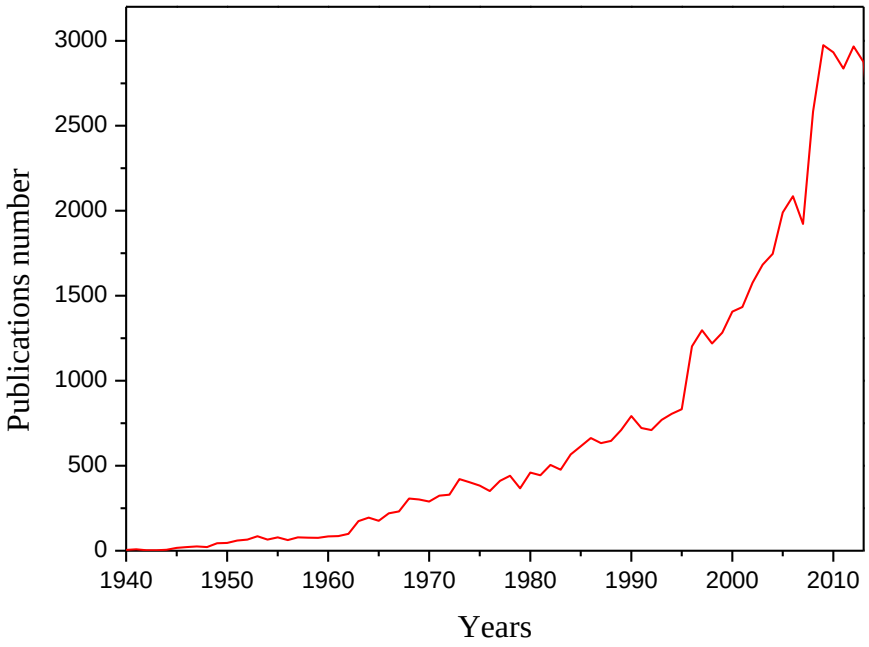

Figure 5: Publications number about porphyrins (per year) according to Scopus Database (23/09/2015).

These compounds are quite easy to chemically modulate, especially on *meso* and β positions, to increase water solubility or to develop new specific properties for targeted applications.[10–12] Without being exhaustive, one can cited optoelectronics,[13] photosynthesis mimicking,[14] medical applications[15,16] or catalysis.[17] As well, historically, after the major discovery of an isomeric porphyrin called *porphycene* by E. Vogel,[18] which has revolutionized porphyrinoid chemistry, a great variety of porphyrins and their derivatives has become accessible. Among other examples, one can mention calixpyrroles,[19] contracted,[20] expanded,[21,22] heteroatom-exchanged[23] and inverted porphyrinoids.[24–26] Elongation of the π–system using fused polycyclic aromatic rings at the edge of the macrocyclic core has resulted in highly conjugated derivatives.[27] In the same way, a new class of fully synthetic tetrapyrrolic macrocycles has emerged, namely phthalocyanines[28] and its derivatives (*e.g.* subphtalocyanines).[29] Phthalocyanines were discovered accidentally during a study of the properties of 1,2-cyanobenzamide and were reported for the first time in 1907.[30] Then in 1927, Swiss researchers synthesized copper phthalocyanines and other compounds while they were trying to obtain phtalonitriles.[31] Nowadays, modern chemistry provides a whole toolbox with

new synthetic protocols, allows more efficient preparation of novel porphyrinoids with new properties to be explored (Figure 6).

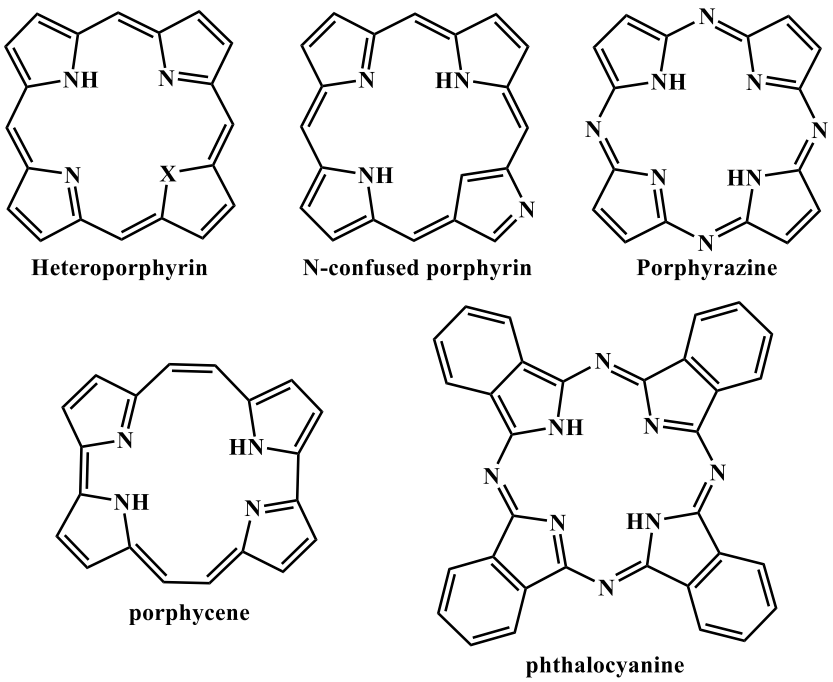

Figure 6: Structure of some porphyrinoids and porphyrin derivatives.

1.2. Structure

Porphyrins are derivatives of porphin (Figure 7). This compound consists of four pyrrole rings joined together *via* methine bridges (=CH-) at their α carbons. It results in two pyrrole (-NH) and two pyrrolenine (=N) units.

The structure of the cyclic tetrapyrrole was first suggested by W. Küster in 1912[32] and subsequent investigations proved the *trans* NH-tautomer was the most stable form. All porphyrins own the same basic structure, however they may have various substituents on the β carbons (positions 2, 3, 7, 8, 12, 13, 17 and 18) of pyrrole core (also named *β-pyrrolic*), or on the *meso* carbons (positions 5, 10, 15 and 20) [33,34].

The two nitrogen atoms at the center can accept protons to form a dication,[35] whereas the two NH groups can lose a proton to form a dianion.[36] Likewise, metallation of porphyrins is likely with many metals through the formation of this dianion. The complexes subsequently obtain are called "*metalloporphyrin*" (as opposed to "*free base*" in the absence of metallation,

Figure 8) and can present a large variety of geometries, depending of the nature of metallic ion.[37]

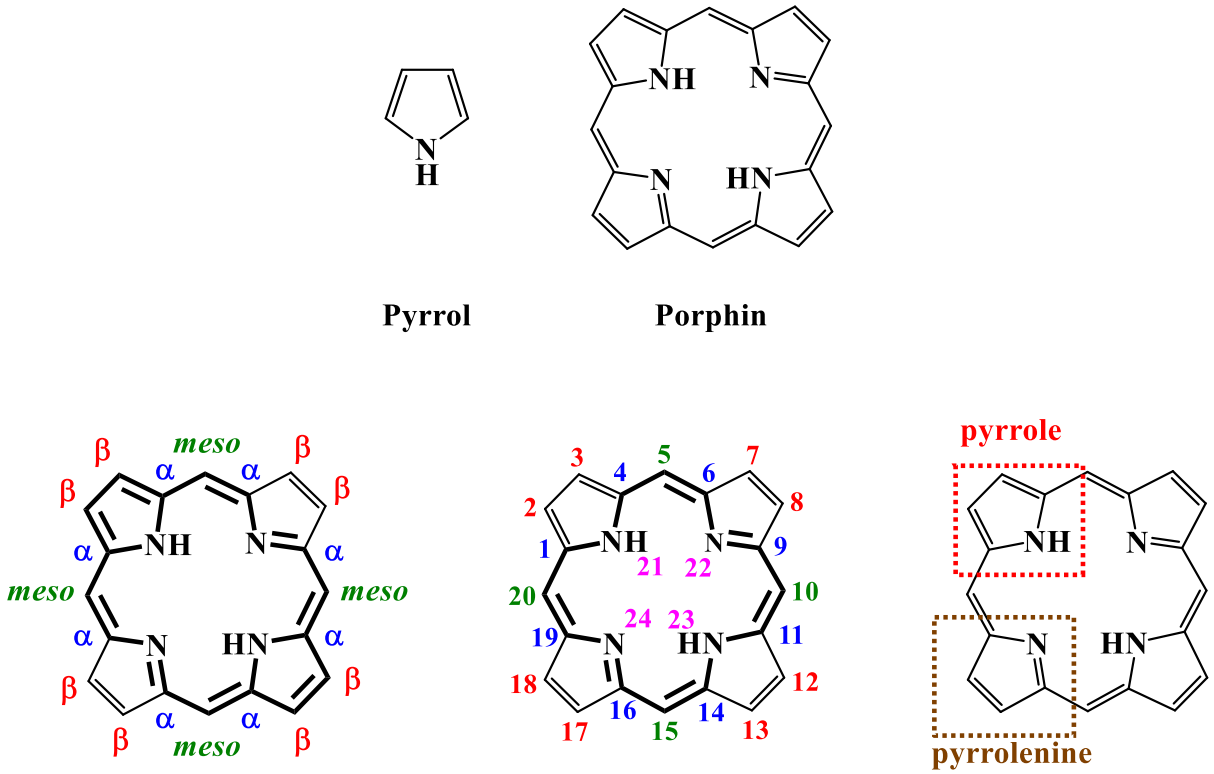

Figure 7: Numbering and naming of the porphyrin positions by means of porphyrin core according to the IUPAC (International Union of Pure and Applied Chemistry).

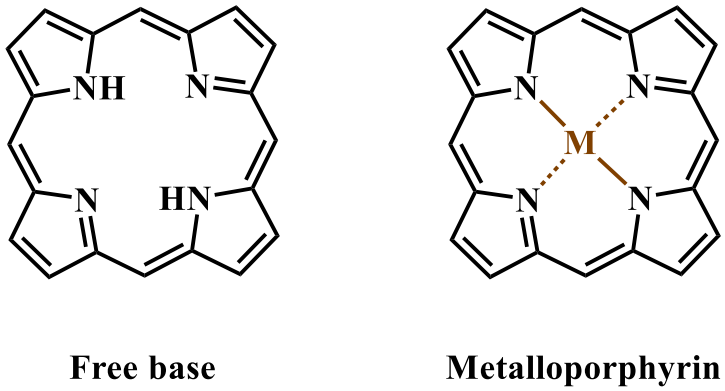

Figure 8: General structure of free base and metalloporphyrin.

It is commonly accepted that aromaticity of porphyrin is unique and comes from the diatropic ring distributed all around the macrocycle. Indeed, the π-system is composed of 22 electrons among which 18 are involved in the porphyrin macrocycle aromaticity and thus obey to the Hückel rules. Nevertheless, due to the similarity with annulene[38] they are sometimes described in the literature as multiple-bridged aromatic di-aza[18]annulene systems.[39]

Chlorins or 2,3-dihydroporphyrin are mainly natural compounds, among which chlorophyll is the major example. Their structure is similar to that of porphyrins with the exception of reduction of a peripheral double bond (Figure 3). Thus, their π-system is composed of only 20 electrons, but still 18 are involved in the macrocycle aromaticity.

A second class of porphyrin derivatives are named bacteriochlorins and were discovered by Van Niel in 1932.[40] The most know, bacteriochlorophylls, are photosynthetic pigments that occur in phototropic bacteria (*e.g.* Purple bacteria, Green sulfur bacteria or *Chloracidobacterium thermophilum*[41]…). These compounds have two reduced double bonds which can be in opposite (bacteriochlorins) or on two neighboring pyrrolic patterns (*iso*-bacteriochlorins)[42] (Figure 3). All the 18 electrons of the π-system are involved in the macrocycle aromaticity.

Phthalocyanines (only founded as traces in Nature) can be considered as synthetic porphyrin derivatives *e.g.*, tetrabenzo-[5,10,15,20]-tetraazaporphyrin (Figure 9). As porphyrins, they are aromatic macrocycles with planar structure possessing 18 π electrons. Their skeleton is composed of 4 *iso*-indoles groups linked in positions 1-3 by nitrogen bridges, which is called tetraazaisoindole macrocycle (Figure 9). They are chemically and thermally stable and as porphyrins they can incorporate different metallic ions into their core.

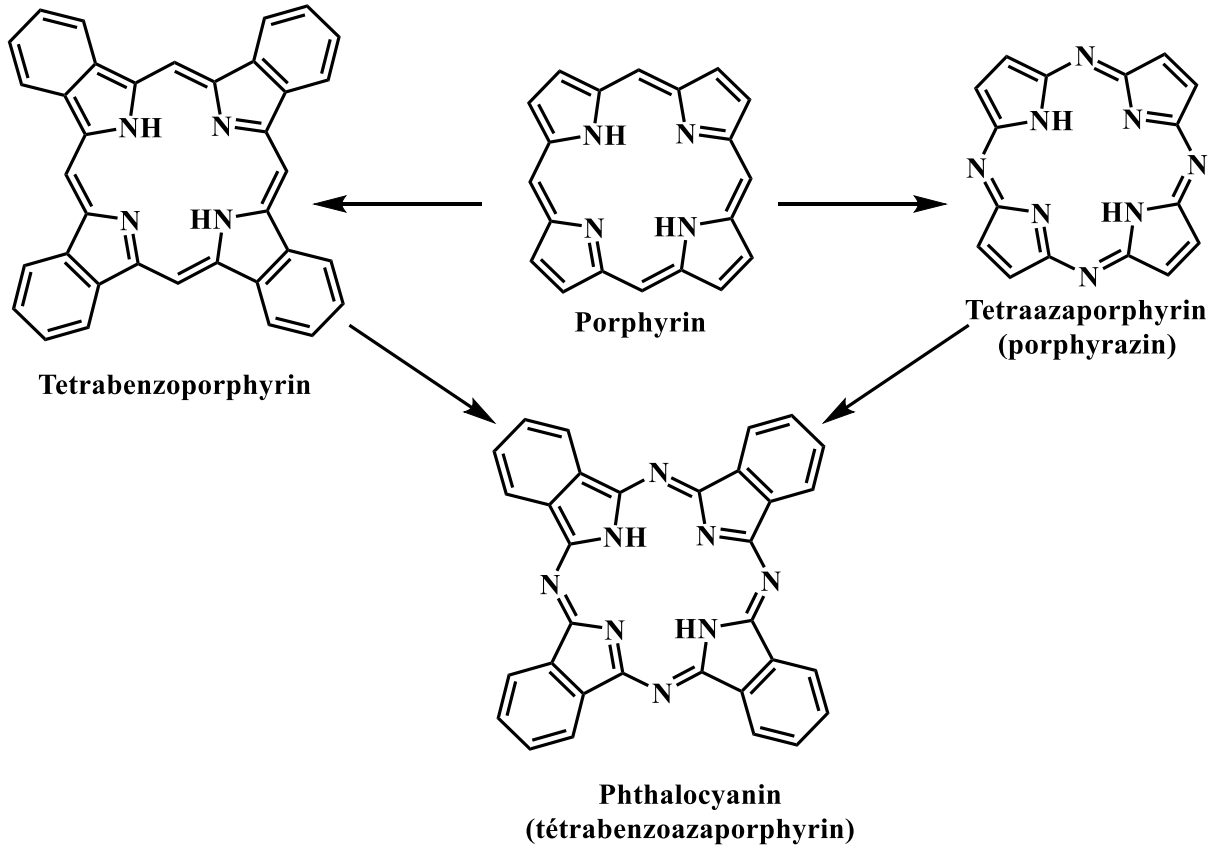

Figure 9: Structural relationships between porphyrins and phthalocyanines.

Grafting different substituents at α and β positions allow modulating their properties (Figure 10). Positions 1, 4, 8, 11, 15, 18, 22 and 25 correspond to α positions or non-peripheral positions, whereas positions 2, 3 , 9, 10, 16, 17, 23 and 24 are called β or peripherals.[33,43] Phthalocyanines are generally synthesized as metallophthalocyanines, the metal atom being most often zinc, copper or aluminum, but also cobalt or silicon.[44]

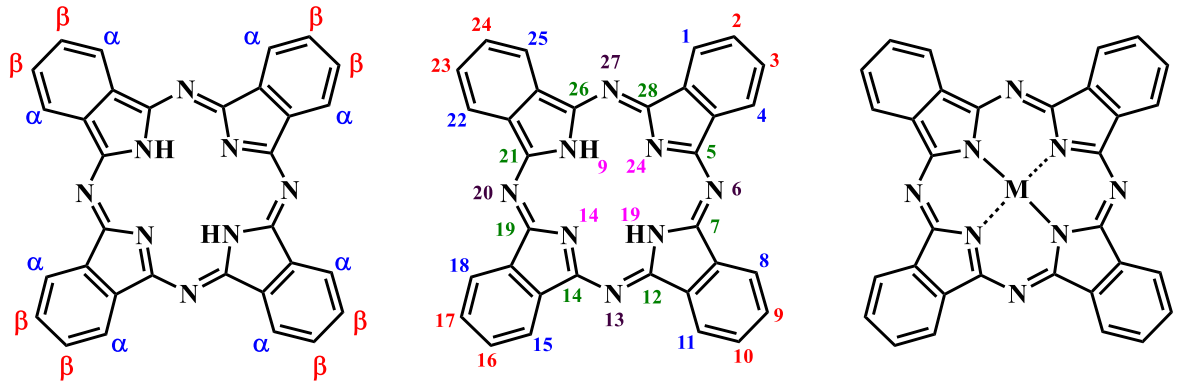

Figure 10: Numbering and naming of the phthalocyanines according to the IUPAC. On the right, general structure of a metallated phthalocyanine.

2. Synthesis pathways

The synthetic routes to obtain tetrapyrrolic macrocycles are too numerous to be exhaustively presented here. Here we first focus on the major routes of porphyrin synthesis. Then the synthesis of chlorins, bacteriochlorins and phthalocyanines is treated with less details.

2.1. Porphyrins

2.1.1. Synthesis from natural pigments

Some tetrapyrollic macrocycles can be isolated from the living kingdom as they come from degradation of animal or plant pigments. This is the case of hemin, an iron porphyrin, which is the most abundant porphyric derivatives into animal organisms. Hemin is the prosthetic group of hemoglobin and myoglobin (Figure 11). It can be obtained from the blood by two methods; Fisher developed the first one and Labbe and Nishida developed the second sixteen years after.

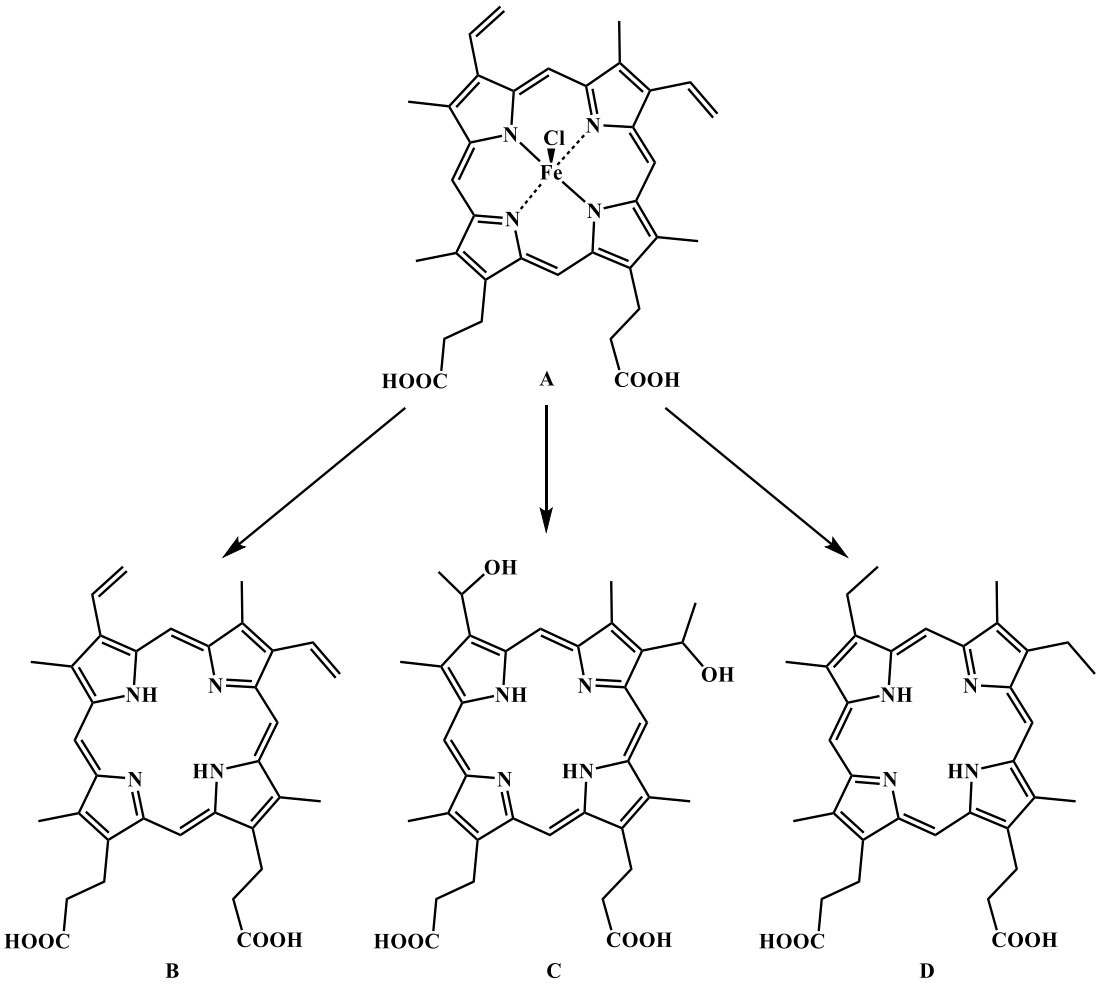

Figure 11: Structure of hemin (**A**), protoporphyrin IX (**B**), hematoporphyrin IX (**C**) and meso-porphyrin IX (**D**).

➢ Fischer method

Described by Fischer in 1941,[45] this process became classical to obtain hemin. It consists in heating defibrinated blood under acidic conditions, then hemin isolation is achieved by filtration or centrifugation during cooling of the mixture. Purification is realized by recrystallization, which allows obtaining about 3 grams of pure molecules per liter of blood.

➢ Labbe and Nishida method

Robert F. Labbe and Goro Nishida have later proposed a new extraction procedure,[46] based on the use of strontium chloride to eliminate the major part of proteins by hot filtration. Hemin crystallizes during the cooling step, then it is purified by recrystallization. The yields obtained by this process are globally similar to those obtained by Fischer's method.

Hemin is then used as a precursor of protoporphyrin IX as obtained by demetallation. Modifications of bay substituents lead to the formation of hematoporphyrin IX (treatment in acidic conditions) or *meso*-porphyrin IX (under mild alkaline conditions) (Figure 11). These

methods are not suitable for an intensive use and do yield only a limited set of compounds. Over the past eight decades, many efforts have made to achieve porphyrin total synthesis.

2.1.2. Total synthesis of macrocycle

All methods that have been developed share a common point, namely the porphyrin core results from two consecutive mechanisms: 1) electrophilic substitutions on positions 2 and 5 of pyrrole units, forming macrocycle and 2) oxidation yielding the aromatic ring. Different strategies (reagents, activation, solvents…) were developed according to the targeted substituents (nature, number and position). All methods can be classified into three groups according to the nature of the macrocycle precursors.[12]

First, the most common and oldest method is based on four pyrrole units' condensation (pathway I). Second, the so-called MacDonald route or [2+2] strategy (pathway II) is an alternative where pyrrole units are replaced by two dipyrromethanes; this allows the control of configuration of the final product (and substituent position). Third, the [3+1] approach is a variant of the MacDonald route using condensation of one pyrrole unit with tripyrrane (pathway III). There is no ideal method, each of the three has its own advantages and limits, for which optimal reaction conditions depend on the desired structure.

2.1.2.1. Pathway I : condensation between pyrrole and aldehyde

- Rothemund synthesis

The first synthesis of porphyrins by condensation between pyrrole and aldehydes was described in sealed tubes by Rothemund, in 1935.[47] In 1939, he obtained several *meso*-tetrakis porphyrins, including *meso*-tetraphenylporphyrin (TPP) also in sealed tubes (142-150 °C during 24 hours). However, he succeeded, later in 1941, especifically in the formation of TPP in sealed tubes by heating at 220 °C for 48 hours.[48] Because of tough experimental conditions, only the most heat resistant aldehydes could form *meso*-tetraryl porphyrins, but with low yields (5-10 %). Chlorins obtained during synthesis (10 to 20 %) were reduced into porphyrin using DDQ (2,3-dichloro-5,6-dicyanoquinone) as oxidant (Figure 12).

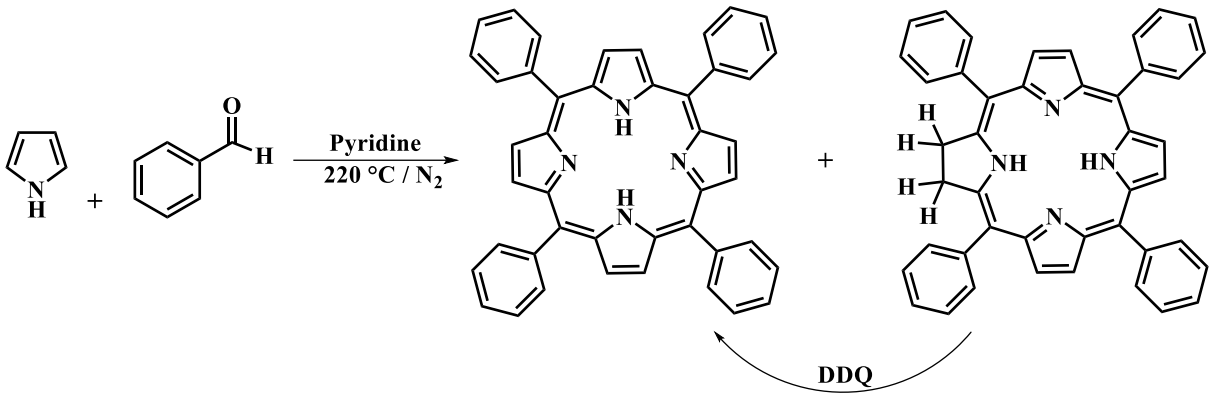

Figure 12: Example of *tetra*-phenylporphyrin synthesis performed according to Rothemund.

- Adler-Longo synthesis

In 1964,[49] Adler and Longo synthesized TPP by refluxing a mixture of pyrrole and benzaldehydes in acetic acid during 30 minutes under air bubbling to oxidize all porphyrinogen intermediates formed during the reaction. Then in 1967,[50] they established a link between condensation yield of pyrrole and benzaldehyde on one hand and acidity, temperature, solvent, and quantities of introduced reactants on the other. Their optimized method consisted in refluxing an equimolar mixture of the two reactants in propionic acid during 30 minutes under aerated conditions. In these conditions TPP is obtained with 20 % yield by washing with methanol then with hot water (Figure 13). Nevertheless, there were still two main limitations to this synthesis. First, air sensitive aldehydes cannot be used, and second concerns purification. Indeed, if TPP crystallizes in propionic acid after cooling at room temperature, this is not true for all porphyrins. Moreover, yields are often not reproducible.

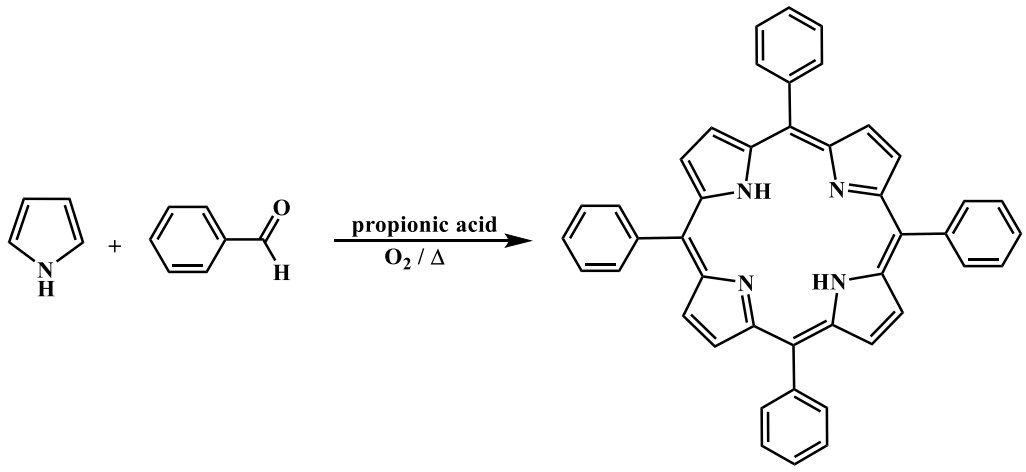

Figure 13: TPP synthesis according to optimized Adler and Longo's method.

➢ Synthesis of Little

Developed in 1975,[51] this method also called "mixed aldehydes method" derives from the Adler and Logo's. In order to obtain non-symmetric *meso*-aryl porphyrins, it consists in refluxing pyrrole and two different aldehydes in propionic acid during 30 minutes (Figure 14).

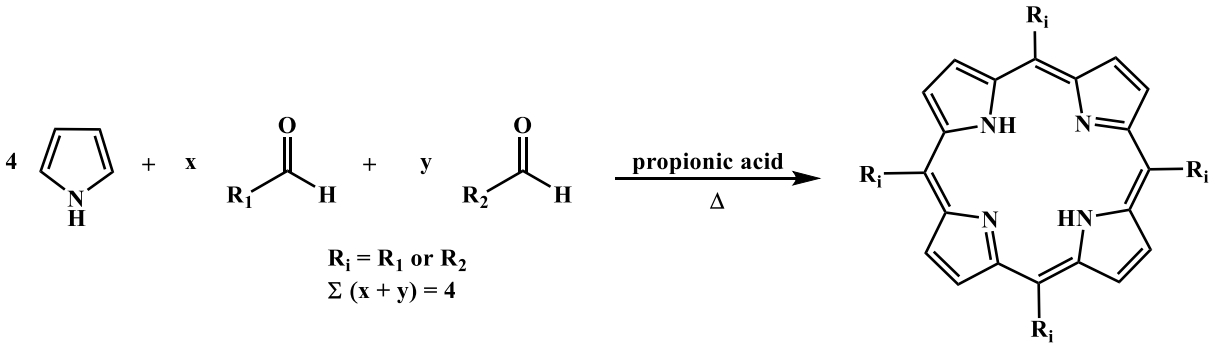

Figure 14: Porphyrins synthesis according to Little's method.

This approach provides a wide range of porphyrins but there is no way to control substituent reactivity during the reaction, which leads to a mixture of six different compounds, namely when two different aldehydes A and B are used, the two parent porphyrins (A_4 and B_4), and four hybrid porph yrins (A_3B, A_2B_2 cis and A_2B_2 trans, AB_3) (Figure 15).

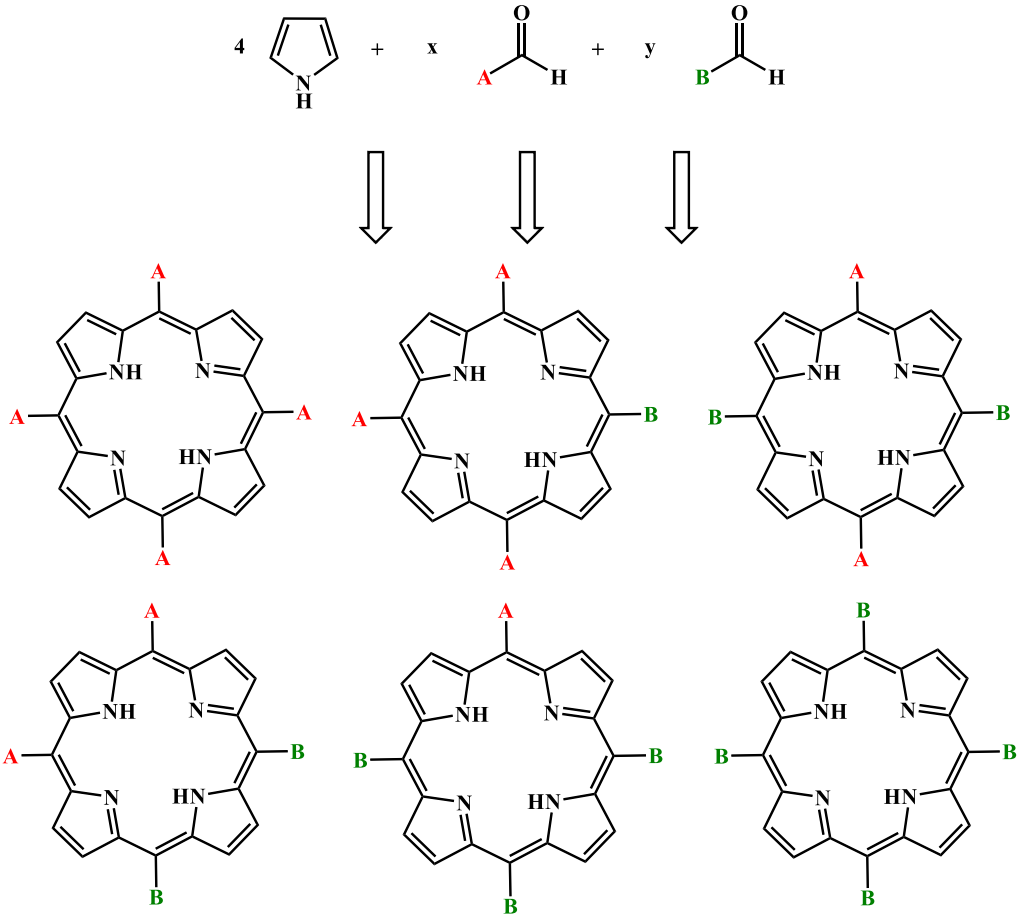

Figure 15: Porphyrins synthesized by using two aldehydes via Little's method.

To favor one compound rather another, one can vary aldehyde equivalents. For example, the mixture can be A_3B-porphyrin enriched by using a greater ratio than 1:1 of the A and B aldehydes. With a 3:1 ratio, the relative concentration of A_3B-porphyrin is 42.2 % *vs*. 25 % as obtained with a 1:1 ratio;[52] it means that for an overall 40 % yield of porphyrins, the A_3B-porphyrin is formed in 16 % yield.[53,54]

- Lindsey synthesis

In 1987,[55] Lindsey proposed a new approach to synthesized symmetric porphyrins, based on the works of Rothemund and Adler and Longo (Figure 16).

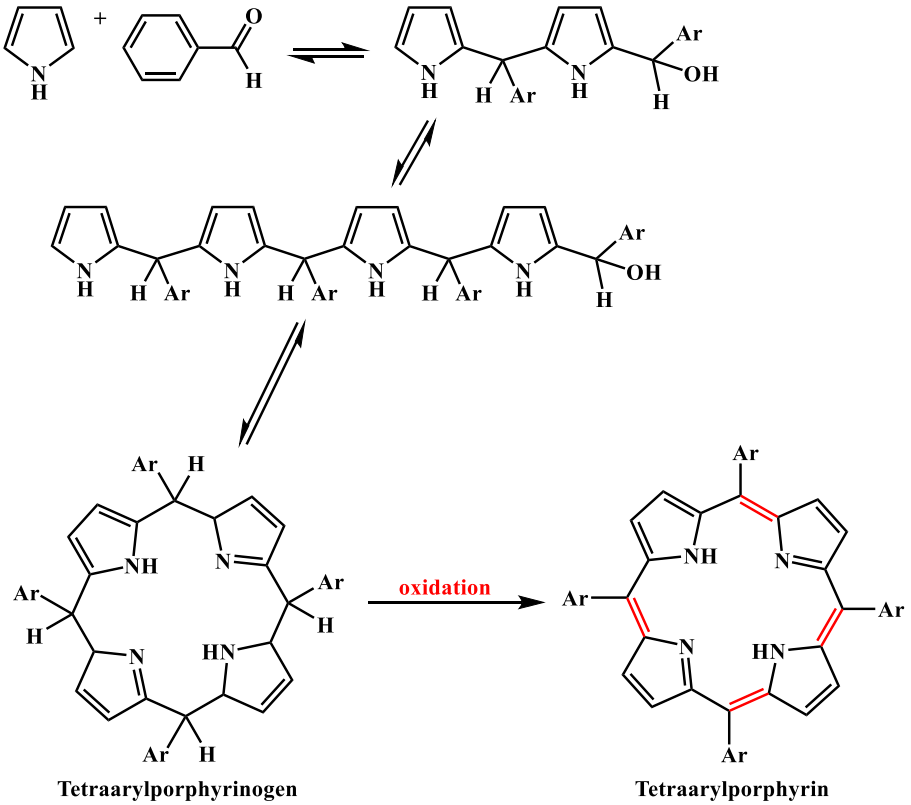

Figure 16: Lindsey's method mechanism.

This method leads to *meso*-tetrakis porphyrins production with good yields (*e.g.* TPP with 35-55 % yield) under mild conditions, which can allow working with thermal sensitive aldehydes and without purification difficulties. In this protocol, a Lewis acid (like BF_3 or BCl_3) was used in catalytic quantity in anhydrous conditions (dichloromethane and TEOA (triethyl orthoacetate) as water scavenger) and under N_2 atmosphere. Such experimental conditions allow obtaining porphyrinogen as the thermodynamically product, which is then eventually oxidized into porphyrins by adding DDQ or *p*-chloranil (Figure 16). With this protocol, maximal yields are reached for dilute solutions ($C < 10^{-2}$ M). However it can even be possible

to use Lindsey's method to synthesize asymmetric porphyrins.[52,56] Nonetheless in all cases, several side reactions may interfere during experiments as pyrrole polymerization, uncontrolled combination of aldehyde and pyrrole patterns, formation of non-cyclized chains, which increase time and difficulty of purification

- Solid phase synthesis

In 1978, Leznoff and Svirskaya realized the synthesis of 5-(4-hydroxy)phenyl-10,15,20-tritolylporphyrin and 5-(3-hydroxy)phenyl-10,15,20-tritolylporphyrin in solid phase,[57] which limits purification steps (Figure 17).

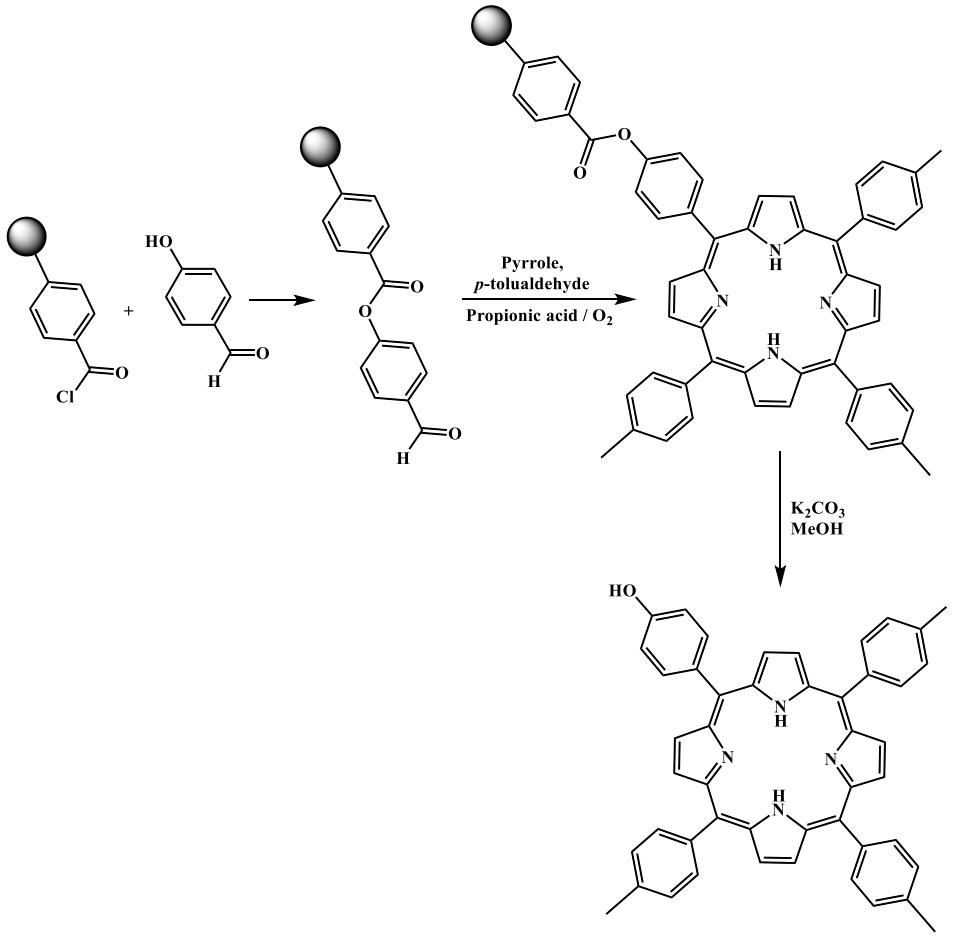

Figure 17: Asymmetric porphyrin synthesis on solid phase.

The procedure is binding of 4-hydroxybenzaldehyde (or its analogue 3-hydroxybenzaldehyde) to a polystyrene resin containing acyl chloride by simple esterification. In a second step, this new polymer is added to *p*-tolualdehyde and pyrrole mixture in propionic acid at reflux for one hour. After filtration, cleavage is realized using potassium carbonate in methanol during 24 h to provide the targeted porphyrin (Figure 17). Although purification has

become easier, this method allows only very poor yields (2 and 4.5 % for 3- and 4-hydroxybenzaldehyde, respectively).

➢ Microwave activations

The use of microwave irradiations in porphyrin synthesis were studied since the 2000s, due to their significant advantages: decrease of reaction time and amount of solvents, high selectivity, no chlorin contamination and relevant alternative to propionic acid.[58] For symmetric porphyrins, it is worth mentioning the study of Nascimento *et al.* who initially used a domestic microwave oven[59] then a laboratory microwave reactor. Some *meso*-tetra-aryl porphyrins were thus obtained with yield up to 20 % (for TPP), using a mixture of aldehyde and pyrrole in propionic acid and nitrobenzene, activated during 5 minutes. They have also shown the interest of heterogeneous oxidation with manganese dioxide[60] under microwave for *meso*-tetra-arylporphyrin synthesis, which facilitates purification and is less expensive than quinones usually employed (as *p* or *o*-chloranil) (Figure 18).

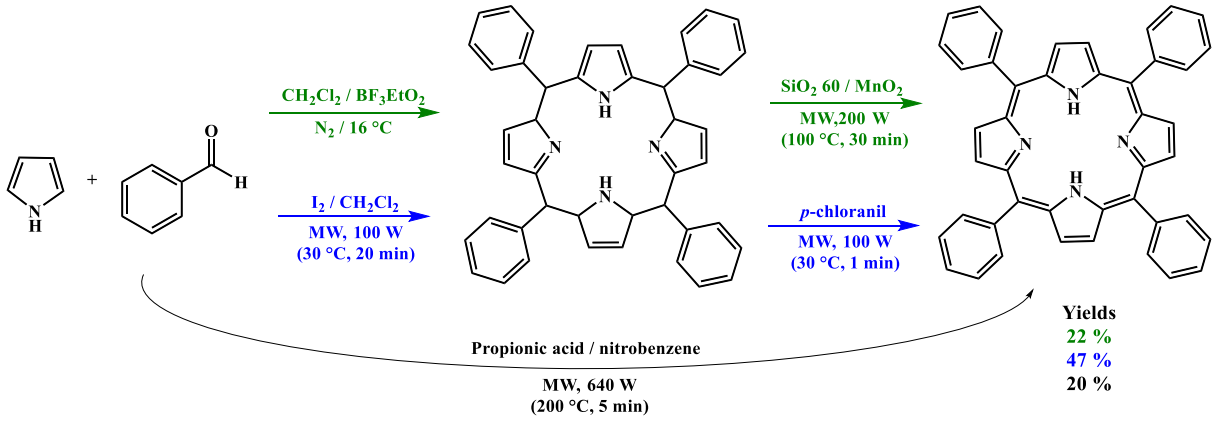

Figure 18: Microwave porphyrin synthesis. Nascimento's works are in green and black, Zerrouki's results are in blue.

In our laboratory, Zerrouki *et al.* have developed a new approach based on diiodine as catalyst. In this method, porphyrinogens are synthetized first, then they are oxidized by *p*-chloranil (Figure 18). The main advantages come from the easier implementation of the procedure and the increased yields compared to classical approaches.[61,62]

Lindsey developed also a synthetic route from pyrrole-carbinols.[56] It consists in treatment of one pyrrole unit by acyl chloride to obtain ketopyrrole, which is then reduced into pyrrole-carbinol. Finally, this compound reacts under acidic and oxygenated conditions to give the corresponding *meso*-porphyrin (Figure 19). For example, TPP was obtained in propionic acid with 41 % yield thanks to this method.

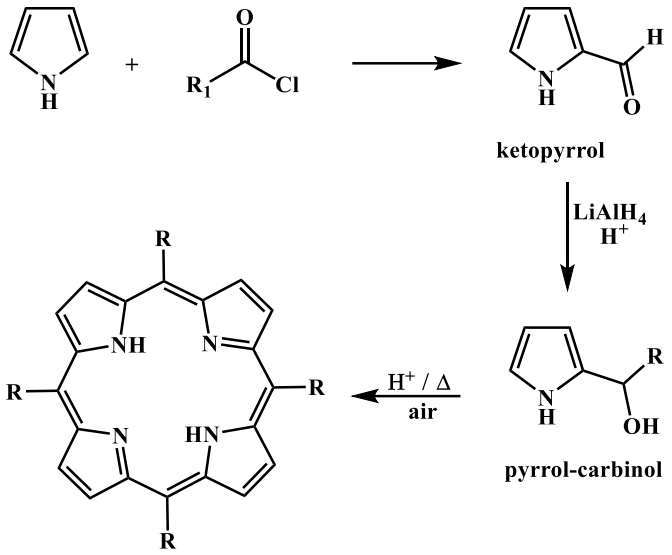

Figure 19: Porphyrin synthesis via pyrrol-carbinol.

- Active charcoal

To overcome the use of solvents and toxic catalysts for the environment, an alternative method was developed in our laboratory by Vignaud *et al.*[63] This approach allows to obtain *meso*-tetraarylporphyrins without solvents through the use of active charcoal (pretreated with nitric acid) which plays the role of acid promoter.[63] Symmetric meso-porphyrins as tetra-tolyl or tetra-anisyl porphyrins were obtained with relatively high yields, 40 and 33 %, respectively (Figure 20).

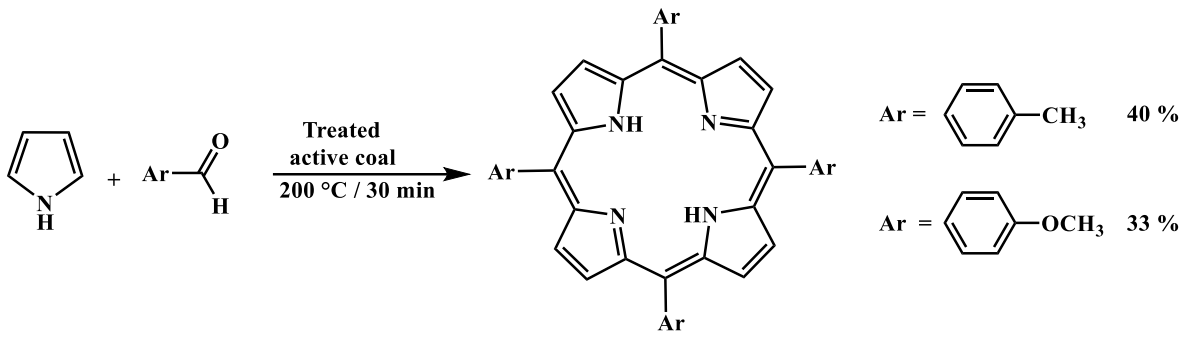

Figure 20: Synthesis catalyzed by active charcoal.

However, no matter the approach, preparing unsymmetrical porphyrins from pyrrole invariably leads to the formation of a mixture of porphyrins requiring rigorous purification.

2.1.2.2. Pathway II: the "[2+2] route"

This approach consists in coupling two dipyrrolic intermediates, and allows obtaining a broad range of asymmetric β-substituted porphyrins. The next section deals with dippyromethanes and dippyromethenes (or dipyrrins),[64] which are the most commonly used (Figure 21).

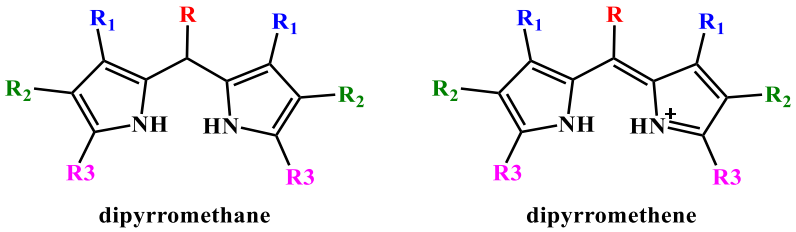

Figure 21: General structures of dipyrromethane and dippyromethene. In dipyrromethane, R_3 = H or aldehyde.

➢ Dippyromethanes

Dipyrromethanes are generally obtained by condensation of two pyrrole units (or derivatives) with an aldehyde pattern, under acidic catalysis (Figure 22).[65–67] For *meso*-substituted porphyrins, formaldehyde was first used, but it is possible to replace it by a large variety of aliphatic or aromatic compounds (the only limitation is the presence of an aldehyde function).[68–70]

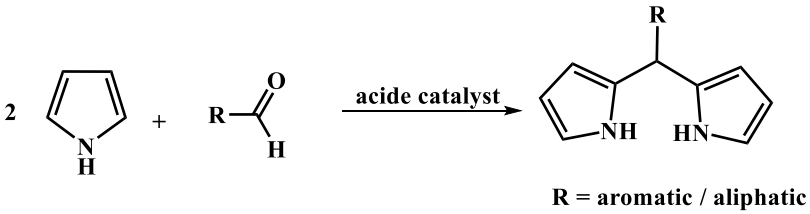

Figure 22: General procedure of dippyromethanes synthesis.

In 1960-61, MacDonald and Woordward synthesized porphyrins from two dipyrromethanes.[71,72] This reaction yields porphyrinogen intermediates, which are oxidized (with air) to produce the corresponding porphyrin (Figure 23). In MacDonald's synthesis, the reaction between substituted and unsubstituted dipyrromethanes allows very good yields (50 to 60 %).

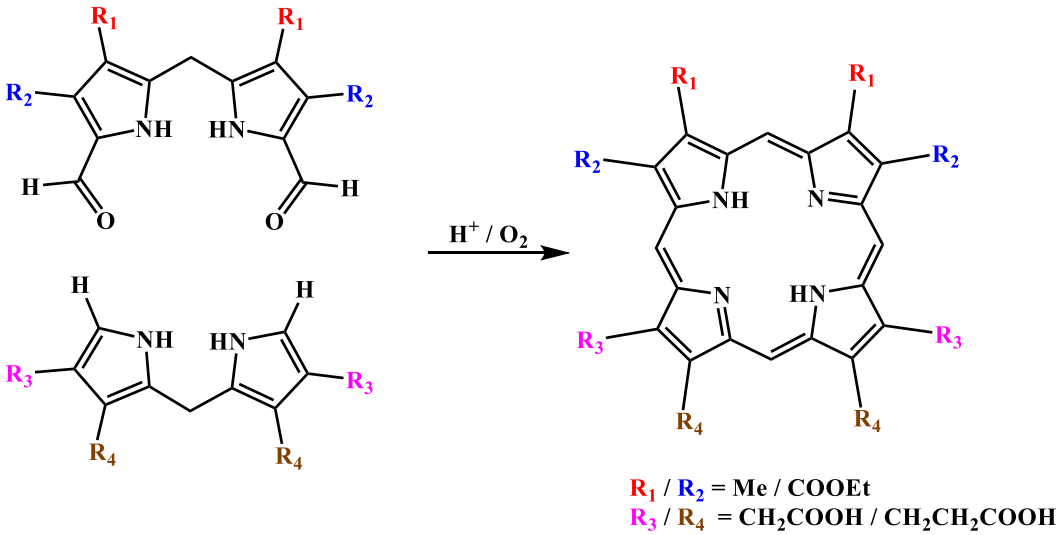

Figure 23: Synthesis scheme according to MacDonald and Woodward methods.

In 1978, Ogoshi *et al.* developed a variant of the former apporach by using aromatic aldehyde, benzene as solvent and TFA as acid catalyst (Figure 24). This approach has led to some 5,15-diarylporphyrin creation with yields ranging from 30 to 40 %.[73]

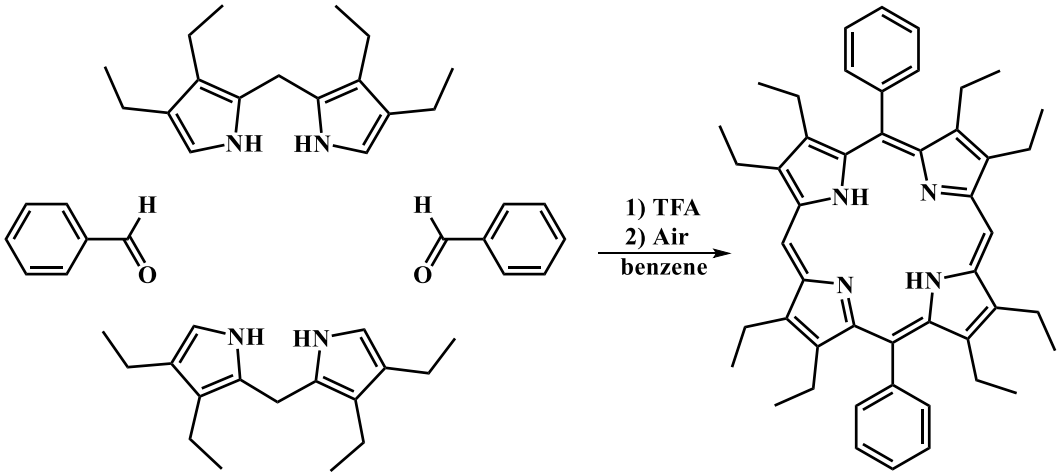

Figure 24: 5,15-diarylporphyrins synthesis according to Ogoshi *et al.*

In 1989, Manka and Lawrence obtained 5,15-diarylporphyrins with high yields (73-92 %).[74] The main difference with their predecessors is the use of a quinone (chloranil) instead of air as oxidant agent (Figure 25).

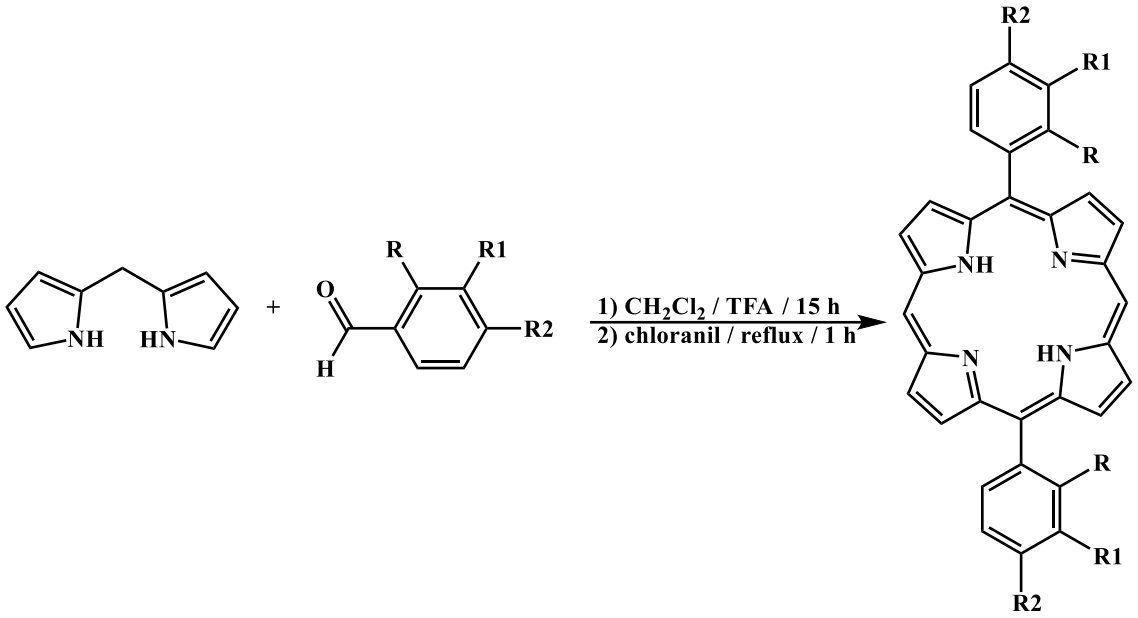

Figure 25: 5,15-diarylporphyrins according to Manka and Lawrence.

As Leznoff and Svirskaya, some scientists have also tried to use solid phase in dypyrromethane chemistry. In 2000, Montierth *et al*. reported dypyrromethane synthesis based on MacDonald's technique (Figure 26).[75] Here, a first dipyrromethane is linked to a Merrifield Resin; then coupling the supported compound to a second dipyrromethane provides an intermediate which is finally transformed into porphyrin (15-20 % yield) using TFA, *p*-toluenesulfonic acid and benzaldehyde (Figure 26).

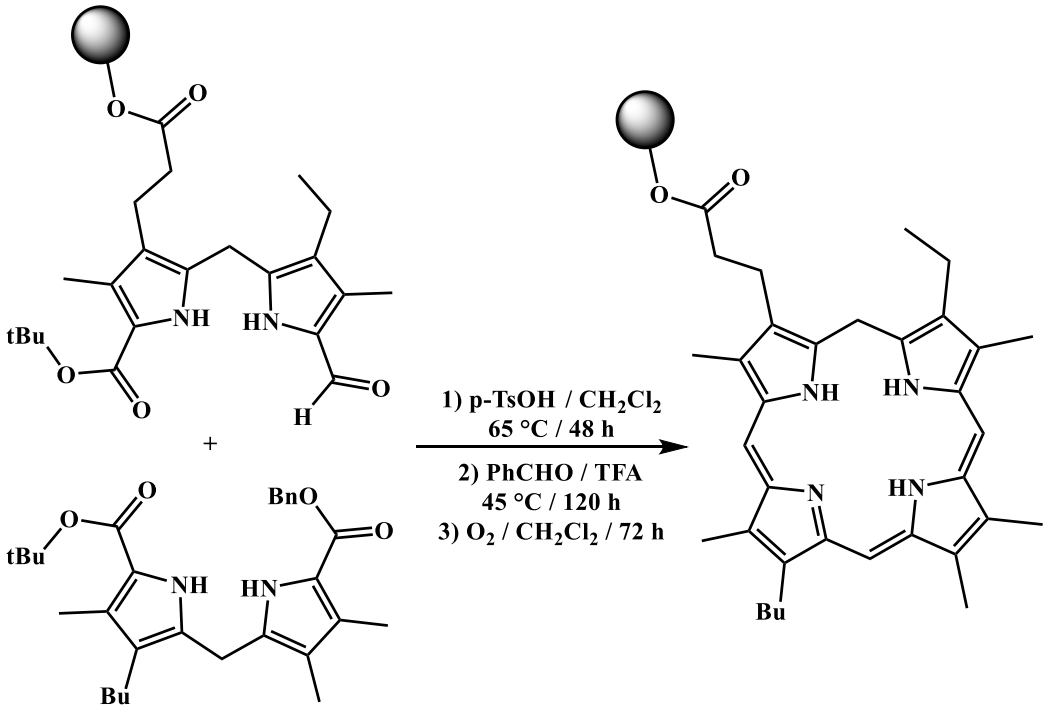

Figure 26: Solid state synthesis *via* dipyrromethanes process.

In 2003, Naik and coworkers presented another solid state synthesis based on Manka and Lawrence methodology, but using cation exchange resins (Amberlist-15, IR-120, Tulsion T40-42-63, Indion-130…) instead of Merrifield resin to synthesize *meso*-tetrakis porphyrins with rather high yields (18 to 68 % depending on substituents).[76]

All these methods have in common the requirement of an aldehyde function. In 2009, Temelli published a different approach (still based on MacDonald's route) using dipyrromethanes in association with N-tosyl-imines.[77] This reaction is catalyzed by metal triflate (best results being obtained with $Cu(Otf)_2$) in dichloromethane, and with DDQ as oxidizing agent (Figure 27).

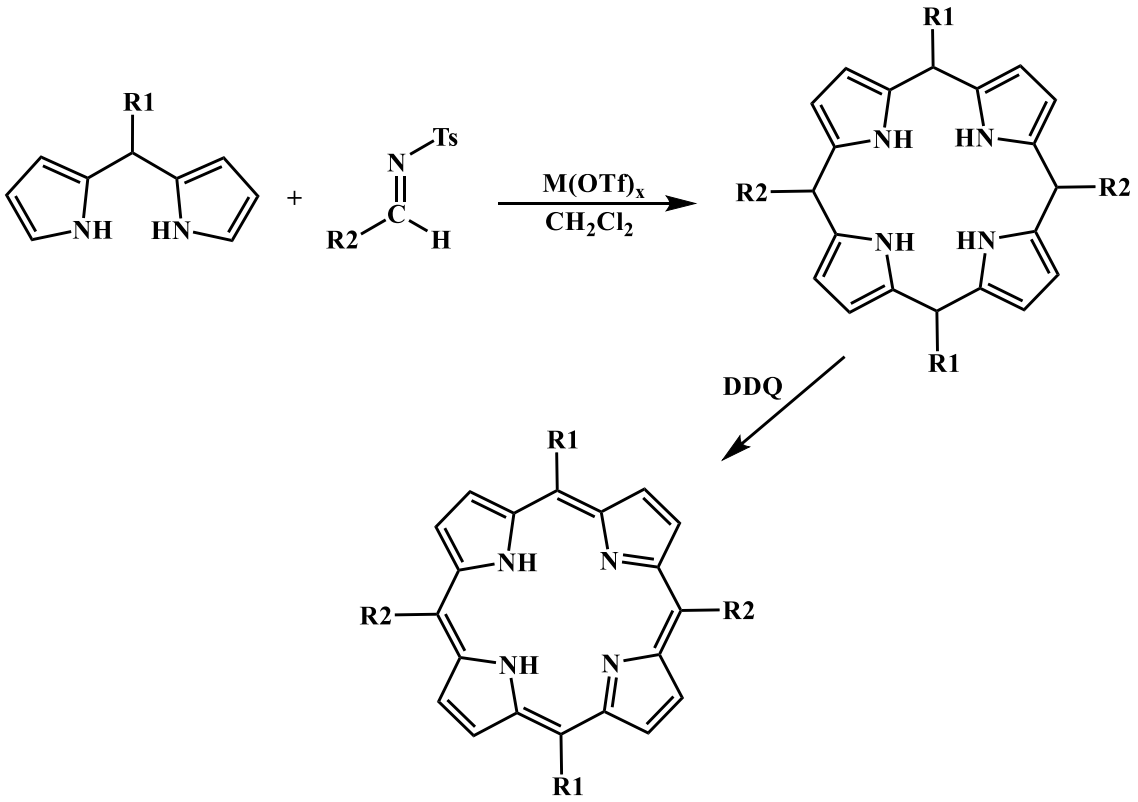

Figure 27: General protocol according to Temelli *et al.*

- Dipyrrins / dippyromethenes

The second way consists to create dipyrromethenes, which are cationic compounds as molecular brick for porphyrin synthesis. They can be obtained under acidic conditions from dipyrromethanes, or by condensation between 2,3-dimethylpyrrole and 2-formyl-3,5-dimethylpyrrole units (Figure 28).[78] The charge dramatically modifies properties, as decreasing stability and increasing reactivity compared to their dipyrromethane analogues.

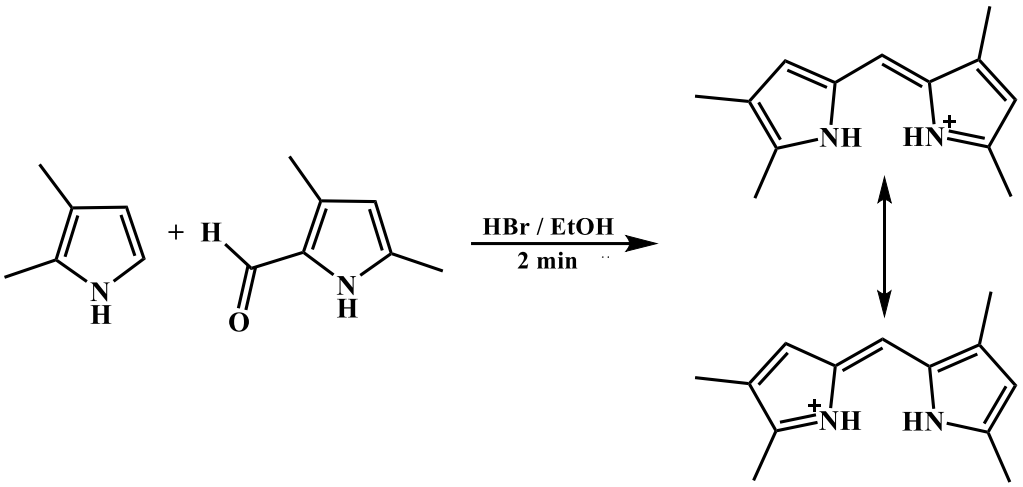

Figure 28: Dippyromethene cation synthesis.

The pioneer use of dipyrromethenes is attributed to Hans Fischer (Nobel Prize in 1930) who synthetized some naturally occurring porphyrins, with yields ranging from 0.2 to 20 %.[79] Condensation of two dipyrromethenes was achieved in acidic medium (tartaric acid) above 200 °C. Due to rather extreme conditions, it was limited to symmetric porphyrins.[80] Later, some advanced syntheses showed that using formic acid with bromine allowed yields up to 40 % (Figure 29).[81]

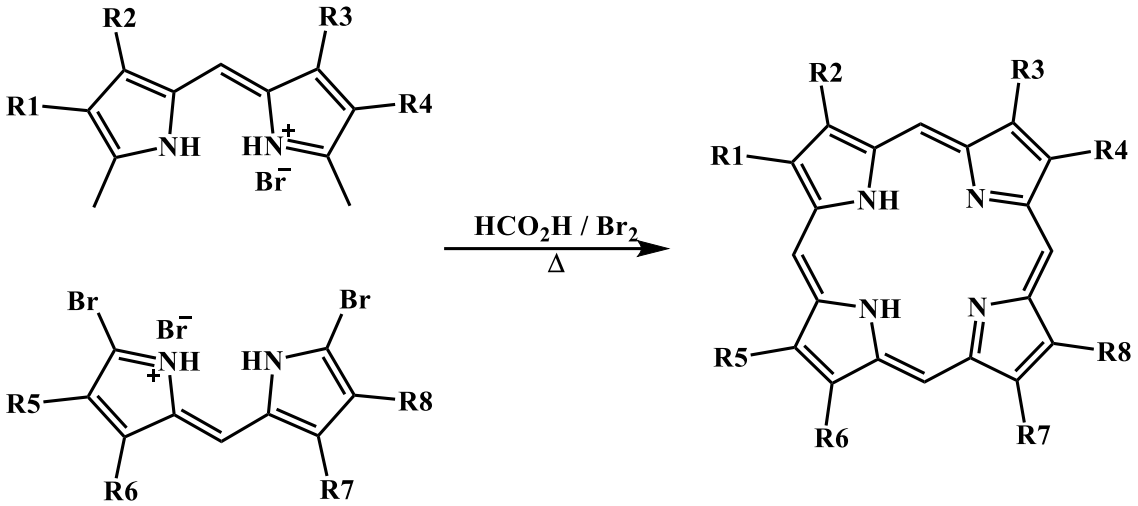

Figure 29: Synthesis protocol of porphyrins *via* dipyrromethenes.

In 1988, Paine *et al*. improved this process by demonstrating dipyrromethene bromination efficiency, with yields up to 90 % (80-90 %), in a DMSO / pyridine mixture (Figure 30).[82]

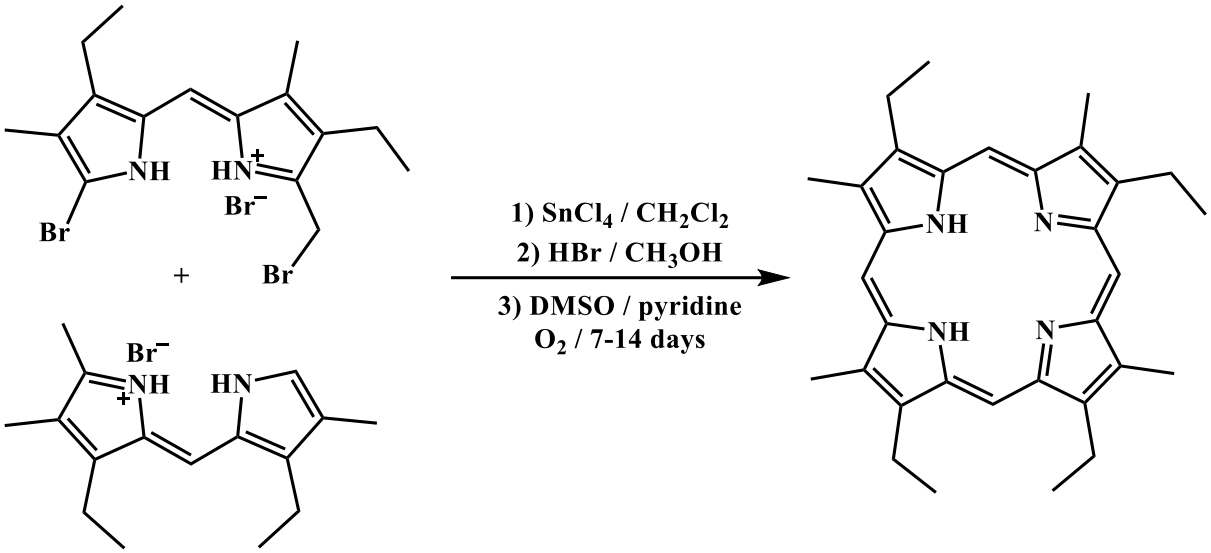

Figure 30: Optimized porphyrin synthesis *via* dipyrromethenes route according to Paine *et al.*

2.1.2.3. [3+1] synthesis

The [3+1] method consists in reaction of a tripyranne compound (with carbons in position 1 and 14 free) with a pyrrole bearing two alcohols (Figure 31).

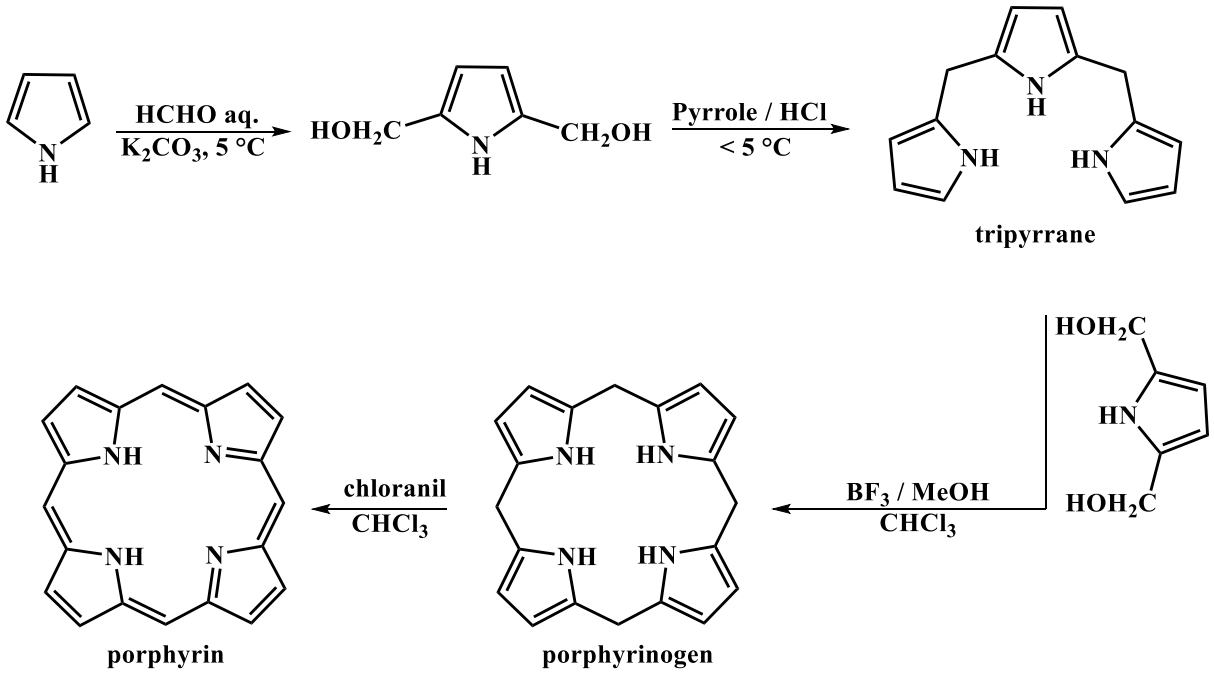

Figure 31: Synthesis pathway of porphyrin core by [3+1] method.

In a first step, synthesis of diol and corresponding tripyranne is achieved with pyrrole and potassium carbonate in acidic conditions for the simplest compounds. Then, these two moieties react together to form porphyrinogen, which is finally oxidized into porphyrin (Figure 31).[83–85]

More recently, Hatscher and Senge proposed a modified version of this procedure.[86] It is based on the reaction of tripyranne with pyrrole and aldehydes instead of diol. Synthesis of some mono or di - substituted porphyrins was then achieved with yields between 4 to 75 % depending on used aldehydes (Figure 32).

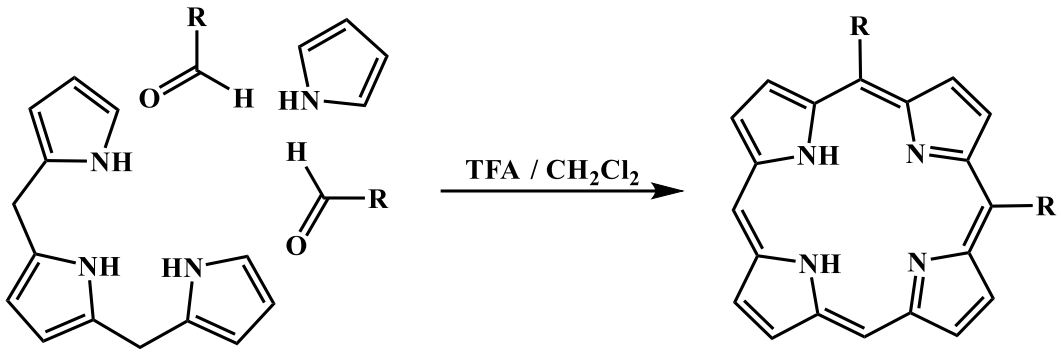

Figure 32: Substituted porphyrins synthesis via [3+1] method according to Hatscher and Senge.

As tripyrranes, their tetrapyrrane analogues can also be used in porphyrin synthesis *via* the [3+1] procedure. In 2008, Saltsman and co-workers described microwave-assisted formation of tri, tetra and penta – pyrranes (Figure 33).

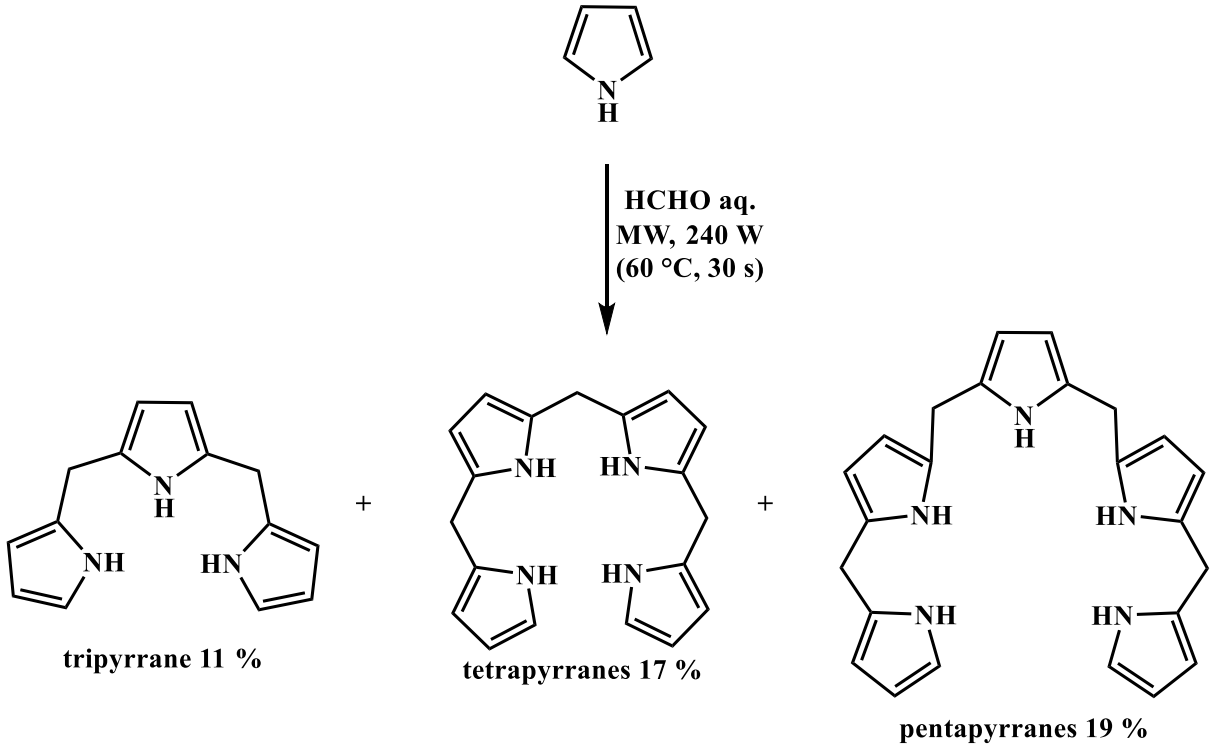

Figure 33: Microwave-assisted synthesis of tri, tetra and pentapyrranes.

The first two poly-pyrranes can then be used for porphyrin formation as described above.[87] This method extremely decreases reaction time, and provides a wide range of intermediates.

In 2007, Lindsey *et al.* studied metalloporphyrin formation by bilane cyclisation. Indeed, metal-templating is expected to favor intramolecular cyclization over competing polymerization.[88,89] Moreover, as with the [2+2] route, this process allows obtaining porphyrins bearing four different substituents (named ABCD porphyrins). Optimal conditions require DBU (1,8-Diazabicycloundec-7-ene) and $MgBr_2$ in toluene, at 115 °C under air during two hours (Figure 34). The metallated corresponding porphyrin is obtained with yields up to 65 %, and if required magnesium atom is removed by simple acidic treatment to give the free base molecule.

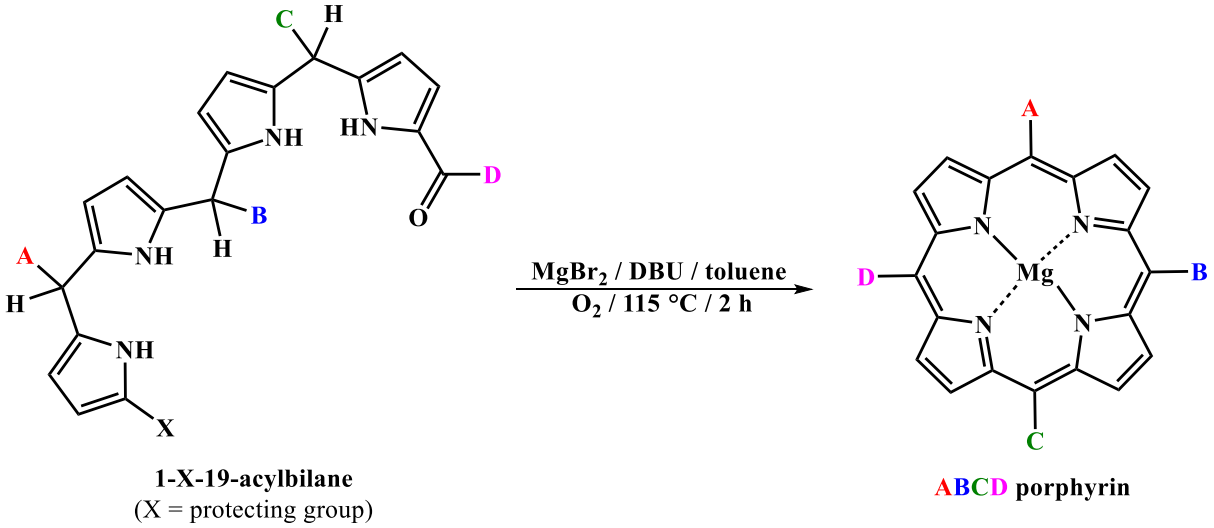

Figure 34: ABCD porphyrin synthesis *via* bilane.

In principle there are three ways to obtain ABCD porphyrins, which are mixed condensations, total synthesis and functionalization. Here it is worth noting a last procedure, which is based on the third way. Senge *et al.* have developed a new method where a "simple model" of porphyrin (native or bromine substituted) is functionalized with A, B, C, D residues.

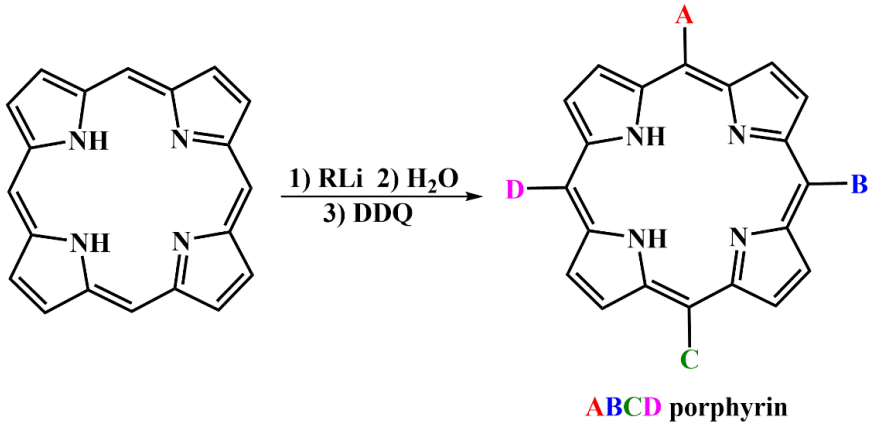

Figure 35: General procedure for ABCD porphyrins.

Thanks to the intrinsic reactivity of *meso* positions of these compounds for electrophilic reactions, organolithium reagents (strong nucleophiles) or Pd catalyzed reactions can result in production of a wide range of ABCD porphyrins (Figure 35).[90,91]

2.2. Chlorins and bacteriochlorins

As for porphyrins, chlorins and bacteriochlorins can be obtained by numerous ways that will not be exhaustively reported here. The next sections present only three global processes to synthetize these compounds.

2.2.1. From porphyrins

As said above, chlorins and bacteriochlorins are porphyrin derivatives and the first method to obtain these molecules is porphyrin reduction (Figure 36).

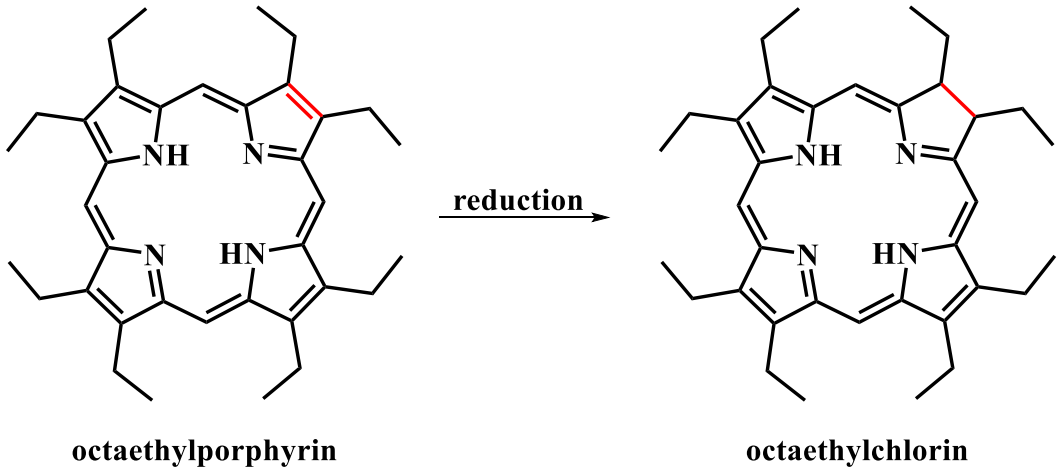

Figure 36: General reduction of porphyrin into chlorin *e.g.*, octa-ethylporphyrin.

The first successful attempt was conducted by Treibs *et al.*, in 1929.[92] By using sodium in alcoholic solvent at 185 °C, a mixture of chlorins was obtained in good yields (20 %). Afterwards, different studies reported synthesis of chlorins using similar conditions, even if the structure was fully elucidated only 40 years later by X-ray crystallography. For example, in 1950 Schlesinger *et al.* reduced *etio*-hemin thanks to sodium in isoamyl alcohol (3-methyl-1-butanol) under hydrogen flux with 79 % yield (mixture of chlorins and dihydrochlorins).[93] As well, in 1957 Eisner *et al.* obtained octa-ethylchlorin from octa-ethylporphyrin with a yield of 32,5%.[94]

The main problem in chlorin synthesis from porphyrin comes from the second reduction of chlorins into bacteriochlorins. To avoid this drawback, Whitlock *et al*. proposed to use

diazene (diimine) on octa-ethylporphyrin, in 1969. In association with *p*-toluenesulfonylhydrazine (*p*-TSH), this allows obtaining in a first step a mixture of chlorins and bacteriochlorins (respectively 62 and 38 %). Then *o*-chloranil is added to oxidize selectively bacteriochlorines into the corresponding chlorin with a yield of 72 %.[95] A lot of asymmetric compounds were realized using this procedure.[96] Since then, conditions to reduce the porphyrin macrocycle have been widely explored. Chlorins derivatives can also be obtained using acid-catalyzed rearrangements or reduction.[97,98] For example, sulfuric acid in association with hydrogen peroxide give the corresponding oxochlorin,[99] while carbene form cyclopropylchlorin,[100] and osmium tetroxide chlorins bearing two hydroxyl groups on the reduced bond (Figure 37).[101]

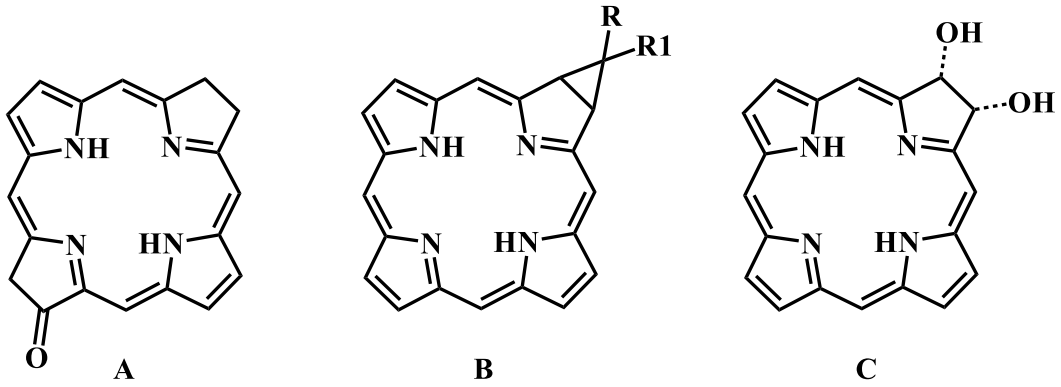

Figure 37: General structure of chlorin like. A: Oxochlorin; B: Cyclopropylchlorin; C: Dihydroxychlorin.

More recently, microwave assisted synthesis was also developed. As for porphyrin synthesis, reaction time is reduced and this provides a wide range of free and metallated compounds (Figure 38).[102]

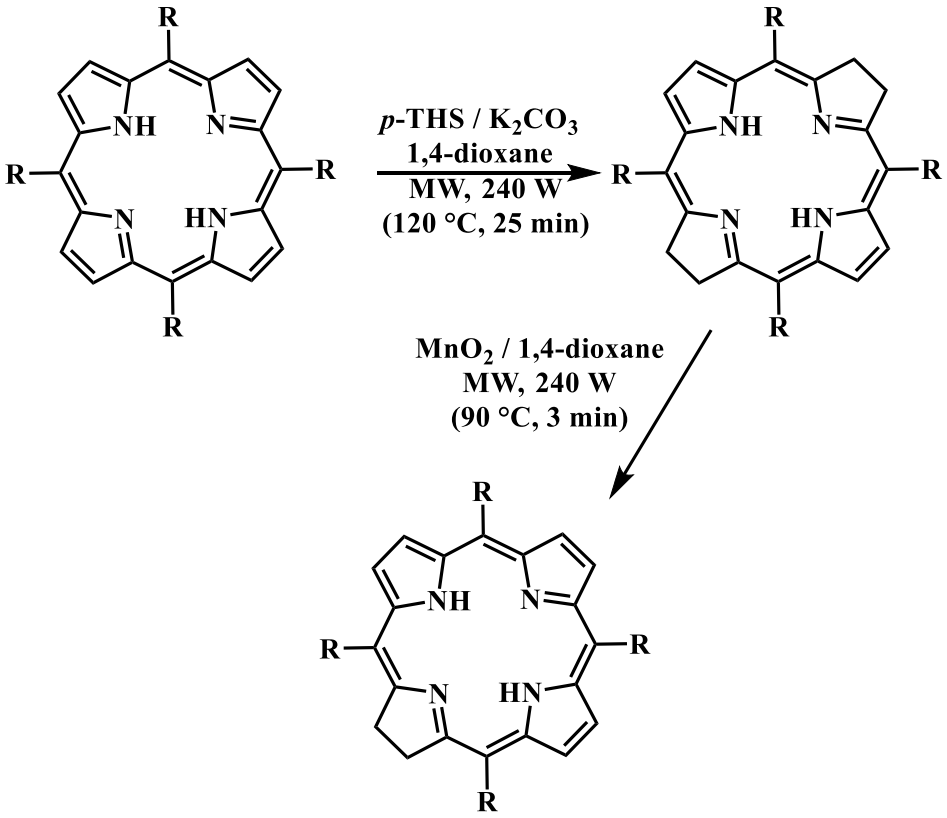

Figure 38: Microwave-assisted of chlorin synthesis.

2.2.2. [2+2] synthesis

As for porphyrins, chlorins and bacteriochlorins can be obtained using a [2+2] strategy based on direct coupling of two dipyrrolic intermediates.[103] The pioneer works of Battersby *et al.* have allowed producing several substituted chlorins, in which localization and nature of substituents can be controlled.[104–106] In this method, the two moieties (called "western" and "eastern" halves) are joined to form an intermediate (called dihydrobilene-*a*), followed by oxidation and cyclization thus yielding chlorin.[107] Two activation modes are possible (Figure 39):

- Thermal route that is performed in the presence of a metal and gives the metallated molecule. The free base chlorin can then be obtained by simple demetallation under acidic condition.
- Photochemical activation that directly forms free base chlorin but requires prolonged irradiations of dilute solutions.

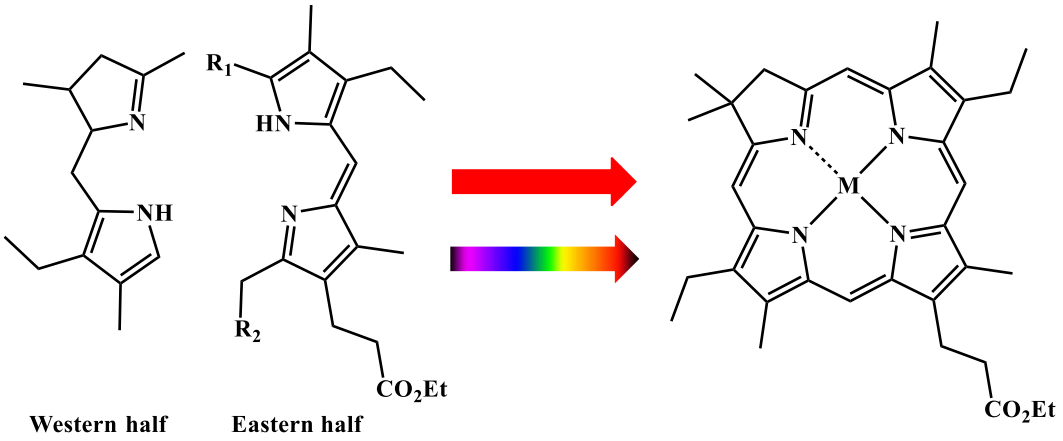

Figure 39: Battersby's routes to chlorins.

2.2.3. Synthesis *via* natural compound extraction

Chlorins and bacteriochlorins are naturally present in Nature, the best example being chlorophyll. As porphyrins is possibly obtained from animal pigments (see section I.2.1.1), chlorins can be extracted from vegetal pigments. For example, one of the most interesting molecules is purpurin-18, which is a chlorophyll-like derivative and could be used as starting material to obtain several original chlorins. A simple synthetic route for this molecule with quantitative yield (> 99 %) was described by Drogat *et al.* (Figure 40).[108]

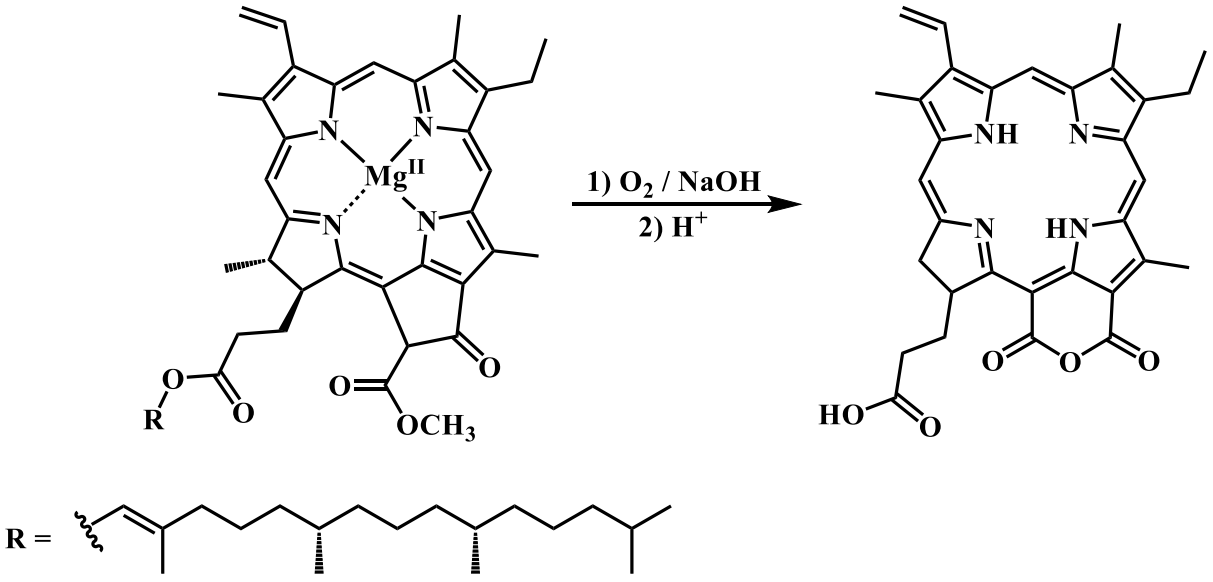

Figure 40: Purpurin-18 synthesis from chlorophyll-a.

The first step consists in extracting pigments from the *Spirulina maxima* alga, which exhibits the highest chlorophyll content. In a second step, the isolated pigments are oxidized by oxygen in basic conditions (NaOH), which give a mixture of unstable chlorins. Finally, an acidic treatment gives purpurin-18 simply by protonation of carboxylic acid functions. This protocol was also used to obtain bacteriopurpurin-18 from bacteriochlorophyll-a (as extracted from *Rhodobacter sphaeroides*, aquatic photosynthetic bacteria).[109]

2.3. Phthalocyanins

The first discovery of phthalocyanines was accidental. In 1907, Braun and Tcherniac observed the formation of a blue impurity when refluxing *o*-cyanobenzamide in ethanol that was made to obtain phthalonitriles; the phthalocyanine named H_2Pc was obtained (Figure 41).[30] Later in 1927, Diesbach and Von der Weid synthesized copper phthalocyanine (23 % yield), copper naphthalocyanine, and copper octamethylphthalocyanine in an attempted conversion of *o*-dibromobenzene into phthalonitriles.[31] Phthalocyanine structure discovery was only made later in the 1930s by Linstead *et al.*, who had later developed several metallated phthalocyanine synthesis processes.[110] Since then, as for porphyrins or chlorins, numerous methods were developed to obtain phthalocyanins (Pc). A large part of them consists to the tetramerization of small molecules.

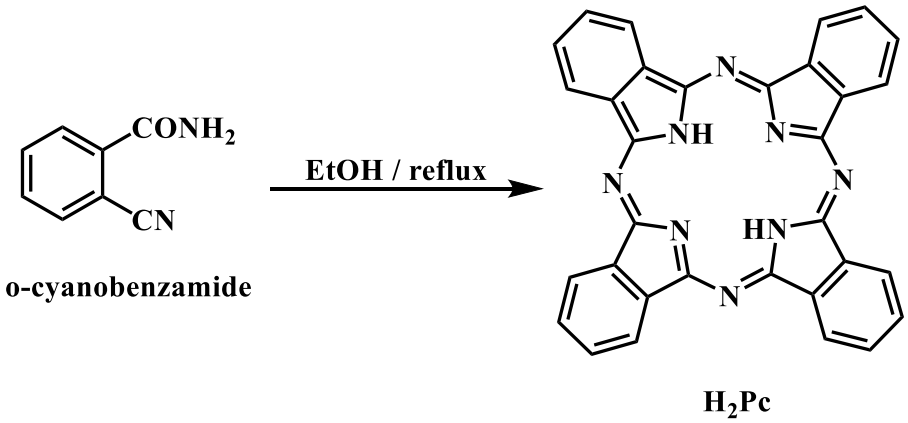

Figure 41: H_2Pc synthesis.

2.3.1. Synthesis *via* a single precursor (tetramerization)

In this case, small molecules like *ortho*-substituted benzene (*e.g. o*-dibromobenzene, *o*-cyanobenzamide….),[111] phthalonitriles, phthalic anhydride or acid, but also phthalimides derivatives are used as precursors (Figure 42). Indeed, all these compounds present some

advantages: they allow achieving good yields for metallated phthalocyanines (except for mercury and silver) and they are popular in academic synthesis.

For all such compounds, operating conditions require reflux and metal template (except for phthalimides for which metal are used but is not mandatory).[112,113] In case of phthalonitriles, the usual conditions are heating at reflux in the presence of a metal template and also an alkoxide lithium to activate reagents in quinoline or N,N-dimethylaminoethanol (DMAE) as solvent.[113, 114] Phthalic anhydrides are used in industrial processes because they are cheap and requires to use molybdenum salt as catalyst and urea, at reflux.[115]

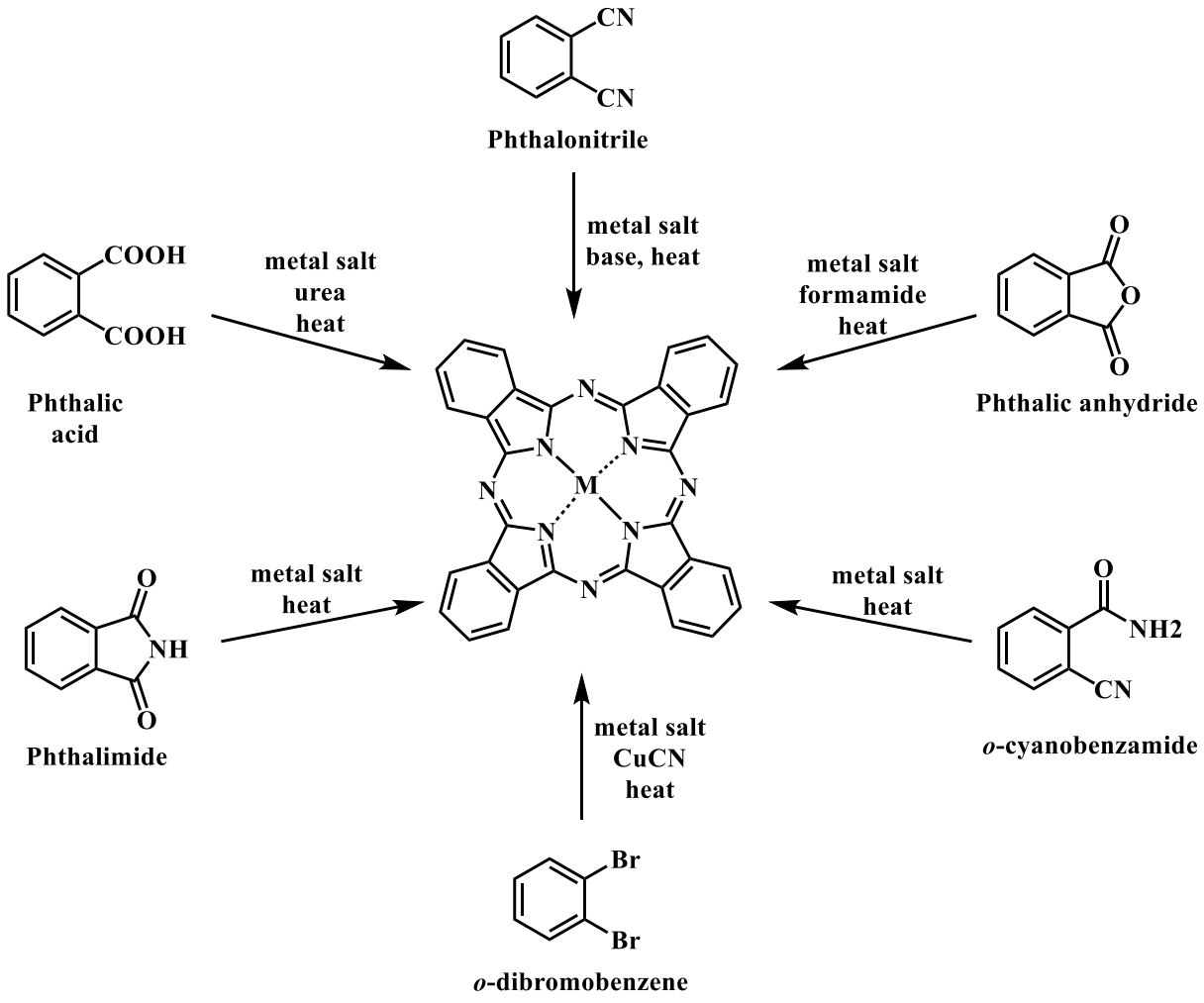

Figure 42: Synthetic routes to metallophthalocyanines via tetramerization of various precursors.

2.3.2. Tetramerization of two (or more) precursors

To obtain asymmetric phthalocyanines, the most common way is condensation of two different phthalonitriles, diiminoisoindoles, or related derivatives, which yield a statistical mixture of six compounds. Isolation of the desired product is often laborious due to difficulties in separation of such similar species. Another approach has been widely used: supported solid phase synthesis. Leznoff *et al.*,[116] used a diiminoisoindoline resin (phthalimide like) with 24 % yield, while Wöhrle *et al.* in 1986[117] used a resin of divynilbenzene-styren. More recently, Erdem *et al.* have developed a new method using PEG-based resin, which enable quick and easy synthesis of a variety of asymmetrical phthalocyanines that do not require intensive purification steps (Figure 43).[118]

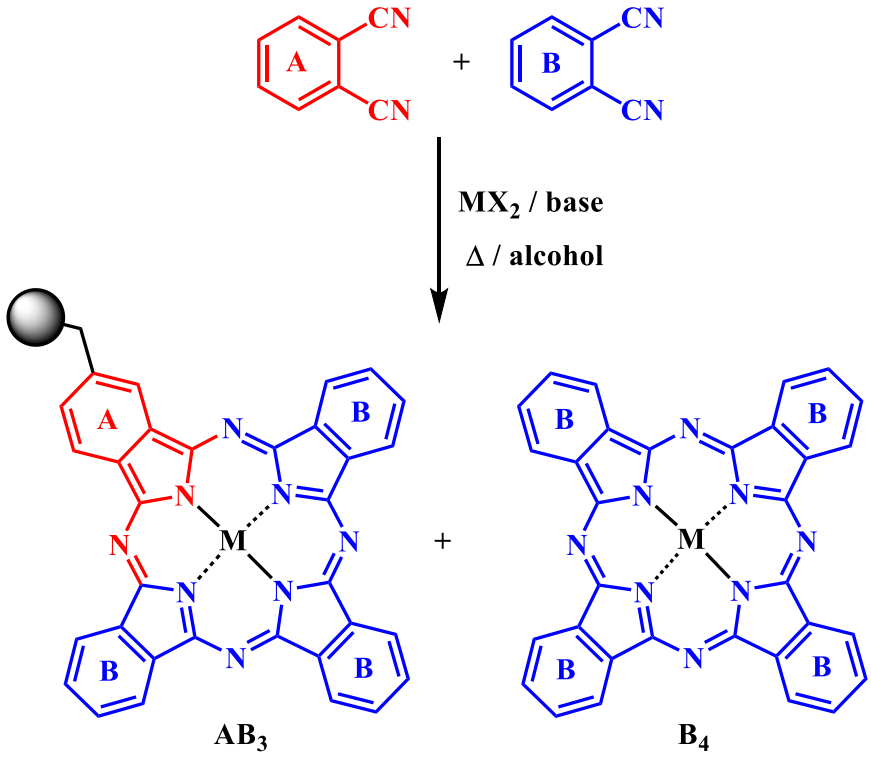

Figure 43: Synthesis of AB_3 compounds according to Erdem protocol. M = H_2 / Cu / Ni / Zn.

Phthalocyanines are poorly soluble in common organic solvents such as ethanol or dichloromethane and particularly in water. In the latter case, some strategies were developed to avoid this drawback, which have led to new hydrophilic derivatives.[119–121]

3. Photophysical properties

Porphyrins are colored compounds, which is attributed to their extended π-conjugation. These molecules (and its derivatives) exhibit various other interesting photophysical characteristics.[122] The photosensitive properties explain their use in various applications. This section details their absorption properties and processes that can occur in excited states of porphyrins.

3.1. UV-Vis absorption properties

The classical absorption spectrum of porphyrins can be described as follows in the following way:

- A intense absorption band between 400 and 430 nm ($\varepsilon \approx 250\text{-}300.10^3$ L.mol^{-1}.cm^{-1}), which is named B band or most commonly Soret band. This band is narrower when purity increases, for unprotonated forms and when aggregations do not occur. The Soret band results from a $\pi \rightarrow \pi^*$ electronic transition from ground state to a higher excited state.
- Four bands (IV, III, II and I) at wavelengths ranging from 480 to 700 nm ($\varepsilon \approx 1\text{-}20.10^3$ L.mol^{-1}.cm^{-1}), which are named Q bands. Their intensity is 10 to 20 times lower than the Soret band. These absorptions result from a weak $\pi \rightarrow \pi^*$ electronic transition, leading the compound from its ground state to the first excited state ($S_0 \rightarrow S_1$).[123,124] Depending on the substituents, Q bands profile can take 4 forms that are described according to their relative intensities:[125]

IV > III > II > I ➔ the spectrum is said *etio-type* and porphyrins are called *etioporphyrins*. Six or more β-positions bear saturated groups (*e.g.* alkyl groups).
III > IV > II > I ➔ *rhodo-type* (*rhodoporphyrin*). Substituents with π-electrons (*e.g.* carbonyl or vinyl groups) are attached directly to β-positions.
III > II > IV > I ➔ *oxo-rhodo-type* (*oxo-rhodoporphyrin*). Substituents are the same than in *rhodo-type*, but they are on opposite pyrrole units.
IV > II > III > I ➔ *phyllo-type* (*phylloporphyrin*). Substituents are positioned on *meso*-position.

Reducing the macrocycle leads to significant changes in the absorption features of the molecule. Indeed, for the chlorins, the Q_I absorption band is red-shifted at *ca*. 650 nm and it is 10 times more intense than for porphyrins. In case of bacteriochlorins, the Q_I absorption band is also 10 times more intense but red-shifted at *ca*. 760-800 nm. Concerning the Soret band, its intensity is decreased and it is blue-shifted upon first reduction (chlorins) whereas its full width

at high maximum (fwhm) increases. After second reduction step (bacteriochlorins), the Soret band is even more shifted in the UV area, around 350 nm.[126]

Phthalocyanines, being colored from blue to green, have the Soret band in the UV range in between 300 and 400 nm, and it is less intensive than in porphyrins. Conversely, their Q bands exhibit a intense absorption in the red (*ca.* 650 nm) because of their more extended π-conjugation system (Figure 44).

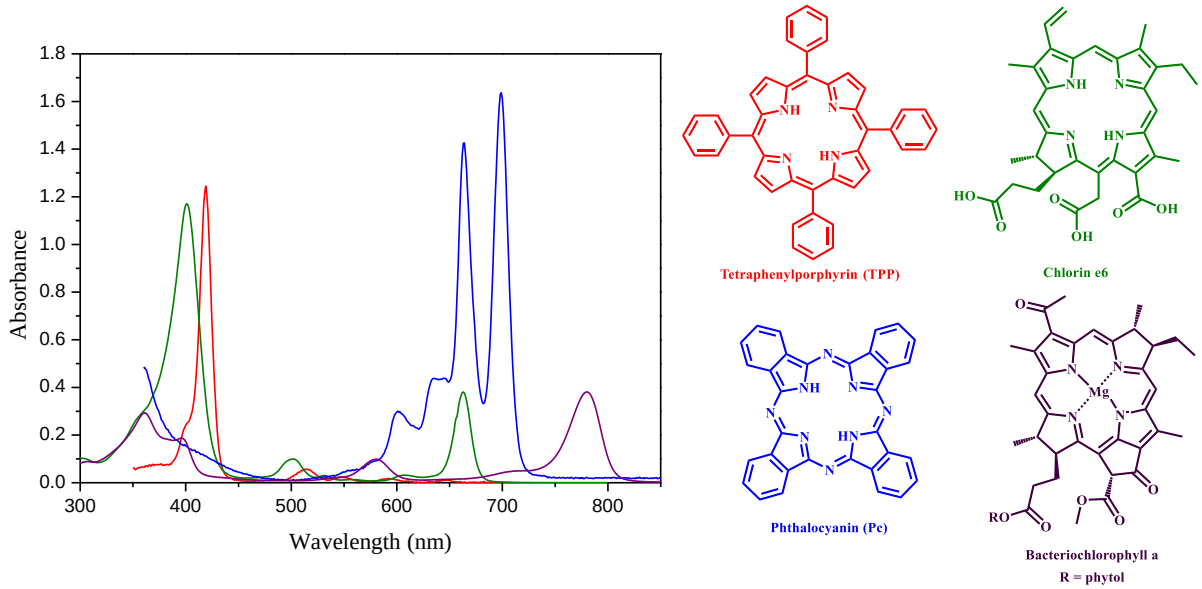

Figure 44: Absorption spectra of tetrapyrrolic molecules. TPP (in toluene), Chlorin e6 (in ethanol), Phthalocyanine (in chloronaphtalene) and Bacteriochlorophyll a (in toluene).

Source: PhotochemCad 2.1.

Upon metallation, the four Q bands characteristic of free-base vanish but are replaced by two bands (α and β) (Figure 45), being also Q bands. This phenomena is due to the fact that metalloporphyrins are more symmetric than free-bases, thus the involved orbitals are fully degenerated. In free-bases, a slight break of degeneracy explains occurrence of 4 Q bands instead of 2.[123,124] Moreover, it can also exist an orbital overlap between transition metal d_π (d_{xy} and d_{yz}) orbitals and the π* orbital of the porphyrin core. Then, a distinction must be made, depending on the metal electronic structure between *regular* metalloporphyrins containing closed-shell metal ion (d^0 or d^{10}, *e.g* cadmium, mercury or zinc…) and *hypso*porphyrins containing d^6 to d^9 metals (*e.g* iron, nickel, gold, cobalt, copper… from groups VIII to IB) where the d_π orbitals are filled (Figure 46).[127] These latter can interact with empty π* orbitals centered on porphyrin's core. By the way, metal orbitals (d_π) are stabilized and the π-π^* energy gap is higher, resulting in a hypsochromic shift of the whole spectrum. In the case of *regular* metalloporphyrins, the low energy metal orbitals have only little effect on the porphyrin π-π*

energy gap and the possible transitions are confined to the delocalised π-system of the core porphyrin ring.[128] For metals with partially occupied d_π orbitals (d^1-d^5, *e.g.* manganese, titanium, chromium…), the resulting (d-type) *hyper* spectra show additional bands in the UV region. These are due to the possibility of a charge transfer from the filled porphyrins π-orbitals to the empty metal's d-orbital.

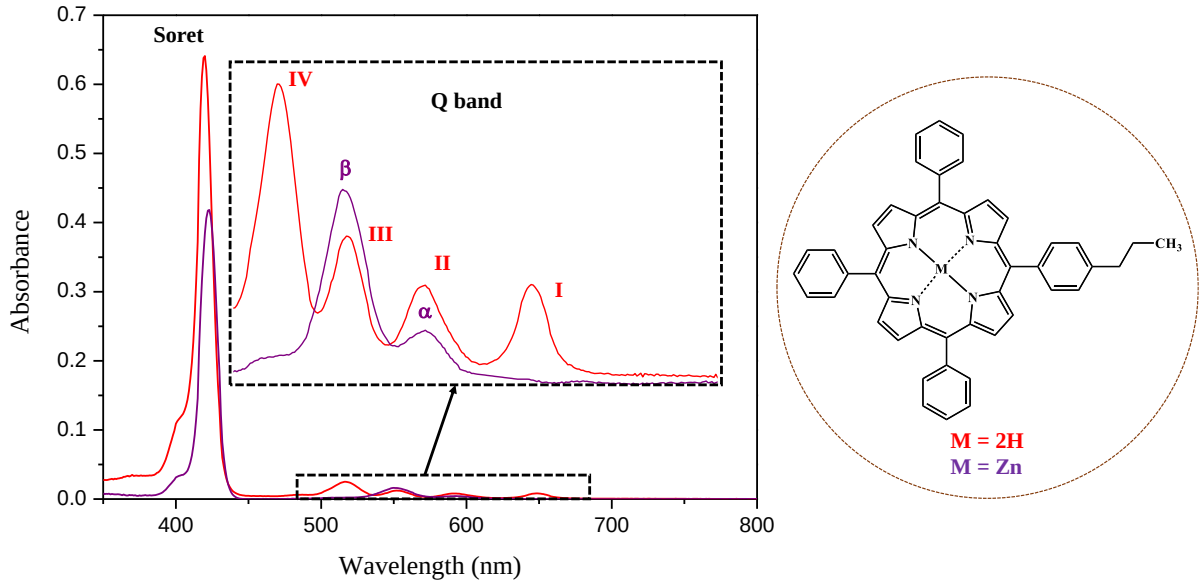

Figure 45: Absorption spectra of porphyrin free base (red) and metallated (purple) in chloroform. Compounds synthesized in our laboratory.

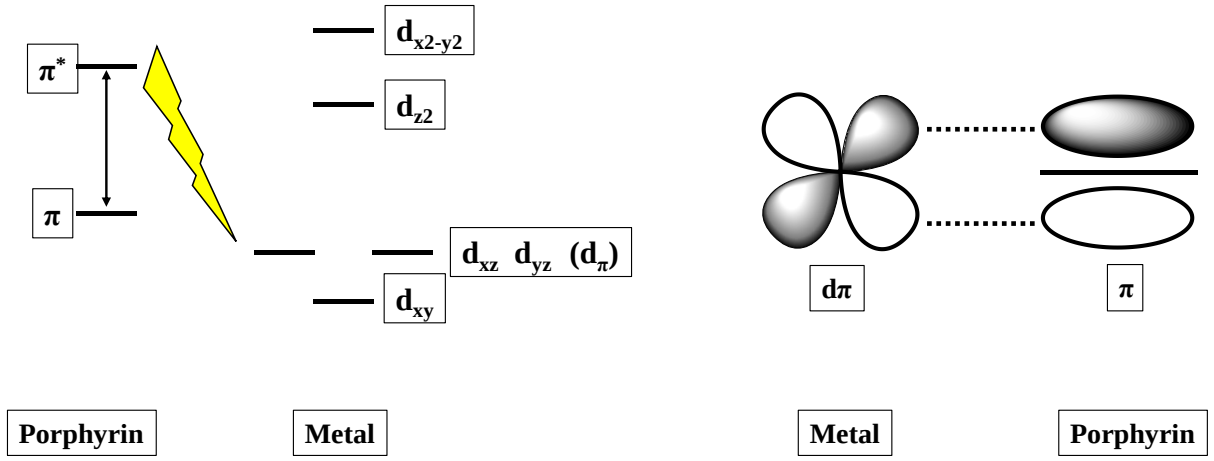

Figure 46: On the left, simplified molecular orbital diagram according to Marsh and Mink. Interaction between metal d_π and π^* porphyrin orbitals (*hypso*porphyrins). On the right, overlap between d_π metal orbital and π system of the porphyrin ring.

3.2. De-excitation to ground state: underlying mechanisms

3.2.1. Background

As it was said above, porphyrins and derivatives are a class of photosensitive molecules, so-called photosensitizer (PS). The following section deals with photophysical and photochemical mechanisms that can occur during relaxation phenomenon. All these processes are summarized in the Perrin-Jablonski diagram (Figure 47). [129]

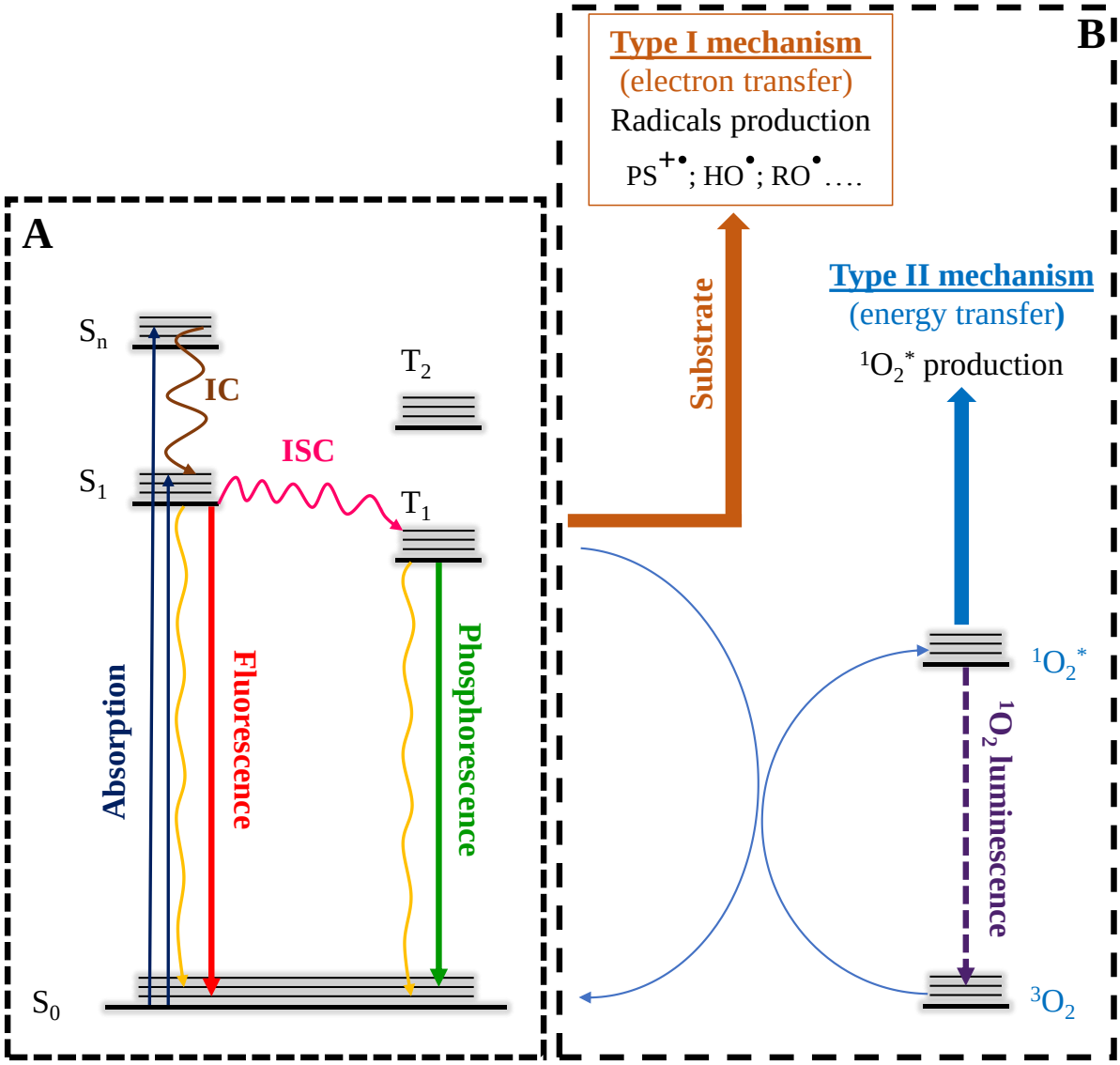

Figure 47: On the left, simplified Perrin-Jablonski diagram of processes in photosensitive molecules (**A**). On the right, interaction with surrounding environment (**B**).

In the ground state (S_0), most of PS are in singlet state, characterized by paired electrons, a total spin S of 0 and a spin multiplicity (2S+1) of 1. Upon light excitation, one-photon absorptions populate excited states S_x (x=1, 2, 3…) in agreement with the selection rules in

particular without changing spin state and according to the energy absorbed. In a simple molecular orbital picture, excitations can be described by promotion of electrons to upper molecular orbitals ($\pi \rightarrow \pi^*$ electronic transitions). After excitation (10^{-13} to 10^{-10} second), the excited PS (PS^*) then has to return back to the ground states *via* excited states of lower energy. This is likely to occur by internal conversions (IC) and vibrational relaxation (VR) through the first excited state. The de-excitation to the ground state then occurs by two different pathways, either non-radiative (heat emission, conformational change...) or radiative (fluorescence emission). Another process can compete, namely triplet excited state (T_1) formation by intersystem crossing (ISC). This process involves spin inversion, which is formally forbidden by selection rules.[130] $^3PS^*$ can relax trough the ground state again by non-radiative and/or radiative (phosphorescence) processes. In this case, the radiative process is a forbidden $T_1 \rightarrow S_0$ transition, which results in longer lifetimes for the triplet (≈ µs to ms) than for the singlet (≈ ns) excited state. Consequently, interactions of triplet excited states ($^3PS^*$) are likely with environment, in particular with surrounding molecular oxygen to produce reactive oxygen species (ROS).

To sum up for the case of porphyrin and derivatives, after light excitation, de-excitation is likely to follow three possible processes:

i) non-radiative de-excitation, without spin change

ii) fluorescence emission

iii)ISC and thus transfer to triplet excited state. Usually the de-excitation then occurs through non-radiative pathways (vibrational relaxation or specific interactions with environment, these latter involving photochemical reactions and opening the way for biological applications).

3.2.2. Fluorescence emission

Porphyrins can have a dual emission. Indeed, in few cases,[131] after excitation of Soret Band, an emission centered at 400-500 nm can be observed. It corresponds to the $S_2 \rightarrow S_0$ transition and thus does not respect the Kasha rule. Indeed according to this rule, emission comes from the lower excited state, namely S_1.[132] However, usually observed fluorescence emission ($S_1 \rightarrow S_0$) is centered between 550 and 800 nm (Figure 48), depending on macrocycle substituents, solvents, and metals (the nature of metal being important).[133] Free-base emission exhibits a vibrational structure with two bands, while metallated derivatives have only one band.

In the case of chlorins, bacteriochlorins and phthalocyanines, fluorescence emission is also observed in the same wavelength range (Figure 48), but the second fluorescence band (if any) is weaker than in case of porphyrins. As for porphyrins, the emission characteristics (intensity and wavelength) depend on functionalization.[134–136] For all these compounds, photophysical investigations can be difficult (and sometimes impossible) due 1) to low stability of chlorines and bacteriochlorins, which can oxidize by air into porphyrins; 2) strong affinity of phthalocyanines to form aggregates in common solvents, particularly for metallated ones;[137,138] and 3) more generally due to their low solubility.

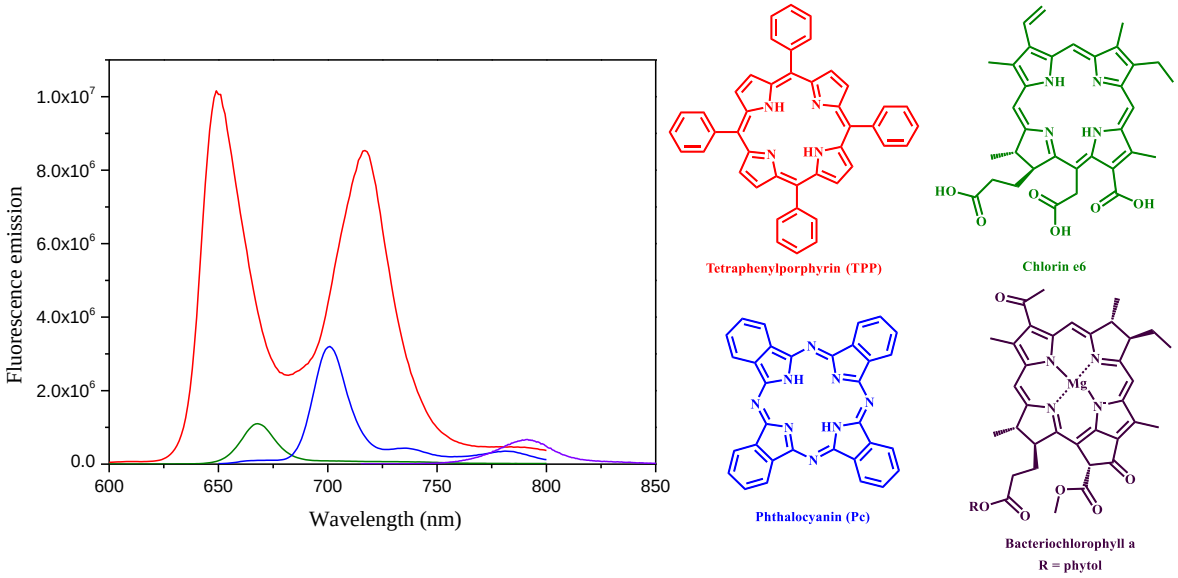

Figure 48: Fluorescence emission spectra of tetrapyrrolic molecules. TPP (in toluene), Chlorin e6 (in ethanol), Phthalocyanine (in chloronaphtalene) and Bacteriochlorophyll a (in toluene). **Source:** PhotochemCad 2.1.

The efficiency of radiative mechanism can be evaluated by the fluorescence quantum yield Φ (Equation 1),[139] defined as the ratio of the number of emitted photons over the number of absorbed photons:[133]

$$\Phi = \frac{\text{Number of emitted photons}}{\text{Number of absorbed photons}}$$

Equation 1: Fluorescence quantum yield formula.

Φ depends on various factors including temperature, pH, capacity to form aggregates and metalation.

Most of porphyrins and derivatives exhibit very poor quantum yields (usually lower than 0.2), mainly in metalloporphyrins.[140–142] This can be explained by the existence of other

non-radiative de-excitation pathways, especially the transfer towards triplet state thanks to ISC which can be very important (see next section I.3.2.3).

In case of chlorins and bacteriochlorins, fluorescence quantum yields are higher than 0.2 for chlorins,[143] and between 0.2 and 0.4 for bacteriochlorins.[144]

Finally, for phthalocyanines, as described above, fluorescence emission and so fluorescence quantum yields are extremely dependent on solvent nature, pH and concentration. This is the reason why in this case quantum yields can range from 0.1 to 0.7, for a wide range of metallated compounds.[145]

3.2.3. Intersystem crossing and ROS production

Another crucial de-excitation process from excited porphyrins is, as outlined before, intersystem crossing. Indeed, according to molecular structure, this process can be predominant. For example, in the case of tetra-phenylporphyrin, in DMF, Φ_{ISC} equals 0.72.[146] Thus as said in paragraph I.3.2, interactions with surrounding molecular oxygen or substrates are then likely leading to reactive oxygen species (ROS) production following two possible mechanisms, namely type I (based on electron transfer and formation of radical species, such as superoxide anion $O_2^{\bullet -}$) and type II (based on energy transfer; leading to formation of singlet oxygen $^1O_2^*$). Here, these mechanisms and properties of major produced ROS are described, the resulting applications will be developed in paragraph 4. ROS being highly toxic, their production can indeed be responsible for several oxidative damages on number of biomolecules (lipids, steroids, enzymes or nucleic acids).

3.2.3.1. Type I mechanism

As said above, de-excitation from the triplet excited state can lead to some photochemical reactions. The first type is named Type I, which results in the formation of free radicals due to electron transfer from the $^3PS^*$ to biological substrates (Equation 2).[147]

$$^3PS^* + Substrate \rightarrow PS^{\bullet -} + Substrate^{\bullet +}$$

$$^3PS^* + Substrate \rightarrow PS^{\bullet +} + Substrate^{\bullet -}$$

$$PS^{\bullet -} + {}^3O_2 \rightarrow {}^1PS + O_2^{\bullet -}$$

Equation 2: Primary photochemical reactions of photosensitive compounds.

As described in Equation 2, at triplet state the photosensitizer first react with substrate by oxidative or reductive electron transfer. Then the subsequent radical anion can interact with molecular oxygen producing superoxide anion that can in turn abstract a proton from any surrounding molecule to form hydroperoxyl radical (Equation 3, 1) and leads to hydrogen peroxide production (Equation 3, 2). Finally, hydrogen peroxide can react with superoxide anion according to the Haber-Weiss reaction to form two new ROS, hydroxide anion and hydroxide radical (Equation 3, 3).[148]

$$O_2^{\bullet -} + H^+ \leftrightarrows HOO^{\bullet} \quad (1)$$

$$2\,HOO^{\bullet} \rightarrow H_2O_2 + O_2 \quad (2)$$

$$O_2^{\bullet -} + H_2O_2 \rightarrow O_2 + OH^- + OH^{\bullet} \quad (3)$$

Equation 3: Primary photochemical reactions of oxygen.

All these species have in common high reactivity and are very powerful oxidant to biomolecules including DNA, lipids or amino acid side chains (tryptophan, histidine, methionine)[149] or even other radicals.[150]

3.2.3.2. Type II mechanism

Type II photochemical reactions consist in a triplet-triplet energy transfer from $^3PS^*$ to molecular oxygen in its ground state, that is in triplet state. To make feasible this process, the energy gap between T_1 and S_0 of PS must be larger than the difference in energy between $^3O_2$ (T_0, ground state) and $^1O_2{}^*$ (S_1, first excited state) *i.e.,* 94 kJ.mol^{-1}.[151,152] This energy transfer leads to the formation of singlet oxygen $^1O_2{}^*$ and de-excitation of PS to its ground state (Equation 4).[147]

$$^3PS^* + {}^3O_2 \rightarrow {}^1PS + {}^1O_2{}^*$$

Equation 4: Energy transfer reaction with molecular oxygen.

As for fluorescence, the production of singlet oxygen is given by a quantum yield Φ_Δ (Equation 5):

$$\Phi_\Delta = \frac{\text{Quantity of produced singlet oxygen}}{\text{Quantity of absorbed photons}}$$

Equation 5: Singlet oxygen production yield formula.

3.2.3.3. ROS production of tetrapyrrolic macrocycles

Some relationship can be evidenced between the efficacy of ROS production and fluorescence quantum yield. Both properties depend on similar parameters, for example, presence of metal (*e.g.*, copper, zinc, magnesium…) temperature, pH, solvents or aggregate formation.

In porphyrins and chlorins, ROS production strongly depend on macrocycle substitution or metallation.[153] For example, tetraphenylporphyrin (H_2TPP) which is the most common porphyrin, is very sensitive. In 1999, Figueiredo *et al.* obtained for H_2TPP Φ_Δ values of 0.11 and 0.073 in toluene and in acetone, respectively;[141] in 2002, De Rosa obtained Φ_Δ values ranging 0 to 0.88 for metallated derivatives in benzene, thus underlined metal influence. Indeed for Cu, Mg, Zn, Pd and Cd, the corresponding Φ_Δ were <0.06, 0.62, 0.83, 0.88 and 0, respectively.[151]

Phthalocyanines are very bad singlet oxygen producers due to their propensity to aggregate in common solvents, which strongly decrease ROS production.[154] The most simple phthalocyanine structure (Pc) exhibits a Φ_Δ value of 0.16 for free base and 0 for metallated (with copper or cobalt) in methanol.

4. Applications

The purpose of this section is not a comprehensive list of applications, is not adapted to this manuscript, but simply to stress importance of these molecules in everyday life.

Nature has developed complex molecular systems, porphyrins, chlorins and bacteriochlorins being perfect example of this fact as being constituents of some proteins involved in vital oxidation and transportation processes. The iron porphyrin, called *heme* (Figure 4A), allows human (and animals) life as being such a constituent of hemoglobin and myoglobin (Figure 49). These two proteins are required to transport oxygen in the blood,[155] but they are also involved in nitric oxide degradation (oxidizing molecule due to the respiratory process). *Heme* is also a subunit of catalase and peroxidase enzymes, which are capable of elimination of toxic compounds like peroxides (*e.g.* hydrogen peroxide dismutation into water and oxygen). These reactions are essential to the correct functioning of the respiratory system.[156] *Heme*-carrying proteins were also postulated to have been present in the last common ancestor of Bacteria and Archaea.[157]

Still in animal organisms, vitamin B12 (Figure 4B), tryptophan-2,3-dioxygenase and cytochrome P450 family are linked to porphyrins. The first is necessary to the brain activity and human cell metabolism; the second is an enzyme that contains *heme* as a co-factor and is involved in the oxidation process of tryptophan catabolism (which is crucial because it can lead to some neurological disorders or suppression of T-cells proliferation);[158,159] cytochrome P450 family are enzymes involved in redox reactions of various compounds including xenobiotics and metabolites . The most common reaction catalyzed by these enzymes consists on addition of an oxygen atom on organic substrate to obtain alcohol function.[160]

In plants and bacteria, chlorins and bacteriochlorins are involved in photosynthesis. Indeed, chlorophylls (a and b) are chlorins containing a magnesium ion, which give the green color to plants (Figure 4B). Due to their high aromaticity, they can play the role of sunlight energy antenna in photosynthesis (see section II.2.3.1).[4]

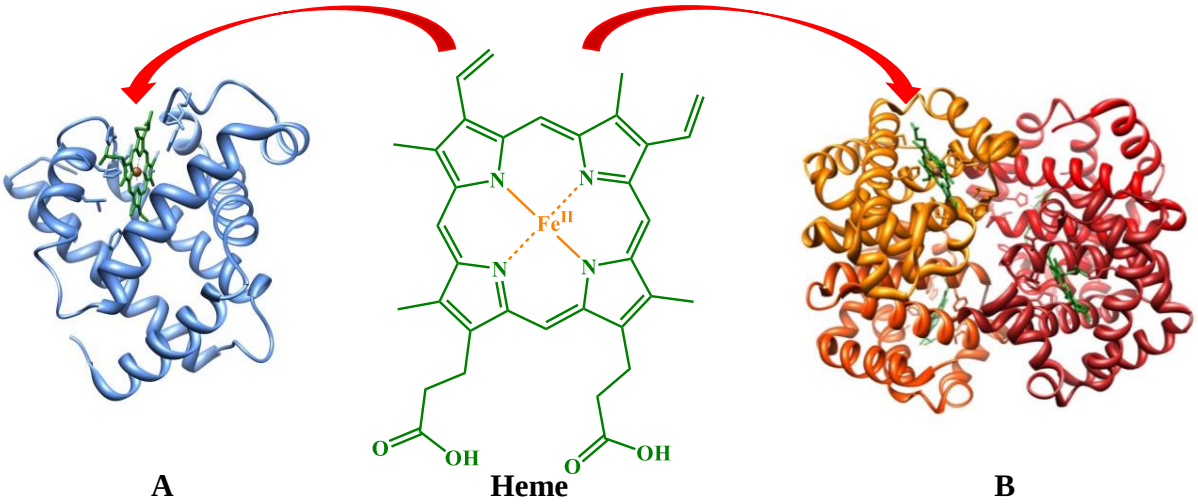

Figure 49: Structure of myoglobin (A) and hemoglobin (B).

From observations of these natural phenomena and as outlined in introduction, tetrapyrrolic macrocycles have attracted much interest over the last century. Thanks to recent progress in synthesis (see section I.2), a wide range of artificial compounds has been created in response to the needs of the most common applications that can be classified as a "Big 5": energetic, technologic, industrial, therapeutic and finally environmental issues.

4.1. Energetic applications

The limited fossil resources (*e.g.*, oil and gas), their related pollution (*e.g.*, coal), and the dramatic increase in energetic needs would sooner or later lead to severe energy crisis if no other technologies are developed and massively used. Although nuclear power is an alternative, the inherent risk of nuclear disasters (*e.g.* Tchernobyl or Fukushima) and recycling/storage of radioactive nuclear waste are major drawbacks, which require finding other alternatives.[161] In this context tetrapyrrolic macrocycles could be used in various other energetic solutions.

- Solar cells[162]

Renewable energy is a viable alternative, especially solar energy. Currently, commercial solar panels are only based on silicon (amorphous or crystalline) with yields ranging from 7 to 14%.[163,164] However, the real challenge is to reduce significantly the cost of produced kilowatt/hour. Silicon offers the best yield but its purification and treatment lead to very high costs, keeping in mind that very toxic manufacturing processes are used. Recycling silicon-based solar cells is also a major drawback.

Because of their capacity to absorb sunlight, porphyrins or phthalocyanines can efficiently be used as dyes in dye-sensitized solar cells. (Figure 50). For example, in 2010, 11% power conversion efficiency was reported for such a device based on porphyrinic dye.[165] Since then, several improvements were performed, for example in association with TiO_2 nanoparticles for specific solar cell applications,[166–168] and it leads to a new record in 2014 with a metalloporphyrin (Zn) that provided a 13 % yield.[169] This makes this class of compounds promoising as being as efficient as the more commonly used ruthenium bipyridyl derivatives (around 15 % power conversion), [170,171] and by extension for commercial use.

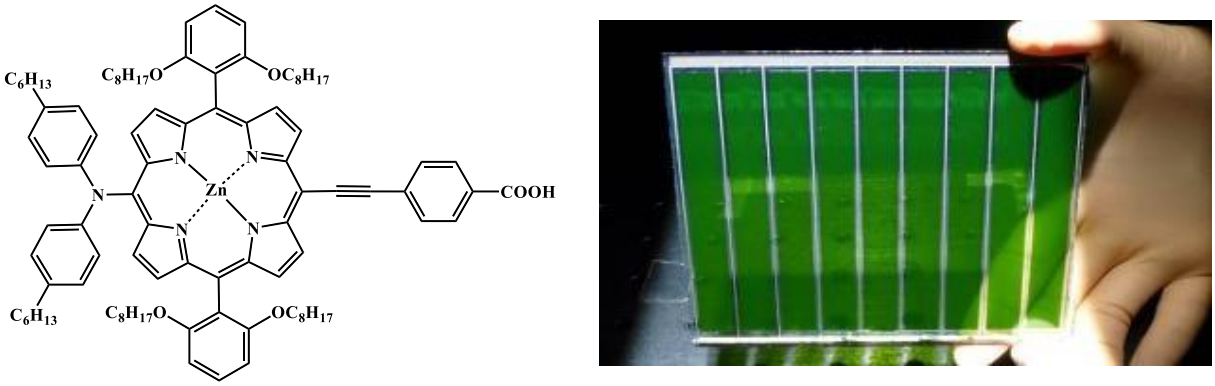

Figure 50: Solar cells containing zinc-porphyrin (12.3 % energy conversion).

Sources: A) chem.fsu.edu and B) *Science* **2011**, *334* (6056), 629–634.

Moreover, because of their electrochemical properties, tetrapyrolic macrocycle, especially phthalocyanines, are also used in association with electron acceptors (*e.g.* quinones or fullerenes…) to generate charge after light absorption process that can used in organic photovoltaic devices or OPVs (see for more details on electron transfer processes, section tagged porphyrins).[172,173]

➢ Artificial photosynthesis

The greatest source of inspiration for human resided in Nature. Complexity and efficiency of natural structures have always fascinated scientists, who systematically try to mimics them. Photosynthesis is the most efficient process of solar energy conversion to date and developing artificial photosynthesis has attracted much interest.[174–178] The key component in photosynthesis is an antenna, which trap and convert solar energy. In nature, this role is played by chlorophyll that can be replaced by synthetic tetrapyrrolic macrocycles.

As outlined in Figure 51, such green processes can be used for hydrogen production from water and thus leads to other applications (*e.g.* fuel cell).[179]

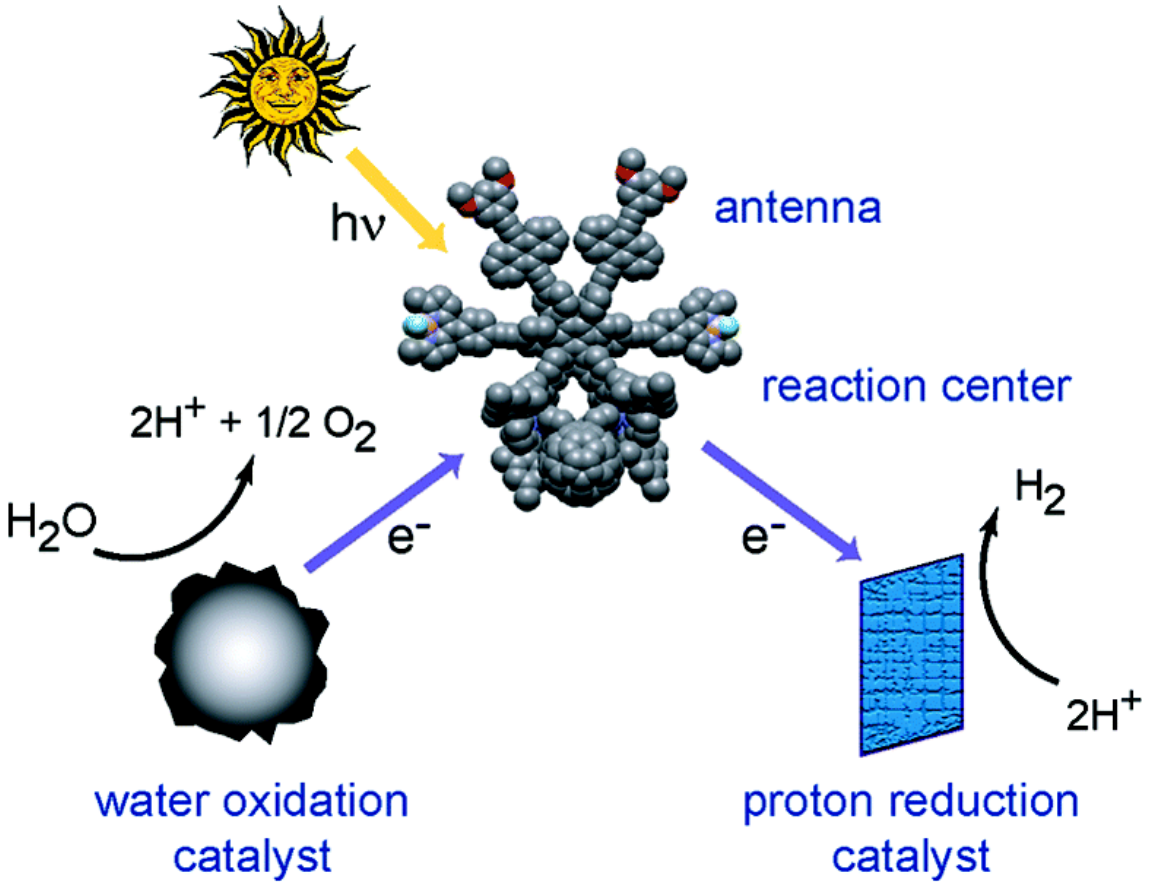

Figure 51: Simply artificial photosynthesis scheme. This green process product hydrogen from water. **Source:** *Acc. Chem. Res.* **2009**, *42* (12), 1890–1898.

4.2. Organic electronic devices

Electron transfer is likely to be obtained in organic electronics.[180,181] This is a new and fast developing sector of microelectronics which aims, as photovoltaics, either to cover applications that are not reproducible with conventional silicon semiconductor technology or to decrease the cost of devices using organic materials. It is based on small molecules and polymers, which have in common to exhibit conductivity properties and flexibility. Small molecules are usually used in construction of organic semiconductors (which exhibit degrees of electrical conductivity between those of insulators and metals); while polymers are used as transistors (or in solar cells). The research is focused on three axes: charge transport with organic field-effect transistors[182,183] (OFETs); electric to photon energy conversion with light-emitting diodes[184,185] (OLEDs); and light to electric energy conversion with organic solar cells (or OPV, described in section I.4.1). In this domain phthalocyanines[186,187] and porphyrins have been extensively studied, as dimers or coupled with other molecules as fullerenes.

Electronic devices based on organic compounds are nowadays widely used, with many new products under development e.g., flexible electronic paper (e-paper) or memory devices; chemical sensors (blood, vapors…); radio-frequency tags (locks, bank cards…). (Figure 52). More recently, Sony or Samsung have developed and marketed flexible OLED television.

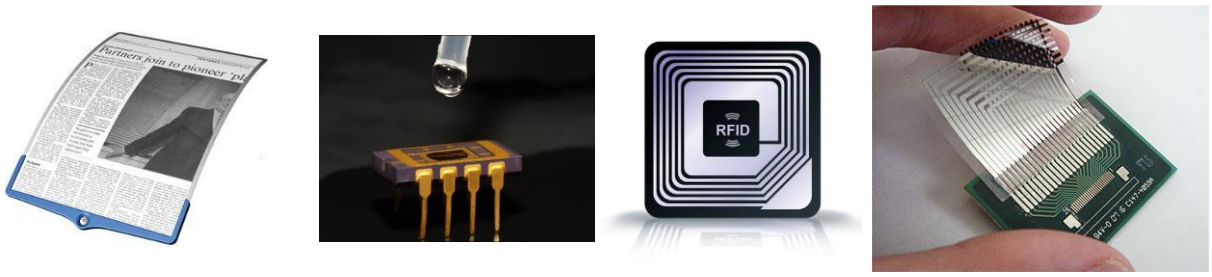

A **B** **C** **D**

Figure 52: Some examples of organic electronics. From left to right: A e-paper, B chemical sensor, C radio-frequency tags and D memory device**. Sources:** tu-dresden.de; research.ibm.com and rcs.org.

4.3. Industrial

Due to their so specific properties, tetrapyrrolic macrocycles are used in addition to the aforementioned applications, in a wide range of other areas at an industrial scale, playing successively the role of catalyst, pigment, or even analytical systems.

➢ As catalyst

As cytochromes P450 in Nature that are capable of catalyzing numerous bioreactions, metalloporphyrins are a class of versatile catalysts[32] with the capacity to functionalize saturated and unsatured C–H bonds *via* several well-defined atom/group transfer processes. The corresponding hydroxylation, amination, and alkylation reactions provide direct approaches of catalytic conversion of abundant hydrocarbons into value-added functional molecules through C–O, C–N, and C–C bond formations, respectively.[17,188,189] In 2012, Elouarzaki *et al.* reported the use of a rhodium-metalloporphyrin for glucose oxidation, in fuel cell applications.[190] Likewise, since the first example of asymmetric oxidation by Groves and Myers in 1983,[191] several chiral metalloporphyrins have been developed for stereoselective catalytic conversion. In the same way, metallophthalocyanines exhibit some interesting catalytic properties. Oxidation reaction of methane, olefins, alcohols or sulfur compounds or C-C bond formation are a few part of their potential.[192] In wood industry, phthalocyanines are also used to catalyze oxidation reaction implied in the bleaching process of wood pulp, this method being less toxic than chlorine oxidation or reaction with hydrogen peroxide.[193] As this process is carried out in order to decrease color of various types of pulp, it is of upmost importance in industrial sectors such as paper mill.

➢ As pigment

In pigment as dyes industry, approximately 25% of all artificial organic pigments are phthalocyanine derivatives (Figure 53).[194] These molecules find extensive use in various areas of textile and spin dyeing in paper industry or in manufacture of high-speed CD-R media.[195,196] A second industrial application concerns LCD (Liquid Crystal-Display) technology. Indeed, phthalocyanines (and especially copper ones) are used as pigment (blue and green) for automotive paints and printing inks.[195,197,198]

➢ In analytical chemistry

Porphyrins and phthalocyanines have also application in analytical chemistry. Indeed, due to their capacity to accept metallic ions and also accepting ligands around them, they can be used for spectrophotometric determination of cation concentration, as membranes of Ion Selective Electrode (ISE) in potentiometry or voltammetry, as biosensors and as stationary phases in HPLC.[199,200] Moreover, recent works have showed that metalloporphyrins and derivatives are able to bind and stabilize G-quadruplex in DNA (structure involved in some biological processes), which make them new potential tools for DNA recognition.[201,202]

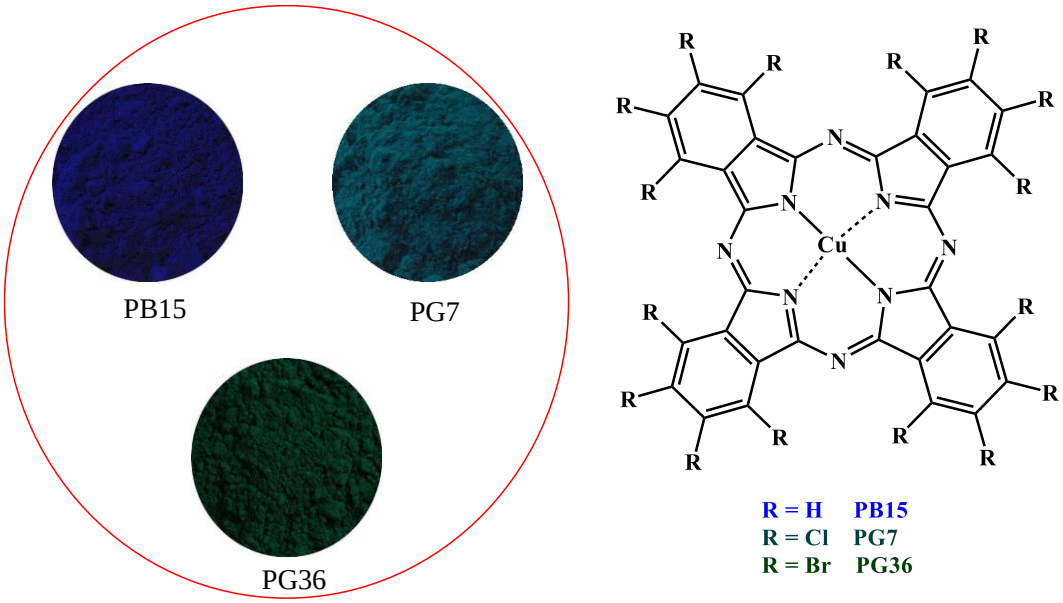

Figure 53: Some examples of phthalocyanines dyes used in industry.

4.4. Therapeutic and environmental issues

Based on their photophysical properties after photoexcitation, porphyrins, chlorins and phthalocyanines have potential applications in medical imaging and photomedicine (photosensitive drugs) (Figure 54).[203,204]

➢ Medical imaging

Porphyrins can be imaging probe as photo-acoustic (which couple spectroscopy accuracy with scan resolution)[205,206] or fluorescent imaging.[207] Due to their capacity to complex atom in their core, different applications are likely. For example, PET/CT (Positron Emission Tomography/Computed Tomography) which can depict the spatial distribution of metabolic or biochemical activity in the body,[208] by labeling tetrapyrrolic macrocycles with radionuclides as indium or technecium.[209] Also, when the metallic ion is manganese, new contrast agents for Molecular Magnetic Resonance Imaging were obtained.[210]

➢ Photosensitive drugs

Conversely to medical imaging application, the capacity of porphyrins to produce ROS is at stake in this case. Nature and effects of these compounds were described in section I.3.2.3. Depending on targets, the name given to this technique is different but the general principle remains the same: a nontoxic light-sensitive compound (like porphyrins, phthalocyanines or

chlorins) is introduced in a given environment; it inactive in the dark, and it produces ROS upon light exposure, possibly at a specific wavelength. The oxidant species created react and damage surrounded organic molecules.

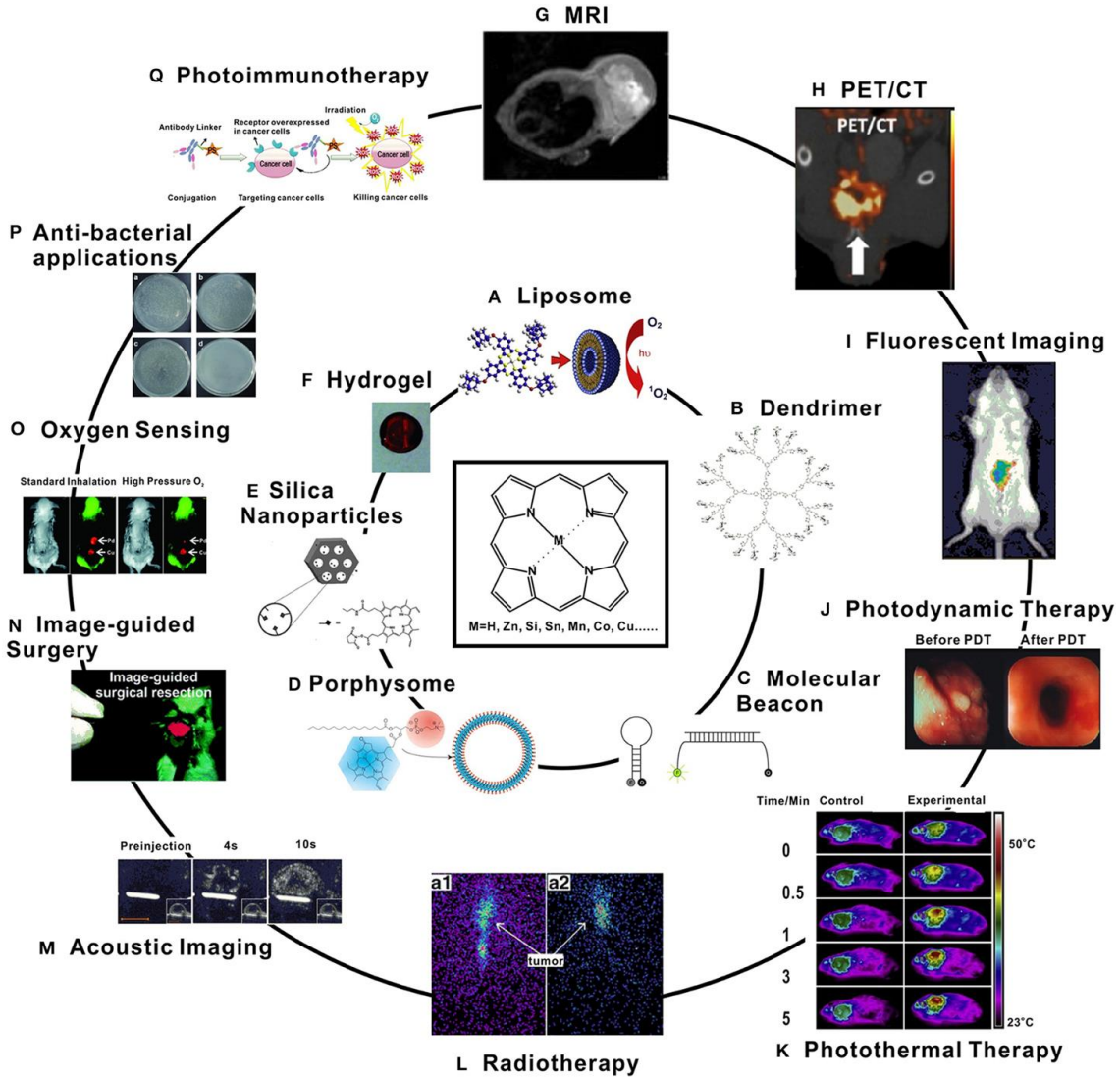

Figure 54: Examples of porphyrin-based biomaterials (inner circle) and applications (outer circle). **Source:** frontiersin.org.

Three applications have been developed and are already used. The first is in precancerous lesions and various cancers (superficial skin, esophageal and cell lung)[211] treatment as photodynamic therapy (or PDT). It consists in a non-invasive technique (contrary to surgery), which destroy malignant and other disease cells. It is also employed in dermatology against severe acne and macular degeneration.[16,212–218] Currently some commercial treatments based on porphyrin structure are used, like PhotofrinII® and Foscan®. Moreover, this procedure could be coupled with other treatments where porphyrins are also the active substance (but withouth light illumination) *e.g.*, radiotherapy[219,220] if porphyrin is coupled with radioactive metal or photothermal therapy.[221] Bacteria can be targeted as human cells, in Photodynamic

Antimicrobial Chemo-Therapy (PACT).[222–227] As PDT, the goal is to destroy planktonic bacteria or biofilm[228,229] as well as to prevent contamination, for example *via* direct application on materials (like medical equipment) in order to decrease the risk of diseases (*e.g*. nosocomial infections).[230–233]

Always based on ROS production, porphyrins were tested as phytosanitary products. They are capable of playing a role as photoactivable insecticide.[234,235] In 1995, Rebeiz *et al.* evidenced their efficiency against *Trichoplusiani* larvae, which is a devastating and invasive species.[236] More recently, Jori *et al.* performed several works against larvae or protozoa, which are pathogenic agents of dengue or malaria.[237–239] Porphyrins and phthalocyanins exhibit interesting insecticide capacities to kill mosquitos and other disease vectors. In other approach taking their natural presence in nature into account, these compounds are tested as potential photoactivable fungicides. In 1984 Rebeiz *et al.* presented the possibility to use porphyrin precursors.[240] Then, Carré in 1999 and Jori in 2004 exposed fungus to porphyrins and phthalocyanines, respectively.[241,242] A comparison with quantum dots were published in 2015 by Viana *et al.*, porphyrins exhibiting promising results contrary to quantum dots alone which have no effects (Figure 55).[243]

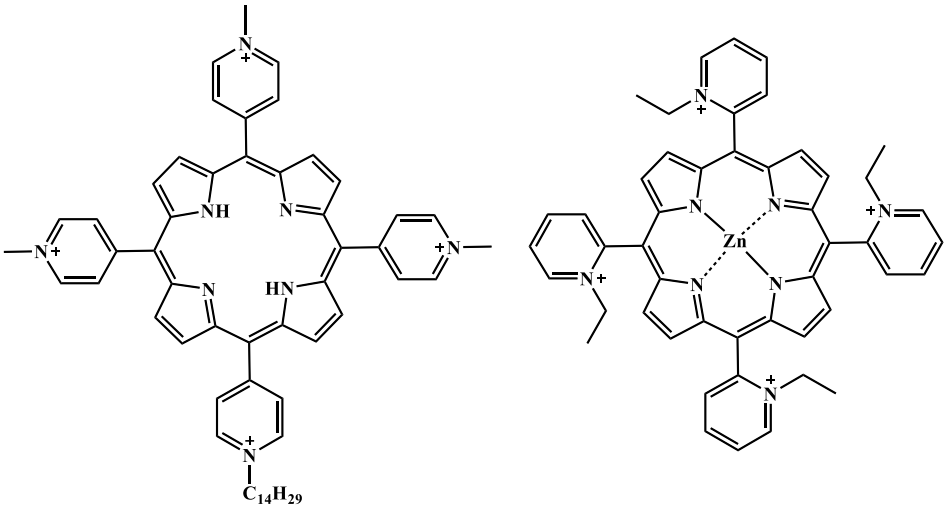

Figure 55: Porphyrins used by Jori as insecticide (**A**) and by Viana as fungicide (**B**).

Porphyrins and chlorins are naturally presents in Nature, and vital for the proper functioning of organisms (*e.g.* hormonal regulation, oxygen transport, photosynthesis...), which make them particularly attractive for development in environmental and therapeutic applications. However, in plants they are mainly used in biological processes through the porphyrin pathway (see II.2), but use as herbicide substances is to be evaluated

II. HERBICIDES

1. History and background

To tackle herbicides a proper definition is required. According to dictionary, an herbicide is a chemical substance of mineral or organic origin that is used to reduce or stop plant growth. An herbicide is said total if it destroys all kinds of plants, and it is said selective if only the undesired plants are targeted. Herbicides are a major class of pesticides, which include herbicides, insecticides, and fungicides. Herbicide chemistry is definitely intricate with agronomical issues. As an important parameter to consider is that herbicides are marketed and used by professionals (grain farmers, market gardeners) as well as by private individuals.

After a brief history aiming at better understanding the current situation the section details the different herbicidal ways of action as well as limitations and drawbacks. At the end of this section potential contributions of porphyrins to herbicides are discussed.

1.1. History

In the Middle Ages, ash and sea salt were used to control cultures, which is the first example of chemicals acting on plant growth reported so far.[244] The extension of herbicide usage has really started in Europe after the great famine in Ireland (1848-1850) caused by potato blight also called mildew, which had ravaged potato farms (potato being the main food source at this period). To fight against this scourge and prevent any other such disasters chemicals had been developed. The early 1880s was marked by the discovery of *Bordeaux mixture* by Gayon and Millardet, who were chemist and botanist, respectively.[245,246] It consists in copper salt and slaked lime, and it was first used as fungicide for vine plants. In 1896, observations were made that this mixture was allowing control of certain weeds, which led to the use of copper sulfate as a selective weed killer to control charlock (wild mustard) in cereals.[247] Later, during the First World War, because field weeding was still manual and men were away at war, sulfuric acid had been used to treat cereal crops (mainly barley, oats, wheat)[248] soon followed by solutions of iron sulfate, copper nitrate, and ammonium or potassium salts.[249] The first synthetic herbicides appeared in 1932,[250] namely 4,6-dinitro-*o*-cresol (DNOC) and other dinitrophenols (Figure 56). They had only been shown as killing living organisms unselectively.

During the Second World War, the developments on potential use of chemical agents as biological weapons gave way to a second breakthrough to herbicidal research.[251] In 1941, 2,4-D (2,4-dichlorophenoxyacetic acid) was discovered.[252] Due to its capacity to mimic plants'

hormones, it was quickly adopted to control broad-leaved weeds in corn, sorghum, small grains, and grass pastures, as well as in lawns and other ornamental turf.

Finally, during the 1950-1970 period, an important class of herbicides was developed that is still used nowadays, for example phenylureas, phenylcarbamates, triazines and glyphosate, best known as Roundup® (Figure 56).[253–257]

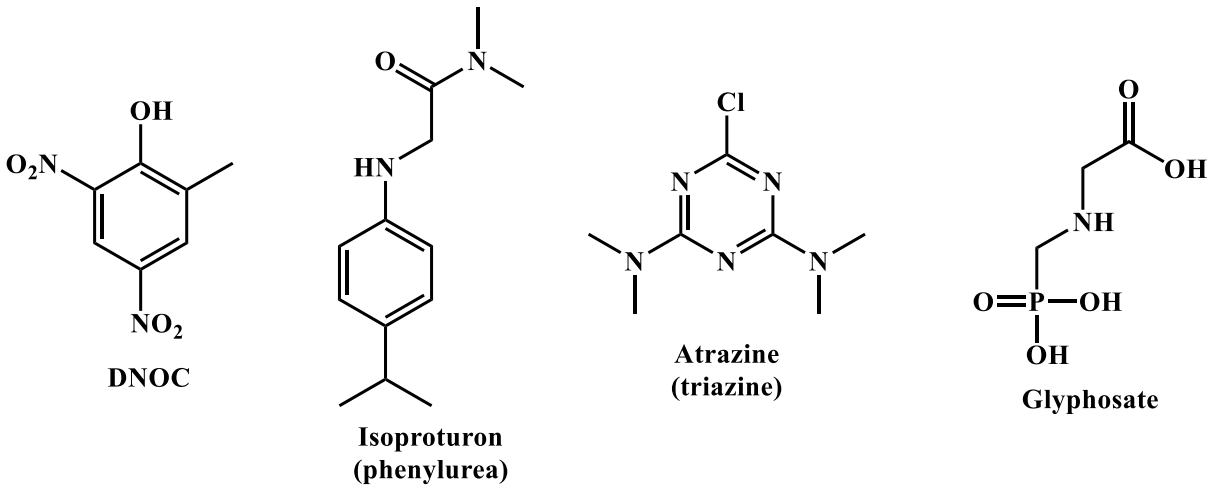

Figure 56: Some examples of herbicide substances.

1.2. Current situation in European Union

At the present time, the market of herbicides is controlled by five multinational companies, and it is constantly expanding; the market estimation is 30 billion dollars by 2019, according to provisional data. The market is approximately distributed as follows: North America 32.2 %; European Union 20 %; South America 11.7 %; Asia 23.2 %; Africa 9.8 % and Oceania 3.1 %.[258] These numbers are in relation with both agricultural area and living standards of the countries. Indeed, tropical countries use less herbicides but more insecticides than Europe or North America; beside, Oceania has only little usable surfaces compare to the oether World regions.

In European Union, although in theory all countries need to work towards common standards, profound inequalities exist. Indeed, in terms of herbicide consumption, France, Great-Britain, Holland and especially Belgium are heavy users.[259] This can be explained by the fact that these countries do not practice or slightly "off-floor" culture that is why their needs are more important than those of Spain or Portugal.

1.3. In France

From 1954 to 1995, the number of active substances and traded compounds has continuously increased in France, as shown in Figure 57. This phenomenon has followed return to economic growth and reconstruction stages after the World War II. This had been accompanied by an increase in consumption (manufactured goods as well as agricultural products). At these periods, herbicides had appeared the best solution to increase production and cover food needs. After 1995 and until the late 2000s, this trend had been reversed, because of the new legislation (EU Directive 91/414)[260] resulting from publications on deleterious effects of some substances on human (Figure 57).[261]

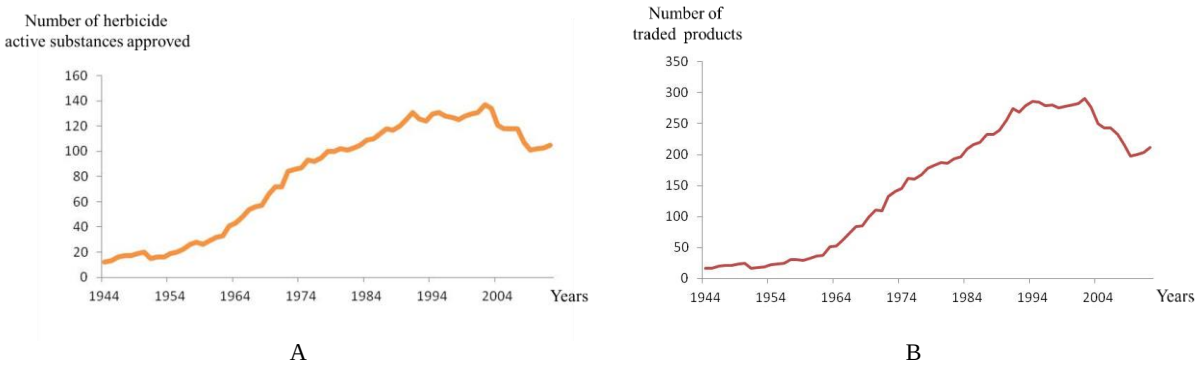

A B

Figure 57: Herbicide evolution of A) active substances approved and B) traded products; in France during 1944 and 2004. **Source:** senat.fr.

More recently the use of pesticides, including herbicides, has increased by *ca*. 5% between 2009 and 2013, and more worryingly by 9.2% between 2012 and 2013 according to the Ministry of Agriculture. This tendency consists mainly in an increase in the use of herbicides. Nowadays, the French herbicide consumption is of 26 000 tons per year, which represents about 40 % of total French pesticide consumption and a market of more than 2 billion dollars (source: Ministry of Agriculture).

Herbicides and the current agriculture are hardly separable. Decreasing their usage or replacing toxic compounds by safe herbicides is a critical ecological and economical challenger. To tackle and develop sustainable and alternative solutions, it is important to know their mechanisms of action.

2. Mechanisms of action

Herbicides are actually thousands of substances with differences in chemical structure or in their action on the plant. There are numerous classifications, either depending on penetration (through the roots *via* the soil or by contact on leaves), or affected areas (roots, stem…), or even the area of application (viticulture, cereals...). Whatever, the most used classification was established by HRAC (for Herbicide Resistance Action Committee), which is an industry-based group supported by Crop Life International, an international federation of companies and professional organizations in the field of crop protection and plant biotechnology (*e.g.* Monsanto, BASF, Bayer or Syngenta…). This classification is based on mechanisms in plants, and is composed on 23 groups and subunits noted A to Z (W, X and Y do not exist already).[262] In the next sections the different classes of herbicides are detailed according to their actions.[251]

2.1. Broad spectrum of action (non-specific of plants)

All these herbicides are non-specific to plants. Indeed, these molecules may be inhibitors of primary cell metabolism or physiological processes present in animals, microorganisms and plants. Lipid or amino acids synthesis, cell division or pH control are common to all alive organisms (Table 1).

- pH control

The active compounds of this category make cell membranes permeable to protons, thus lowering pH of cells and causing death by necrosis and drying of plant tissues. For example, benzene derivatives and dinitrophenols (like DNP), which are used as contact herbicides can be cited. They are also toxic to human beings and environment (Figure 58).

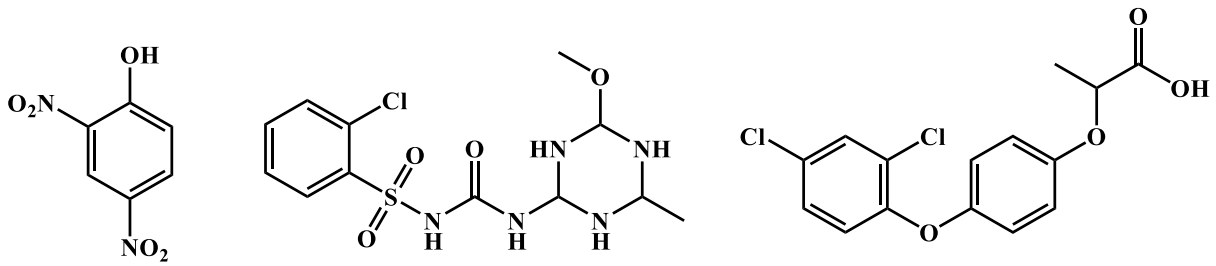

DNP (pH) | **Chlorosulfuron (Amino-acids synthesis)** | **Diclofop (Lipid synthesis)**

Figure 58: Examples of non-selective herbicides and their targets.

➢ Primary metabolism

Some compounds are also capable to inhibit production of vital molecules to plants including lipids and amino acids. They can act by two mechanisms called competitive and noncompetitive inhibition (Figure 59).

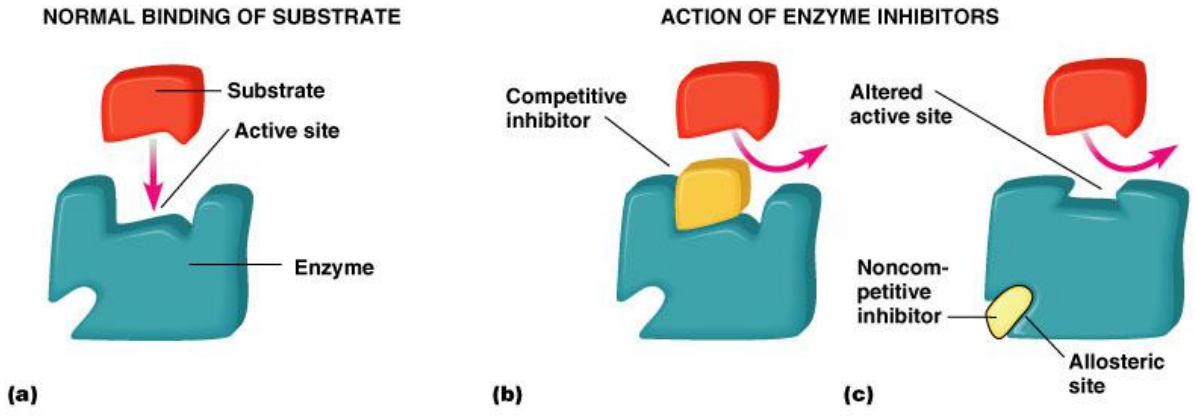

Figure 59: Enzyme inhibition mechanisms. **Source:** Pearson Education 2005/ legacy.owensboro.kctcs.edu.

In the competitive mechanism, herbicides, because they have a structure which allows its recognition and binding to the enzyme active site, inhibit the reaction between substrate and enzyme on the active site to give desired compound. Most herbicides exhibit this character. Instead, in the case of the noncompetitive mechanism, herbicides can be recognized by a site that differs from the active site (allosteric site). Fixing the inhibitor causes a conformational change that affects the active site and prevents substrate binding.

The usual targets are the inhibition of:

i) Acetyl Coenzyme A carboxylase (or ACoA), involved in the first step of lipid Production (Figure 58).

ii) Acetolactate synthase / ALS (also known as acetohydroxyacid synthase / AHAS), which is essential for linear and ramified amino-acid synthesis (valine, leucine, isoleucine) and of course for plant growth. Used for cereal crops or in order to destroy all plants, herbicides used here (mainly sulfonylurea, imidazolinones, triazolopyrimidines and sulfoanilides) exhibit a high efficiency due to their persistence in soil (several months). Moreover, they are minimally toxic for humans (and animals) who are synthesizing these amino acids conversely to microorganisms.

iii) 5-Enolpyruvoylshikimate-3-phosphate synthase (EPSP), involved in aromatic amino-acids (*e.g*. tyrosine, phenylalanine and tryptophan) biosynthesis like. This mechanism is a major interest because the most used herbicide, *N*-(phosphonomethyl)glycine or glyphosate or commercially named Roundup® (Figure 56), behave by this behavior (Figure 58).

➢ Cell division

Molecules (Figure 60), which are capable of inhibiting cell division can target different steps of cell division as:

i) Folic acid synthesis. Carbamates for example are used as dihydropteroate synthase (DHP) inhibitors. This enzyme allows folic acid and other derivative production, which are essential in DNA and RNA synthesis and more generally for production of new cells.

ii) Mitosis.

iii) Microtubule assembly and thus herbicide stop root growth.

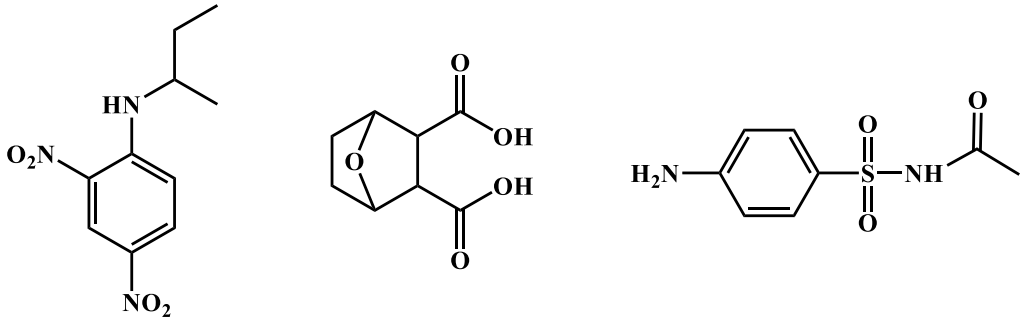

Butraline (Microtubule inhibition) **Endothall (Mitosis inhibition)** **Asulam (DHP inhibition)**

Figure 60: Examples of non-selective herbicides acting on cell division.

All these compounds have in common to be only slightly toxic for mammals and to exhibit persistence in soils from 2 to 6 months.

Table 1: Classification of major large broad spectrum herbicides.

Target	HRAC code	Family	Action	Molecules
pH	M	Dinitrophenols	Permeabilize membranes	DNOC (dinitro-ortho-cresol), Dinoterb, Dinoserb
Lipid synthesis	A	Aryloxyphenoxypropionates	ACCase inhibition	Diclofop
		Cyclohexandiones		Clethodim, Sethoxydim
	N	Thiocarbamates	AcoA conjugation	Butilate, EPTC
Amino acids synthesis	B	Imidazolines	ALS inhibition	Imazamox, Imazapic, Imazapyr
		Sulfonylureas		Amidosulfuron, Chlorsulfuron, Nicosulfuron
		Triazolopyrimidines		Florasulam, Pyroxsulam
		Sulfonylaminocarbonyltriazolinones		Flucarbazo
		Pyrimidinylthiobenzoates		Pyrithiobac
	G	Glycines	EPSP inhibition	Glyphosate
Cell division	I	Carbamates	DHP inhibition	Asulam
	K1	Dinitroanilines	Microtubule assembly inhibition	Benfluraline, Butraline
		Pyridines		Dithiopyr
		Benzamides		Tebutam
		Benzoic acids		DCPA
	K2	Carbamates	Mitosis inhibition	Barban,
	NC	Dicarboxylic acids		Endothall

2.2. Against plant growth

Some herbicides particularly target plant cell division and eventually plant growth. Plant cells are eukaryotic cells, differing in many aspects from cells of other eukaryotic organisms.[263] Here we briefly describe plant cells and their mechanism of division and growth before developing herbicide's mechanisms.

2.2.1. Plant cell

As shown in Figure 61, a plant cell is a complex organite constituted of a plurality of organelles, a nucleus and a protective shell,[264] each separate component having a specific role. Their main difference from animal cells comes from the cell wall. In plant cells, it is constituted of two protective layers, sometimes called cellulosic and cell membranes, which protect cell integrity.[265,266]Their main difference from animal cells comes from their cell wall. Indeed, cell wall have two protective layers, called cellulosic and cell membranes. Their main function is to protect cell integrity and its contents.[265,266]

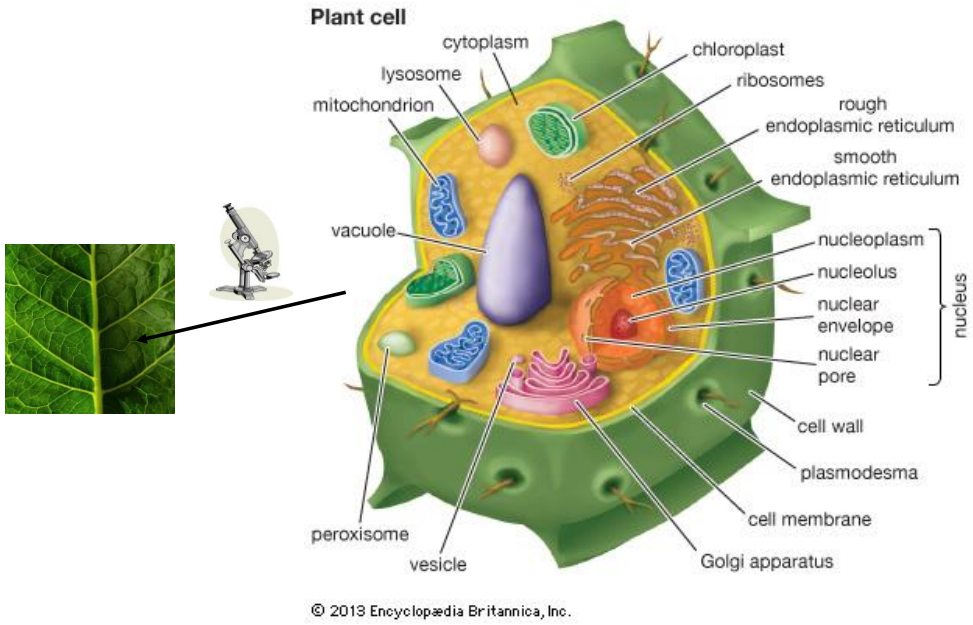

Figure 61: General structure of plant cell. **Source:** Encyclopædia Britannica.

- Pecto-cellulosic wall is characteristic of plant cells. It is constituted of two layers, namely the primary and secondary cell walls forming a skeleton that provide rigidity, preventing deformation, and enough elasticity, allowing cell division and growth. Although their compositions depend on plant type, age and cell role, they contain mainly cellulose and hemicelluloses (up to 90 %). The primary wall also contains pectin, enzymes, structural glycoproteins (2-10 %) and a few phenolic esters (< 2 %), and the secondary wall (which is

directly in contact with the cytoplasmic membrane) contains small proteins or lignin. Inclusion of lignin makes the secondary cell wall less flexible and less permeable to water than the primary.[265,267,266]

- Cell membrane, also called cytoplasmic membrane, encloses cytoplasm. Constituted of an amphiphilic phospholipidic bilayer with embedded proteins, it is selectively permeable to ions or organic molecules.[268]
- Plasmodesmata are microscopic channels through cell wall; they enabletransport (*e.g.* proteins, messenger RNA…) and communication between cells. A typical plant cell may have around 10^5 plasmodesmata, which corresponds approximately to about 1 to 10 per μm^2.[269,270]

2.2.2. Cell division and growth

Cell division is crucial for plant growing (Figure 62). Mitosis is cell division, transforming a mother cell into two daughter cells (Figure 62, M and Figure 63). This phenomenon is preceded by the replication of genetic material (DNA) during a step called interphase. This phase is divided into three stages: (Figure 62) G1 for cell growth; S phase for DNA replication; G2 that precedes mitosis, during which cell is still growing and is preparing for division.[271]

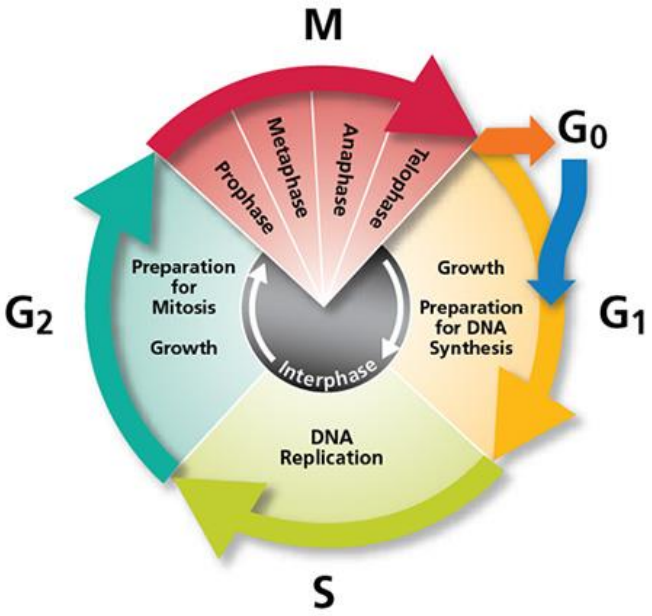

Figure 62: General cellular cycle. **Source:** CNRS.

In plant cells only, mitosis (and more specifically prophase) is preceded by a pre-prophase stage. Indeed, for highly vacuolated cells, the nucleus has to migrate into the center of the cell before mitosis can begin (Figure 63).

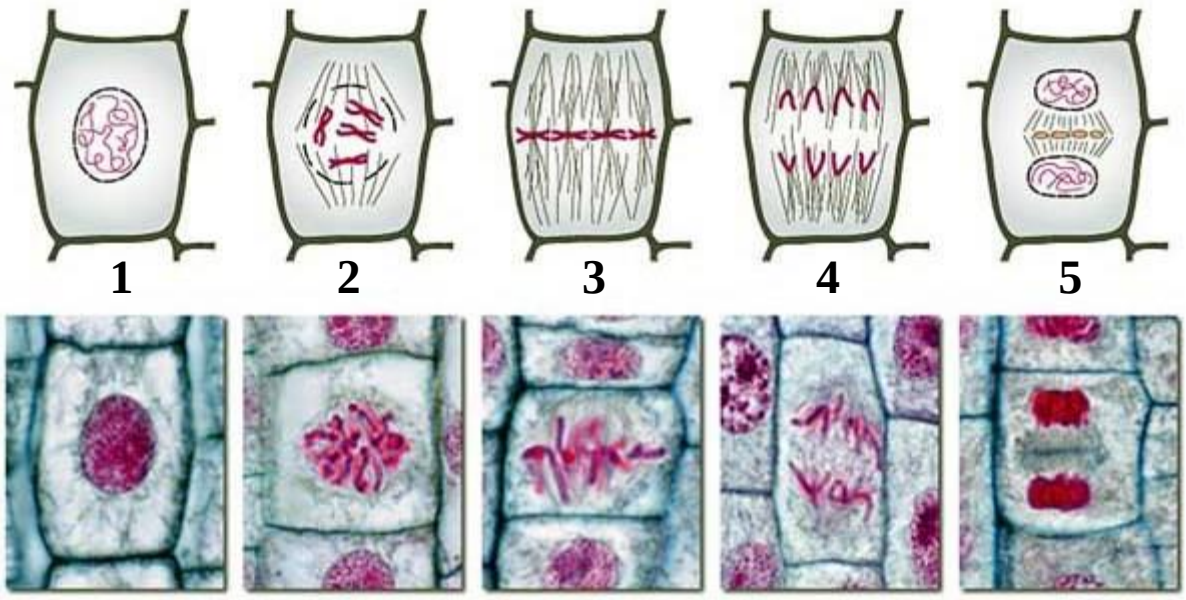

Figure 63: General mitosis cycle.
1) Prophase, 2) Prometaphase, 3) Metaphase, 4) Anaphase, 5) Telophase.

2.2.3. Herbicide mechanism

There are five major families of growth factors: auxins, gibberellins, cytokinins, abscisic acid (ABA) and ethylene. Naturally synthesized, they travel throughout plant. Their effects are different depending on their localization in plants and their concentration, which is generally very weak (*ca*. nanomolar) but may vary during plant's development.[272] Some herbicides (Figure 64) are able to act on plant growth, more specifically on auxin regulation and transport. Their effects can be classified into three groups (according to HRAC) (Table 2).

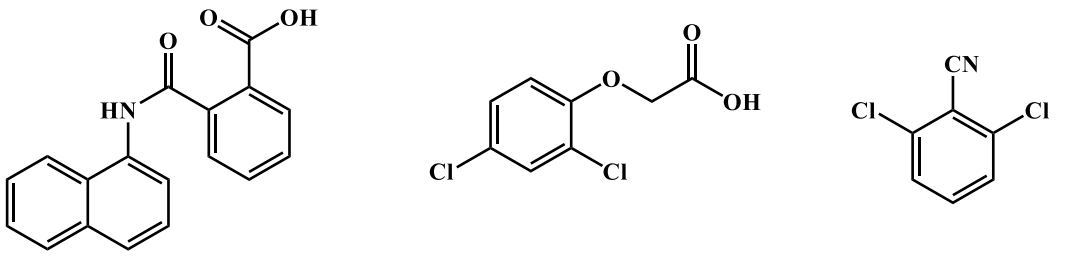

Naptalam (Auxin transport inhibition) **2,4-D (Auxin like)** **Dichlobenil (Cellulose biosynthesis inhibition)**

Figure 64: Examples of herbicides specific of plant growth.

Table 2: Classification of major growth inhibitors.

HRAC code	Family	Action	Molecules
O	Phenoxycarboxylic acids	Auxin-like	2,4-D (2,4-dichlorophenoxyacetic acid)
	Benzonitriles		Dicambo
L	Nitriles	Cellulose biosynthesis inhibition	Dichlobenil
	Benzamide	Cell wall synthesis inhibition	Isoxaben
P	Phthalates	Auxin transport inhibition	Naptalam

- Cellulose biosynthesis inhibition, essentially by nitrile-based compounds. As cellulose is the major component of cell walls, the inhibition of its synthesis results in inability of cell to grow.[273]

- Disruption of auxin regulation (auxins like)[274] by carboxylic compounds such as benzoic, phenoxycarboxylic, pyridine carboxylic, and quinoline carboxylic acids. These herbicides act similar to that of endogenous auxin although the true mechanism is always not well understood. Nevertheless, the primary action of these compounds appears to affect cell wall plasticity and nucleic acid metabolism. Indeed, they stimulate proton-pump which results in cell elongation by increasing the activity of enzymes responsible for cell wall damaging. Moreover, depending on their concentration, they have two other effects:

i) Low concentration of auxin-mimicking herbicides in plants stimulate RNA polymerase resulting in increase in RNA, DNA, and protein biosynthesis, which lead to uncontrolled cell division (and growth) and finally vascular tissue destruction.

ii) High concentration inhibits cell division and growth. Indeed, synthesis of abscisic acid (hormone involved in plant development) is stimulated and leads to an inhibition of CO_2 assimilation. It results in ROS production then senescence and cell death.

- Auxin transport inhibition[275] by phthalates that are capable of inhibition transport of 1) naturally occurring auxin, 2) indoleacetic acid (IAA) (which is an auxin regulator) and 3) synthetic auxin-mimicking herbicides. It leads to an abnormal accumulation of IAA and auxins in meristematic shoot and root regions, which affects profoundly growth and ability of plants to respond to gravity and light.[276]

2.3. Photosynthesis inhibition

Photosynthesis is a very complex process, using several pigments (chlorophylls, β-carotenoids), water, carbon dioxide, electrons and protons, hence possible targets for herbicides are numerous and vary from one herbicide to another. Moreover, the effect of herbicide can target different photosynthetic processes (electron or proton transfer, carbohydrates synthesis, light energy transfer….) (Table 3).

Table 3: Classification of major herbicides inhibiting photosynthesis.

HRAC code	Family	Action	Molecules
C1	Triazines	PSII inhibition: No electron transport No light energy transport	Atrazine, Cyanazine
	Triazinones		Metribuzin, Oxyfluorfen
	Uracils		Bromacil, Terbacil
	Phenyl-carbamates		Desmedipham
	Pyridazinones		Pyrazon
C2	Ureas		Chlortoluron, Diuron
C3	Nitriles	Low concentration: photosynthesis disrupting High concentration: Cell membranes disrupting	Bromoxynil
	Phenyl-pyridazines		Pyridate
D	Bipyridyliums	PSI inhibition	Diquat, Paraquat
E	Diphenylethers	PPO inhibition	Bifenox, Lactofen
	Triazolinones		Azafenidin
C2	Amides	Carotenoids biosynthesis inhibition	Propanil
F1	Pyridazinones		Norflurazon
F3	Triazoles		Amitrole
H	Phosphinic acids	Glutamine synthetase inhibition	Glufosinate

2.3.1. Photosynthesis

According to Gest, « photosynthesis is a series of processes in which electromagnetic energy is converted to chemical energy used for biosynthesis of organic cell materials; a photosynthetic organism is one in which a major fraction of the energy required for cellular syntheses is supplied by light ».[277]

The global equation of chemical reaction occurring during photosynthesis is (Equation 6):

$$6\ CO_2 + 6\ H_2O \xrightarrow{h\upsilon} C_6H_{12}O_6 + 6\ O_2$$

Equation 6: photosynthesis global equation.

In plants and algae, photosynthesis takes place in organelles called chloroplasts (Figure 65), discovered by Hugo von Mohl in 1837 (19 years after chlorophylls discovery by French scientists Pelletier and Caventou),[263,278,279] A typical plant cells contains approximately 10 to 100 chloroplast.

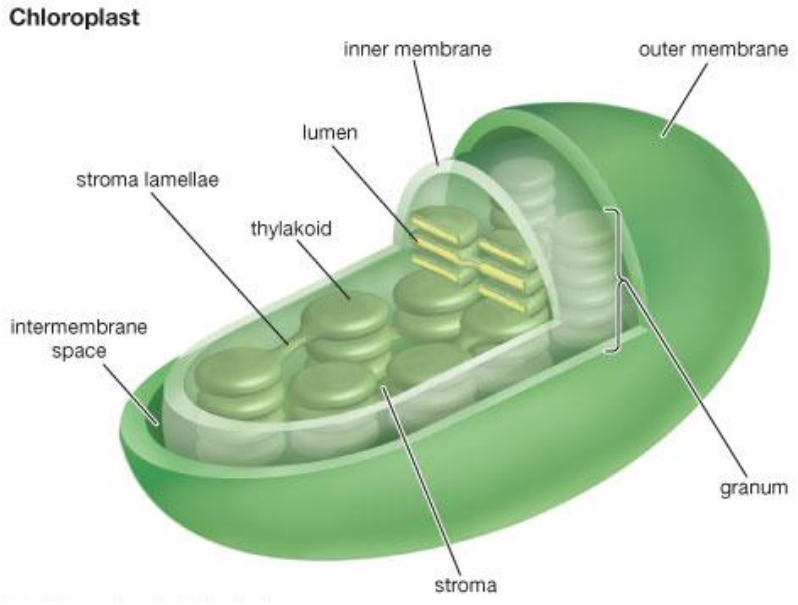

Figure 65: Chloroplast structure**. Source:** Encyclopædia Britannica**.**

The inner part of chloroplast is embedded in two phospholipidic membranes (inner and outer) separated by an intermembrane space containing an aqueous fluid called stroma. Stroma also contains thylakoids stacked into grana. Thylakoids are flattened-disk in shape, delimited by a membrane containing the thylakoid space or lumen (Figure 65).[279] Photosynthesis takes

place precisely in thylakoid membrane, which contains pigments that absorb light energy, namely photosystems I and II (Figure 66).[271,278]

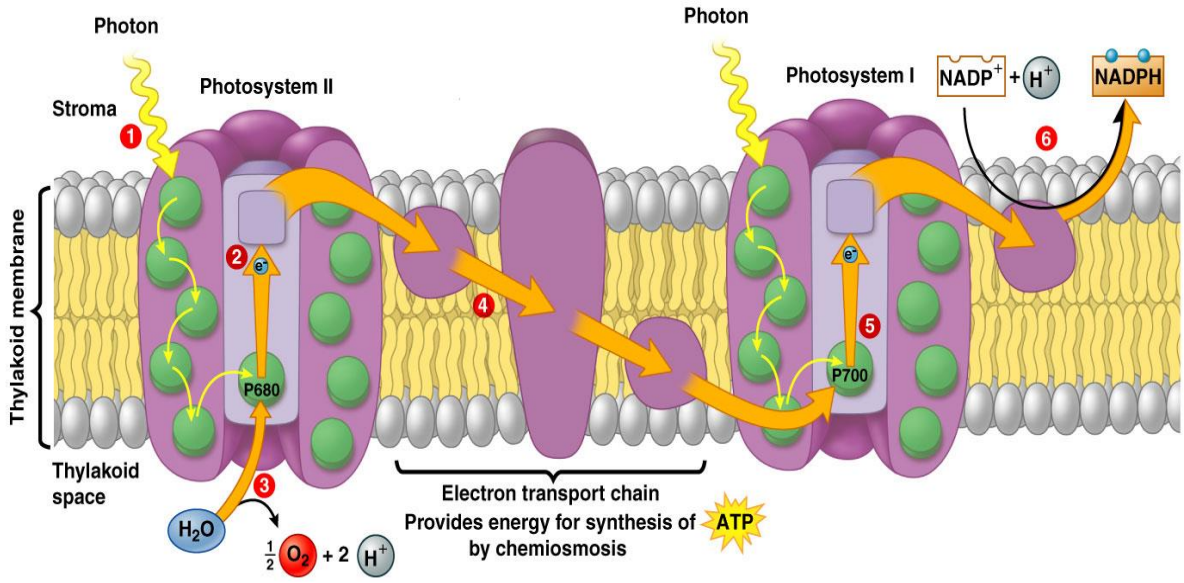

Figure 66: Photosynthesis mechanism. **Source:** Pearson Education 2005/ legacy.owensboro.kctcs.edu.

As sunlight is absorbed (**1**), the energy travels to the reaction-center complex of the photosystem II where an electron flow is set off, resulting in $P680^+$, formation, the strongest biological oxidizing agent (**2**). In order to fill up the missing electron, an enzyme catalyzes water splitting (**3**) into oxygen and protons (pumped into the thylakoid lumen, providing proton-motive force for chemiosmotic synthesis of ATP *via* ATP synthase. Then, electrons are transferred *via* electron carriers to photosystem I (**4**). Meanwhile, in photosystem I, sunlight is also absorbed by chlorophylls and trapped energy is transferred to the reaction center complex (P700) of photosystem I. Then, as for photosystem II, it results in $P700^+$ formation (**5**). This $P700^+$ complex can then act as an electron receptor for the electrons coming from photosystem II.[280] From the primary acceptor of photosystem I, electrons pass through another electron carrier chain. At the end of the chain, the enzyme $NADP^+$ reductase catalyzes $NADP^+$ reduction into NADPH (**6**). This reaction requires two electrons from the linear electron flow, and one proton from the stroma. NADPH and ATP generated during the light reactions phase are used in the Calvin cycle to synthesize sugars.

2.3.2. Herbicide targets

Five main targets in photosynthesis inhibition can be identified:

- Photosystem II inhibitors (Figure 67)[281]

Phenylcarbamates, pyridazinones, triazines, triazinones, ureas, uracils, benzothiadiazinones, nitriles, and phenylpyridazines are examples of herbicides that inhibit photosynthesis by binding proteins of photosystem II complex in chloroplast thylakoid membranes. It results in an inhibition of electron transport and thus of photosynthesis and ATP / $NADPH_2$ production.[282,283] Moreover, excited chlorophyll molecules cannot return to the ground state by normal process. However, they can switch *via* ISC to triplet excited state and thus lead to ROS production (Figure 47). Reactive oxygen species react with unsaturated lipids to produce lipid radicals (Equation 2 and Equation 3) and thus initiate the lipid peroxidation chain reaction; this results in a loss of chlorophylls and carotenoids, but also in membrane destruction leading to rapid drying and destruction of cells and cell organelles.[284]

- Photosystem I inhibitors (Figure 67)

In this approach, herbicides trap electron from photosystem I and forms a radical. Then, by type I mechanism (Figure 47) it reduces molecular oxygen into superoxide anion, being the first step of ROS production, very toxic to plants. Indeed, $O_2^{\bullet -}$ and H_2O_2 may oxidize various organic compounds whereas $OH^{\bullet}$ destroys unsaturated lipids, including membrane fatty acids and chlorophylls. They all produce lipid radicals, which react with oxygen to form lipid hydroperoxides and another lipid radicals to initiate a self-perpetuating chain reaction of lipid oxidation. Such hydroperoxydes destroy cell membranes integrity allowing cytoplasm to leak into intercellular spaces and leads to rapid leaf wilting and desiccation.[285]

- Protoporphyrinogen oxidase inhibition (Figure 67)

Protoporphyrinogen oxidase (PPO or Protox) is an enzyme that catalyzes oxidation of protoporphyrinogen IX (PPGIX) into protoporphyrin IX (PPIX, precursor of both chlorophylls and heme). Its inhibition leads to PPGIX accumulation in cell and even overflows in thylakoids membranes. They are then slowly oxidized into PPIX, due to the high concentration of O_2 being produced in chloroplasts. Finally, as for photosystem II, light absorption leads to ROS production and thus lipid peroxidation, chlorophylls and carotenoid destruction and so cell death.[286,287]

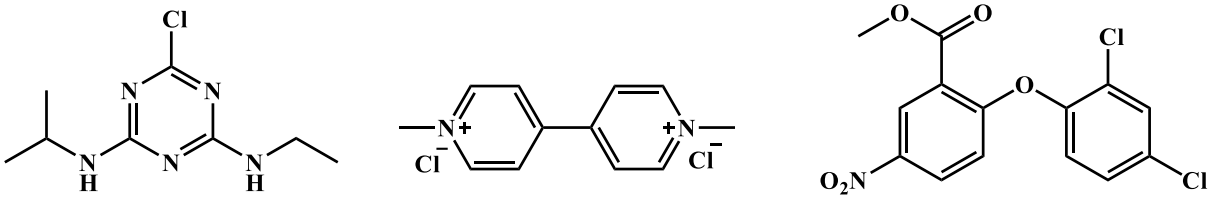

Atrazin (PSII inhibition) | **Paraquat (PSI inhibition)** | **Bifenox (PPO inhibition)**

Figure 67: Examples of herbicides targeting photosynthesis.

➢ Carotenoids biosynthesis inhibition (Figure 68)

Amides as pyridazinones are examples of compounds that block carotenoids synthesis by inhibition of phytoene desaturase (enzyme involved in carotenoids synthesis). Carotenoids play an important role in dissipating oxidative energy of singlet $^1O_2{}^*$. Indeed, if in healthy plants carotenoids and other protective molecules quench singlet oxygen, when they disappear ROS accumulate including the radical species, leading to cell death.[288,289]

➢ Glutamine synthetase inhibitors (Figure 68)

Phosphinic acids inhibit glutamine synthetase activity, this enzyme converts glutamate and ammonia into glutamine. Accumulation of ammonia in plants destroys cells and inhibits directly photosystems I and II reactions.[289]

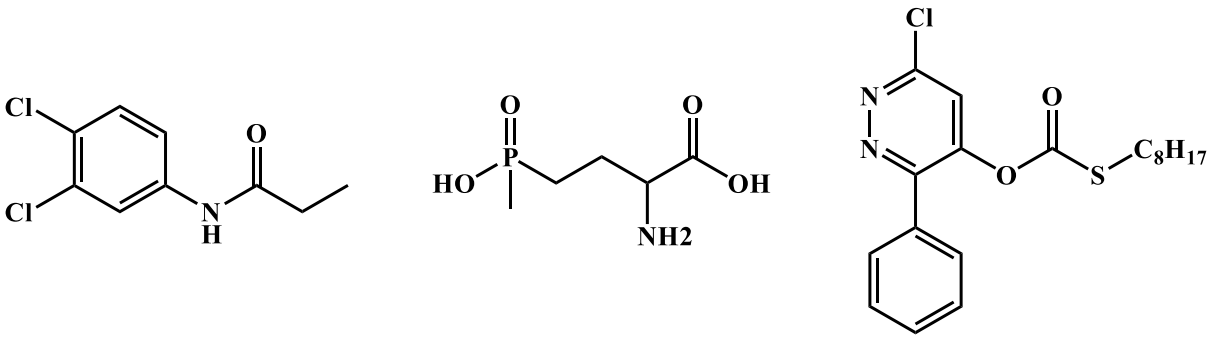

Propanil (Carotenoids biosynthesis inhibition) | **Glufosinate (Glutamine synthetase inhibition)** | **Pyridate (Photosynthesis / cell membranes disrupting)**

Figure 68: Examples of herbicides targeting photosynthesis.

All herbicides described above exhibit various mechanisms, but in reality they are rarely used alone. Indeed, according to the diversity of plants that should be eradicates (and protected), combination of herbicides is often required. The majority of commercial herbicides are mixtures of several herbicides in order to maximize effects.

3. Drawbacks and limitations

As with any chemical substance, using herbicides can present a series of potentials risks. These can concern environmental, sanitary, economic but also in this case ethical and legal issues.

3.1. Environmental drawbacks

When speaking about herbicides and drawbacks, people are particular concerned by pollution issues. Even if their toxicity is supposed to target only unwanted species and thus no crops (and environment in general), their massive use is a source of contamination of water, soil and air.

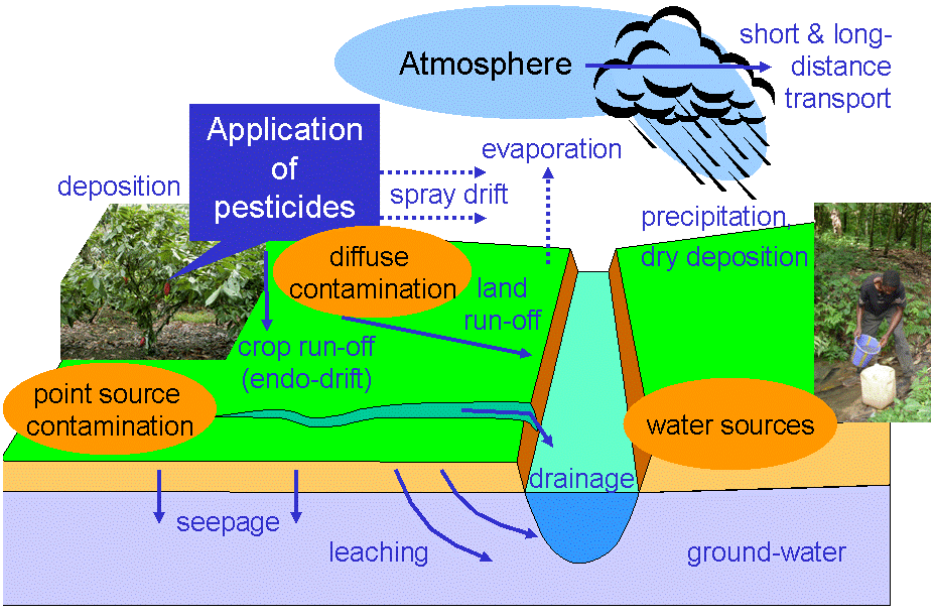

Figure 69: Environmental contamination with pesticides. **Source**: Roy Bateman 2008.

3.1.1. Water contamination

Due to their physicochemical properties, most herbicides have weak adsorption coefficients in soil. They are therefore poorly absorbed in ground, and as a result end into streams and groundwater. Moreover, toxicity is usually determined for native herbicides, and do not take the products of degradation into account (often much more mobile and unfortunately also dangerous) and nature of soil. In addition, herbicides have often extended lifetime in the water, which increase the risk of accumulation and thus increase contamination of water environments.[290–293] As an example in 2013, in France, the General Commission for Sustainable

Development (GCSD) believed that contamination of rivers "is almost universal in France, mainly by herbicides", such as glyphosate, triazines (with atrazine desethyl, a decomposition product of atrazine) and substituted urea.[294] In 2014, the latest results showed that up to 93 % of watershed are contaminated, and sometimes with prohibited substances for 10 years.[295] More worryingly, herbicides level higher than 0.5 µg/L were observed, which is the maximum allowed in drinking water (Figure 70). A major consequence of stream contamination by herbicides is the increase of some nutrients' quantities, particularly nitrogen and phosphorus, creating an imbalance in the growth of marine plants and algae proliferation (synergistic phenomenon with the massive use of fertilizers). It leads also to an impoverishment of oxygen content in rivers and thus excess in mortality of aquatic species.

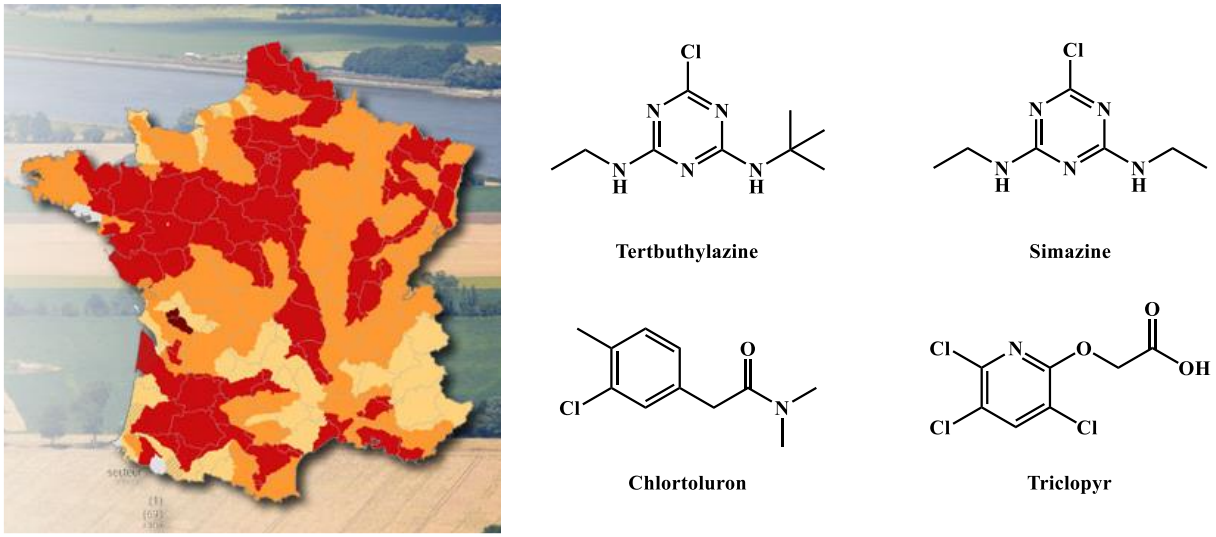

Figure 70: Water contamination by herbicides in 2014. In red: concentration of herbicides >0.5 µg/L, in yellow between 0.1 and 0.5 µg/L and in beige <0.1 µg/L. **Source:** Ministry of Ecology.

3.1.2. Soil

Herbicides with high adsorption coefficients will not be affected by runoff. Nevertheless they will often have a very low penetrating power in soil and thus will deteriorate it directly at the point where they were spread. As consequence, this changes nature and physicochemical properties of soil, creating a contamination thereof.[296,297] Another source of contamination is not caused by the herbicide as such, but again by its degradation. In the case of chlorinated compounds, the mineralization and bacterial degradation emits in environmental chemicals such hydrochloric acid (HCl).[298] Coupling with an intensive use of fertilizers, it leads to an acidification of soil, being not toxic by itself. The problem is actually indirect, coming from the

fact that low pH values increases solubility of many toxic elements (such as ionic species of lead, aluminum, manganese or copper), which are thus absorbed by plants.[299,300]

3.1.3. Air

Atmosphere was not spared by herbicides. Indeed, some herbicides are very volatile, particularly those based on esters. A large part of them is scattered in atmosphere during their application on crops (Figure 71) but also by evaporation from plants or soils on which they were dispersed.[301–303] Carried by wind (sometimes far from their spreading), they fall with rain directly on water systems (rivers, lakes...) and soils on which they are drained into aquatic environments by runoff and infiltration (Figure 69).

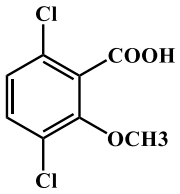

Dicamba

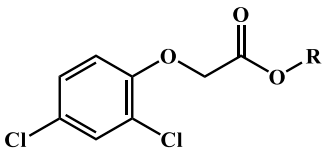

2,4-D esters (R = alkyl chain)

Figure 71: Spraying herbicides and examples most volatile compounds used.

Source: Ministry of Ecology.

3.1.4. Human negligence (soil, water and atmosphere)

So far, human beings have developed environment contamination by herbicides after their applications on crops. However, the most important source of contamination remains human negligence e.g., storage in inadequate and illegal conditions; defective application techniques; carelessly rejection of waste or surplus; accidental contaminations; and the list is not exhaustive.

It is worth mentioning the Seveso disaster in 1976 (Italia). A chemical plant (belonging to Icmesa company), which produced 2,4,5-Trichlorophenoxyacetic acid (or 2,4,5-T, a synthetic auxin used as a defoliant), accidentally released a toxic cloud of TCDD (2,3,7,8-tetrachlorodibenzo-p-dioxin), considered as the most dangerous compound in dioxin family (Figure 72). This dioxin is a by-product due to uncontrolled temperature during the 2,4,5-T synthesis process. About 2000 hectares of land were contaminated, 3300 animals killed (and

81000 were shot down for safety reasons) and 37000 people affected.[304] A second industrial disaster took place in 1984 in Bhopal (India), where a chemical plant belonging to Union Carbide and producing herbicides and pesticides for Indian agricultural program released also a toxic cloud of methyl isocyanate (precursors of carbamates, Figure 72), which killed 3500 people the first night, 8000 the first week and 25000 in total. In addition, this company has buried toxic waste in soil and contaminated effluents and thus rivers. As a consequence, the long-term effects have generated more than 350000 victims affected in varying degrees.[305]

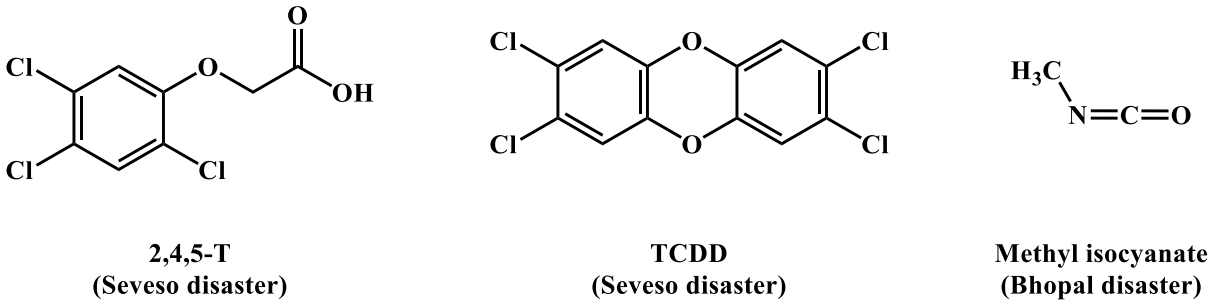

2,4,5-T (Seveso disaster) | **TCDD (Seveso disaster)** | **Methyl isocyanate (Bhopal disaster)**

Figure 72: Molecules involved in Bhopal and Seveso disasters.

3.2. Human health

The link between diseases and plant protection products is a subject of perpetual debate between industries, victims and scientists. The effects listed below are those whose causality is not questionable, or for which the great majority of the scientific community fully agrees.

Pollution induces by herbicides affects both animals and plants. Direct effects are likely or bioaccumulation in food (animal and vegetable) or in water. Short-term effects are often by severe burns due to skin contact, headache and in some cases breathing difficulties. Long-term effects are usually more deleterious. Herbicides have carcinogenic and teratogenic effects. Three disasters have unfortunately allowed to figuring out consequences, namely the industrial disasters of Seveso and Bhopal, and Vietnam War. Indeed, during the conflict in Vietnam, US army had intensively used the herbicide called Orange Agent. It was a mixture of 2,4,5-T and 2,4-D (2,4-dichlorophenoxyacetic acid), which are two synthetic auxins. The 2,4,5-T used to produce this herbicide was contaminated with 2,3,7,8-tetrachlorodibenzodioxin (TCDD). In some areas, TCDD concentrations in soil and water had been hundreds of times greater than the levels considered as safe, and caused several diseases (blindness, diabetes, prostate and lung cancers or birth defects) and pollution. Moreover, due to high stability of this herbicide, 50 years later, the effects are still visible.[306–308] Similar carcinogenic and teratogenic effects have been observed due to Bhopal and Seveso disasters, still seen 30-40 years after.

More recently, Roundup® and glyphosate derivatives have hit the headlines (Figure 73). This substance, which is the most used as herbicide by individuals, has been suspected of carcinogenic, teratogenic, cardiovascular and hormone deregulation effects in humans.[309–311]

Figure 73: Roundup active substance and marketed products.

3.3. Economic issues and resistance phenomenon

The intensive use of herbicides eventually causes a phenomenon of adaptation of plants, which become less and less sensitive to these substances (as microbes for antibiotics). Resistances result for ability of weed to survive a herbicidal treatment.[281,312,313] Weed resistances are developed against one specific herbicide or for several (multi-resistance). [314] Since 1957 and since the first discovery of resistant herbicide weeds,[315] there have been over 249 weed biotypes resistant to herbicides discovered in 47 countries worldwide; and this number increases year after year (Figure 74).[262,316] Some management practices increase the likelihood of weeds to develop resistance:

- Resistance is more likely to occur when the same herbicide (or herbicides) belonging to the same groups are used repeatedly which is encouraged by monoculture.
- Along the same line, using different herbicides (in terms of chemical structure) but using similar mechanisms of action may lead to resistance development. This also the case with specific herbicides (developed for one or two particular species), and for which intensive use promotes resistance gene development.
- If targeted species exhibit an ability to produce a lot of seeds (like annual weeds), a resistance phenomenon can occur only statistically. For example, if only 5 % of specie develops a resistance gene to an herbicide, each survivor can produce hundred (or thousand) seeds, so in a few years all weeds are resistant. Moreover, lethal effects of herbicide increase resistance in plants.

➢ Finally, in line with the latest technological advances, a new resistance training was born. Indeed, although their potential risks are still unknown and subject of debate, GMOs have a scientifically proven blackhead. As described below in section II.3.4, some of them are herbicide resistant. However, in last years, some cases of "natural" crops contamination were reported,[317] which ultimately leads to the proliferation of their resistance genes.

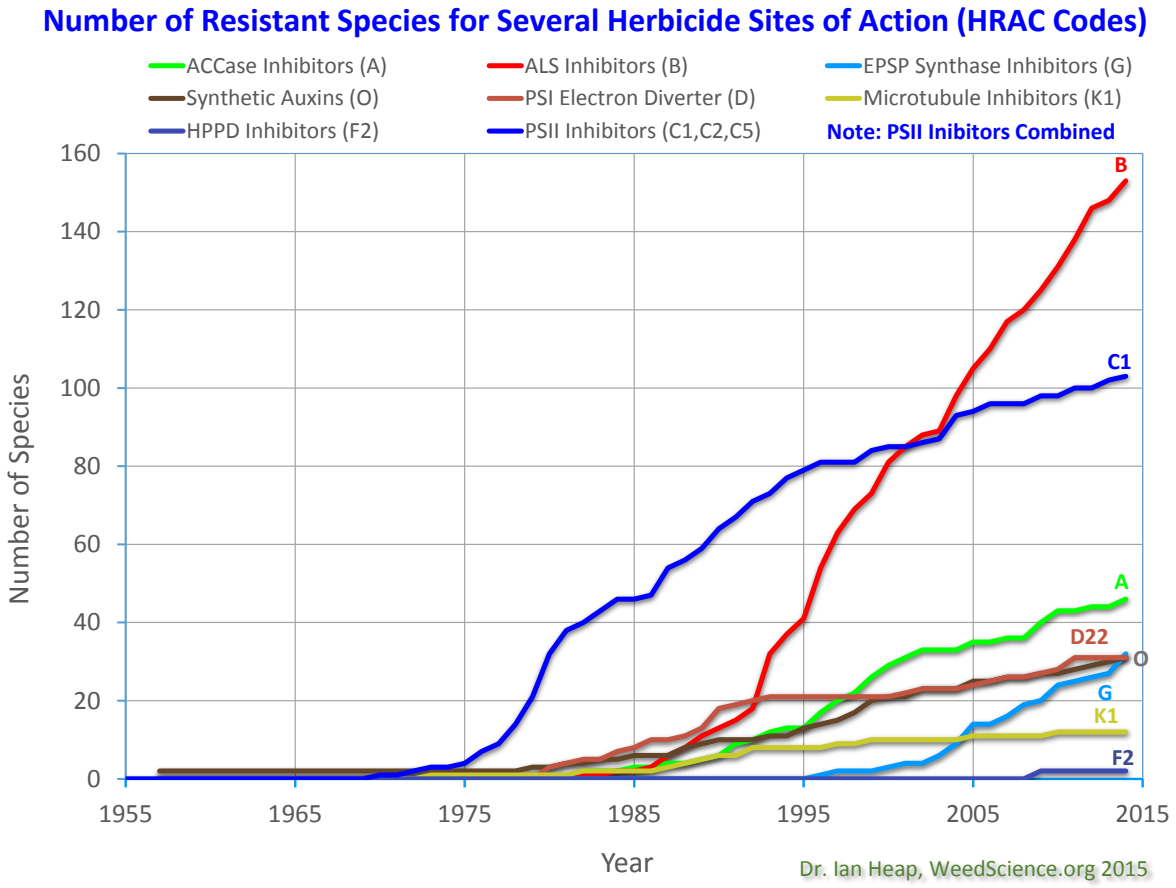

Figure 74: Chronological increase in herbicide resistance. **Source:** weedscience.org

This resistance has a cost, both for farmers who have to adapt their herbicide usage, but also for consumers who pay more for the same product, due to yield reduction.

3.4. Herbicide and genetics

Misuse, pollution of groundwater, effects on human health attributed to herbicides are a matter of intense and sometimes controversial debates. Genetically modified organisms (GMO), such genetically modified crops that have emerged in the 1990s, are particularly controversial, because many of them are herbicide resistant (70 % of GMO crops were specifically designed to be herbicide resistant). Soybean, cotton, maize, oilseed rape and beet

resistant to glyphosate were introduced in the United States in 1996 and are now well established in many other countries as Canada, Brazil and Argentina. Today, genetically modified crops are grown by more than 10 million farmers in 22 countries and cover 100 million hectares. According to the United States department of agriculture, in 2012, more than 93 % of soy planted and 73 % of corn were "herbicide tolerant" .[318] Genetic manipulation of plants raises societal and ethical debates. Consumers ask to scientists: What are the risks for neighboring non-modified crops? Are there effects on humans? If yes, which effects? Are they long-term or short-term effects? Indeed, if GMOs are results of the latest advanced technologies, feedbacks cannot be mature so far. Moreover in theory, making plants resistant to a particular herbicide should enable using only one herbicide, therefore reduce the overall herbicide consumption. Nevertheless, several recent studies suggested that it is not the case. Indeed, in the United States (one of the biggest users of GMO), herbicide-resistant crop technology has led to a 239 million kilograms increase in herbicide use from 1996 to 2011, while they have reduced insecticide applications by 56 million kilograms.[319] In addition, accidental contamination of culture by GMO have been recently identified, which increases distrust in GMO crops.[320] Thus, if GMOs are allowed in Europe and present in consumer products (although at very low levels), their culture is prohibited in France, and henceforward Scotland has decided to ban them.

3.5. Military uses

Historically, the destruction of crops and food reserves has helped to reduce the resistance of the opponent. From 1943 to 1944, up to 12000 defoliants were tested in the United States and more than 7000 products were discovered. The research continued after the war and in 1950 the British Army was the first to use herbicides during the war against the guerrillas in Malaysia.[321] The Vietnam War unfortunately and undoubtedly perfectly illustrates that herbicides can be turn into deadly destructive weapon. Indeed, when the war began and intensified, the United States government has exercised its power conferred by the Defense Production Act to contract with seven chemical manufacturers to procure 15 herbicides, which were used for military purposes against opposing forces, the most famous of them remaining Agent Orange, (see section II.3.2).[322] More recently, herbicides were used for fighting drugs production in South America and Afghanistan. Over the past decade, more than 300,000 hectares of coca and opium poppy fields in Colombia, but also marijuana crops, have been sprayed with glyphosate for coca and opium and paraquat for marijuana (Figure 67, Figure

73).[323] Although the fight against drugs is an important cause, the aerial fumigation cycle causes pollution affecting humans, animals and vegetation, and destroys the livelihoods of peasant and indigenous communities.

3.6. Legislation

All the points discussed above, pollution, health risks, military use or genetic modification have led to several laws, establishing limitations or even prohibition of herbicides in agreement with recent scientific advances. However, these laws vary from one country to another. This is for example the case of atrazine (PSII inhibitors) that is banned in Europe because carcinogenic, but it is extensively used in the rest of the World, in particular in United States.[324] It is also worth noting the case of paraquat (PSI inhibitors), a very toxic compound forbidden in Europe since 2007, but only since August 2015 in Tahiti (French island).[325] For all these reasons, the number of authorized or effective herbicide substances will decrease over the next years. This makes research in herbicide science crucial to establish clear technical specifications. New compounds must be readily degradable into non-toxic products, not persistent in soil and groundwater, and not dangerous for human health (and more generally for all living organisms, animals and vegetal). Finally, they have to be easy to manipulate in order to decrease (or suppress) accidents.

4. Porphyrins as herbicides

4.1. Choice of exogenously pathway

Porphyrins and their derivatives are involved in several crucial processes such as photosynthesis or those implied hemic-proteins; all of them constituting the porphyrin pathway, one of the most important metabolic processes. As well, a wide range of herbicides inhibits production, regulation or functions of endogenous tetrapyrrolic compounds, causing their accumulation then ROS production, lipids oxidation and cell death. Nevertheless, it exists another possibility to act on porphyrin pathway, which was virtually overlooked as herbicide's target and only few publications deal with this possibility.[326] By using herbicides based on exogenous porphyrin precursors, it may be possible to trigger in green plants an undesirable accumulation of metabolic intermediates of the chlorophylls metabolic pathways, namely tetrapyrroles. Finally, the porphyrin overexpression in plant results in ROS overproduction.[327]

This idea was first applied in 1984 by Rebeiz *et al.*[240] in order to promote the production of tetrapyrrolic intermediates. Cucumbers were sprayed with two chemicals: δ-aminolevulinic acid (ALA) and/or 2-2'-dipyridine (Figure 75). The first, a biodegradable amino-acid, is a tetrapyrrole macrocycle precursor whereas the latter is an activator of the chlorophylls biosynthetic pathway. Then cucumbers were placed in a dark growth chamber during one night allowing the dark biosynthesis and accumulation of tetrapyrrolic intermediates.

δ-aminolevulenic acid **2,2'-dipyridyl**

Figure 75: Chemicals used by Rebeiz in 1984.

Even after 10 days with normal sunlight period, the authors observed that ALA or 2-2'-dipyridine alone did not exhibit significant cytotoxic effect. However, under the same experimental conditions (dark incubation and then light exposition), a spray of both ALA and 2-2'-dipyridyl caused severe damages, in a few hours. Moreover, these photodynamic effect seems species dependent; for example cucumber mustard or lamsquarter exhibit damages up to 85 % whereas cereal crops (corn, oat and wheat) are not affected. Unfortunately, the direct use of exogenous porphyrins on plants was not tried at this time, because it was considered too expensive and possibly dangerous for health.[328] Later in 1988, Kouji *et al.* published their works on diphenylethers (already used as herbicides). Thanks to a study on tobacco cells, they have demonstrated that diphenylethers stimulate 5-aminolevulinic acid production and thus porphyrin overproduction in plants.[329] In addition, diphenylethers exhibit some interesting advantages compared to Rebeiz's systems: already marketed, cheaper and usable for the same final mechanism.

4.2. Cationic porphyrin and DNA

Although the use of porphyrins as potential herbicides is rejected and replaced by more profitable substances such as diphenylethers, Villanueva *et al.* pursued research indirectly. Indeed, they worked on photodynamic therapy and more precisely damages induced on DNA. Unfortunately, such photodynamic damages are difficult to figure out in mammalian cells, or

tissues. One preliminary approach consists in studying simplified model systems as liposomes and red blood cell membranes. The only limitation is that the studied subject must be an eukaryotic organism. In this context an *in vivo* plant system has some advantages and provides useful information about photodynamic effects. Their studies were performed on *Allium cepa* roots, with two cationic porphyrins (Figure 76), meso-tetra(4-N-methylpyridyl)porphyrin (T_4MPyP) and its zinc complex (ZnT_4MpPyP).[330,331] Results showed that cationic porphyrins were able to enter into cells, and even in the nucleus (with an affinity to chromatins) where they induced DNA photodamages (by ROS production). Therefore they concluded that porphyrins are capable of killing plant cells by exogenous application. However, these authors did not document the mechanism of porphyrins uptake by the nucleus.

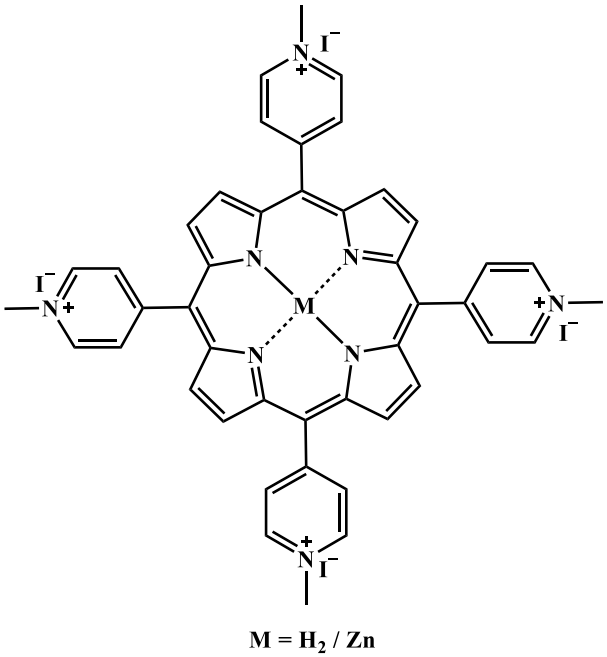

Figure 76: Cationic porphyrins used by Villanueva *et al.*

4.3. Current situation

As described earlier, the agricultural world is in crisis. Herbicide-resistant plants, hazardous chemicals, pollution are many new drawbacks that have emerged in the last 20 years. Concerning the few herbicides acting on the chlorophylls biosynthesis pathway, most of them are now prohibited or will soon be so. For examples, over the last decades, diphenylethers have evidenced many effects on human health. Nitrofen, first marketed compound of this family, is known to increase risks of developing cancer and teratogenic effects. This is why it was banned in Europe and United States in 1996.[332,333] More recently, two other compounds of this family,

chlornitrofen and oxyfluorfen, were suspected to be toxic.[334,335] Currently classified as "substances of very high concern" by the World Health Organization (WHO), they are likely to be banned in the next few years. In the current environmental context, porphyrins may appear as potential alternatives. On one hand, few publications described since 1986 the lethal effects of exogenous porphyrins on plant cells (see section II.4.2).[330,331] This interesting property can be now associated with recent works which suggest that water soluble porphyrins could pass through different kinds of cell walls, even if they are composed of various molecules (*e.g.* peptidoglycans for bacteria; mannan, glucan or chitin for insects and fungi; or polysaccharides for plants).[331,336] On the other low toxicity of exogenous porphyrins perfectly fit with the recent requirements for commercial herbicides. [328]

This is why since 2013, we have developed new project in our laboratory based on experiments using charged porphyrins on tobacco cells (Tobacco Bright Yellow-2, TBY-2). Preliminary results, performed on anionic and cationic porphyrins, showed that the anionic ones were the more efficient to lead hydrogen peroxide overproduction and thus apoptosis, which make them potential new photoherbicides.[337] Moreover, because of their similarity with natural porphyrins, it is reasonable to believe that these new materials will be naturally degraded. Indeed, degradation of porphyrins and chlorins contained in plants has never led to the formation of products which might contaminate soil and groundwater; the Nature being equipped to recycle these metabolites. Many assays are now required to support the proof-of-concept.

5. Purpose of work

Preliminary researches carried out in our laboratory on the use of charged porphyrins as new photoactivable herbicidal compounds led to interesting results.[337] However, for plant application, porphyrins have weak fluorescence quantum yields, and they are thus hardly tractable in plants, especially in chlorophylls containing plants because of spectral overlap between chlorophyll and porphyrin fluorescence. Therefore, in continuation of these works we aim at developing two intricate axes.

First, we have designed new anionic free base porphyrins, by modulating number (4 or 8) and nature (by replacing sulfonate groups by carboxylate or phosphonate functions) of charges. Their effects on both physicochemical properties (acido-basic behavior, absorption and emission features and ability to produce ROS) and toxicity towards TBY-2 cells were studied (Figure 77).

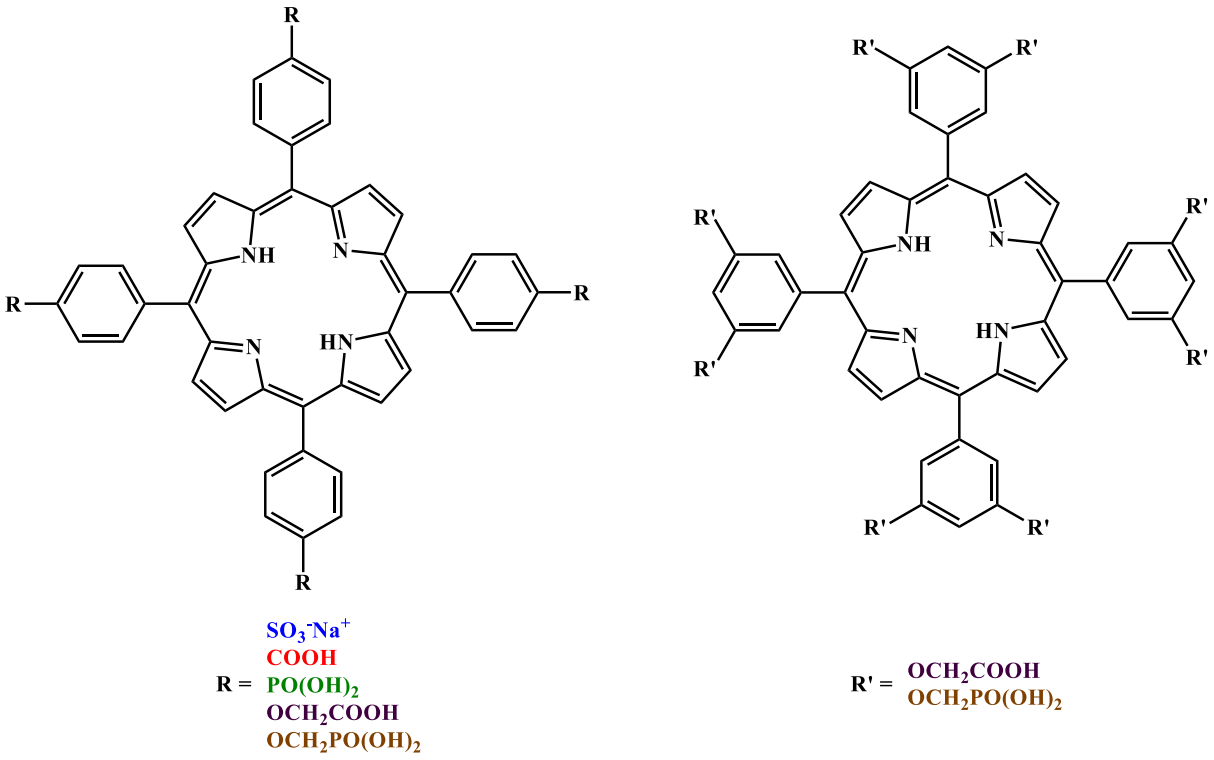

Figure 77: General structure of anionic porphyrins.

Second, localization of porphyrins in plant cells or plants has been carefully considered, using the dyad concept. *In vitro* and *in vivo* localization is of upmost importance to further investigate and understand mechanisms of herbicide action and degradation (uptake, photochemical processes…). In this context, we have designed a series of new dyads, made of porphyrins (metallated or not) labeled by a fluorophore. Molecular modeling has supported experimental photophysical characterizations (Figure 119). Due to its intrinsic non-toxicity for plants, and its specific photophysical properties, fluorescein was chosen as the fluorescent tag. The spacer between porphyrin and fluorescein moieties has deserved a special attention. Indeed this pattern is expected to be responsible for final properties and existence of intermolecular interaction porphyrin and fluorescein.

Moreover, in order to be tested in biological media as potential photo-activable herbicides, all these compounds must be non-toxic in the dark, good ROS producers after photo-activation and be obtained as pure as possible. Therefore, all of them were characterized by NMR (^{1}H and ^{13}C), mass spectra (HRMS, except for commercial compounds), UV-Vis absorption, and fluorescence emission. ROS production was evaluated either by EPR or through singlet oxygen quantum yield evaluation.

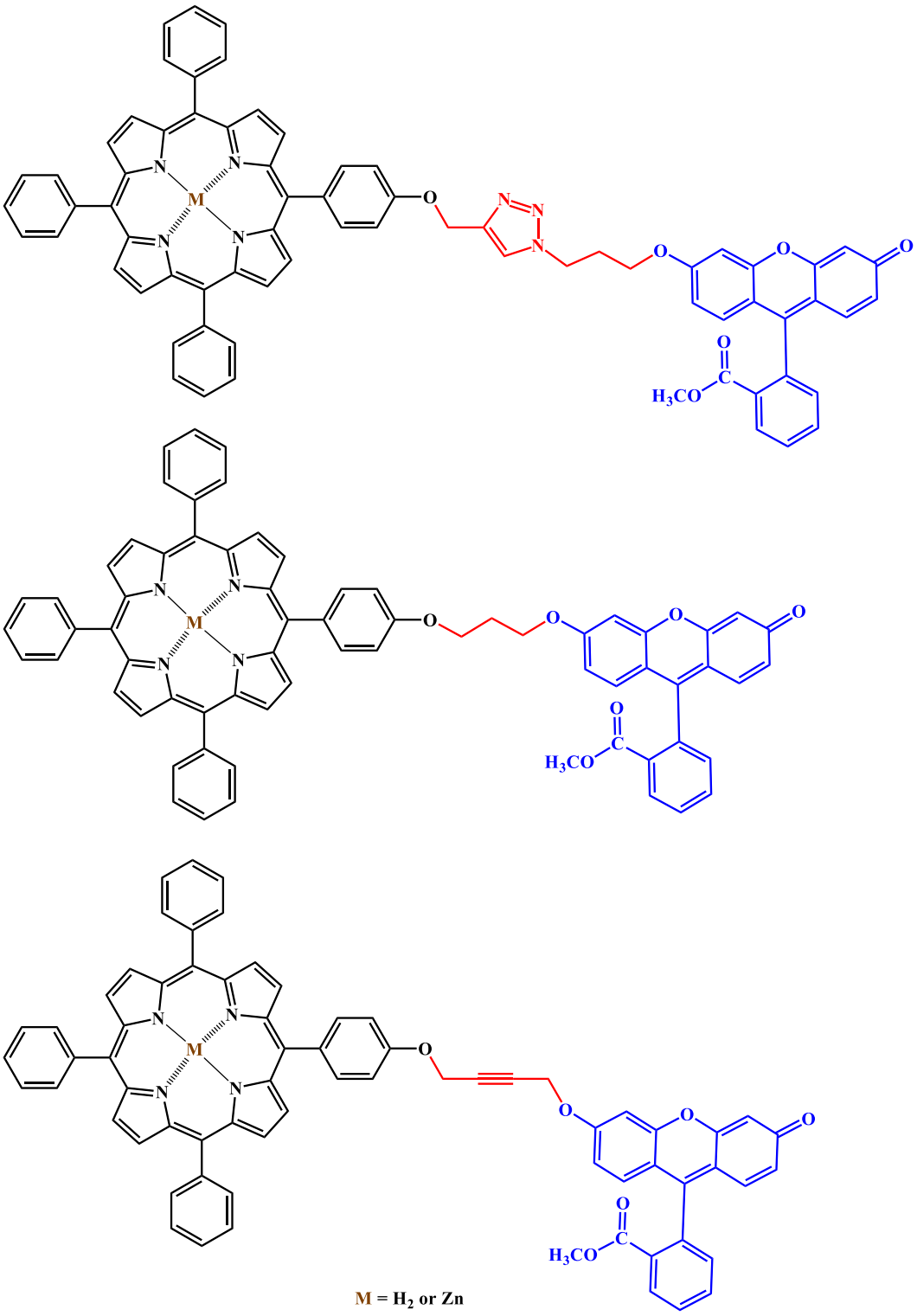

Figure 78: General structures of dyads synthesized.

Anionic Photosensitizers

The choice of anionic porphyrins as potential new herbicides is not trivial and arises from a preliminary study conducted in our laboratory that is described in the first section.[337]

1. Preliminary work

The pioneer works of Rebeiz *et al.*[240] and Villanueva *et al.*[331] have described effects of porphyrins on plants in endogenous and exogenous applications, respectively. Along this line, here we report the study of some porphyrins on plant cells.

1.1. Choice of porphyrins

The study of porphyrins as potential bio-herbicides requires strict specifications. As mandatory requirement to work with plant cells, molecules must be water-soluble; any addition of other solvents classically used as alternative, as DMSO or DMF, triggers cell death, even in low amount (≈ 2 %, v/v). Moreover they must efficiently produce ROS, which are the toxic agent inducing plant cell death.

Keeping these prerequisites in mind, four different compounds were selected, two anionic (**1** and **1-Zn**) and two cationic (**CP** and **CP-Zn**) porphyrins (Figure 79). The charges enable water solubility. Additionally, to study metal effects is feasible when comparing free bases and the corresponding zinc complexes, zinc being known to not modify ROS production.[141]

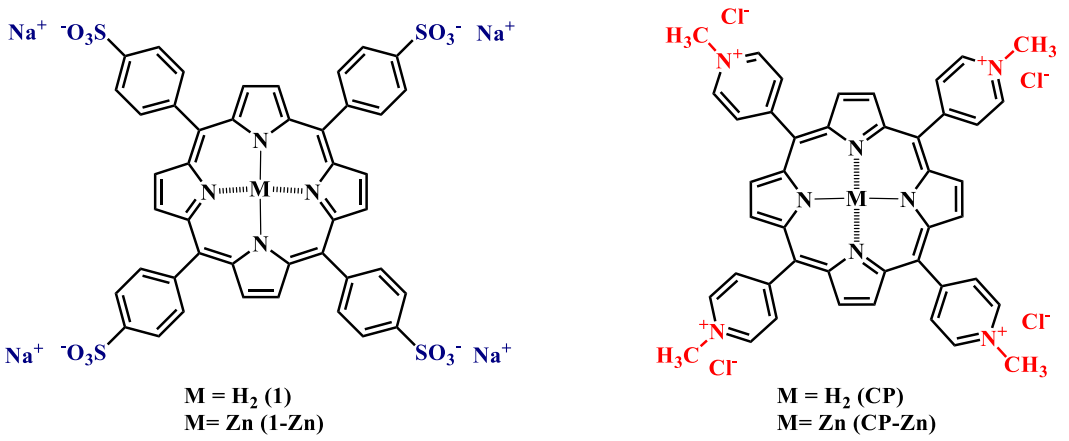

Figure 79: Porphyrins chosen for the preliminary study.

Three of the compounds were purchased, namely **1**, **CP** and **CP-Zn.** The **1-Zn** derivative was synthesized according to the classical porphyrin metalation procedure.[338] Treatment of **1** by zinc(II) acetate in water led, after dialysis, to **1-Zn** in quantitative yield.

1.2. Characterizations

The evaluation of photophysical properties, photostability and ROS production of these four compounds is of upmost importance to establish structure-activity relationship.

1.2.1. Photophysical properties

All measurements were performed at room temperature, in water solution (concentration *ca.* 10^{-6} M). Results are summarized in Table 4.

Table 4: Selected photophysical data in water for **CP**, **CP-Zn**, **1** and **1-Zn.**

Compound	λ_{abs}	ε	$\lambda_{em\ max}$	Φ_f
CP	423	153200	680	0.016
	519	9500		
	555	4200		
	586	4100		
	640	1000		
CP-Zn	437	268100	634	0.025
	565	21700		
	608	6800		
1	414	219000	644	0.046
	516	7300		
	553	3700		
	582	4100		
	636	3900		
1-Zn	422	434700	606	0.03
	557	13700		
	596	5500		

CP and **1** exhibited the typical Soret and Q bands characteristic of free-base porphyrins. **CP** had a *phyllo-type* spectrum whereas **1** is very close to an *etio-type* profile, as already described in the literature.[123] As expected for metallated compounds **CP-Zn** and **1-Zn**, modifications of UV-Vis spectra were observed: 1) a slight bathochromic shift; 2) an increase in molar extinction coefficient (ε) of the Soret band; and 3) a decrease in the number of Q bands

(Table 4). For all these compounds, no aggregation was evidenced at the concentrations used for experiments.

All four compounds presented a weak emission ($\Phi_f < 0.05$ at room temperature) centered from 606 to 680 nm, characteristic of porphyrins. Moreover, fluorescence excitation spectra matched absorption profiles over the entire wavelength range, evidencing purity of both commercial and synthetic compounds.

1.2.2. Photostability

Porphyrins behavior in the TBY-2 growth medium[337] was crucial. Indeed, upon illumination, interactions between porphyrins and medium components could decrease ROS production and cell death. Thus, photostability was evaluated (Table 5) by monitoring absorption spectra after differents illumination times under similar conditions that used for plant cells, that is 3 hours of dark incubation then white light irradiation (5.10^3 $lm.m^{-2}$) of porphyrin solutions ($3.5.10^{-6}$ M) in TBY-2 growth medium. Variations in the Soret band intensity and potential modification in the UV-Vis spectrum profile were carefully followed as these parameters indicate photobleaching and/or photodegradation (Table 5).

Table 5: Photostability of **CP, CP-Zn**, **1**, **1-Zn** (obtained from 2 or 3 independent experiments).

	Photostability (%)			
	CP	**CP-Zn**	**1**	**1-Zn**
Dark time (h)	**Dark incubation**			
0	100	100	100	100
Illumination time (h)	**Illumination period**			
0	84.7 ± 24.7	99.6 ± 2.0	79.3 ± 3.0	84.1± 9.8
1	55.7 ± 3.9	74.3 ± 21.1	39.6 ± 10.1	22.4 ± 4.5
4	51 ± 0.9	66.5 ± 18.5	31.2 ± 5.5	1.8 ± 2.1

No changes in absorbance spectra were observed after 4 hours irradiation for **1**, **CP** and **CP-Zn**. For **1-Zn**, a shoulder at 444 nm appeared after 2 hours illumination that is possibly attributed to aggregation. New bands in the UV region (300-400 nm) were also recorded, evidencing some photo-transformation of **1-Zn**. All attempts to isolate and identify degradation products have failed, as photochemical reactions involved seemed not reproducible, and analytical methods required are rather difficult to develop in presence of growth medium.

Whatever, this identification should bring valuable information on PS modifications. We hypothesize that macrocycle can open upon oxidation.[339,340] **1-Zn** exhibited the lowest photostability, namely 22.4 % and 1.8 % of the initial Soret band absorption was kept after only one and four hour illumination, respectively. Moreover, the Soret band decreased in intensity during dark incubation for all compounds, whereas these molecules were perfectly stable in water. This stressed that specific interactions between PS and growth medium may exist.

All these results allowed concluding that **1**, **CP** and **CP-Zn** did not undergo phototransformation, but only photobleaching. No aggregates or protonation were found at the concentration used in TBY-2 growth medium. The cationic porphyrins were more stable than the anionic porphyrins.

1.2.3. ROS production

ROS production was evaluated for **1**, **CP** and **CP-Zn** (**1-Zn** being unstable) by Electron Paramagnetic Resonance (EPR) in collaboration with Dr Calliste (LCSN). Due to short lifetimes of ROS, and the non-radical nature of singlet oxygen, specific spin traps were used. TEMP, in phosphate buffer, was used to spin trap singlet oxygen while DMPO in DMSO was used to spin trap superoxide anion (see experimental section for more details). Results are summarized in Figure 80.

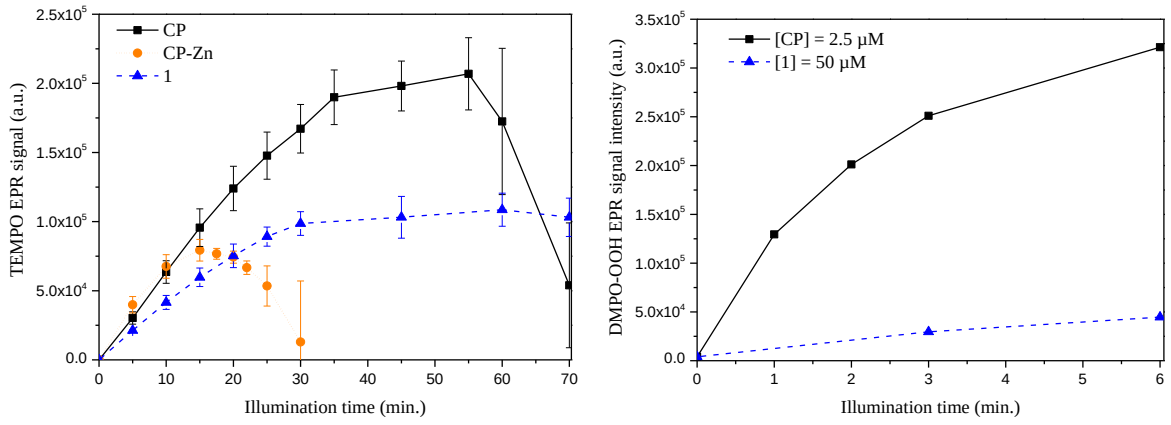

Figure 80: EPR signal of TEMPO generated by irradiation of **CP**, **CP-ZN** and **1** (c = 40 µM) **(A)**. EPR signal of DMPO-OOH generated by irradiation of **CP** and **1 (B)**. Values represent the means ± S.D. obtained from 3 independent experiments for **A**.

Figure 80A shows that the two free-base porphyrins (**CP** and **1**) exhibited better singlet oxygen production than the other two. **CP-Zn** was rapidly degraded, probably by ROS produced upon photoactivation of **CP-Zn** itself. **CP** and **1** produced also superoxide anions

(Figure 80B), but **CP** being more efficient (more than 240 times) than **1**, even if the concentration used was 20 times lower (2.5 and 50 µM, respectively). The capacity of **CP** and **1** to produce both singlet oxygen and superoxide anion made them relevant candidates for photoherbicide applications.

1.3. Biological experiments

To assess the herbicidal potential of the four PS, a biological study was conducted by Dr C. Riou (LCSN) on tobacco cells (TBY-2)[341]. This plant was chosen for several reasons. First, TBY-2 cells are commonly used as a relevant vegetal model. Second, they are non-chlorophyllic cells, therefore the porphyrin-PS can be tracked by fluorescence. Third, TBY-2 are fast growing plant cells, with cell multiplication ratio being up to 100 times within one week in adequate culture medium and environmental conditions and in addition these cells are capable to growth into darkness.

In practice, experimental conditions were carried out as following: exponential growth phase cells were incubated with porphyrins (concentration = $3.5.10^{-6}$ M) for 3 hours under dark conditions and orbital agitation (140 rpm). Then, cells were centrifuged to throw away excess of porphyrins, and new growth medium was added. After five hour illumination ($6.5.10^{3}$ $lm.m^{-2}$), cells were placed in the dark for 18 hours, then cell death percentage was determined using Trypan blue (blue staining of dead cells). Two kinds of control experiments were also performed, without porphyrins and without light.

Results are shown in Figure 81. Control experiments evidenced that in absence of light exposure, porphyrins did not induce cell death and thus were not cytotoxic for plant cells, and that both light and porphyrins are necessary to induce cell death. Indeed, all porphyrins tested upon irradiation induced significantly TBY-2 cell death. This probably occurs *via* ROS production (cf. paragraph III.1.2.3) which lead to lipid oxidation and subsequently to membrane disruption and cell death (cf paragraph II.2.2.3).[284]

The presence of metal atom (zinc) seems not to alter porphyrin properties. Indeed, both **CP** and **CP-Zn** produce ROS, they have the same photostability level and they similarly induce cell death. A direct comparison of **1** and **1-Zn** was prevented by the very low stability of **1-Zn**. Although cationic porphyrins are the most used in PDT (human cells) and PACT (bacteria), anionic molecules appeared more efficient to induce death on tobacco cells. Compound **1** appeared as the most efficient photosensitizer, which induced more than 90 % cell death whereas the other porphyrins induced less than 40 %, at the tested concentration (3.5 µM).

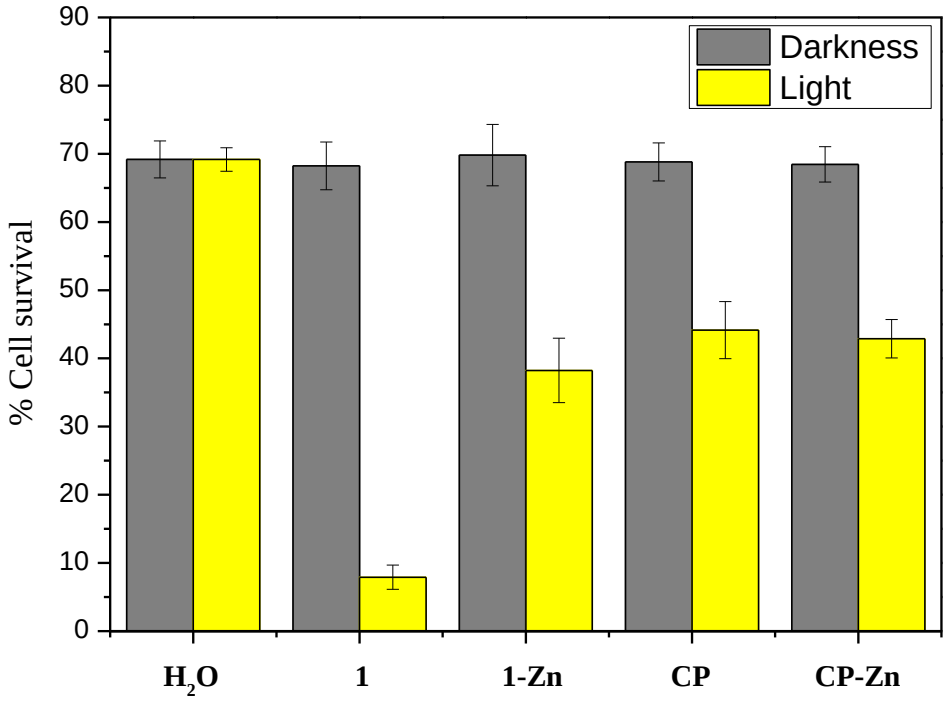

Figure 81: Percentage of TBY-2 cell survival after 5-hour illumination. Porphyrins were tested at concentration of 3.5 µM.

In conclusion to this section, although **1** is less effective than **CP** in terms of ROS production (both singlet oxygen and superoxide), it was more efficient than cationic porphyrins to induced TBY-2 cell death. These results led us to consider the development of new anionic free-base porphyrins in order to study influence of charge (number and/or nature of chemical functions) on ability to induce cell death.

2. New targeted anionic porphyrins

2.1. Strategy

To evaluate porphyrins as potential herbicide substances, our strategy was to modulate number and nature of charges. In this context, carboxylic acid and phosphonate functions were selected, as being well studied in the literature and that allow obtaining one anionic charge per function at pH values higher than 5. Indeed, pKa values are 4.2 and 1.42/6.92 for benzoic acid[342] and aryl phosphonic acid,[343] respectively while the pH value of TBY-2 growth medium is 5.8. Two of the targeted compounds were commercially available: 5,10,15,20-(tetra-4-

carboxyphenyl)porphyrin (**2**) and 5,10,15,20-(tetra-4-phosphonatophenyl)porphyrin (**5**) (Figure 82).

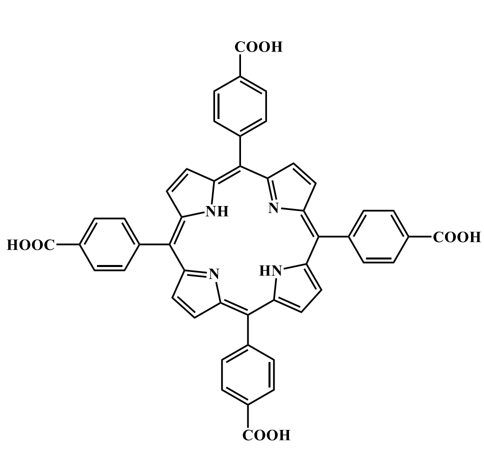

2

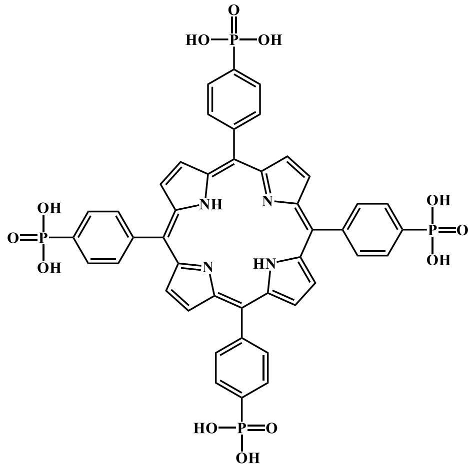

5

Figure 82: Commercial porphyrins **2** and **5**.

To modulate charge number, 5,10,15,20-(tetra-3,5-dihydroxyphenyl)porphyrin (**9**) has been chosen as precursor of octa-substituted-porphyrin **11** and **12** (Figure 83).

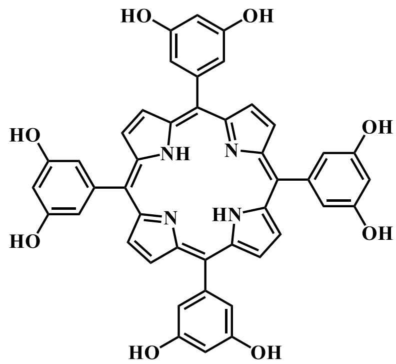

9

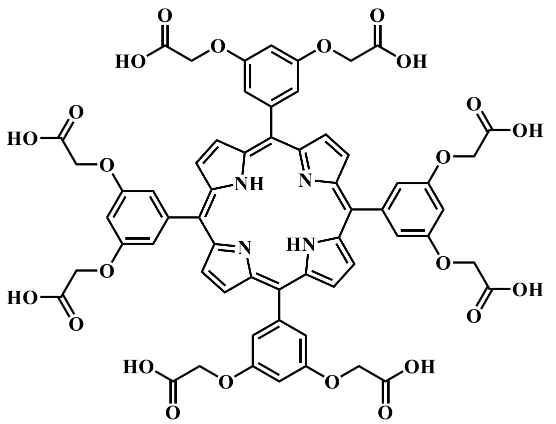

11

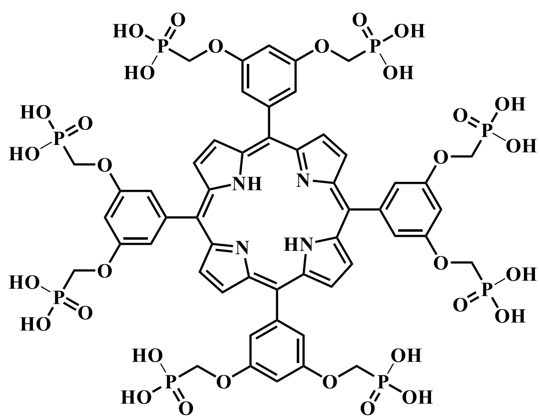

12

Figure 83: Structures of octa-anionic porphyrins **11** and **12**, as well as their precursor **9.**

However the strategy employed has required the use of an O-CH_2 linker between the phenyl rings on the porphyrin and acid or phosphonate functions. Thus, in order to evaluate the influence of this spacer on PS properties and stability, two more tetrakis analogues of **2** and **5** (**4** and **7,** respectively) were also synthesized from the same commercial porphyrin (Figure 84).

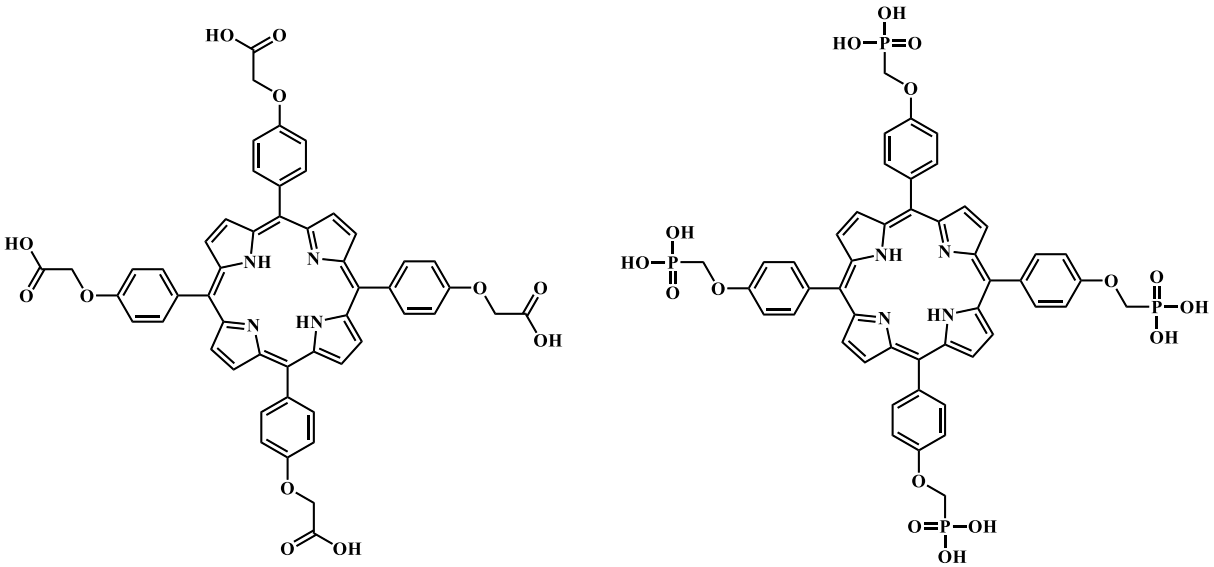

Figure 84: Structure of tetrakis anionic porphyrins **4** and **7**.

2.2. Synthesis of targeted compounds

2.2.1. Tetrakis porphyrins synthesis

Compounds **4** and **7** were synthesized from commercial 5,10,15,20-(4-hydroxyphenyl)porphyrin using similar protocol. The first step consisted in grafting a synthon bearing the protected acid or phosphonate function by simple Williamson reaction, followed by deprotection to obtain the desired compound.

2.2.1.1 *Tetra*-carboxylic acid porphyrin (**4**) synthesis

The protected analogue of **4** (compound **3**) was initially obtained by a simple Williamson reaction between 5,10,15,20-(4-hydroxyphenyl)porphyrin and an excess of *tert*-butyl bromoacetate (Figure 85). Reaction was made in DMF, at 70 °C, which is an adapted solvent for nucleophilic substitution. Reaction progress was monitored by TLC until complete disappearance of the starting porphyrin, and crude product was purified on chromatographic column after removing salts to give compound **3** with high yields (82 %).

Parameters such as temperature and *tert*-butyl bromoacetate equivalents were varying to study their influence on reaction yields (Table 6).

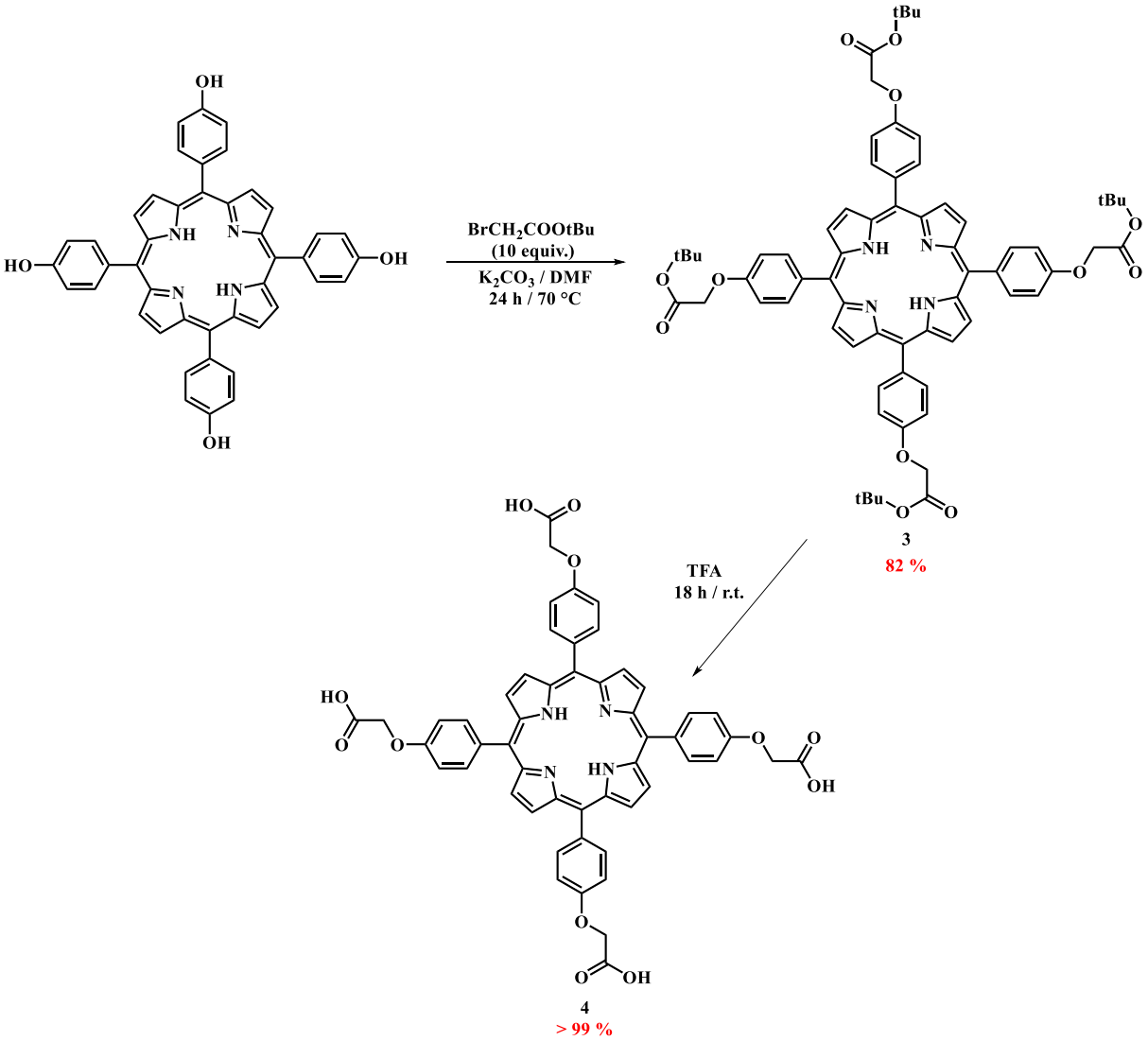

Figure 85: Synthesis pathway of compound **4**.

Table 6: Experimental conditions tested for **3** synthesis.

Entry	Equiv. $BrCH_2COOtBu$	Time (h)	Temperature	Yields (%)
1	8	24 (up to 48)	r.t.	27
2	10	24	70 °C	82
3	4	24	70° C	53
4	10	48	70 °C	79
5	20	48	70 °C	81

This study showed that, as it was expected, heat was required (Table 6, Entry 1). In addition if less equivalents of *tert*-butyl bromoacetate gave the desired product with low yields

(< 60 %, Table 6, Entry 3), more equivalents did not significantly increase yields, this might be partly explained by the occurrence of an emulsion that complicated treatment (Table 6, Entry 5).

The tertio-butyl protecting groups were eventually removed with TFA to give **4** with quantitative yield (Figure 85). By products formed during deprotection were eliminated by evaporation, and acid residues were removed by washing the final product with diethyl ether.

2.2.1.2 Tetraphosphonic acid porphyrin (**7**) synthesis

As for compound **4**, compound **7** was obtained thanks to nucleophilic substitution in DMF with an excess of diethyl-iodo-methylphosphonate (Figure 86).

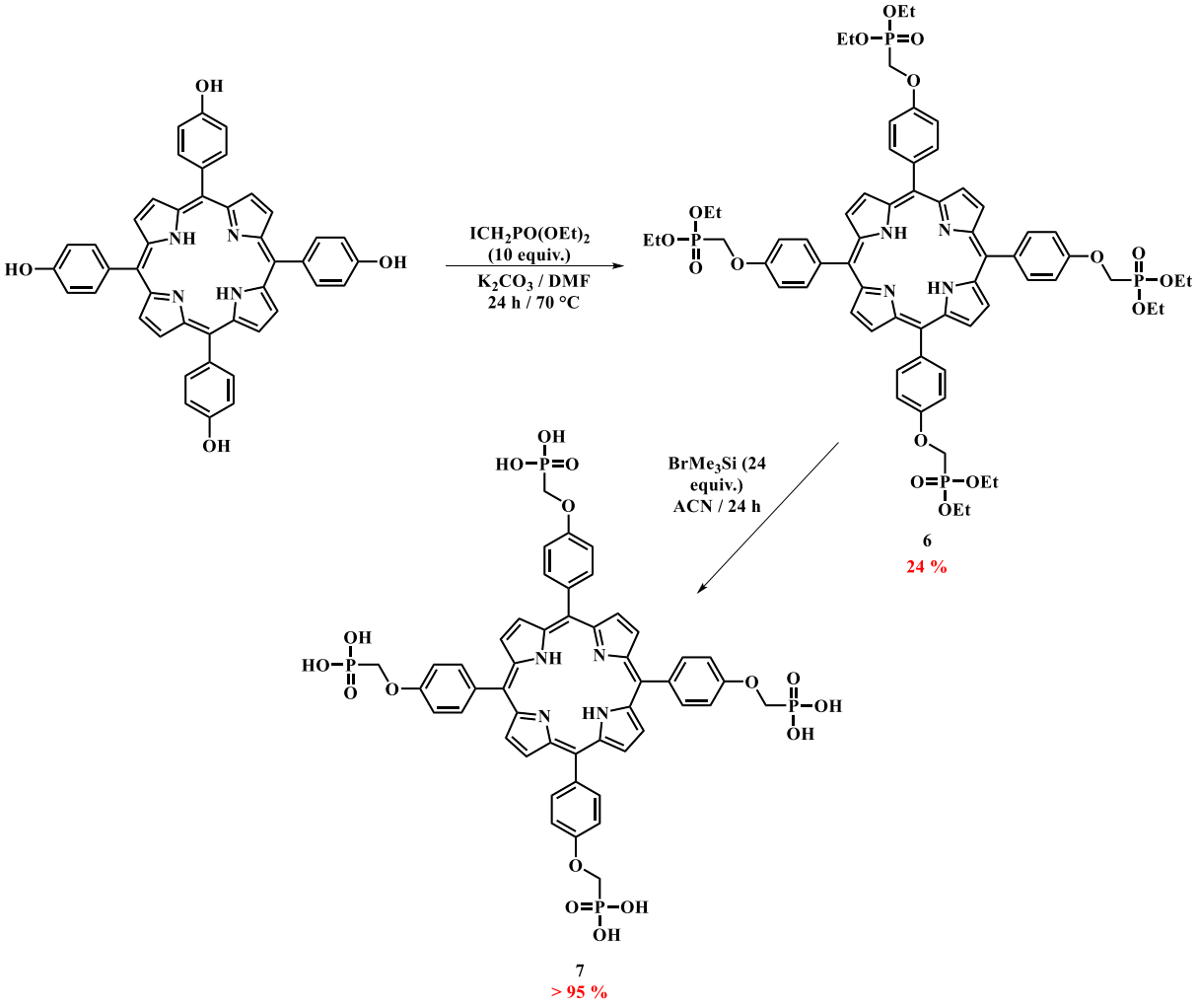

Figure 86: Synthesis pathway of compound **7**.

After 24 h at 70 °C, the solution was evaporated to dryness, then it was washed to remove salts. Following this step, an emulsion was formed in the separatory funnel, regardless of number of equivalents used. Release with NaCl was necessary to recover organic phase, which contained porphyrin mixture. After purification by chromatographic column, compound **6** was

obtained with 24 % yield. In order to increase this yield, modulation of operating conditions was tested (Table 7) without success, the optimal experimental conditions being the same than for **3** but leading to a lower yield (Table 6 and Table 7, Entries 2).

Table 7: Experimental conditions tested for **6** synthesis.

Try	Equiv. $ICH_2PO(OEt)_2$	Time (h)	Temperature	Yields (%)
1	8	48 (up to 96)	r.t.	6
2	10	24	70 °C	24
3	10	72	70 °C	15
4	8	72	70 °C	17
5	16	72	70 °C	degradation
6	10	2x8 min	M.W. (200 W / 120 °C)	-

This was surprising considering that iodine is a better leaving group than bromine. Based on this observation, two main options were possible. First, another counterion than K^+, better at solvating the iodine atom, could be used. However K_2CO_3 has advantage to be removed by simple filtration after reaction. The other option would consist in using another leaving group. Indeed, iodine can be replaced by tosyl or analogous as chlorophenylsulfonyloxy group. According to a patent,[344] the use of diethyl-4-chlorophenylsulfynoxymethyl phosphonate allows to obtain the diethylphosphonate derivative in high yields (up to 91 %). This solution should be tested soon in the laboratory

To obtain the corresponding phosphonic acid **7**, deprotection was performed using two methods, according to the literature.[345]

- Strategy 1: use of trimethylsilylchloride with sodium bromide, at 60 °C and under argon. In this case, remove the NaBr salt was very difficult for two main reasons. First liquid/liquid extraction was impossible due to the weak solubility of the deprotected porphyrins, and second during dialysis tests, porphyrins adsorbed onto membranes and were impossible to recover.

- Strategy 2: use of trimethylsilyl bromide (Figure 87). Porphyrin **6** was dissolved in acetonitrile with trimethylsilyl bromide (highly volatile) during 24 hours. Unfortunately, reaction progress was very difficult to observe. Indeed, reactant **6** has a very close frontal report on TLC compare to the silyl intermediate formed. Distillated water was added and the reaction solution was stirred for two hours in order to hydrolyze the silyl ether previously formed. To complete synthesis, compound **7** was obtained by simple evaporation as it removed solvent

(acetonitrile, boiling point: 82 °C) as well as byproducts (trimethylsilol 99 °C and bromoethane 32 °C).

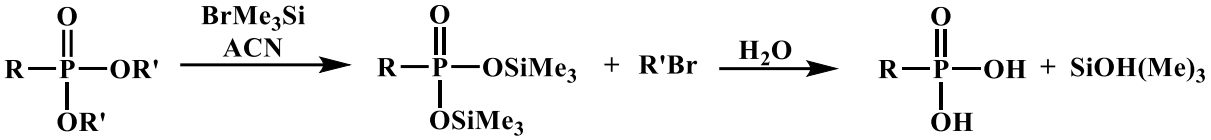

Figure 87: Cleavage of phosphonate diesters to phosphonic acid using $BrMe_3Si$.

2.2.2. Octacarboxylic acid porphyrin 27 synthesis

2.2.2.1 Octahydroxyl porphyrin (**9**) synthesis

As for tetrakis compounds **4** and **7**, nucleophilic substitution on hydroxyl group was performed. To this end, porphyrin **9** was synthesized but not directly with high yield due to the presence of 8 hydroxyl groups that could complicate the purification step. Therefore, the methoxy derivative (compound **8**) was first formed as porphyrin precursor (Figure 88).

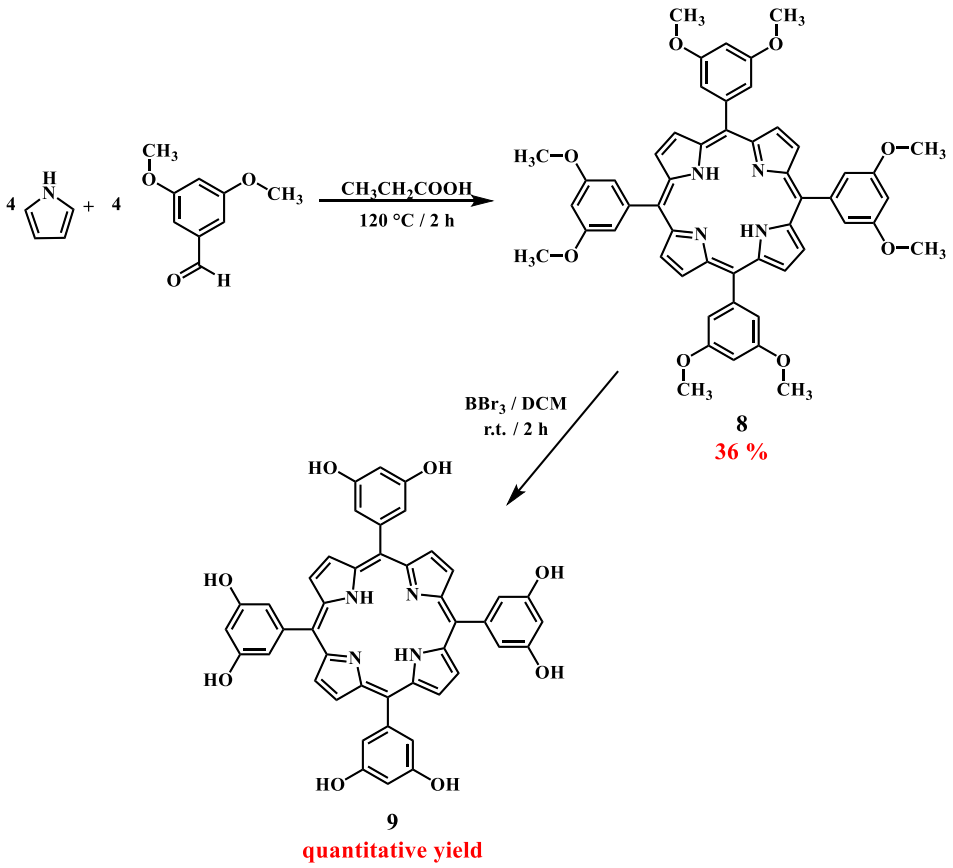

Figure 88: Synthetic pathway of compound **9**, precursor of compounds **11** and **12**.

In that purpose, 3,5-dimethoxybenzaldehyde and pyrrole reacted according to Little's method to give compound **8** with good yields. Then, methoxy groups were transformed into hydroxyls. The most commonly used solutions are mixtures of pyridine and hydrochloric acid at 220 °C,[346] or boron tri-halogenated (BBr_3 or BCl_3).[347,348] The last one was chosen as it needed milder conditions: BBr_3 in DCM and at room temperature (Figure 89).

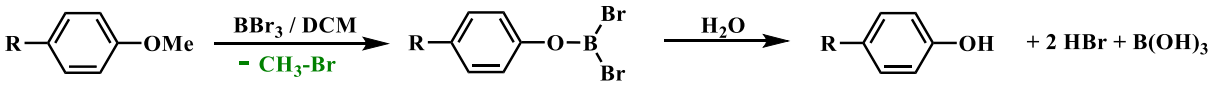

Figure 89: Mechanism of BBr3 on methylether function.

Reaction was stirred during 24 h in the dark, and solution took a green color due to HBr release and protonation of the porphyrin core. Then distillated water was added to cleave the O-Br bonds and formed alcoholic function. Finally, compound **9** was obtained after evaporation (bromomethane formed as a weak boiling point: 4 °C) and treated with Et_3N to remove acidity. Presence of boron salts prevents to calculate yields, but mass spectra and NMR confirmed disappearance of starting porphyrin **8**.

2.2.2.2 Octacarboxylic acid porphyrin (**11**) synthesis

Using the same protocol than for compound **3**, compound **10** was obtained using an excess of *tert*-butyl bromoacetate (20 equiv.) in DMF and at reflux during 48 h (Figure 90). TLC monitored the progress until complete disappearance of the starting porphyrin, and crude product was purified on chromatographic column, after salt removing, to give compound **10** with high yields (73 %). As previously mentioned for compound **3**, increasing equivalents of *tert*-butyl bromoacetate did not result in a significant gain of yields but it increased number of purification steps. Then, the tertio-butyl protecting group was removed with TFA to give **11** with quantitative yield (Figure 90). Byproducts formed during deprotection were eliminated during evaporation, and the acid residues were removed by washing with diethyl ether.

We have not been able to complete the synthesis of compound **12** yet, however the precursor **9** was obtained in sufficient amount, thus synthesis of **12** should be completed soon.

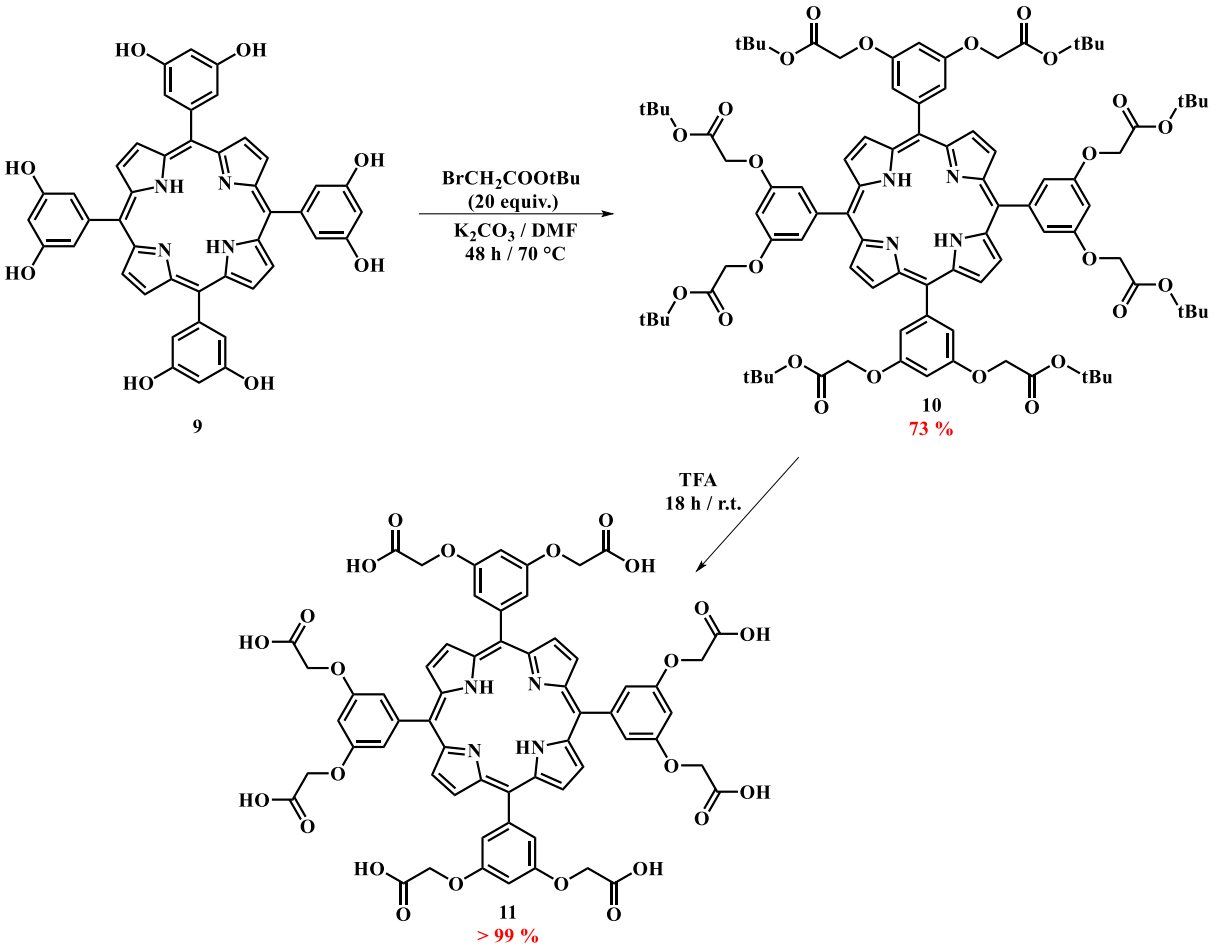

Figure 90: Synthesis pathway of compound **11**.

2.3. NMR characterizations

Although final compounds and precursors have different solubility properties, all NMR analyzes were performed in a common solvent: DMSO-d_6. The analyses of compounds **5** and **7** are still under progress due to their low solubility. Indeed, the evaluations already performed in organic solvents (methanol and DMSO) and the tests in D_2O (containing a few drops of sodium hydroxide itself dissolved in D_2O) were not conclusive as providing non-interpretable spectra, probably because of the sample dilution. For compounds **5**, **6** and **7**, ^{31}P, ^{1}H and ^{13}C NMR spectra were recorded.

- Compounds **3**, **4** and **6** (Table 8)

Compounds **3**, **4** and **6** have very similar structures. β-pyrrolic protons were the most de-shielded and appeared as a singlet. As expected, 2,6-aryl and 3,5-aryl protons were coupled, as evidenced by their respective coupling constants.

For compound **6**, protons of the O-CH_2 appeared as a doublet contrary to those of compounds **3** and **4**, which is attributed to the presence of phosphorus. Indeed, a proton-phosphorous coupling occurs, which is characterized by a coupling constant J higher than for the same proton-proton coupling. The same effect is observed with CH_2 of ethyl group (Table 8).

For compound **4**, acidic protons behave as expected *i.e.*, de-shielded and as a slightly intense and very broad singlet.

^{13}C NMR was also performed for all compounds and agreed with results of ^{1}H spectra. Disappearance of aliphatic signals between **3** and **4** confirmed total removing of tBu protecting groups. Because C-1 and C-2,6 aryl are very close, HMQC / HMBC analyzes should confirm their allocations.

In addition, ^{31}P NMR spectrum was realized for compound **6**. It exhibited only one signal at 19.9 ppm, in agreement with the literature.[349] Moreover, although we have not yet been able to obtain interpretable proton and carbon spectra, ^{31}P analysis of compound **7** exhibited only one signal at 13.1 ppm, which seems to confirm deprotection.

Table 8: ^{1}H NMR of compounds **3**, **4** and **6** in DMSO-d6. δ are in ppm.

H	**3**	**4**	**6**
β-pyrrolic	8.84 s (8H)	8.85 s (8H)	8.85 s (8H)
2,6-aryl	8.12 d (8.5 Hz) (8H)	8.13 d (8.1 Hz) (8H)	8.14 d (9.0 Hz) (8H)
3,5-aryl	7.35 d (8.5 Hz) (8H)	7.36 d (8.2 Hz) (8H)	7.48 d (8.5 Hz) (8H)
O-CH_2	4.96 s (8H)	4.99 s (8H)	4.74 d (10.0 Hz) (8H)
NH_{int}	-2.90 s (2H)	-2.90 s (2H)	-2.89 s (2H)
Tertbutyl	1.55 s (36H)	--	--
CH_2 (ethyl)	--	--	4.26 m (16 H)
CH_3 (ethyl)	--	--	1.50 t (7.0 Hz) (24 H)
OH (acid)	--	13.18 s_{el} (4H)	--

- Compounds **8**-**11** (Table 9)

As for tetrakis compounds, β-pyrrolic protons appeared as singlet in the same area for the four molecules. 2,6-aryl and 4-aryl protons were coupled, with characteristic meta-coupling constants (around 2 ppm). The slight shift observed for **9** might be explained by an effect of hydroxyl groups.

^{13}C NMR was also performed for all compounds and agree with results of ^{1}H spectra. Aliphatic area is particularly critical, indeed disappearance of signal at 55.4 ppm in compound **9** was characteristic of the complete demethylation. Then, as for tetrakis porphyrins **3** and **4**, ^{13}C signals show grafting of protected acid functions (**10**) then removing of tBu protecting groups (**11**).

Table 9: ^{1}H NMR of compounds **8-11** in DMSO-d6. δ are in ppm.

H	**8**	**9**	**10**	**11**
β-pyrrolic	8.91 s (8H)	8.94 s (8H)	8.90 s (8H)	8.94 s (8H)
2,6-aryl	7.37 d (2.5 Hz) (8H)	7.06 d (2.2 Hz) (8H)	7.37 d (2.1 Hz) (8H)	7.39 d (2.1 Hz) (8H)
4-aryl	6.98 t (2.5 Hz) (4H)	6.70 t (2.2 Hz) (4H)	6.98 t (2.1 Hz) (4H)	6.98 t (2.1 Hz) (4 H)
NH_{int}	-2.99 s (2H)	-3.02 s (2H)	-2.99 s (2H)	-3.00 s (2H)
$O\text{-}CH_2$	--	--	4.87 s (16 H)	4.88 s (16H)
$O\text{-}CH_3$	3.93 s (24H)	--	--	--
OH (alcohol)	--	9.30 s_{el} (8H)	--	--
Tertbutyl	--	--	1.41 s (72H)	--
OH (acid)	--	--	--	12.87 s_{el} (8H)

2.4. Mass spectra

Structural analysis of porphyrins **3-4** and **6-11** was confirmed by mass spectra (Table 10). All compounds showed the $[M+H]^+$ molecular peak. Compound **11** requested several analysis tests. Indeed ionization of the compound was limited by the presence of the eight acid functions. For this compound, “ion trap” technique was used, in which the sample was directly introduced and energies applied to ionize were higher than with the technique used for the other PS.

Table 10: m/z values of $[M+H]^+$ ions for compounds **3-4** and **6-11**; obtained by HRMS.

Porphyrins	Chemical formula	Monoisotopic mass	$[M+H]^+$
3	$C_{68}H_{70}N_4O_{12}$	1134.50	1135.7179
4	$C_{52}H_{38}N_4O_{12}$	910.25	911.3003
6	$C_{64}H_{74}N_4O_{16}P_4$	1279.20	1280.3453
7	$C_{48}H_{42}N_4O_{16}P_4$	1054.15	in progress
8	$C_{52}H_{46}N_4O_8$	854.33	855.3385
9	$C_{44}H_{30}N_4O_8$	742.21	743.2129
10	$C_{92}H_{110}N_4O_{24}$	1654.75	1655.7662
11	$C_{60}H_{46}N_4O_{24}$	1207.25	1208.3457

As for NMR, HRMS analysis confirmed the expected structures of all compounds.

3. Photophysical properties of tetrakis compounds

UV-Vis absorption, in water and as a function of pH values, and fluorescence emission properties of **1-2** and **4-5** were performed. Moreover, as preliminary work, ROS production was evaluated by EPR while photostability in TBY-2 growth medium by UV-Vis absorption. The study of compound **7** was postponed because NMR and MS did not yet confirmed its structure.

3.1. UV-Vis absorption

UV-Vis absorption spectra of compounds **1-2** and **4-5** were performed in water, at room temperature and at a concentration of *ca*. 2.10^{-6} $mol.L^{-1}$. Except for **1**, direct water solubilization was not possible. Therefore, the same protocol (in agreement with biological testing protocols) was used for all PS, that is addition of sodium hydroxide (3.75 equiv. by function) to obtain charged functions and thus complete water solubility. All results presented were from at least 3 independent experiments. UV-Vis spectra are shown in Figure 91 and the main characteristics are collected in Table 11. UV-Vis spectra were characteristic of free-base porphyrins. Indeed, a strong absorption band around 415 nm is observed, and other four less intense bands between 510 and 640 nm (Q bands). Compounds **4** and **5** exhibit a characteristic *etio-type* spectrum. The spectra of **1** and **2** are very similar to *etio-type*, but the intensities of the Q bands were particularly close to each other. Interestingly, **2** exhibited a much greater absorption intensity

than the other PS, particularly at the Soret band. This phenomenon could be due to the extension of the conjugation, especially compared to **4**.

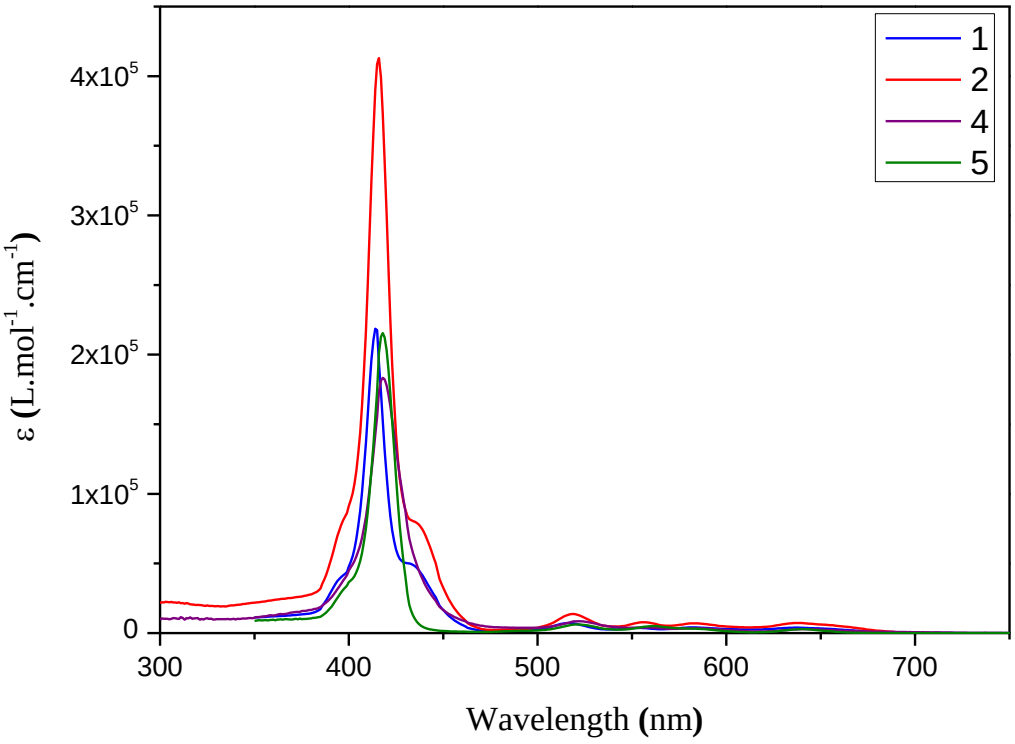

Figure 91: UV-Vis spectra of compounds **1-2** and **4-5**, in water.

Table 11: UV-Vis absorption of compounds **1-2** and **4-5** in water (pH = 8.2). All ε presented are the mean of three independent experiments.

Porphyrins	Absorption λ_{abs} (nm) and ε (10^{-3} L.mol.$^{-1}$.cm^{-1})				
	Soret	Q bands			
1	414 (219)	516 (7.3)	553 (3.7)	582 (4.1)	636 (3.9)
2	416 413)	518 (13.7)	556 (7.8)	583 (7)	638 (7.3)
4	418 (216)	521 (6.2)	561 (5)	586 (3)	640 (2.9)
5	418 (183)	522 (8.5)	558 (3.9)	583 (3.5)	640 (2.8)

The influence of pH on absorption profiles was assessed for the four PS as this parameter is of upmost importance in plant cells (Figure 92). As the protocol for solution preparation used NaOH (1 M), this study was made by acidification *via* controlled additions of fresh dilute hydrochloric acid solutions, at 10^{-4}, 10^{-3} and 10^{-2} M, successively. Porphyrin solutions were magnetic stirred in between each acid addition (and therefore each UV monitoring), in order to

homogenize. Finally, reversibility of porphyrin protonation phenomena was tested by controlled additions of NaOH at 10^{-2} M.

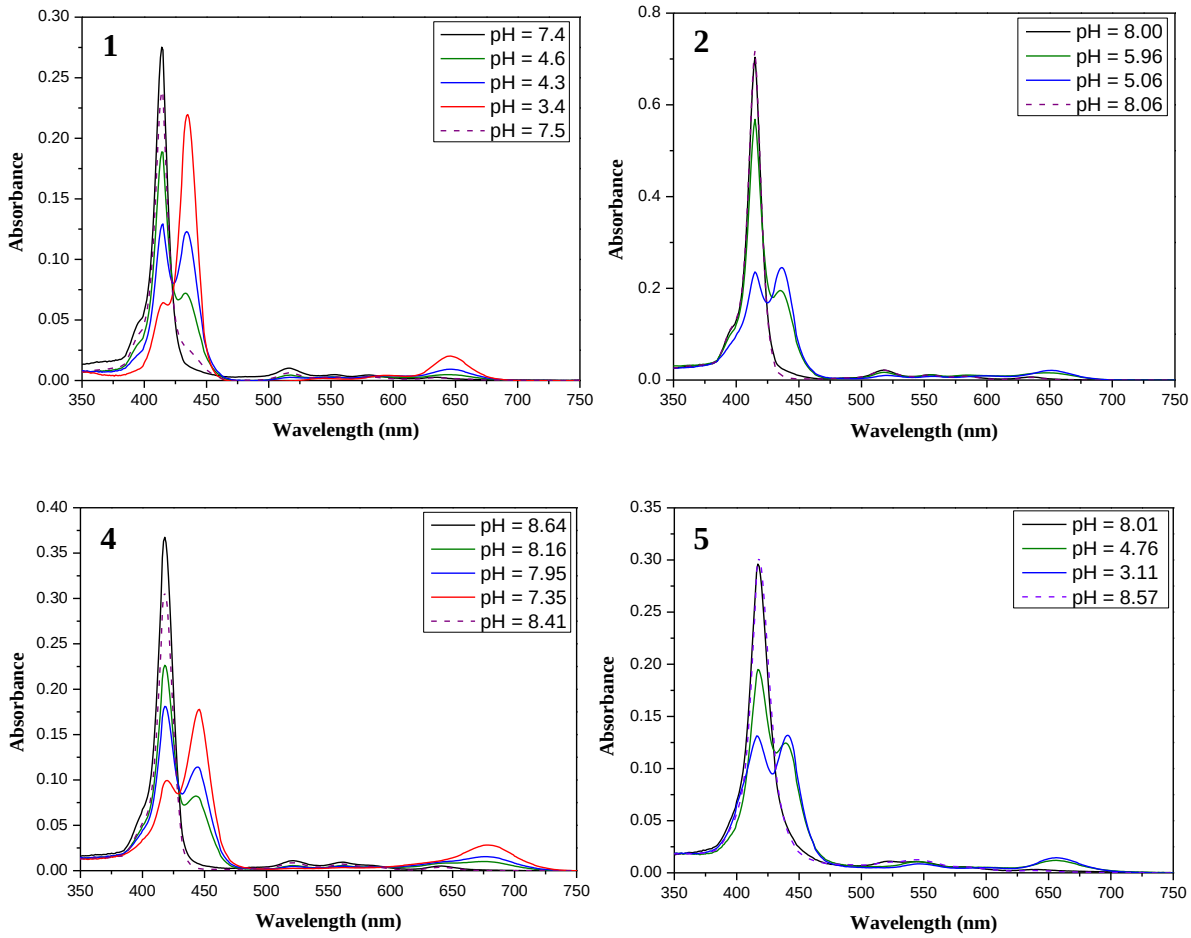

Figure 92: UV-Vis absorption spectra at different pH values. All spectra were performed in water and at a concentration of 2.10^{-6} M. Purple dashed lines represent the reversal process.

All compounds exhibited similar profiles. Indeed, when pH values decreased, new zwitterionic species appeared, characterized by two new red-shifted absorption bands. Having in mind the PS structure, the first band was observed from 440 to 460 nm and was assigned to the Soret band of the new species, and the second band was recorded from 650 to 700 nm, being assigned to the Q-bands. The spectral shifts were attributed to protonation of porphyrin cores (Figure 93).[350] Indeed, because of their internal environment, nitrogen atoms have a higher pKa value than the substituents, and thus are the first to be protonated (Figure 93).[351] It leads to an increase in symmetry and bathochromic (red) shifts, resulting in color change of PS, from purple to green (Figure 93).[350]

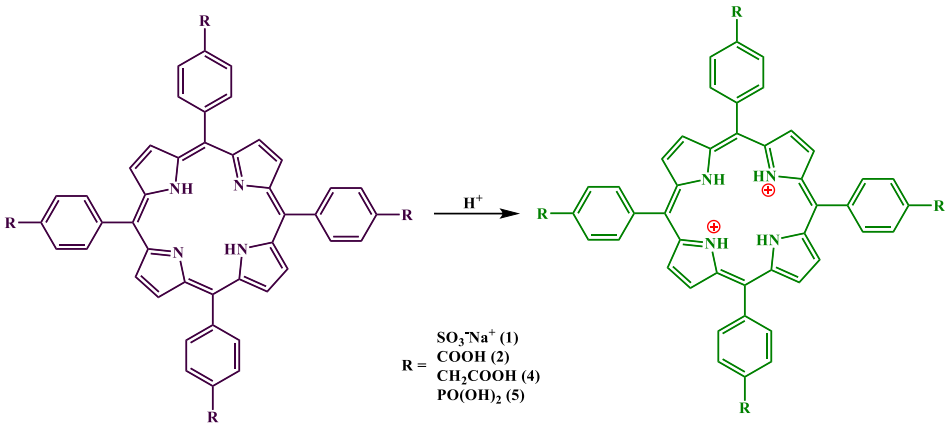

Figure 93: General structure of protonated porphyrins.

In all cases, observation of an isobestic point indicated that the stoichiometry did not change along charge state changes. It means that no side reactions occurred during the time of analysis. Assuming that molar extinction coefficients are virtually the same for both forms, the pH value at which they should exhibit the same maximum absorption of the Soret band should correspond to the pH at which the two forms are present in solution at the same concentration *i.e.*, pKa values corresponding to the nitrogen protonation. Namely, it is observed at pH values of 4.30, 3.11, 5.06 and 7.35/7.95 for **1**, **5**, **2** and **4**, respectively. Substituent effects on the porphyrin rings could explain these differences. Indeed, protonation of **4,** which is the only compound having four mesomeric donor effects *via* oxygen covalently linked to phenyls, occurs at a much higher pH than the other PS, which exhibit mesomeric attractor substituents. This is particularly relevant with **2** that it is structurally very close to **4**, and for which protonation occurs at a pH value of 5.06 (*vs.* 7.35 for **4**). Thus, as TBY-2 growth medium has a pH value of 5.8, compound **4** might exist exclusively in its zwitterionic form under these conditions, whereas **2** might exist in its both forms. In the case of **1** and **5**, only the non-protonated form occurs in the TBY-2 growth medium. Moreover, for **5**, only one of the two hydroxyl groups of phosphonic functions was in its charged form, due to the difference in pKa between them (6.92 and 1.42, respectively).

Reversibility of protonation was also evaluated by pH value increase with a dilute sodium hydroxide solution. Results are showed in Figure 92 as purple dashed lines. As expected for the four PS, higher pH fully gave back the neutral form *i.e.*, total reversibility.

3.2. Fluorescence emission

Corrected emission spectra of compounds **1-2**, **4** and **5** were performed in water, at room temperature, at a concentration *ca.* 10^{-6} M (Figure 94) and at an excitation wavelength λ_{exc} = 555 nm. Because no oxygen effect was observed on spectra, non-degassed solutions were used. All spectroscopic data of the four PS are summarized in Table 12. In addition, excitation spectra were conducted and exhibited similar profiles than UV-Vis spectra over the whole wavelength range, confirming the degree of purity required for biological testing.

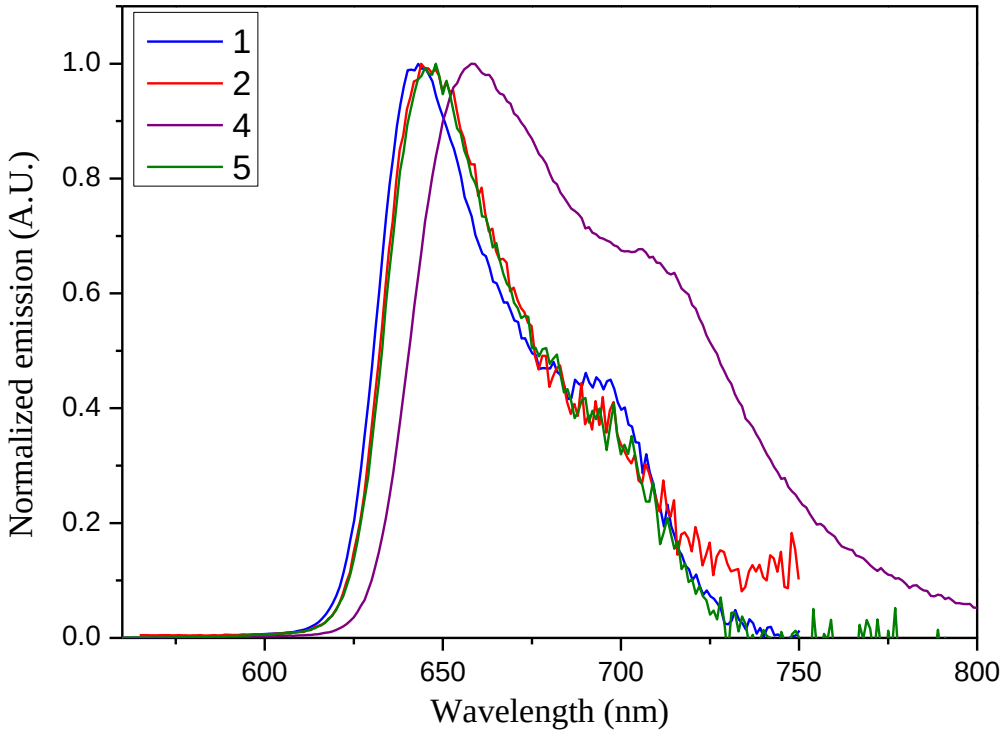

Figure 94: Fluorescence emission spectra of compounds **1-2** and **4-5** (λ_{exc} = 555 nm) in water.

As expected, all four PS exhibited the typical of free-base porphyrin profile, with emission at around 650 nm. Red-shift of the maximum of emission was observed for **4**. All compounds exhibited low fluorescence quantum yields, except **4**. Thus it may exist preferential non-radiative de-excitation pathways such as ISC that allows ROS production for all these compounds. For **4**, the behavior observed (red-shifting and higher fluorescence quantum yield compared to the other PS) could be due to the occurrence of J-aggregates that are known to favor red-shifted luminescence.[352–354] These aggregates are likely to be formed in the ground state, but can hardly been visualized. Moreover anionic porphyrins are known to form such aggregates according to their protonation degree and thus pH,[355] even if usually this

phenomenon is also observed at the ground state which is not the case for **4**. Whatever, this results underlined that **4** seems to be prone to aggregation compared to the other studied PS.

Table 12: Spectroscopic characteristics of compounds **1-2**, **4** and **5** in water (pH = 8.2). Fluorescence quantum yields are obtained from three independent experiments.

Porphyrins	λ_{max} (emission) (nm)	Φ_f *
1	643	0.05 (± 0.01)
2	644	0.15 (± 0.02)
4	658	0.28 (± 0.01)
5	648	0.09 (± 0.01)

λ_{exc} = 555 nm, in water (n = 1.333) at room temperature. H_2TPP in chloroform (n =1.446) was chosen as standard (Φ_f = 0.11).[356]

3.3. ROS production

Type I and II mechanisms may occur simultaneously and the ratio between these processes depends both on PS's nature and concentration, as well as other compounds involved in the reaction mainly oxygen and substrate. Thorough characterization of ROS production by photoexcitated porphyrins is a crucial step to figure out the preferred mechanism and effects on plant cells.[147]

Various identification methods exist according to ROS nature. The most convenient for singlet oxygen production is the direct observation of its emission spectrum at 1268 nm.[151] Nevertheless, this method does not quantifying superoxide anion production, while with Electronic Paramagnetic Resonance (EPR) both singlet oxygen and superoxide anion can be observed. A direct observation is however prevented due to very small lifetimes of these ROS ad non-radical nature of singlet oxygen. Spin traps were used, namely TEMP and DMPO for both singlet oxygen and superoxide anion; subsequently transformed into TEMPO and DMPO-OOH (Figure 95).[357,358]

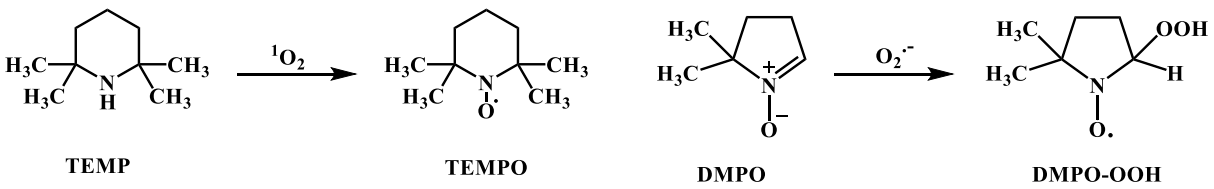

Figure 95: Singlet oxygen and superoxide detection using TEMP and DMPO as ROS spin traps.

Experiments were performed at room temperature, under visible illuminations (white light, 20 W halogen lamp, and 20.10^3 lm.m^{-2} intensity) and at a 40 µM concentration. Results obtained are presented in Figure 96 and Figure 97 for singlet oxygen and superoxide anion, respectively.

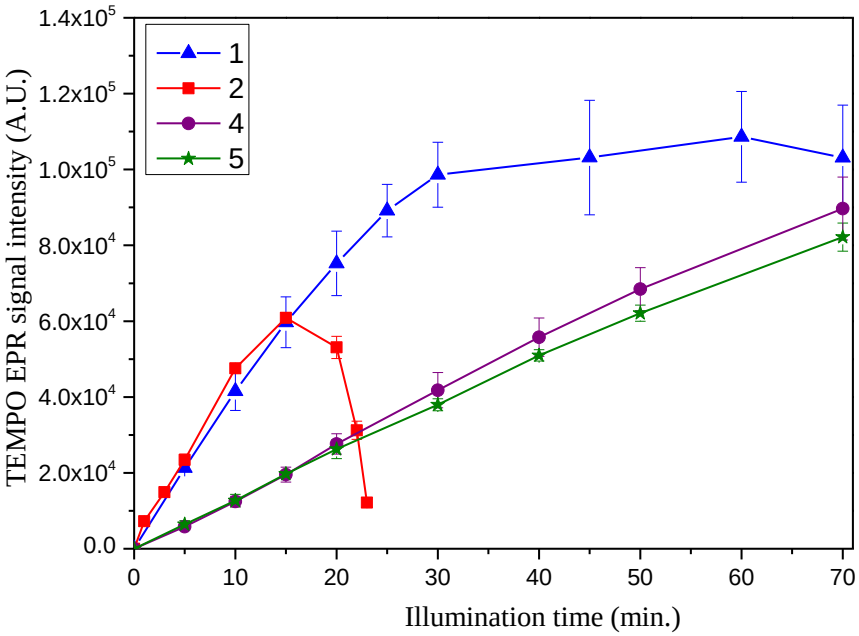

Figure 96: EPR signal of TEMPO generation upon irradiation. Values represent the averaged value ± S.D. obtained from 3 independent experiments.

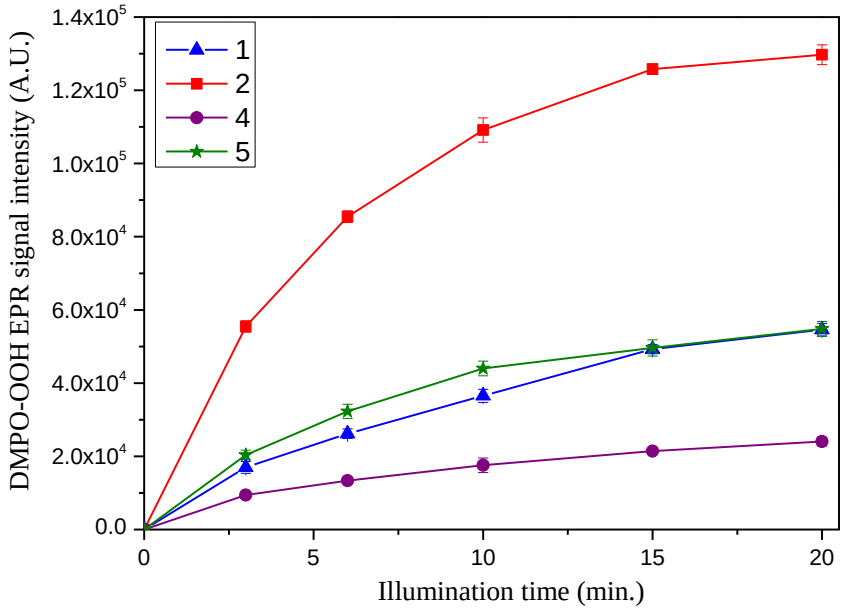

Figure 97: EPR signal of DMPO-OOH generation upon irradiation. Values represent the averaged value ± S.D. obtained from 3 independent experiments.

As shown in Figure 96 it seems that **1** and **2** produce more singlet oxygen than **4** and **5**. Interestingly, after 15 min irradiation, a dramatic decrease of ROS production was observed for **2**. A similar behavior was observed for **CP-Zn** (Figure 80), mostly probably attributed to porphyrin degradation by the ROS produced by the PS itself upon photoactivation. Compound **2** produces 2 to 6 times more superoxide anions than the three other porphyrins (Figure 97).

These results, coupled with the low fluorescence quantum yields observed, allow concluding that after excitation, ISC then reactions with environmental oxygen strongly contribute to the de-excitation process. For both type I and II mechanisms, **2** seems to be the more efficient compound, which is partly explained by the fact that this molecule is also the best absorber (UV-Vis spectra, Figure 91), whereas **4** is the weakest one. The higher fluorescence quantum yield of this compound compared to the other is also in agreement with less efficient ROS production. The behavior of **1** is also particularly interesting as this compound is a good producer of singlet oxygen but a bad producer of superoxide anion. Thus, the comparison of the effect of these PS on plant cells and their ROS production ability together should allow us to conclude on the type of mechanism involved in the plant cells.

After studying the behavior of these different molecules in the water, as in the preliminary study, investigation in culture medium may lead to further information.

3.4. Photostability study

Photostability of the four PS in the TBY-2 growth medium was also studied (Figure 98). For this purpose, their absorption spectra were monitored for different illumination times under the same conditions than those used with plant cells (white light and concentration of 2.10^{-6} M). Soret band intensity and other modulation of the UV-Vis spectrum profile were carefully monitored as reflecting photobleaching and/or photodegradation.

For **1**, **2** and **5**, no modification of the absorption profile was observed even after 5-hour illumination, except on peak intensities. It means that these three PS did not undergo phototransformation but only photobleaching. On the contrary, compound **4** showed a profound change in its UV-Vis spectrum with appearance of new bands at 485 nm and 728 nm after slightly more than 2 hours under darkness (Figure 99). Moreover, low stability was evidenced because after 3-hour incubation under darkness a decrease of more than 50 % of Soret band intensity was monitored.

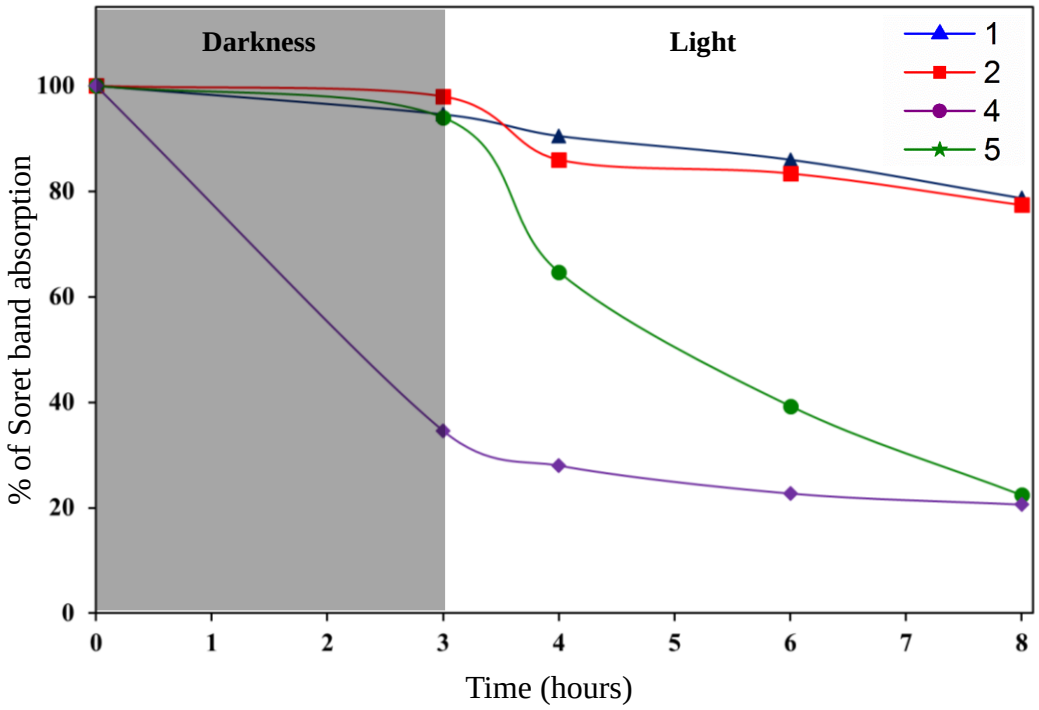

Figure 98: Photostability of compounds **1-2**, **4** and **5** in TBY-2 growth medium. Results are from 3 independent experiments.

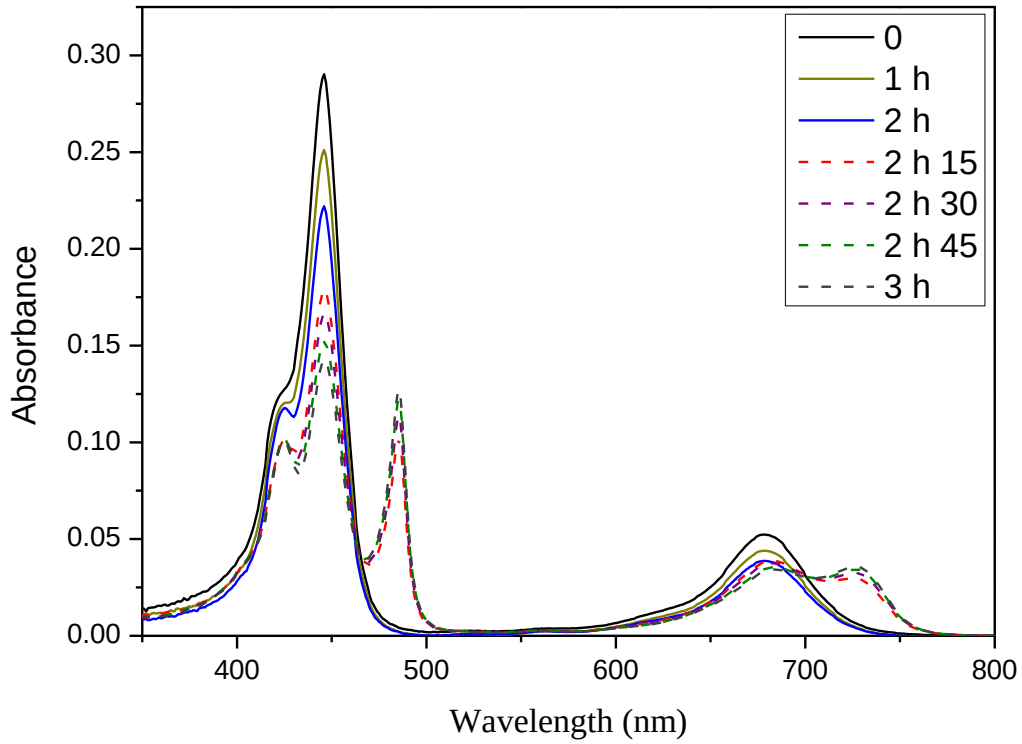

Figure 99: UV-Vis spectra of compound **4** aggregates formation during 3 hours in obscurity, in TBY-2 culture medium (C = $3.5.10^{-6}$ M)

Aggregate formation could rationalize these low stability and spectral changes. Indeed, the culture medium has a pH value of 5.8 while compound **4** undergoes protonation of the central nitrogen at pH values higher than 7 (Figure 92). Thus, in medium, **4** is rapidly protonated as indicated by the occurrence of the Soret band at 450 nm and Q band at 679 nm. Then, 2 hours after incubation under darkness (T = 2 h 15, Figure 99), aggregates may appear with a new red-shifted band at 728 nm. As described in 1994 by Ribó et *al.* with *meso*-tetrakis(4-sulfonatophenyl)porphyrins (Figure 100),[355,359] edge-to-edge aggregation (J-aggregates) is likely between the negative charges of carboxylate functions and the positive charges of the core nitrogens. These aggregation phenomenon can partly explain the decrease in Soret band intensity, which is therefore not only due to photobleaching processes.

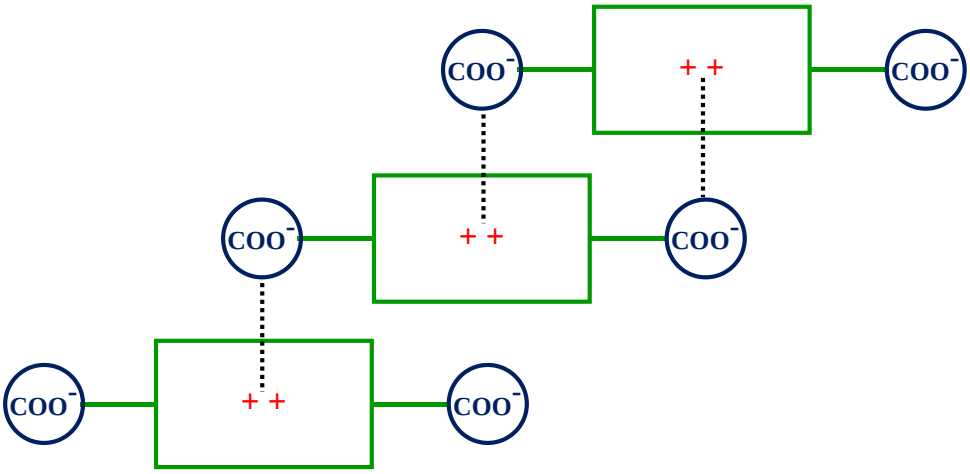

Figure 100: Edge-to-edge aggregation (J-aggregates) through intermolecular stabilized zwiterrion, according to Ribó et *al.*

Finally, in the case of **5** a sudden decrease of Soret band intensity is observed after 1-hour illumination. As no absorption spectrum modification was recorded, aggregate formation is ruled out and we can argue that this behavior is due to photo-induced ROS production that could degrade **5**. Moreover, because this phenomenon was not observed during EPR measurements, we can conclude that 1) longer illumination (hours for this study *vs* minutes for EPR) and 2) specific interaction of this particular PS and compounds contained in the TBY-2 growth medium used (2,4-dichlorophenoxyacetic acid, thiamine nicotinic acid, glycine…) are involved.

4. Bioassays

Biological experiments were performed on the TBY-2 tobacco cells (Dr. C. Riou, LCSN) following similar experimental conditions than for the preliminary study: exponential growth phase cells were incubated with porphyrins (C = 2.10^{-6} M) for 3 hours under dark and agitation. Then cells were centrifuged to throw away the excess of porphyrins and new TBY-2 growth medium was added. After 3-hour illumination, they were placed in the dark for 18 hours, then cell death percentage was determined using Trypan blue (staining method of dead cells) (Figure 101).

As in the preliminary work, controls without light exposition (darkness in Figure 101) and without porphyrin addition (data not shown) showed that both porphyrins and light are required to induce cell death and thus that porphyrins alone were not cytotoxic for plant cells at the tested concentration (2 µM). On the contrary, irradiated porphyrins induced significant TBY-2 cell death, up to 70 % after 3 hours, probably *via* ROS production that trigger oxidation of essential cell components such as lipids, proteins and DNA, which consequently led to cell death (Figure 101). However, after 3-hour light irradiation, induction of cell death was very different from one porphyrin to another (Figure 101).

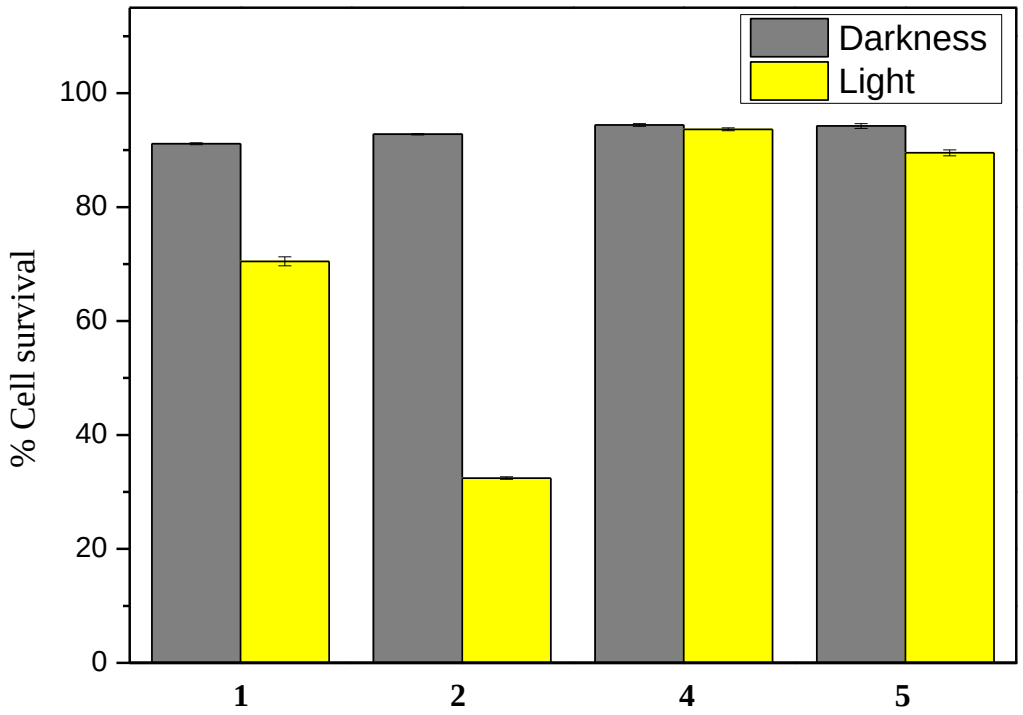

Figure 101: Percentage of TBY-2 cell survival. Results presented are from at least 3 independents experiments (C = 2 µM).

On one side **4** and **5** exhibited very few or no effects whereas on the other side, **1** and **2** induced significant cell death. In case of **4**, the total lack of effect may be partially due to aggregation phenomena as evidenced in the culture medium. Aggregates cannot efficiently interact with cells to allow penetration, which means that they are systematically removed during rinse step. Thus, when cells were exposed to light, the medium did not contain porphyrins at all (or only very low concentrations to enable any observable effects), so no ROS were produced and no cell death was observed. Moreover, even if some **4** molecules could interact with cells (according to Figure 98, some were not aggregated), ROS production produced by this compound was very low compared to the other PS (Figure 96 and Figure 97).

For **5**, a slight phototoxic effect (10 % of cells death after 3 hours illumination) was observed. This low efficiency may be explained by its weak photostability (Figure 98). Indeed, **5** was degraded very rapidly after light irradiation (1 h) and thus cannot produce ROS anymore and as a consequence induce cells death. Moreover, **5** slightly produced more superoxide anion than **4** whereas these two PS had the same production profile concerning singlet oxygen Figure 96 and Figure 97). So, type I mechanism could be the most important mechanism involved, as only **5** showed cell death ability.

Compounds **1** and **2** induced a higher percentage of cell death, namely 29.5 and 67.6 % respectively (Figure 101**).** Some experiments as showed that **1** exhibited similar herbicidal effects than **2**, but for concentration 1.75 time higher ($3.5.10^{-6}$ M). This difference in efficiency confirms the previous hypothesis and the favored occurrence of Type I mechanism. Indeed, if **1** and **2** had similar photostability and initial singlet oxygen production (Figure 96 and Figure 98), **2** was much more efficient in superoxide anion production (Figure 97). Moreover, higher coefficient absorption (see Table 11 and Figure 91) for **2** could reinforce its efficiency, even if its quantum yield (0.15 ± 0.02; Table 12) was higher than for **1** (0,05 ± 0.01; Table 12), but probably not that much.

Even if **1** and **5** had similar efficiency at producing superoxide anion, greater herbicidal effects of **1** with respect to **5** could be explained by, as mentioned previously, a different photostability (Figure 98) but also by a partial occurrence of Type II mechanism as both mechanisms are usually concomitant.[147,360] Moreover, confocal microscopy investigations showed that **1** was trapped in cell wall whereas **2** was capable of cell and nucleus penetration. On the contrary, **5** seemed not to penetrate cells, highlighting the role of chemical function on cell penetration.

5. Conclusion

The use of exogenous charged porphyrins on tobacco cells was achieved as a proof of concept for using porphyrins as new herbicides (Figure 81). Then, a series of anionic porphyrins was suggested, among which some were synthesized. All compounds were characterized by UV-Vis absorption and fluorescence emission spectroscopy, as well as by NMR (^{1}H, ^{13}C and ^{31}P if appropriate) and mass spectra. For tetrakis compounds, ROS production (both superoxide and singlet oxygen), pH influence and photostability in TBY-2 growth medium were also evaluated. Biological assays on tobacco cells have been initiated as well, providing encouraging results for **2** (Figure 101). Further studies will be conducted to confirm all hypotheses formulated thanks to this study. In particular, along this line and with the sake of establishing accurate structure-activity relationship, investigation on anionic porphyrins will continue. Octo-porphyrin **11** is currently studied to i) confirm importance of mesomeric donor substituents and their position on acid-base properties; ii) evaluate photostability; iii) rationalize the impact of the eight substituents on aggregation; iv) elucidate their localization in plant cells as confocal microscopy already showed that PS penetration depend on their chemical structure. Likewise **12** will be synthesized soon and will allow a quantitative comparison between carboxylate and phosphonate derivatives.

Although promising, these results obtained on tobacco cells must now be transferred to plants (e.g. tomato). Indeed not only chemical composition of cells (organic molecules or environmental oxygen) but also substrate availability change from one species to another. For example, green plants use photosynthesis and they are thus rich in oxygen, which can promote type II mechanism. Moreover, assays on plant cells remains far from those on plant organisms, which are more complex (*e.g.* cellular interactions in plant, influencing defensive response in the event of oxidative stress). This is the case for cationic porphyrins, which are less efficient on tobacco cells than anionic but more on tomato (non-published works) and other plants.[240,331]

Moreover, the weak fluorescence quantum yields of porphyrins prevent any fine localization in plants (or in chlorophyll cells). In this context, tagged porphyrins with fluorophores is a promising solution.

Tagged Porphyrins

1. State of the art in molecular systems such dyads

According to the dictionary, "dyad" has several definitions. It can be a group of two people in sociology; a set of two notes in music; a group of two students working together in pedagogy; a pair of sister chromatids in biology; a product in mathematics; or symmetry in genetics. So whatever the field of application dyad is pair. Going back to the etymological roots the Greek *dyo* indeed means two. Here we are going to focus on pairs of chromophores.

1.1. Generalities

1.1.1. Definition

In chemistry a dyad is generally a molecular assembly consisting of two patterns (or molecules) often covalently linked and possibly interacting together. This definition is the simplest that can be given, however this category of molecules is vast and encompass a wide range of structures and numerous different properties.

The design of a dyad is always though in response to a particular expectation. Such molecular systems are attractive because joining two molecules exhibiting different properties and thus may lead to derivatives having dual action. One can even expect new effects coming for example from synergic actions. Dyads can consequently find place in a large scale of applications (*e.g.* energetics, sanitary…). Moreover, the properties of dyads can also be modulated by their global chemical structure: covalent bond, metal complexation,[361] presence of a spacer,[362] conjugation extension…[363,364] All these parameters (in relation to constituting moieties) can have an influence of the final outcome.[365] For example, the final purpose may be Photo-induced Electron Transfer (PET) thanks to association of an electron donor (D) and an acceptor (A). PET reactions are crucial for energy storage in both biological and photovoltaic systems.[365] There are numerous possible molecular combinations that could favor PET, and it is far from the scope of this work to detail all of them. Historically, ruthenium(II) α-diimine complexes are among the most popular photosensitizers for electron (but also energy) transfer.[366] Fullerenes is an attractive electron acceptor and have been used in many dyads,[367] in association with a wide range of donors. Porphyrins and similar derivatives (phthalocyanines, corolles, diazaporphyrins...)[368–371] but also BODIPY or ferrocene are few examples often depicted in literature (Figure 102).[372–374]

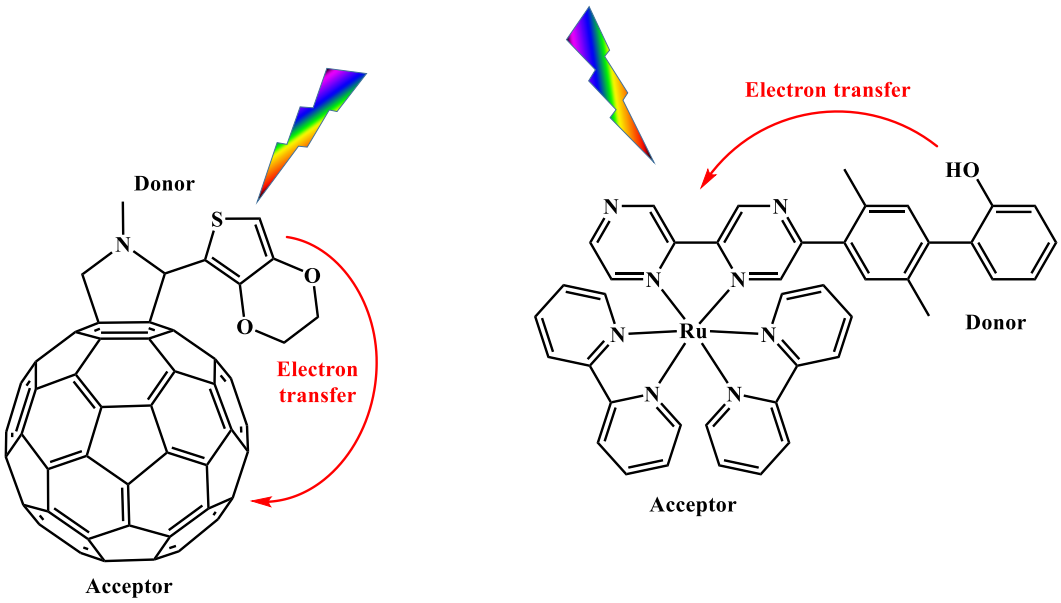

Figure 102: Examples of structure allowing electron transfer.

Dyads also represent an attractive way to favor energy transfer. In this case, one part of the dyad acts as a collecting energy antenna whereas the second moiety is the acceptor. This goal may be pursued for example to improve absorption properties of acceptors. As for electron transfer, there are numerous candidate compounds but BODIPYs,[375] fullerenes[376] or perylene diimide[377] can be cited as particularly relevant compounds (Figure 103).

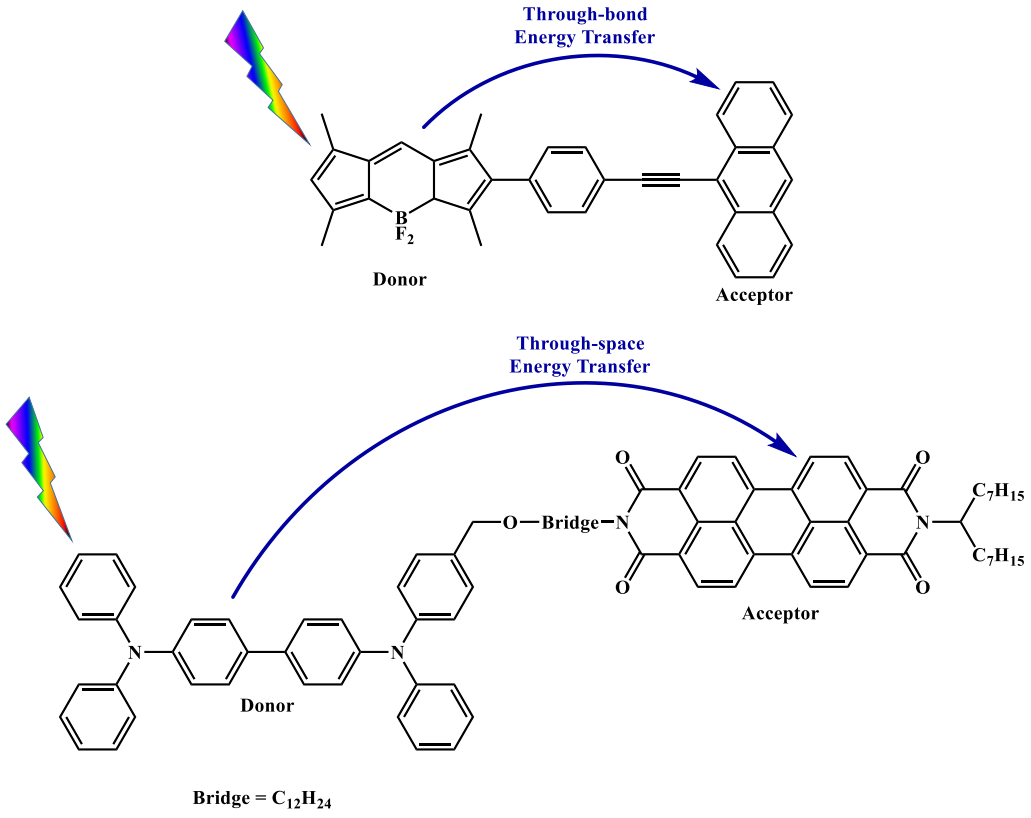

Figure 103: Example of structures allowing energy transfer.

Based on electron and energy transfer processes, fluorescence switches have attracted increasing interest due to their potential applications in molecular switches, optical data storage, fluorescent biological markers and other molecular devices. In such dyads, a molecule with a particular property dependent on an external stimulus (electrochemical,[378] chemical,[379] pH,[380] thermal[381]…) is anchored to a fluorescent moiety, and thus modulate fluorescence emission characteristics of the fluorophore in the dyad. Among others examples, BODIPY and anthracene fluorophore are widely used in this field due to their specific photophysical properties. For example, Thilagar and De Souza have recently developed a series of boryl-BODIPY dyads[382] and anthracene derivatives, respectively (Figure 104).[383] In addition, the synthesis of new compounds capable of answering to different stimuli has been explored e.g., Dou *et al.* have designed new molecules, for which fluorescence emission color changes depending on stimuli (heating, pH or grinding).[384]

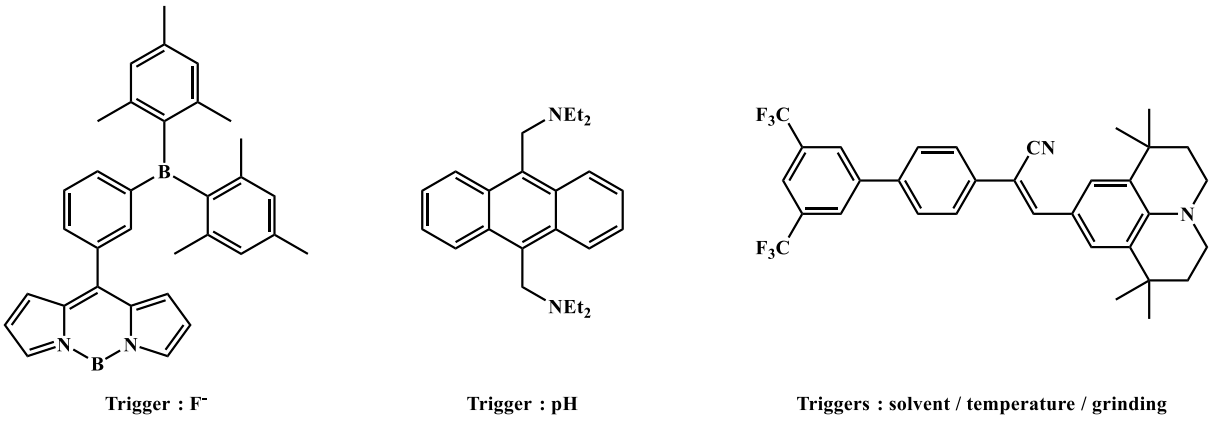

Figure 104: On-off fluorescence switches dyads according to Thilagar (left), De Silva (middle) and Dou (right).

All these processes are photo-induced. However, for the special case of biological applications, active substances can also be coupled to fluorophore (*e.g.* rhodamine, fluorescein…) with the sake of fluorescent labelling. There are various reasons requiring such labelling: weak quantum yields of the biologically compounds; same fluorescence emission wavelength than environmental molecules (*e.g.* chlorophylls in plants); or just no fluorescence properties at all. In such a use, both the biologically active compound and the fluorophore tag should keep their own properties when being in dyad. For example, protein can be tagged with a fluorescent one.[385] Fluorescein is also often used, especially covalently bounded to a drug molecule like peptide or antibody (Figure 105) in order to locate their receptors.[386]

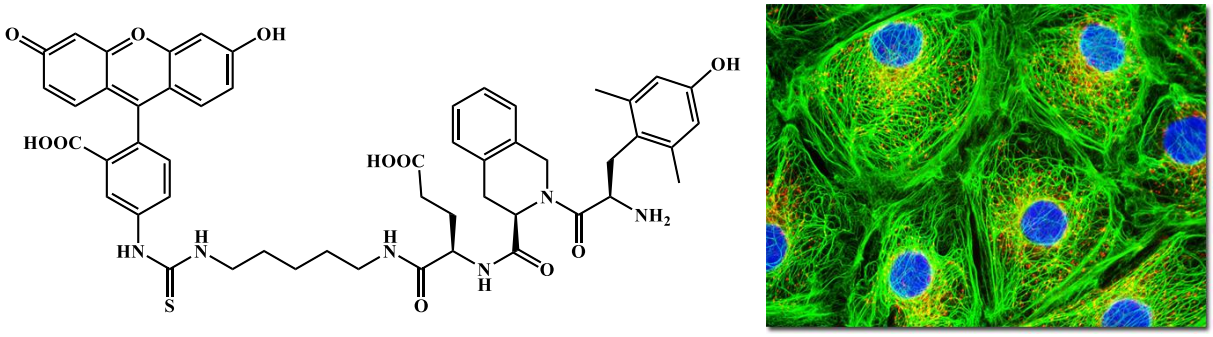

Figure 105: On left peptide labelled with fluorescein. On right Kangaroo Kidney Epithelial Cells (PtK2) tagged with fluorescein. **Source:** micro.magnet.fsu.edu.

1.1.2. Potential applications

Due to all possibilities that are offered by dyad systems, the field of applications seems to be infinite: in artificial photosynthesis, where dyads make possible synthesis of structures containing collecting antenna coupled to energy acceptor unit; in organic electronics; in dye-sensitized solar cells (DSSCs) and organic photovoltaic devices (OPV); in photodynamic therapy, where absorption properties of porphyrins (which are used as photosensitizers) can be improved by the use of two-photon absorption antenna.[387] For all these applications, to control interactions between both moieties of dyads is a prerequisite. Thus, in the next section, we will discuss on all information that could help at characterizing these interactions.

1.2. Ground state characterizations

UV-Vis absorption spectra may provide preliminary but precious information concerning interactions into the dyad at the ground state. In case of no interactions, the sum of the UV-Vis spectra of both patterns must perfectly overlap the dyad spectrum. If not, and if some new absorption band are observed in the dyad spectrum, this points the existence of a strong interaction between the two moieties within the dyad. For example, in the case of strong electron donor and acceptor association, an internal charge transfer (ICT) can occur, the corresponding absorption band (position and intensity) being sensitive to solvent. Usually in such dyads, both moieties are linked through a conjugated spacer or they are even merged (Figure 106).[388] Such effect may also occur in dyads made with organometallic patterns (*e.g.* ruthenium or lanthanides). Depending on the direction of CT the transition involved are called either ligand-to-metal[389] (LMCT) or metal-to-ligand (MLCT) charge transfer.[390,391]

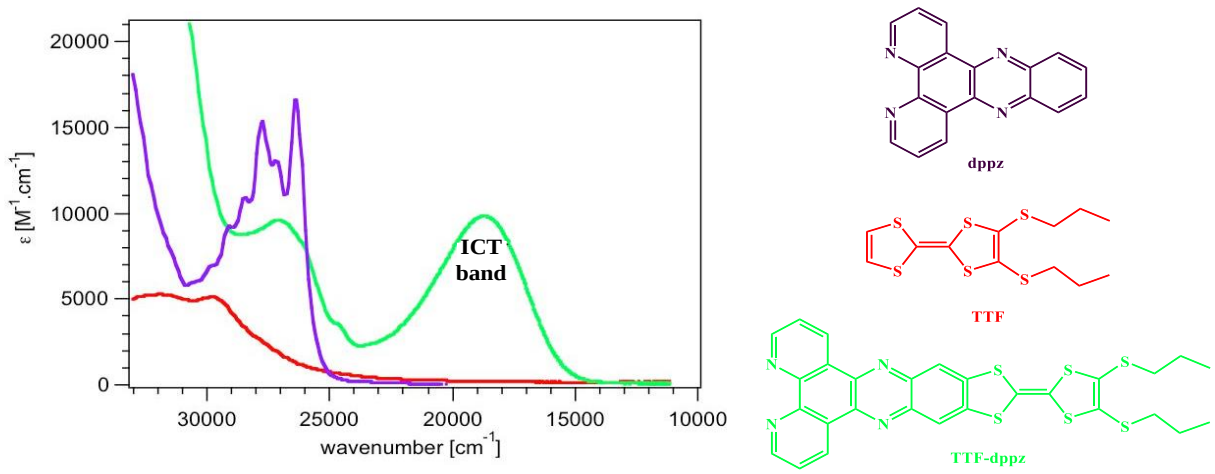

Figure 106: Example of ICT character on UV-Visible spectrum.

Source: Geneva University (Science Faculty).

1.3. Photo-induced process

Absence of ICT band at ground state does not mean that there's no interaction in dyad. Indeed, main phenomena take place after excitation of the molecule, which may lead to electron or energy transfer.

1.3.1. Electron transfer

The photoinduced electron transfer (PET) can occur according to two possible pathways depending of exciton position.

In a simple molecular orbital picture, one-photon absorption by a donor induce one electron excitation from HOMO to LUMO. The excited electron is then transferred to the LUMO of the acceptor, being lower in energy; this results in the creation of a separated charge state (Figure 107). This process can simply be seen as an oxidation by electron transfer.

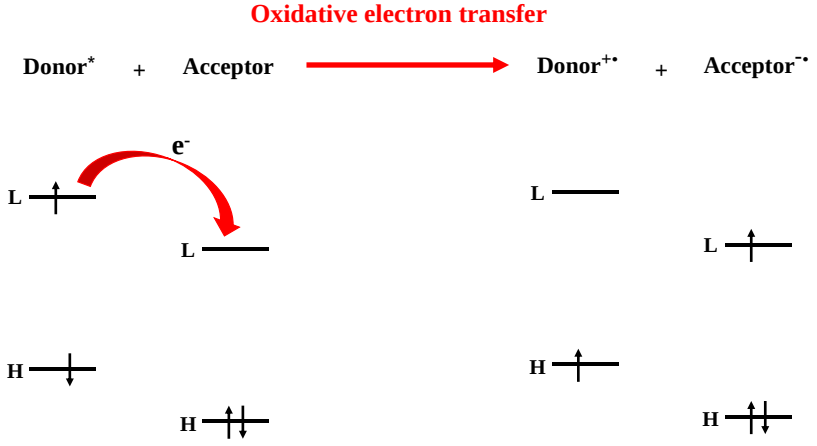

Figure 107: Oxidative electron transfer.

Conversely, one-photon absorption by the acceptor promotes an electron to the LUMO of the acceptor, leaving a lack in the HOMO that is fulfilled by electron transfer from the HOMO of the donor (Figure 108). This is a reduction by electron transfer.

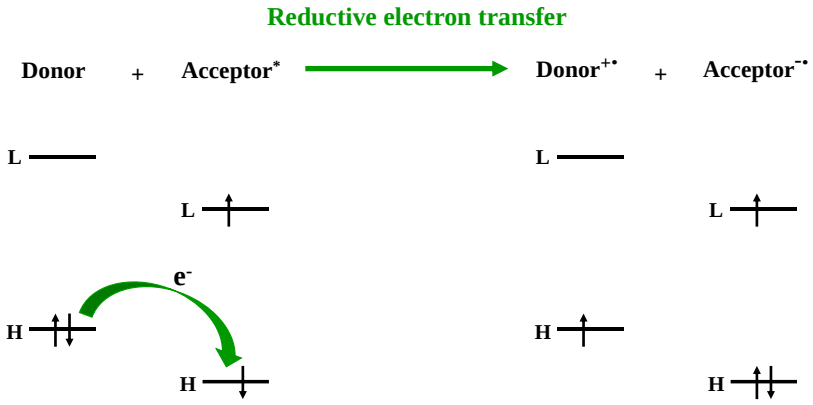

Figure 108: Reductive electron transfer.

To know if an electron transfer between a donor and an acceptor is thermodynamically allowed, one can determine the feasibility of electron transfer from the singlet state to the charge-separated state (CSS). For that purpose, energy levels of the involved states (Equation 7**a**) can be determined according to the Rehm-Weller equation (Equation 7**b**):[392,393]

$$\textbf{(a)}\ E_{CSS} = E_{S1} + \Delta G^{0}$$

$$\textbf{(b)}\ \Delta G^{0} = E_{(ox)} - E_{(red)} - E^{0\text{-}0} - \frac{e^{2}}{4.\pi.\varepsilon.r}$$

Equation 7: (1) Separate charge state equation and **(2)** Rehm-Weller equation.

Where:

- E_{CSS} (in eV): charge-separated state energy
- E_{S1} (in eV) = first excited state energy
- $E_{(ox)}$ (in eV): first oxidation potential of the donor, into dyad.
- $E_{(red)}$ (in eV): first reduction potential of the acceptor, into dyad.
- $E^{0\text{-}0}$ (in eV): fundamental transition value of excited moiety.
- $\frac{e^{2}}{4.\pi.\varepsilon.r}$ (in eV): Coulombic term.

1.3.2. Energy transfer

Energy transfer is only possible if the donor's emission spectrum overlaps (even partially) the acceptor's absorption spectrum. If the process is repeated, excitation successively transfers from one to another molecule, allowing excitation energy transport also called energy migration. Energy transfer is either radiative and or non-radiative.

➢ Radiative energy transfer:

Radiative transfer (also called *trivial transfer*) is a 2-step process (Equation 8). A photon is first emitted by the donor and then absorbed by the acceptor, both partners being either different (*hetero-transfer*) or identical (*homo-transfer*).

$$1)\quad \mathbf{D^*} \longrightarrow \mathbf{D} + h\nu$$

$$2)\quad h\nu + \mathbf{A} \longrightarrow \mathbf{A^*} \text{ or } h\nu + \mathbf{D} \longrightarrow \mathbf{D^*}$$

Equation 8: Radiative energy transfer.

Such a transfer requires no interaction between both partners, but it depends on the spectral overlap and on concentration of the species. One consequence of the radiative energy transfer is a decrease in fluorescence intensity in the spectral region of overlap. Such distortion of the spectrum is called inner filter effect (the greater the overlap, the greater the distortion).

➢ Non-radiative energy transfer:

The non-radiative transfer requires interaction between a donor and an acceptor. It can only happen if the donor emission spectrum overlaps the absorption spectrum of the acceptor, which allows a match between donor and acceptor vibronic energy levels. All possible transitions are coupled in a resonant way, the whole process being called "resonance energy transfer" (RET). Energy transfer may result from Coulombic interactions or molecular orbital overlap (Figure 109).

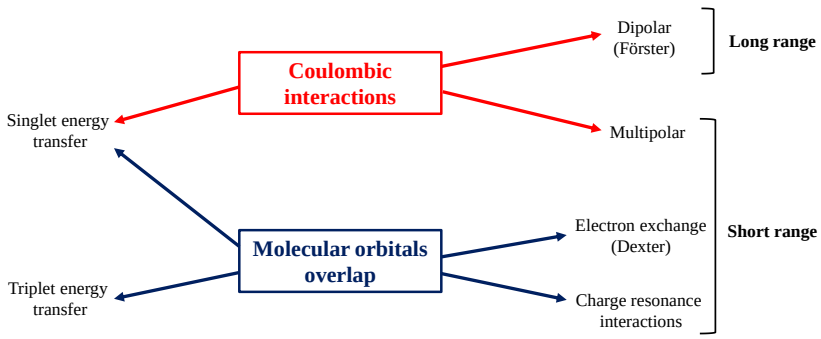

Figure 109: Type of interactions involved in nonradiative transfer mechanisms.

For Coulombic interactions, long-range dipole-dipole interactions (Förster mechanism),[394] and short-range multipole type can be distinguished. In contrast, interactions involving molecular orbital overlap are only observed at short distances between A and D (Dexter mechanism mainly).[395] The theories rationalize these two contributions as two energetic terms, Coulombic and exchange, constituting the total energy (Figure 110). The former term corresponds to energy transfer occurring when the excited electron (in LUMO) in D relaxes to the HOMO of D, this relaxation being accompanied by excitation of one electron from HOMO to LUMO in A (Figure 110). The exchange term corresponds to the concomitant transfer of two electrons, namely the excited electron in D to LUMO of A, and an electron from HOMO of A to HOMO of D (Figure 110).

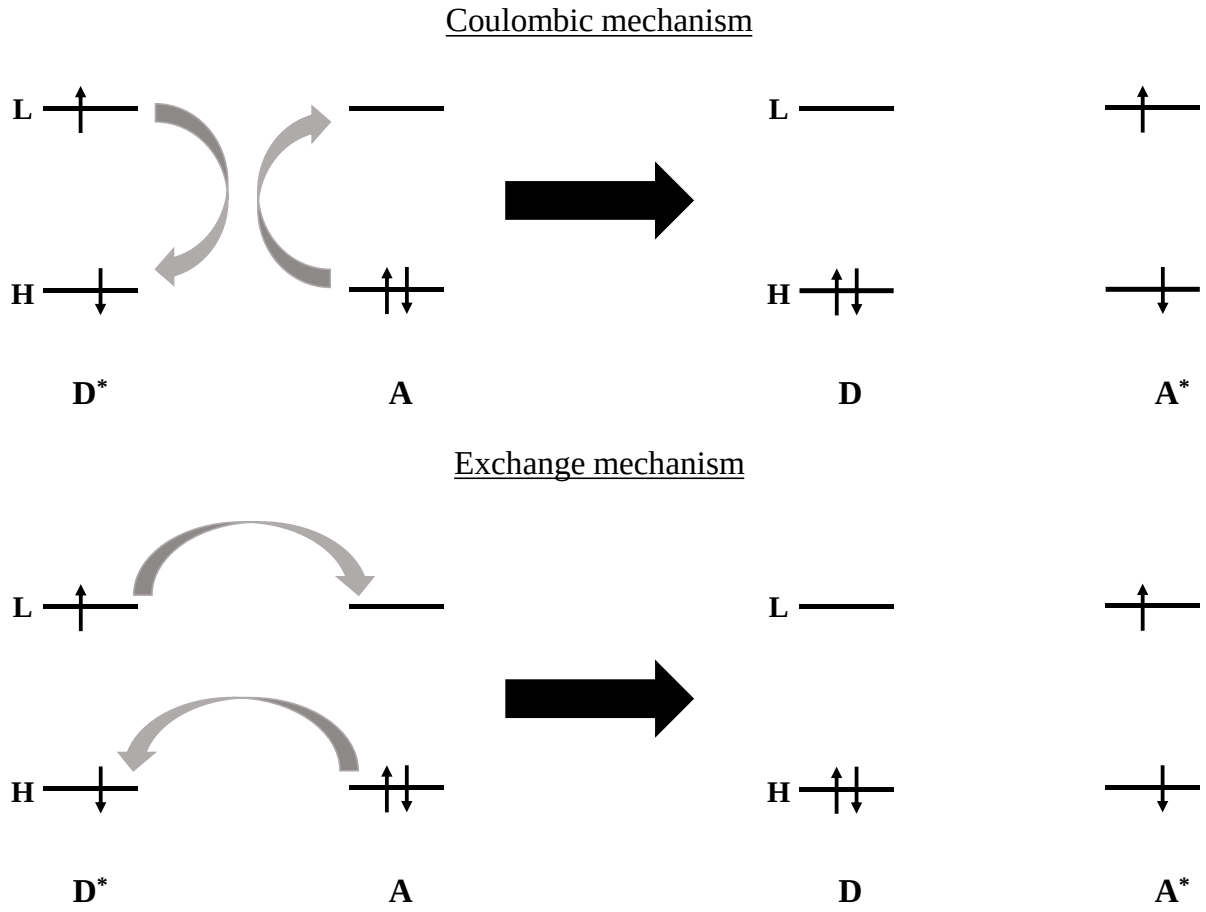

Figure 110: Schematic representation of Coulombic and exchange mechanisms of excitation energy transfer.

According to selection rules, energy transfer is generally made between energy levels of same multiplicity, that is singlet-singlet or triplet-triplet energy transfer. When transitions involving both donor and acceptor are permitted, Coulombic interactions predominate, even at short distances. When they are forbidden, the Coulombic interaction term is negligible and only

the exchange mechanism is at stake. However, this mechanism is only possible when inter-partner distances are shorter than 10 Å, to allow sufficient molecular orbital overlap. Conversely, the Coulombic mechanism remain possible at distances up to 80-100 Å. Experimental consequences of such photo-induced energy transfers is quenching of donor fluorescence emission and decrease of its excited state lifetime, whereas the acceptor keeps its excited state properties (Φ_f and τ_f).

- Förster theory (FRET):

In the late 1940s, Theodor Förster defined FRET (Förster Resonance Energy Transfer) as a non-radiative energy transfer (*i.e.*, without light emission) resulting from dipole - dipole interaction between two molecules (donor and acceptor). This physical phenomenon requires energy compatibility between the two moieties, which means that donor's emission spectrum must overlap (at least partially) acceptor's absorption spectrum.

Then, he had developed a theory to express energy transfer efficiency Φ_T (Equation 9).[396]

$$\Phi_T = \frac{1}{1+\left(\frac{r}{R_0}\right)^6} = 1-\left(\frac{\tau}{\tau_0}\right)$$

Equation 9 : Förster theory.

Where:

- R_0 (in Å) is the Förster radius (or critical distance): distance at which transfer and spontaneous de-excitation of the donor are equiprobable,
- r (in Å) is the distance between donor and acceptor,
- τ and τ_0 are donor lifetimes with and without acceptor, respectively

It is clear that the higher the distance between donor and acceptor, the lower the efficiency. The Förster radius (R_0) is the distance at which transfer efficiency is 50 %, it is generally in between 15 and 60 Å and it can be determined from spectroscopic measurements according to the following equation (Equation 10):[394,396]

$$R_0 = 0.2108.\left[\kappa^2 \phi_D^0 n^{-4} \int_0^\infty I_D(\lambda)\varepsilon_A(\lambda)\lambda^4 d\lambda\right]^{1/6}$$

Equation 10: Förster radius equation.

Where:

- κ is the orientation factor (κ^2 may in principle take values ranging from 0 to 4),
- Φ^0_D is the emission quantum yield of the reference donor,
- $I_D(\lambda)$ is the corrected fluorescence intensity of the donor with the total intensity normalized to unity,
- n is the refractive index of the solvent,
- ε_A is the molar absorption coefficient of the acceptor ($L.mol^{-1}.cm^{-1}$),
- λ is the excitation wavelength.
- When molecules can freely rotate at a much higher speed than the de-excitation speed of the donor, κ^2 value is 2/3 (isotropic dynamic average). The relationship between energy transfer efficiency and donor-acceptor distance (so Förster radius) is schematically exemplified in Figure 111.

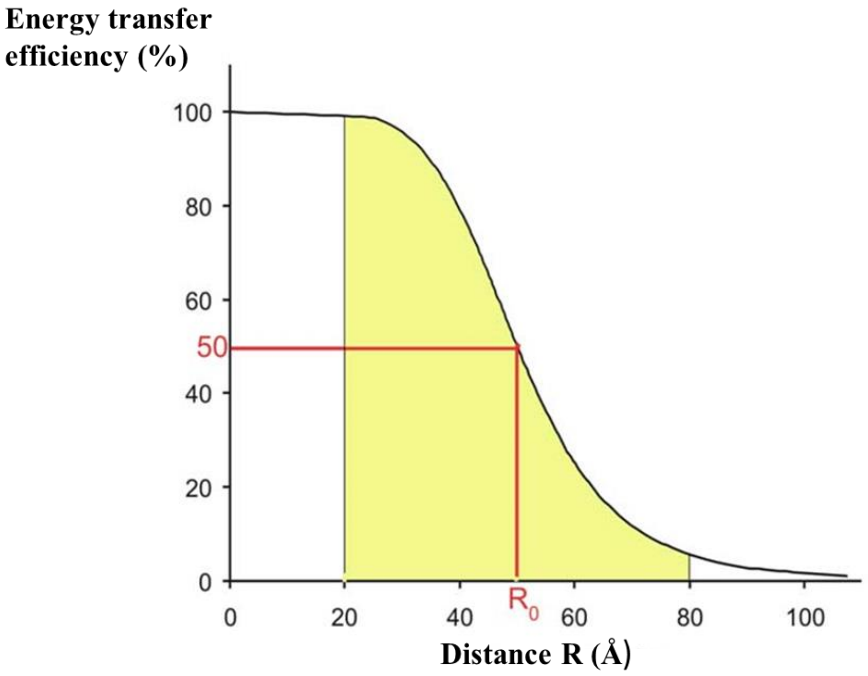

Figure 111: Distance-dependency of FRET-efficiency.

1.4. Porphyrins-fluorophore dyads

Dyads containing porphyrin patterns have been extensively studied due to their efficient electron donor capacities, *e.g.* combined with the acceptor properties of fullerenes have opened up promising applications. However, there are only a handful of publications on labeling porphyrin with fluorescent molecules (Figure 112) and even less without intention of

establishing interaction between the two patterns (energy or electron transfer). The porphyrin pattern is covalently (or not) coupled to the fluorophore. Several studies reported boron-dipyrrin (or BODIPYs) as a fluorophore, the dyad acting as a collecting antenna through singlet-singlet energy transfer towards porphyrin.[397,398] In 2013, Ngen *et al*. synthesized a rhodamine B-porphyrin dyad, with the aim of enhancing singlet oxygen generation by FRET (from rhodamine B* to porphyrin).[387] In 2009 Li *et al.* used napthalimide to develop a new imaging probe for Hg^{2+},[399] as Moura *et al.* Did with chalcone to develop new metallic ions sensors (*e.g.* Zn, Cd, Ag…) in 2014.[400] Fluorescein was also chosen to create new metallic (Zn, Ni, Mn and Cu) fluorescein-porphyrins dyads, still with the aim of promoting photo-induced energy transfer between the two moieties.[401,402]

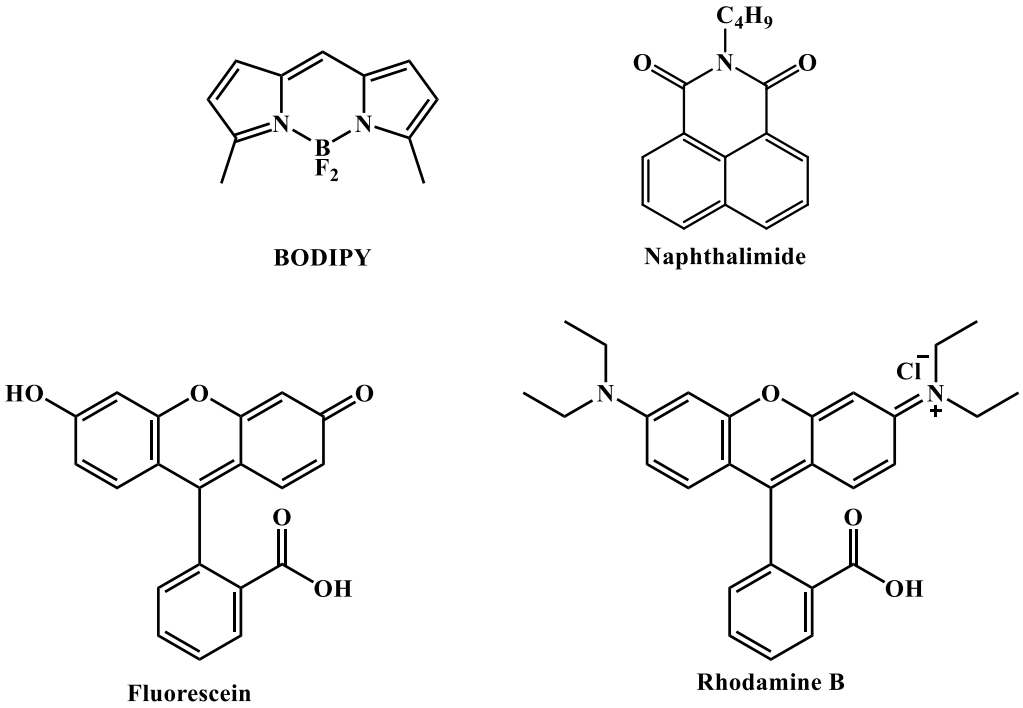

Figure 112: Examples of fluorophores used with porphyrin into dyads.

This situation is particularly surprising, given that as described above porphyrins are naturally present in Nature and seem to be prime targets. Such association is particularly relevant as porphyrin itself exhibits very low fluorescence quantum yields, whereas this property is crucial for visualization and tracking in biological media. Moreover, due to similar chemical structure, porphyrins have similar optical properties than chlorophyll, which is an additional serious drawback to localize them in plants without using an appropriate fluorescent tag. Having these drawbacks in mind, the design of molecular systems associating a porphyrin unit with a fluorescent tag has appeared as a novel and suitable solution to develop new kind of molecular bio-tracer and thus to better understanding some biological mechanisms (in human

as well as in plant cells). However, it is first necessary to use an optimized molecular design strategy to perfectly control dyad structures and avoid any interfering effects.

2. Basic knowledge in molecular modeling

2.1. A few introductory words

Behind the "Molecular modeling" or "Theoretical chemistry" terms stand a huge number of techniques for calculating physical-chemical properties of molecular systems, with more or less complexity. The aim of these calculations is to mimic as best as possible the physicochemical reality of gas phase, solution or solid state. Doing so, all intra- and intermolecular interactions should be accurately evaluated. Among other interactions one can mention solute-solute, solute-solvent, solute-metal atoms or ions, small solute (*e.g.* drugs) with macromolecules as membranes, proteins and DNA.[403–405]

Because molecular modeling methods have challenged the limits (Figure 113), the last decades have seen the development of their use in biology, physics, or chemistry.[406] Choosing the proper methods of calculation may help elucidating mechanisms of synthesis or biological actions as a support for experimental data.

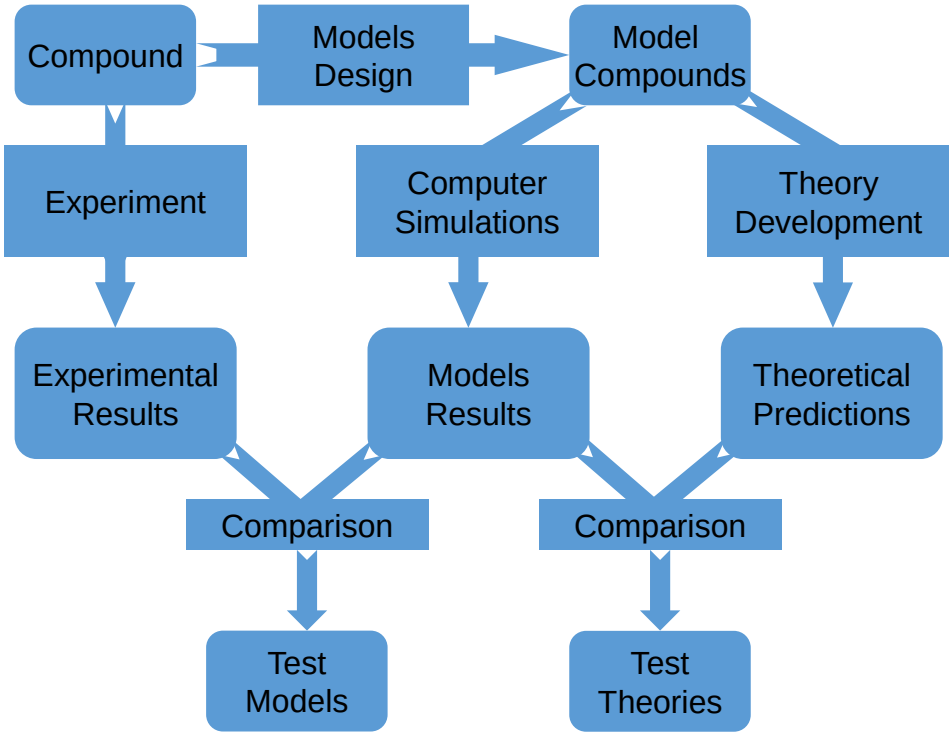

Figure 113: Molecular modeling overview.

2.2. Basic principles

Two major methodologies have been developed, namely molecular mechanics and quantum chemistry calculations.[408,409]

- Molecular mechanics and molecular dynamics focus on the movement of atoms, without distinguishing the movement of electrons. Used for the first time around 1960 (Alder and Wainwright in late 50s, then Gibson *et al.* and Rahman in 60s),[410–412] these methods consider atoms as balls and bonds as springs (so that a given molecule is an assembly of balls and springs). Internal forces are described within the classical mechanics (or Newtonian mechanics) framework, using rather simple mathematical functions and equations. All functions (and by the way constants and coefficients of these functions) and equations that describe interactions ensuring molecular cohesion are called a *force field*. The parameters of a force field are based either on experimental data or on high-level quantum calculations. Molecular mechanics calculations are performed at 0 K and allow optimizing conformations in a potential well. Molecular dynamics introduces temperature (translated in terms of atom velocities), which enables comprehensive conformational analyzes, even when the number of degrees of freedom of the molecular system is high.

- Conversely, quantum chemistry methods consider the movement of electrons and treat nuclei as fixed during electronic energies determination. This is based on Born-Oppenheimer's approximation. The calculation of energy levels and wave functions of a given molecule can be an extremely complex resolution, which requires much approximation as far as the number of electrons is higher than 1. In 1927, Born and Oppenheimer published a theory to simplify such calculations.[407] Their approximation states that in molecules, the movement of nuclei is much slower than that of electrons, which enable decoupling movements of both types of particles. Quantum chemistry calculations require computational times much longer than those of molecular mechanics. However they are the only way to access electronic structure and hence molecule reactivity. Because these methods have been mainly used for this thesis work, here we detail their underlying principles.

2.3. Quantum chemistry

All quantum chemistry methods have a common point, they require somehow solving Schrödinger's equation for a molecular system, as discovered in its time-independent form in 1925 and first published in 1926 (Equation 11):[413]

$$\hat{H}\Psi = E\Psi$$

Equation 11: Schrödinger's equation.

Where:

- E is the total energy of the system;
- ψ is the wave function that is described mathematically as a complex combination of molecular spin orbitals, themselves described as a combination of atomic orbitals;
- Ĥ is the Hamiltonian operator that accounts for kinetics terms of electrons and nuclei (T_e and T_n, respectively) and potential terms, namely all electron-electron (V_{ee}), nucleus-nucleus (V_{nn}) and nucleus-electron (V_{ne}) interactions (Equation 12).

$$\widehat{H} = \hat{T} + \hat{V} = \widehat{T_e} + \widehat{T_n} + \widehat{V_{ee}} + \widehat{V_{nn}} + \widehat{V_{ne}}$$

Equation 12: Hamiltonian operator.

As said above, Schrödinger's equation can only be solved exactly for systems having one electron only. A first step to overcome this limit is to use the Born-Oppenheimer's approximation, so that nucleus movements are omitted from the equation. This means that the electron wave function depends only on nucleus positions and not on their moments, and thus Schrödinger's equation becomes (Equation 13):

$$\widehat{H_{el}}\Psi_{el} = E_{el}\Psi_{el}$$

Equation 13: Electronic Schrödinger's equation.

Here, ψ_{el} is the electronic wave function, and combined with its associated electronic energy (E_{el}), they determine all electronic properties of the corresponding system. However this simplified formulation is still impossible to be exactly solved for multi-electronic systems. In this case, many approximations have been developed and we propose to list some of them. It is worth noting that in many cases, electron velocity is considered small compared to that of light (non-relativistic approximation).[408]

2.3.1. Hartree-Fock and other derived methods

The term *ab initio* (meaning from the beginning) is often used to describe this type of calculations.

- Hartree-Fock:

The Hartree–Fock (HF) method approximates determination of wave function and energy for a many-body system in stationary state. In 1927, soon after the discovery of Schrödinger's equation, D. R. Hartree introduced a procedure, which he called self-consistent field (SCF) method, to calculate approximate wave functions and energies for atoms and ions.[414] In this approximation method, the bielectronic interaction terms (expressed in the Hamiltonian operator H) are not considered explicitly. In place, the polyelectronic system of **n** electrons is transformed into **n** monoelectronic systems. However, this method has accumulated errors and is almost not used anymore in its primary form. In particular, HF methods do not describe properly electron correlation. More precisely the correlation movement due to their charge, and between electrons having parallel spins (or *exchange term*) is well described within the HF formalism. However, the quantum-correlation associated to the movement between electrons having antiparallel spins (or usually termed *correlation term*) is totally omitted in this formalism.

- Post Hartree-Fock methods:

To correct the severe drawback of HF-formalism (lack of correlation description), other methods have been developed based of the HF approximation and thus named *post-HF methods*.[415] They include electron correlation (main weakness of HF-formalism) by various ways, which are grouped either in perturbation MPn (*e.g.* MP2) or in configuration interaction CI (*e.g.* CID) methods. Unfortunately although these calculation techniques can be very efficient, they are extremely greedy in terms of memory and computing time.

2.3.2. Density Functional Theory

Density Functional Theory (DFT) formalism is an interesting alternative to post-HF methods. The DFT popularity has risen thanks to the performing ratio between accuracy and computational time; up to 300-atom molecular system can be treated.[416] In DFT, the formalism is based on electron density **ρ** rather than on molecular orbitals (as in HF). The correlation term is inherently included in equations. All quantities (including energy) are described as functions

of **ρ**, which is itself a function of molecular orbitals *i.e.* functionals (a function of a function is a functional). Functionals have been developed for both exchange and correlation contributions. The development of the most accurate functionals has deserved much attention over the last two decades, among which the local, gradient-corrected and hybrid functional families will be described now.

- Local methods:

The LDA (Local Density Approximation) and LSDA (Local Spin Density Approximation) functionals[417] treat density as a uniform electron gas. This approximation is justified for metals, because uniform electron gas model correctly describes electrons of conduction band of metals. For molecules, in which electron density can change very quickly in small volumes, local methods are rarely appropriate and accurate.

- Gradient-corrected methods:

Because erroneous results obtained with LDA functionals are mainly attributed to their too local character, other functionals have been developed which include density gradient. Among other examples of gradient-corrected methods, so called GGA (Generalized Gradient Approximations), one can quote PW91 (Perdew-Wang 1991),[418] LYP (Lee-Yang-Parr).[419,420] Although GGA functionals provide usually better results (total energy, energy barrier or binding energy) than LDA, they are still not sufficiently accurate. This drawback partially comes from a bad description of exchange term whereas it is known that HF exactly calculates exchange.

- Hybrid methods:

Also called hyper-GGA methods, they were introduced by Axel Becke in 1993.[421] These methods propose to mix HF and DFT exchange whereas correlation is described by a pure DFT functional. Schematically, hybrid functionals is written as follows (Figure 114):

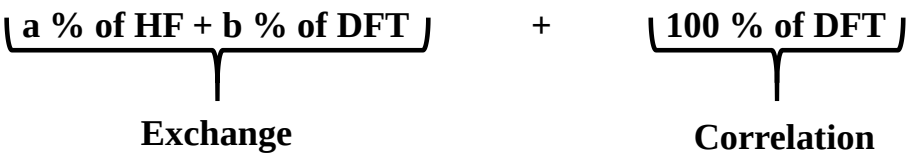

Figure 114: Hybrid functional terms (exchange and correlation) description.

This inclusion of a percentage of HF in the exchange term has dramatically improved predictions of experimental data. For example B3LYP functional uses about 30% HF in exchange term, or BHandHLYP introduces 50% HF.

➢ Time Dependent Density Functional Theory

Time Dependent DFT (TD-DFT) has been developed to allow calculation of time-dependent phenomena.[422] The theoretical foundations of TD-DFT are relatively complex and are far beyond the scope of this work. However, it is worth noting that it allows investigating the properties and dynamics of many-body systems in the presence of time-dependent potentials, such as electric or magnetic fields. The effect of such fields on molecules (and solids) can be studied to extract features like excitation energies, frequency-dependent response properties, and maybe the most important photo-absorption properties and spectra (including energy or electron transfer).

2.3.3. Basis sets

➢ Generalities

For a given theoretical method of calculation (HF or DFT), a basis set must be used which allow describing molecular orbitals as linear combination of mathematical functions. Basis sets used for the calculations will have a direct impact on accuracy. It is therefore crucial to adapt it according to the desired precision, keeping in mind that increasing basis size set may dramatically increase computational time.

Molecular orbitals are thus described as linear combinations of atomic orbitals (LCAO). The atomic orbital are typically Slater Type Orbitals (STO),[423] which correspond to a set of functions that decay exponentially *vs* the distance from the nucleus increases. However, the mathematical use of STO functions is rather complex, in particular in integral calculation. Therefore, it has been suggested by John Pople (Nobel Prize in 1998) to describe atomic orbitals by linear combinations of Gaussian functions, making integrals much easier to calculate.[424]

➢ Minimal basis sets

Minimal basis sets contain a number of functions as small as possible. Here, each atomic orbital is described by a single function, which is a linear combination of Gaussian functions. The most common are minimal STO-nG basis (Slater Type Orbitals-n Gaussians as STO-3G[425]) where n is an integer representing the number of Gaussian primitive functions. Moreover, in this case, there is no distinction between core and valence orbitals, both being described by the same functions. They are nowadays rarely used and give inconclusive results.

➢ Extended basis sets

Technological advances in computer technology have allowed development and use of new basis sets, called extended (or separate valence). In practice it has resulted in an increase

by a factor two of basic functions, leading to the creation of basis set called "double zeta" (or double-ζ). Doubling the number of atomic orbital functions has allowed a better description of electron distribution. In this case, core atomic orbitals are described by a single function (as minimal basis) while valence atomic orbitals are described by two or even more functionals (double-ζ; triple-ζ…). The most used basis sets (or Pople basis sets) are denoted X-YZ G,[424] where:

- X representing number of Gaussian functions which describe atomic orbitals core,
- Y and Z indicate that valence orbitals are composed of two atomic orbitals, both being composed by a linear combination of Y and Z primitive Gaussian functions, respectively.

For example, 6-311G means that core electrons are described by a linear combination of 6 Gaussian functions and valence electrons are described by three functions (triple-ζ), described by three, one and one Gaussian functions.

- Additional functions

Polarization functions can be added, which improve accuracy to describe polarized electron density. For “heavy” atoms for which valence shells are s and p, polarization functions are of *d* type. For "light" atoms (hydrogen) for which valence shells are s, polarization functions are of *p* type. Using such functions allows to "break" the perfect symmetry introduced by Gaussian functions which prevents any flexibility in the description of the electronic distribution. For example, 6-31G(d,p) is a double-ζ basis set (because two functions are used to describe valence orbitals) and for which polarizations are used on all atoms.

Finally, there are diffuse functions noted + or ++.[426] To improve description of electronic effects far from the nucleus, diffuse Gaussian functions are added, flattened at function maximum (center) and extended away from the center. The first + means that one includes these functions only for atoms other than hydrogen, and ++ for all atoms without distinction, *e.g.* 6-31+G(d,p) or 6-31++G(2d,3p).

3. Design of targeted dyads

3.1. Context

Although the concept of porphyrins as potential herbicides has been clearly evidenced, mainly due to their efficient capacity to produce ROS, the capacity to penetrate cells and the mechanism involved remain unknown. To precisely locate porphyrin in plants should provide valuable information to tackle this issue. However, porphyrins cannot easily been seen in plants for two major reasons. First because they have very low fluorescence yields, making them poor fluorescent markers. Second, their emission is hidden by autofluorescence existing in plant cells due to structurally related molecules (*e.g.* chlorophylls, protoporphyrin IX...), which emit in the same spectral range.

To overcome this drawback, our strategy has been to tag porphyrins with a fluorophore. This can only be achieved under mandatory requirements, namely the chosen fluorophore must: 1) absorb and emit at a different wavelength than the natural fluorescent compounds present in plants, ideally wavelength lower than 600 nm; 2) be non-cytotoxic; 3) be easy to handle (for coupling with porphyrin); and 4) be stable in biological media. Fluorescein was chosen as fulfilling these four requirements and being commercially available.[427–429]

Another bottleneck to build such dyads concerns the link between porphyrin and fluorescein moieties. Indeed, both compounds are π-conjugated, which is responsible for their characteristic properties. Direct linking of these two patterns would lead to π-conjugation extension and therefore would dramatically modifying their photophysical properties as well as their capacity to produce ROS. Using a spacer arm has emerged as an adapted solution, allowing linking both moieties while keeping their individual characteristics (Figure 115). As for the fluorescent tag, the choice of linkers has to be well thought *i.e.* non-cytotoxic for plants, chemically inert in biological media, that is to say resistant to enzymes as well as stable at physiologic pH, easy to modulate and so prone to chemical reacting, and last but not least non-conjugated. Having this guideline in hands, the linker selection has been based on classical chemistry considerations and on a molecular modeling study of the dyad conformational space. The dyad was further synthetized with three different linkers.

The last constraint consists to obtain water-soluble compounds. Indeed, it is mandatory to work in biological media. In this context, porphyrins must be modulated with functions able to bring this solubility. Based on works realized with anionic compounds, we have chosen sulfonic acid groups. Indeed, porphyrins sulfonation is a reaction easy to implement with very

high yields. Moreover, sulfonic groups do not necessitate sodium hydroxide (or other basis) addition to bring solubility in water.

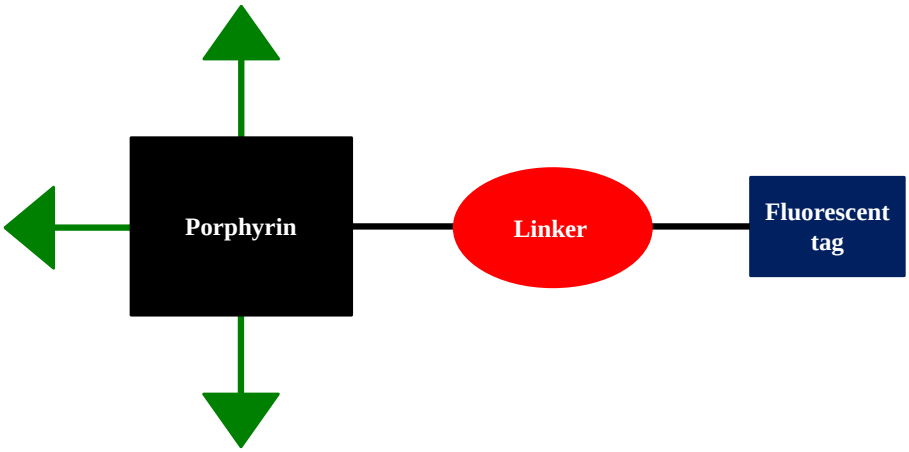

Figure 115: General structure of dyads. Green triangles represent water-soluble functions.

3.2. Choice of linkers

A selection of potential candidates was made based on 1) the literature, 2) their reactivity, but also 3) their commercial availability (Figure 116).

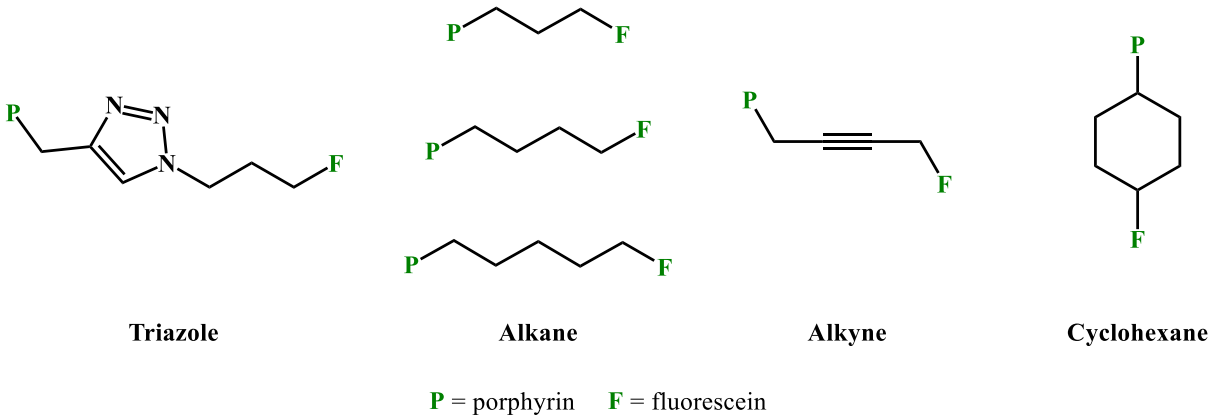

Figure 116: Linker library selected, according to literature, reactivity and availability.

The triazole ring was chosen as it is easy to obtain with high yields by click-chemistry (Huisgen 1,3-dipolar cycloaddition between alkyne and azide functions) and it is often used in pharmaceutical chemistry due to its high stability *vs.* pH or against enzymes.[430,431] The propyl chain is necessary to prevent the extension of aromaticity between fluorescein ring and triazole. The other five compounds were chosen for their capacity to be modified by simple nucleophilic substitution and to ensure different flexibility level in the dyad (Figure 116). Indeed, preliminary conformational study on the triazole moiety alone was carried out within the DFT

formalism. Calculations were performed with B3LYP functional, both in the gas phase and chloroform described as implicit solvent model (Polarizable Continuum Model, PCM). The conformational analysis has highlighted a high degree of freedom, providing eight isoenergetic conformers (Figure 117) within a 2 kcal.mol^{-1} range.

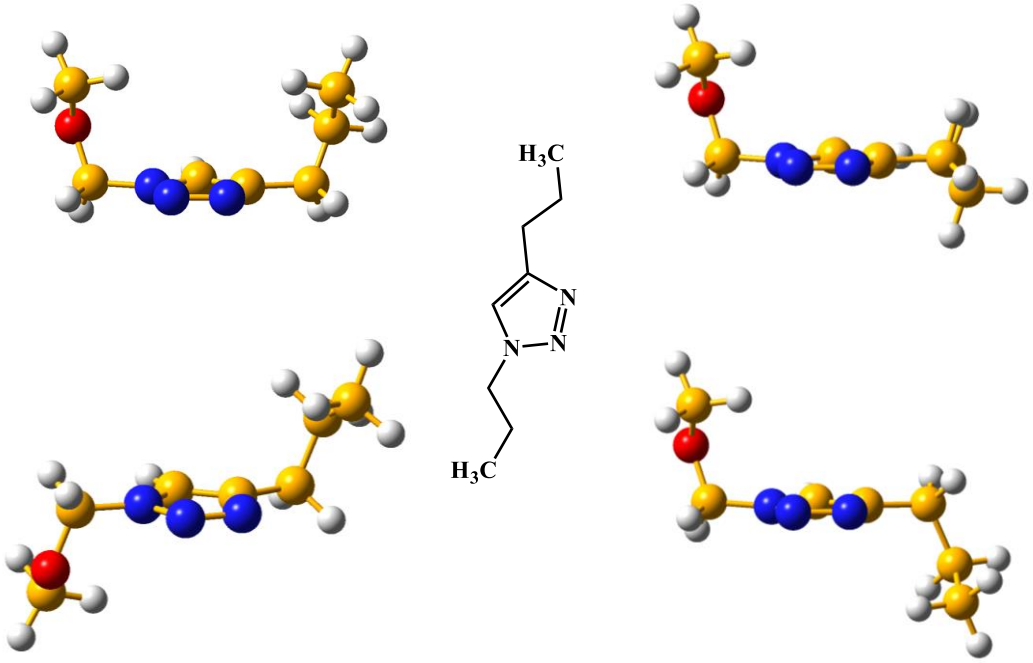

Figure 117: Examples of isoenergetic conformers found for the triazole compound.

Conversely, cyclohexane and alkyne appeared as relevant candidates to ensure rigidity. The former compound was too expensive so the latter was preferred as bearing similar stiffness characteristics. The rigidity of alkane chains depends on their length; compounds with 4 and 5 carbons have high flexibility whereas 3-carbon chain should lead to intermediate flexibility (Figure 118).

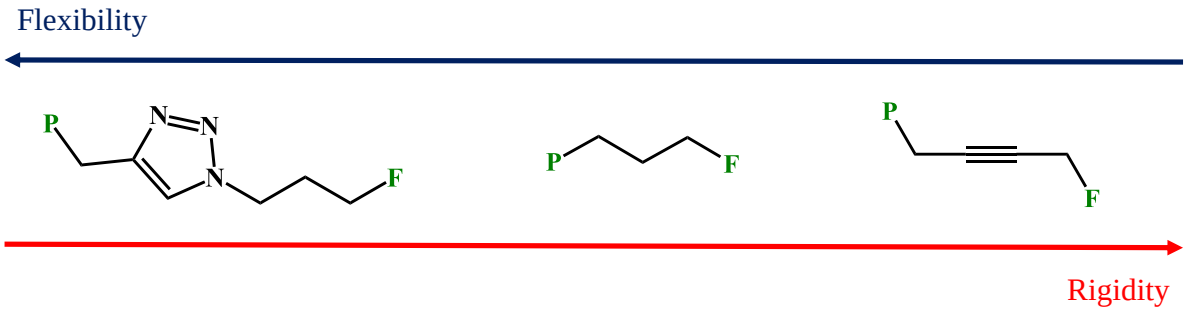

Figure 118: Structure of the 3 chosen arms. **P** means Porphyrin while **F** is for Fluorescein.

This preliminary study allowed us to define three different kind of dyads containing both porphyrin and fluorescein moieties. However, due to the particularity of triazole synthesis (see

below), the corresponding dyad was only obtained under metallated form (**24**) while dyads with alkane and alkyne links were obtained both free-base (**25** and **27**) and zinc-metallated (**26** and **28**) (Figure 119).

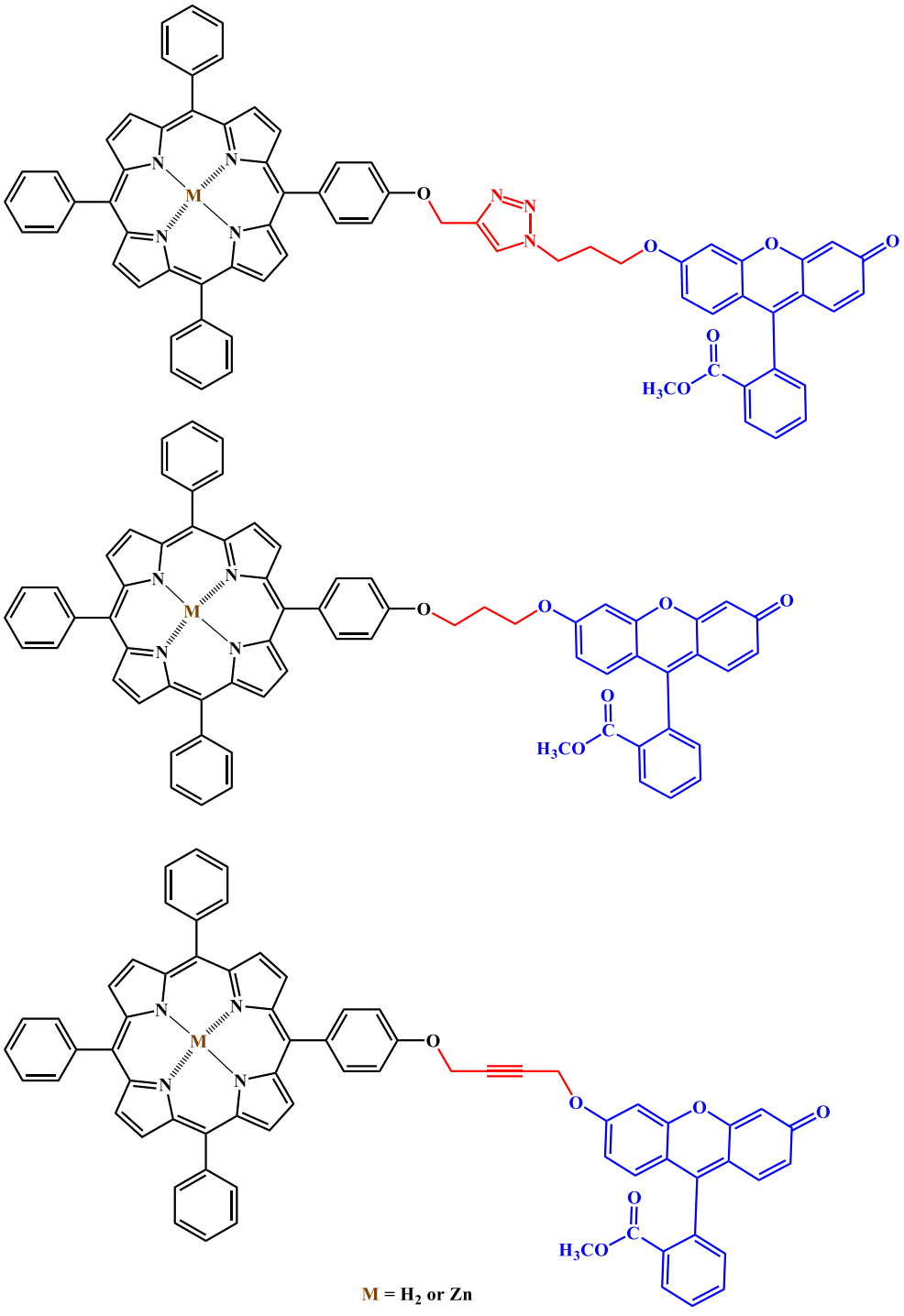

Figure 119: General structures of dyads synthesized.

4. Synthesis

4.1. Strategy

The first synthetic strategy performed in our laboratory was to synthesize fluorescein and sulfonated porphyrin patterns separately and then to couple them together to form the desired dyad.[432] Unfortunately, in the case of the triazole linker, all attempts were unsuccessful probably due to solubility problems. Indeed, sulfonated porphyrin was soluble in water but not (or very little) in common organic solvents (*e.g.* THF, DMF…), while modified fluorescein was not soluble in water. Therefore, as alternative strategy we have chosen to synthesize non water-soluble dyads (Figure 120) and to post-functionalize them after. Water-solubilization, could then be envisaged either by sulfonation or encapsulation of these molecular systems. Moreover, this strategy will allow to study the interaction between fluorescein and porphyrin moieties in non-water-soluble dyads in different solvents and to strengthen these experimental investigations with theoretical results.

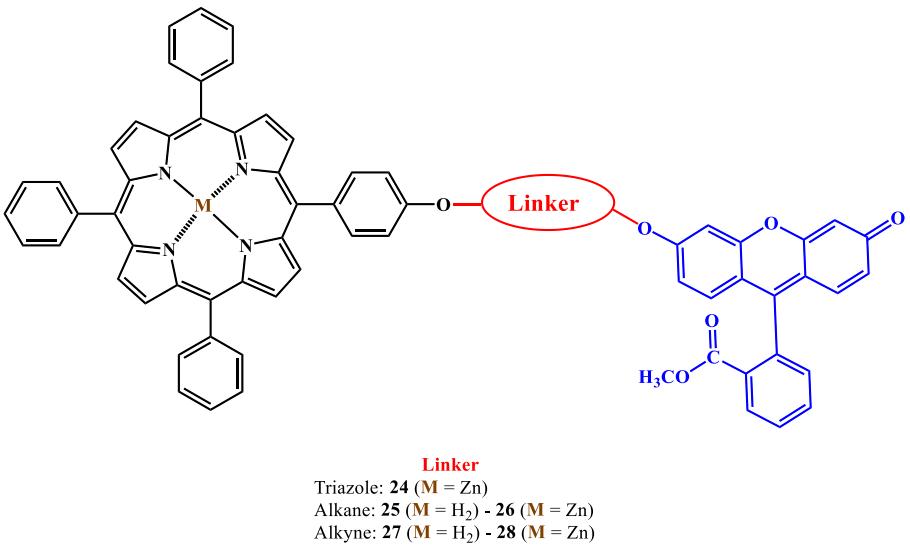

Linker
Triazole: **24** (**M** = Zn)
Alkane: **25** (**M** = H_2) - **26** (**M** = Zn)
Alkyne: **27** (**M** = H_2) - **28** (**M** = Zn)

Figure 120: General structure of dyads (**24-28**) synthesized during this work.

In that purpose, some reference compounds were also synthesized: compounds **14** (free base), **15** (zinc metallated) and **21** for porphyrin and fluorescein moieties, respectively (Figure 121).

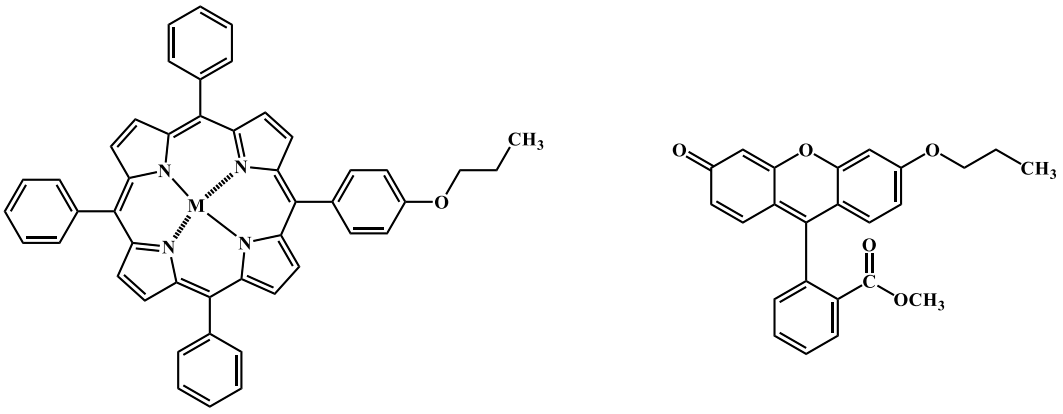

Figure 121: Spectroscopic references **14-15** and **21**.

4.2. Key and reference compounds

Two key molecules, porphyrin **13** and fluorescein derivative **20**, were first synthesized. Indeed, these two compounds were the basis for all subsequent synthesis of dyads (Figure 119) as well as for reference compounds. As reference compounds **14-15** and **21**, were synthesized directly from these two precursors by simple nucleophilic substitution in presence of bromopropane, their synthesis will also be presented here.

4.2.1. Porphyrins

Key porphyrin **13** was achieved according to Little's method[51] by reaction between 1 equiv. of 4-hydroxybenzaldehyde, 3 equiv. of benzaldehyde and 4 equiv. of pyrrole (Figure 122). Indeed the choice of this stoichiometry is recommended for A_3B porphyrin synthesis.[53,54]

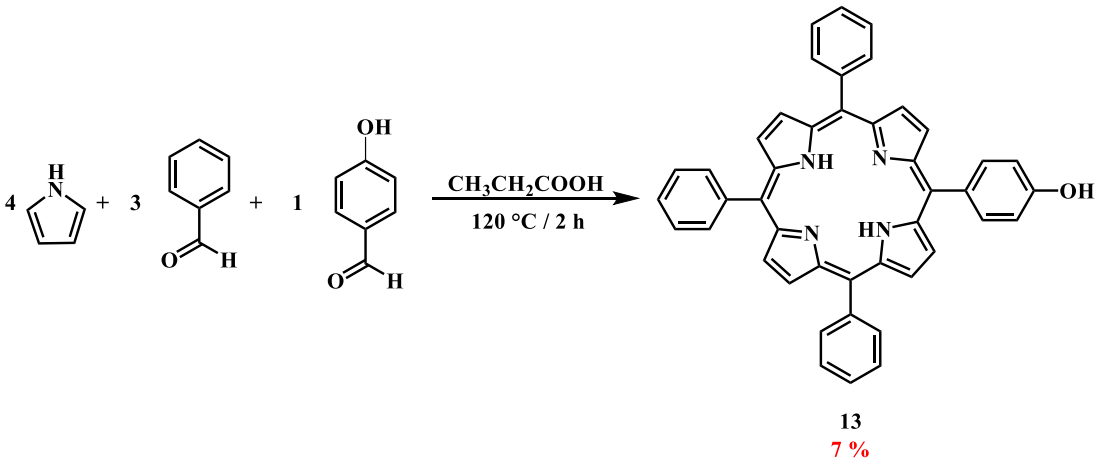

Figure 122: Synthesis of compound **13**, according to Little's method.

First, aldehydes were dissolved in propionic acid and refluxed was activated. Then, fresh distillated pyrrole was added dropwise and reaction was stirred in the dark. After 1 hour, mixture was cooled at room temperature. Then crude product was purified on chromatographic column after acid evaporation to give compound **13** with 7 % yield, in agreement with the literature.

Synthesis of **14** was performed according to a microwave assisted protocol developed in the laboratory (Figure 123). An excess of 1-bromopropane was dissolved in DMF with porphyrin **13**. Reaction was activated using microwave irradiations (2 x 5' / 200 W / 120 °C) and progress was monitored by TLC. After purification on chromatographic column, compound **14** was obtained with good yields (78 %). Then, **15** was obtained by simple metalation of **14** with zinc(II)acetate (in excess) in quantitative yields (> 99 %). Progress was monitored by UV-Vis absorption, until complete disappearance of free-base porphyrin Q bands.

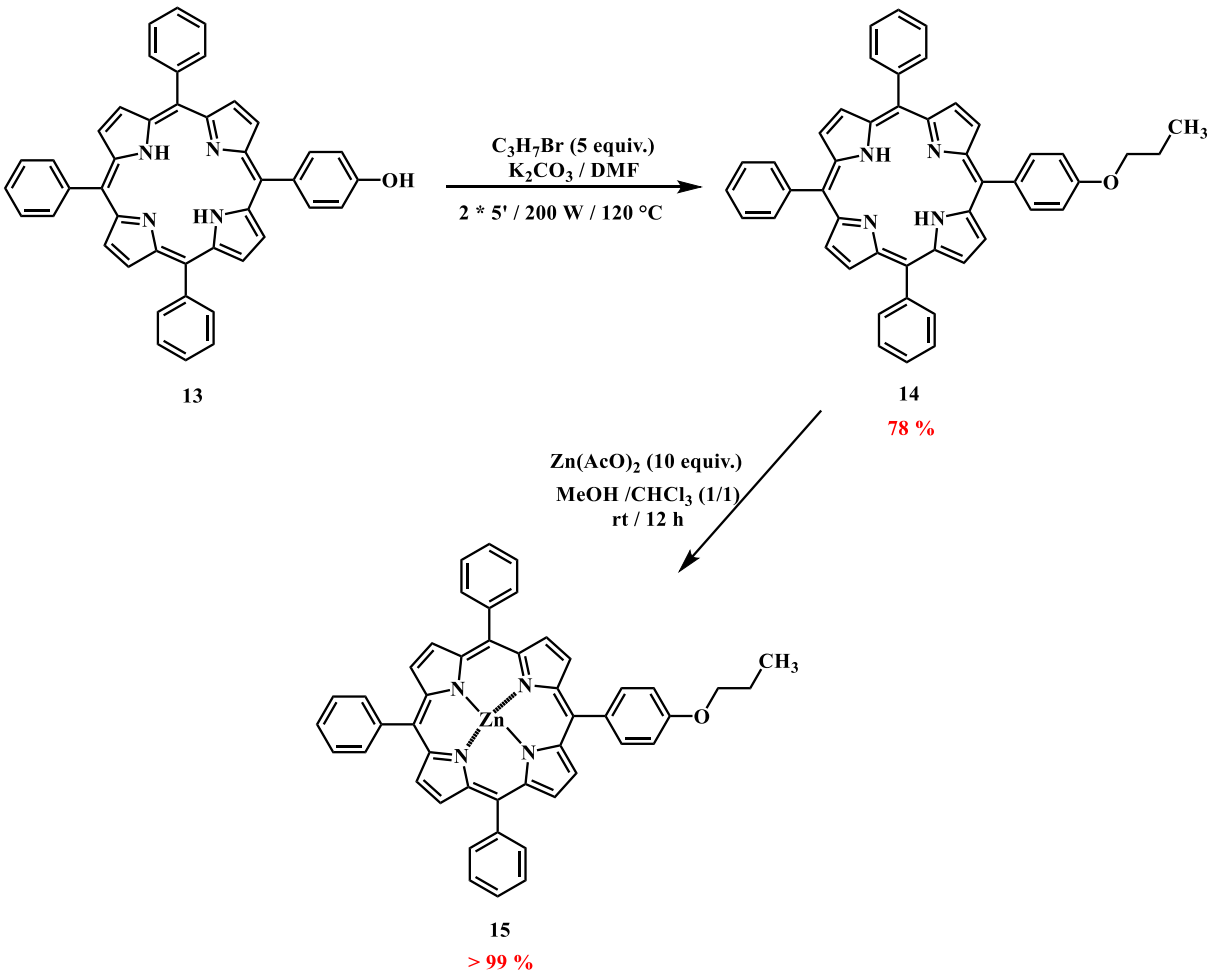

Figure 123: Reference compounds **14** and **15** synthesis.

4.2.2. Fluorescein derivatives

Native fluorescein co-exists in two forms, called quinoid and lactone (Figure 124), depending on its environment (solvents, pH or esterification of the hydroxyl group…). In the first one, the carboxylic acid function is free while in the second one, this same function has undergone an intramolecular cyclisation to form a lactone.[433]

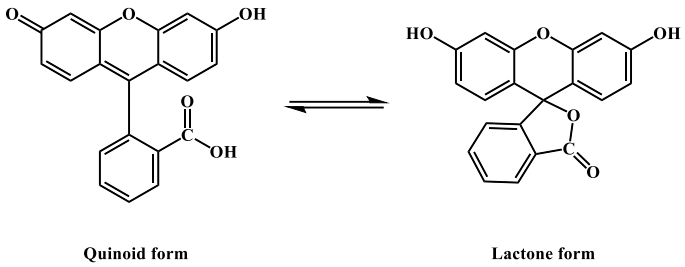

Figure 124: Fluorescein conformers.

In order to prevent coexistence of two dyads in solution (quinoid and lactone conformers), which might increase drastically interactions, quinoid form was chosen because more easy to obtain. Thus, a carboxylic function was first protected by esterification, blocking lactone formation (Figure 125). According to Pérez Guarìn *et al.*,[434] commercial fluorescein was dissolved in freshly distillated methanol in presence of catalytic amount of sulfuric acid, and reaction was stirred in darkness for 18 hours. Addition of cooled water resulted in a precipitation of esterified molecules, then filtration and evaporation to dryness have allowed achieving compound **20** with quantitative yields (up to 90 %).

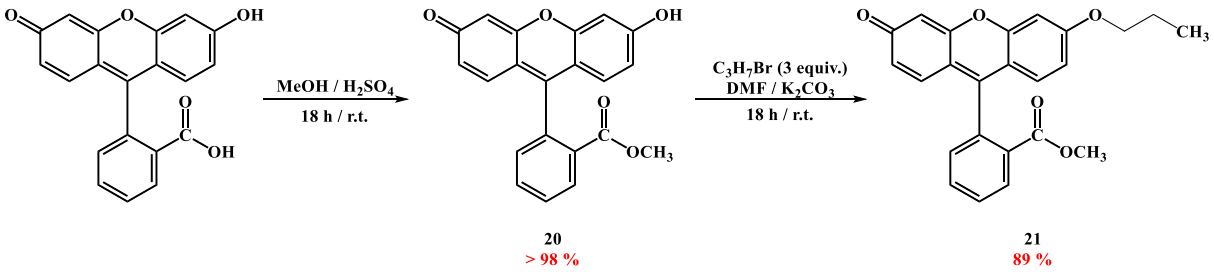

Figure 125: Synthesis of compound **20** and reference **21**.

Reference **21** was obtained by reacting **20** with an excess of 1-bromopropane in DMF (Figure 125). Reaction was stirred in darkness during one night, at room temperature. Finally, crude product was purified on chromatographic column to give **21** with good yields (89 %).

4.2.3. NMR characterizations

All NMR spectra (^{1}H and ^{13}C) were performed in $CDCl_3$ with TMS as internal reference.

➢ Porphyrins **13-15** (Table 13)

Table 13: ^{1}H-NMR of compounds **13-15** in $CDCl_3$. δ are in ppm.

H	13	14	15
β-pyrrolic	8.87 d (4.8 Hz) (2H) 8.83 s (6H)	8.86 d (4.8 Hz) (2H) 8.82 s (6H)	8.87 d (4.8 Hz) (2H) 8.82 s (6H)
2,6-phenyl	8.21 d (7.6 Hz) (6H)	8.21 d (7.6 Hz) (6H)	8.21 d (7.6 Hz) (6H)
2,6-aryl	8.04 d (8.3 Hz) (2H)	8.06 d (8.3 Hz) (2H)	8.06 d (8.3 Hz) (2H)
3,4,5-phenyl	7.75 d (8.2 Hz) (9H)	7.75 d (8.2 Hz) (9H)	7.75 d (8.2 Hz) (9H)
3,5-aryl	7.16 d (8.2 Hz) (2H)	7.15 d (8.2 Hz) (2H)	7.15 d (8.2 Hz) (2H)
NH_{int}	-2.74 s (2H)	-2.74 s (2H)	-
$O\text{-}CH_2$	--	4.32 t (6.8 Hz) (2H)	4.32 t (6.8 Hz) (2H)
CH_2	--	1.84 m (2H)	1.84 m (2H)
CH_3	--	1.04 t (7.3 Hz) (3H)	1.04 t (7.3 Hz) (3H)

As expected the three compounds exhibit very similar spectra. Indeed, the only difference is the propyl chain grafted instead of hydroxyl group, and which has just a slight donor effect. Metalation with zinc results in a loss of internal NH.

➢ Fluorescein **8-10** (Table 14)

To facilitate the interpretation of spectra, fluorescein and its derivatives have been numbered as follows (Figure 126):

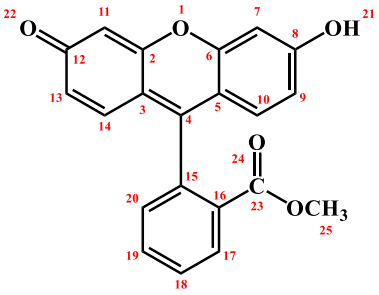

Figure 126: Numbering of fluorescein atoms.

Propyl behavior is the same in fluorescein than in porphyrin. Indeed, there is no significant effects on chemical shifts chain has the same behavior (Table 14).

Table 14: ^{1}H-NMR of compounds **20** and **21** in $CDCl_3$. δ are in ppm**.**

H	**20**	**21**
13	8.25 dd (7.8 / 1.2 Hz) (1H)	8.24 dd (7.2 / 1.2 Hz) (1H)
17	7.74 dt (7.5 / 1.4 Hz) (1H)	7.73 dt (7.4 / 0.9 Hz) (1H)
19	7.66 dt (7.6 /1.4 Hz) (1H)	7.66 dt (7.6 /0.9 Hz) (1H)
18	7.30 dd (7.5 / 1 Hz) (1H)	7.31 dd (7.2 / 1 Hz) (1H)
11	6.96 d (2.4 Hz) (1H)	6.94 d (2.4 Hz) (1H)
14	6.89 d (8.8 Hz) (1H)	6.87 d (8.9 Hz) (1H)
10	6.85 d (9.7 Hz) (1H)	6.84 d (9.7 Hz) (1H)
9	6.74 dd (8.9 / 2.4 Hz) (1H)	6.73 dd (8.9 / 2.3 Hz) (1H)
20	6.55 dd (9.7 / 1.7) (1H)	6.54 dd (9.7 / 1.8) (1H)
7	6.47 d (1.6 Hz) (1H)	6.45 d (1.8 Hz) (1H)
25	3.64 s (3H)	3.63 s (3H)
26	--	4.02 t (6.5 Hz) (2H)
27	--	1.86 m (2H)
28	--	1.06 t (7.4 Hz) (3H)

Moreover, ^{13}C-NMR spectra correlate expected structures for both porphyrin and fluorescein derivatives.

4.2.4. Mass spectra

Structural analysis of compounds **13-15** and **20-21** was pursued by studying their mass spectrum (Table 15). All compounds exhibited the molecular peak $[M+H]^+$.

Table 15: m/z values of [M+H]+ ions for compounds **13-15** and **20-21**, obtained by HRMS.

Compounds	Chemical formula	Monoisotopic mass	$[M+H]^+$
13	$C_{44}H_{30}N_4O$	630.75	631.5248
14	$C_{47}H_{36}N_4O$	672.83	673.3217
15	$C_{47}H_{34}N_4OZn$	734.20	735.2439
20	$C_{21}H_{14}O_5$	346.34	347.0913
21	$C_{24}H_{20}O_5$	388.42	389.1381

As for NMR, HRMS analysis confirmed that the structures were those expected.

4.3. Triazole dyad (**24**)

4.3.1. Synthesis

To form the triazole bridge, it is that necessary to preliminary form alkyne and azide that must react together. Thus, propargylation of porphyrin (Figure 127) and azidation of fluorescein (Figure 128) were performed in parallel.

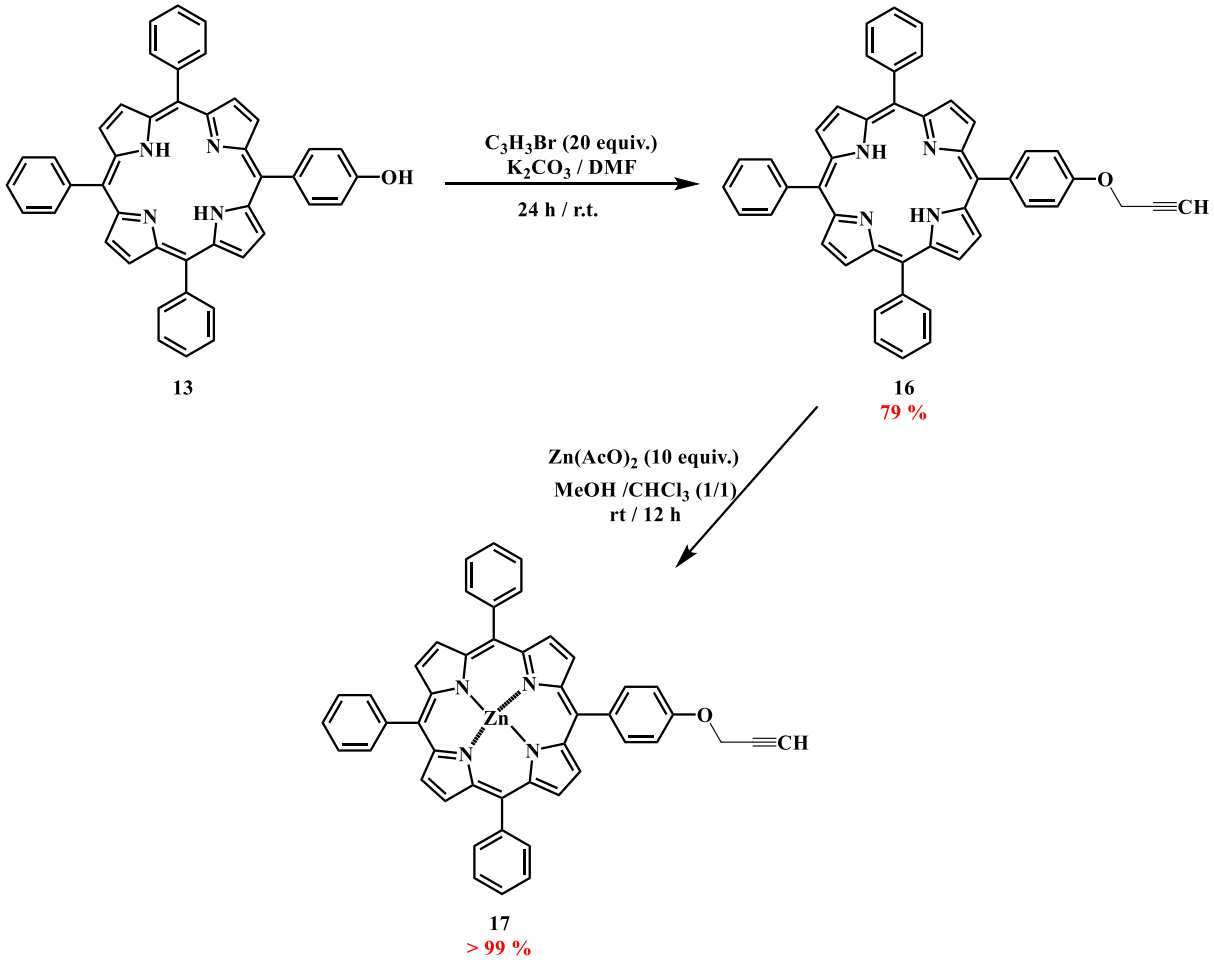

Figure 127: Synthesis of porphyrinic intermediates **16** and **17**.

Propargylation of the hydroxyl group of **13** was conducted through a Williamson's reaction[435] in the presence of an excess of propargyl bromide in DMF. After salt removing and purification *via* chromatographic column, intermediate **16** was obtained with 79 % yield. Then, next step consisted of a zinc metalation of the porphyrin nucleus. This was of upmost importance because dyad **24** was obtained by click-chemistry reaction catalyzed by copper(I)[436] between **17** and **23**. As this metal exhibits high affinity to the porphyrin nucleus, the absence of copper complexation prevention by the porphyrin moiety may decrease the efficiency of

catalysis and hence reaction yields. Moreover, as described by Figueiredo *et al*. in 1999,[141] the production of ROS was dramatically decreased in copper-porphyrin whereas zinc-porphyrins are known to be efficient ROS producers.[141] Therefore metalation of **16** was done with an excess of zinc(II)acetate, to give **17** in quantitative yields (> 99 %). Progress was monitored by UV-Vis absorption, until complete disappearance of free-base porphyrin Q bands.

In parallel, the fluorescein precursor **23**, required for synthesis of **24**, was obtained in two steps from **20** (Figure 128). First, compound **22** was obtained by alkylation of **20** with an excess of 1,3-dibromopropane.

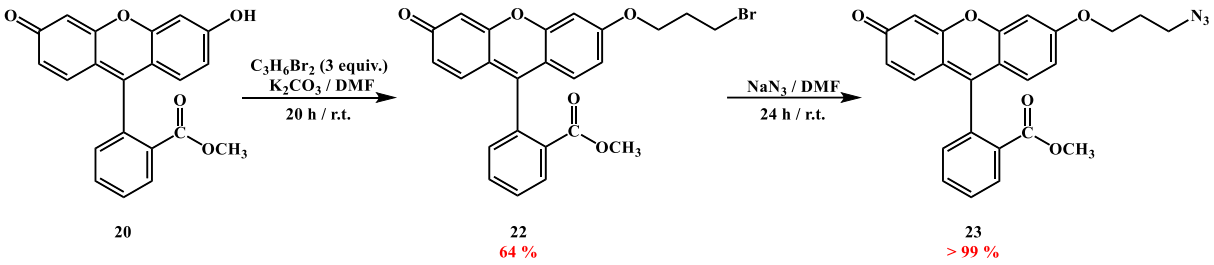

Figure 128: Synthesis of fluorescein precursor **23**.

Reaction was stirred during 20 hours. After salt removing and purification, **22** is obtained with 64 % yield. The difference in yields observed with respect to the synthesis of reference **21** is due to the possibility here of dimer formation (20 %). Then, **22** is subsequently transformed with quantitative yields into **23** by direct reaction with sodium azide based on Singh *et al*. method.[437] However, the product appeared as unstable despite of the usual conservation precautions (low temperature and inert conditions) and thus must be used very quickly.

The porphyrin and fluorescein key-moieties (**17** and **23**) were then coupled by an Azide-Alkyne [2+3] Huisgen Cycloaddition[436,438–440] using Copper(II) acetate/sodium ascorbate (2.7/7 equiv.) as catalytic system (acting as precursor of the real catalytic specie, namely Copper(I), produced *in situ*) (Figure 129). During this coupling step, the solubility of the various reagents was problematic. To overcome this issue, salts (Copper(II) acetate and sodium ascorbate) were dissolved together in distillated water whereas the two precursors (**17** and **23**), were dissolved in THF. Afterwards, the two solutions were mixed. After 24 h reaction at room temperature, salts were removed and after purification step on chromatographic column **24** was obtained with 91% yield.

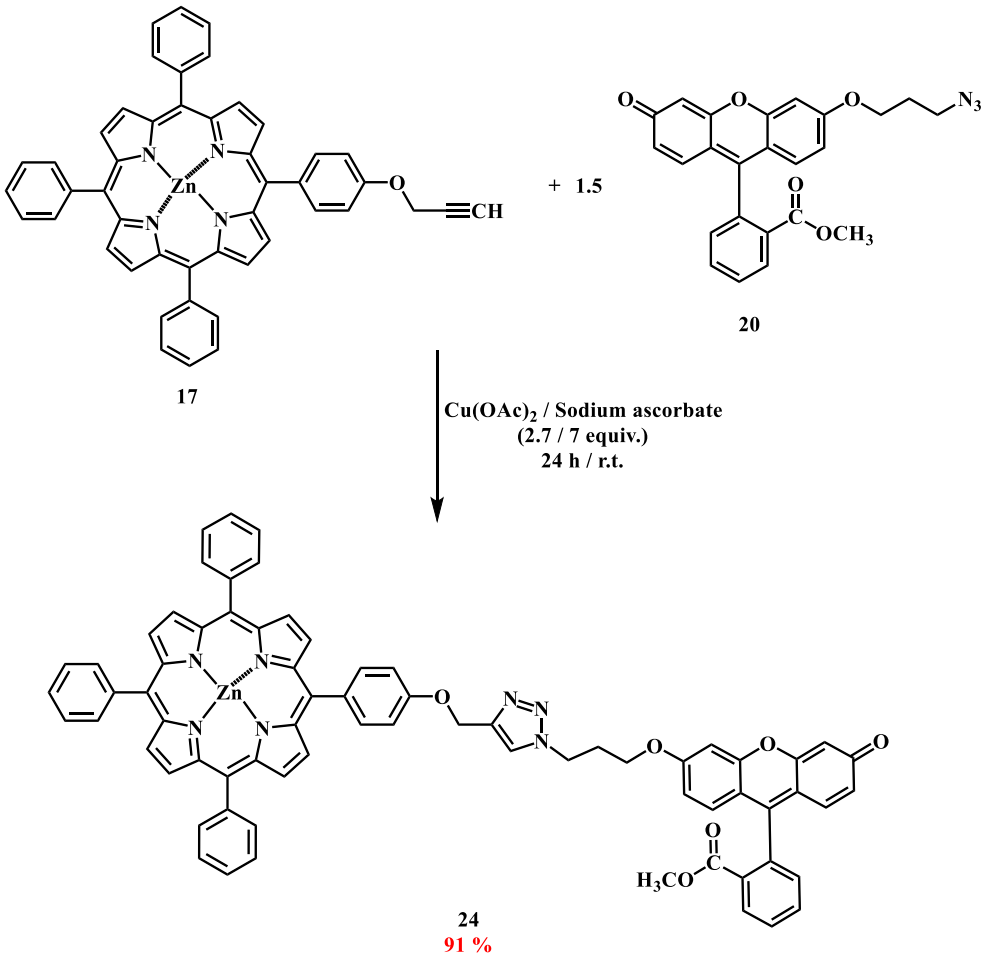

Figure 129: Synthesis of dyad **24** using click-chemistry.

4.3.2. NMR characterizations

All NMR spectra (^{1}H and ^{13}C) were performed in $CDCl_3$ with TMS as internal reference. NMR spectra interpretation of dyad **24** was difficult because both porphyrin and fluorescein moieties have aromatic protons and carbons in the same chemical shift range,. We have therefore chosen to describe separately the two patterns in order to be as clear as possible. ^{1}H-NMR of porphyrins derivatives and moiety in **24** are summarized in Table 16 while ^{1}H-NMR of fluorescein derivatives and moiety in **24** are in Table 17.

As expected, complete metalation of **16** to give **17** is confirmed by disappearance of signal at -2.74 ppm. The formation of the triazole bridge is observed by the appearance of a characteristic proton signal at 8.07 ppm and simultaneously by the disappearance of the proton signal of propargyl function at 2.69 ppm. Moreover, a slight variation of the chemical shifts for protons carried by the porphyrin appears. It can result from a folding between porphyrin and fluorescein patterns, indeed triazole linkage showed a high degree of freedom. The same

difference between fluorescein intermediates and the similar protons into dyad **24** would be consistent with the hypothesis of a folding.

- Porphyrin moieties (**16-17** and **24**)

Table 16: ^{1}H-NMR of compounds **16-17** and **24** in $CDCl_3$. δ are in ppm.

H	**16**	**17**	**24** (porphyrin part)
β-pyrrolic	8.87 d (4.8 Hz) (2H) 8.83 s (6H)	8.88 d (4.8 Hz) (2H) 8.84 s (6H)	8.98 d (4.7 Hz) (2H) 8.94 s (6H)
2,6-phenyl	8.21 d (7.6 Hz) (6H)	8.21 d (7.4 Hz) (6H)	8.14 d (7.7 Hz) (6H)
2,6-aryl	8.04 d (8.3 Hz) (2H)	8.14 d (8.4 Hz) (2H)	8.03 d (8.3 Hz) (2H)
3,4,5-phenyl	7.75 d (7.4 Hz) (9H)	7.75 d (7.4 Hz) (9H)	7.73 m (9H)
3,5-aryl	7.16 d (8.2 Hz) (2H)	7.36 d (8.2 Hz) (2H)	7.36 d (8.5 Hz) (2H)
NH_{int}	-2.74 s (2H)	--	--
$O\text{-}CH_2$	4.98 d (2.3 Hz) (2H)	4.99 d (2.4 Hz) (2H)	5.53 d (2.4 Hz) (2H)
$H_{propargyl}$	2.69 t (2.3 Hz) (1H)	2.69 t (2.3 Hz) (1H)	--
$H_{triazole}$	--	--	8.07 s (1H)

- Fluorescein moieties (**22-24**)

Table 17: ^{1}H-NMR of compounds **22-24** in CDC_{l3}. δ are in ppm.

H	**22**	**23**	**24 (**fluorescein part)
13	8.25 dd (7.8 / 1.2 Hz) (1H)	8.24 dd (7.6 / 1.2 Hz) (1H)	8.24 dd (7.5 / 1.2 Hz) (1H)
17	7.74 dt (7.5 / 1.4 Hz) (1H)	7.74 dt (7.5 / 1.4 Hz) (1H)	7.74 dt (7.5 / 1.3 Hz) (1H)
19	7.66 dt (7.6 /1.4 Hz) (1H)	7.67 dt (7.6 /1.4 Hz) (1H)	7.67 dt (7.6 /1.4 Hz) (1H)
18	7.36 dd (7.5 / 1 Hz) (1H)	7.30 dd (7.5 / 1 Hz) (1H)	7.30 dd (7.5 / 1 Hz) (1H)
11	6.96 d (2.4 Hz) (1H)	6.96 d (2.4 Hz) (1H)	6.95 d (2.4 Hz) (1H)
14	6.89 d (8.8 Hz) (1H)	6.90 d (8.9 Hz) (1H)	6.90 d (8.9 Hz) (1H)
10	6.85 d (9.7 Hz) (1H)	6.85 d (9.7 Hz) (1H)	6.80 d (8.9Hz) (1H)
9	6.74 dd (8.9 / 2.4 Hz) (1H)	6.74 dd (8.9 / 2.4 Hz) (1H)	6.73 dd (8.9 / 2.4 Hz) (1H)
20	6.55 dd (9.7 / 1.7) (1H)	6.55 dd (9.7 / 1.5) (1H)	6.61 dd (8.8 / 2.1) (1H)
7	6.47 d (1.6 Hz) (1H)	6.47 d (1.6 Hz) (1H)	6.42 d (1.6 Hz) (1H)
25	3.64 s (3H)	3.64 s (3H)	3.63 s (3H)
26	4.24 t (5.8 Hz) (2H)	4.17 t (5.7 Hz) (2H)	4.14 t (5.9 Hz) (2H)
27	2.37 quint (6.1 Hz) (2H)	2.10 quint (6.5 Hz) (2H)	2.10 m (2H)
28	3.60 t (6.3 Hz) (2H)	3.53 t (6.5 Hz) (2H)	3.54 s_{el} (2H)

As for porphyrin, the fluorescein pattern's protons of dyad **24** (H_{10}, H_{20} and H_7) showed slight shift. However, if there is no interaction between the two moieties, this modification should not be observed.

In addition, for all compounds, ^{13}C-NMR spectra correlate expected structures.

4.3.3. Mass spectra

Structural analysis of compounds **16-17** and **22-24** was pursued by studying their mass spectrum and results exhibited shown the molecular peak $[M+H]^+$ (Table 18).

Table 18: m/z values of [M+H]+ ions for compounds 16-17 and **22-24**, obtained by HRMS (a) or Maldi-TOF (b).

Compounds	Chemical formula	Monoisotopic mass	$[M+H]^+$
16 (b)	$C_{47}H_{32}N_4O$	668.80	669.2367
17 (b)	$C_{47}H_{30}N_4OZn$	730.17	731.1529
22 (a)	$C_{24}H_{19}BrO_5$	466.04	467.0918
23	$C_{24}H_{19}N_3O_5$	429.43	unstable
24 (a)	$C_{71}H_{49}N_7O_6Zn$	1159.30	1160.3102

As for NMR, HRMS and Maldi-TOF analysis confirmed that the structures were well those expected.

4.4. Alkane dyads (**25-26**)

4.4.1. Synthesis

The synthesis of alkane dyad **25** is done in two steps. First, the porphyrin **13** is functionalized with the spacer arm (Figure 130), then coupled in a second step with fluorescein pattern **20** (Figure 131). In order to compare the different molecules synthesized, an additional metalation step was carried out to obtain metallated analog **26**.

In order to obtain precursor **18**, compound **13** is dissolved in DMF with an excess of 1,3-dibromopropane (Figure 130). Then reaction is stirred during 48 hours at room temperature, and after purification on chromatographic column **18** is obtained with 89 % yields. As for synthesis of modified fluorescein **22**, first yields obtained were decreased by the formation of dimers (Entry 5, Table 19). Several variables have been changed to increase yields (Table 19).

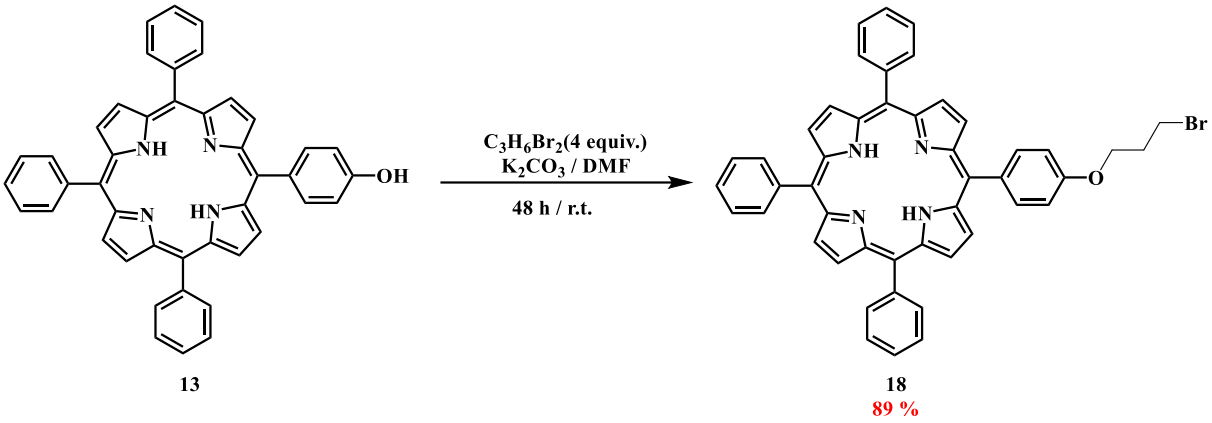

Figure 130: Synthesis of porphyrin precursor **18**.

Table 19: Experimental conditions tested for **18** synthesis.

Entry	Equiv. $C_3H_6Br_2$	Equiv. K_2CO_3	Time (h)	Temperature	Yields (%)
1	10	10	2x8 min	M.W. (200 W / 120 °C)	15
2	20 (dilute)	20	48	80 °C	17
3	20	20	48	80 °C	70
4	20	20	48	r.t.	76
5	8	20	48	r.t.	61
6	4	4	48	r.t.	89

Except for entry number 2, all reactions were performed in concentrated solutions. Heating the reaction causes an increase in the amount of dimers formed and thus a decrease of **18** yields (Entries 2-3). For microwave irradiations (Entry 1), explanation may come from the inability to ensure uniform irradiation power, which prevented to reach desired temperature. Increasing 1,3-dibromopropane equivalents not only complicates salt removing step (formation of emulsions difficult to eliminate), but also increases dimer formation (Entry 4).

Then, coupling with fluorescein precursor **20** was made by nucleophilic substitution in DMF, during 72 hours and at room temperature to avoid reactants degradation (Figure 131). Dyad **25** is obtained with low yields (20 %), however reaction conditions have not been optimized yet.

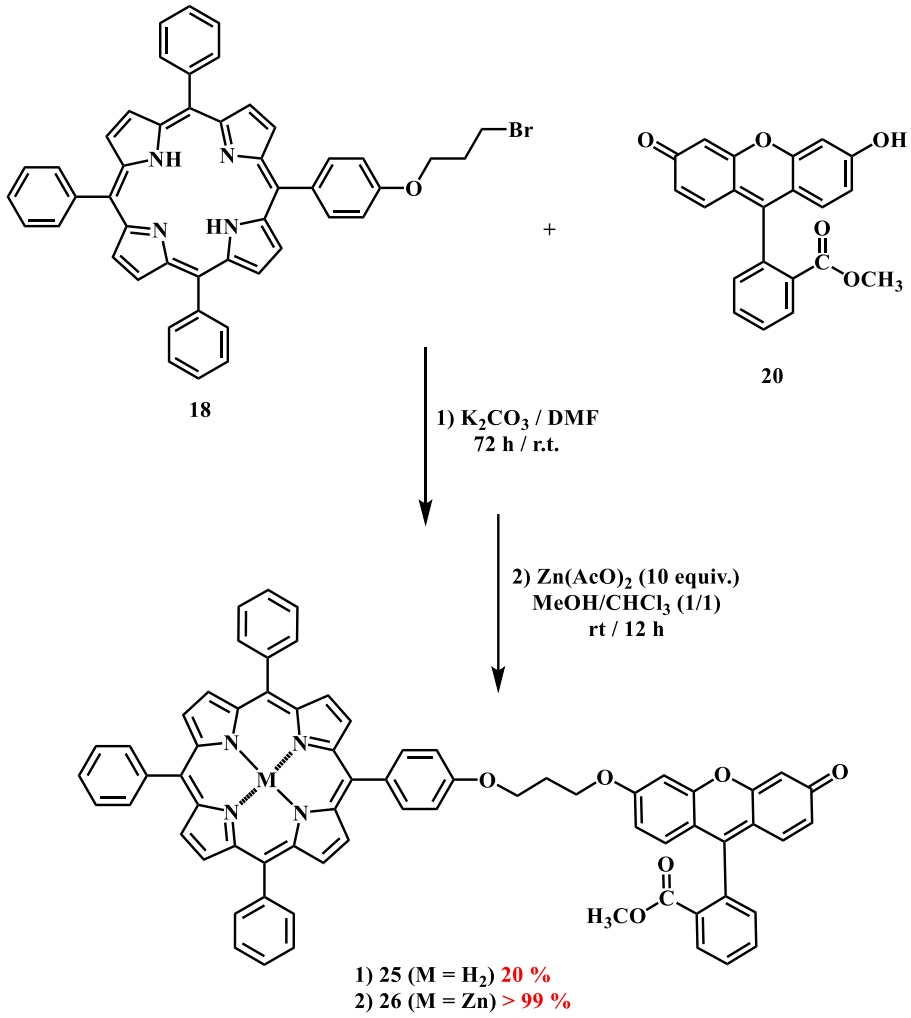

Figure 131: Synthesis of dyads **25** and **26**.

Triazole dyad **24** being metallized with zinc (due to its method of synthesis), so we chose to metallate **25** in the same way (Figure 131). As for porphyrins **15** and **17**, we used the conventional method: an excess of zinc acetate in a mixture of chloroform and methanol (1/1; v/v). The reaction was stirred at room temperature for 12 hours, and monitoring was carried out by UV-Vis absorption spectroscopy. After salt removing and evaporation to dryness, compounds **26** is obtained in quantitative yields (> 99 %).

Thus we will have access to comparable compounds for the purpose of evaluating their photophysical properties. Moreover, it allows evaluating the influence of metal between compounds **25** and **26**.

4.4.2. NMR characterizations

All NMR spectra (^{1}H and ^{13}C) were performed in $CDCl_3$ with TMS as internal reference. As for **24**, interpretation of ^{1}H-NMR of dyads **25** and **26** are described separately for the two

patterns. ^{1}H-NMR of porphyrins are summarized in Table 20 while ^{1}H-NMR of fluorescein in Table 21.

- Porphyrin moieties (**18, 25-26**)

Table 20: ^{1}H-NMR of compounds **18**, **25** and **26** in $CDCl_3$. δ are in ppm.

H	**18**	**25** (porphyrin part)	**26** (porphyrin part)
β-pyrrolic	8.87 d (4.7 Hz) (2H) 8.84 s_{el} (6H)	8.85 d (4.7 Hz) (2H) 8.82 d (6.4 Hz) (6H)	8.85 d (4.7 Hz) (2H) 8.82 d (6.4 Hz) (6H)
2,6-phenyl	8.21 d (7.8 Hz) (6H)	8.21 d (7.5 Hz) (6H)	8.21 d (7.5 Hz) (6H)
2,6-aryl	8.10 d (8.3 Hz) (2H)	8.11 d (8.5 Hz) (2H)	8.11 d (8.5 Hz) (2H)
3,4,5-phenyl	7.76 d (7.4 Hz) (9H)	7.74 m (9H)	7.74 m (9H)
3,5-aryl	7.26 d (8.6 Hz) (2H)	7.27 d (8.6 Hz) (2H)	7.27 d (8.6 Hz) (2H)
NH_{int}	-2.76 s (2H)	-2.76 s (2H)	--
O-CH_2	4.55 t (6.3 Hz) (2H)	4.10 t (6.2 Hz) (4H)	4.10 t (6.2 Hz) (4H)
CH_2-Br	4.35 t (6.0 Hz) (2H)	--	--
CH_2	2.35 q (6.2 Hz) (2H)	2.49 q (6.1 Hz) (2H)	2.49 q (6.1 Hz) (2H)

- Fluorescein moieties (**25** and **26**)

Table 21: ^{1}H-NMR of compounds **25** and **26** in $CDCl_3$. δ are in ppm.

H	**25** (fluorescein part)	**26** (fluorescein part)
13	8.24 dd (7.9 / 1.1 Hz) (1H)	8.24 dd (7.9 / 1.1 Hz) (1H)
17	7.74 dt (7.5 / 1.4 Hz) (1H)	7.74 dt (7.5 / 1.4 Hz) (1H)
19	7.66 dt (7.8 /1.1 Hz) (1H)	7.66 dt (7.8 /1.1 Hz) (1H)
18	7.31 dd (7.6 / 1 Hz) (1H)	7.31 dd (7.6 / 1 Hz) (1H)
11	7.08 d (2.4 Hz) (1H)	7.08 d (2.4 Hz) (1H)
14	6.92 d (8.9 Hz) (1H)	6.92 d (8.9 Hz) (1H)
10	6.85 d (9.7 Hz) (1H)	6.85 d (9.7 Hz) (1H)
9	6.82 dd (8.9 / 2.4 Hz) (1H)	6.82 dd (8.9 / 2.4 Hz) (1H)
20	6.54 dd (9.7 / 1.9) (1H)	6.54 dd (9.7 / 1.9) (1H)
7	6.48 d (1.9 Hz) (1H)	6.48 d (1.9 Hz) (1H)
25	3.64 s (3H)	3.64 s (3H)

^{1}H-NMR spectra confirmed grafting of the bromopropyl arm to the porphyrin. The difference on proton chemical shifts between O-CH_2 and CH_2-Br comes from the electronegativity gap between oxygen and bromine atoms. Protons carried by the carbon

directly bonded to the oxygen of the arms (4.55 ppm) are more de-shielded than those attached by the carbon linked to bromine (4.32 ppm). Disappearance of these signals coupled with simultaneous appearance of a signal at 4.10 ppm (which integrates for 4 hydrogens) is characteristic of coupling between **18** and **20**. In fact, in dyad **25** the two CH_2 groups have a similar chemical environment and therefore the same chemical shift. Disappearance of the signal at -2.76 ppm confirms the complete metalation of **26**. Moreover, all structures were confirmed by ^{13}C-NMR analysis.

4.4.3. Mass spectra

Structural analysis of compounds **18**, **25** and **26** was pursued by studying their mass spectrum (Table 22). All compounds exhibited the molecular peak $[M+H]^+$.

Table 22 : m/z values of [M+H]+ ions for compounds **18**, **25** and **26**; obtained by HRMS.

Compounds	Chemical formula	Monoisotopic mass	$[M+H]^+$
18	$C_{47}H_{35}N_4OBr$	751.73	753.2053
25	$C_{68}H_{48}N_4O_6$	1016.36	1017.3702
26	$C_{68}H_{46}N_4O_6Zn$	1078.27	1079.2247

As for NMR, HRMS analysis confirmed that the structures were well those expected.

4.5. Alkyne dyads (**27-28**)

4.5.1. Synthesis

Synthesis of alkyne dyads **27** and **28** was performed according to the same principle as for dyads **25** and **26**. First porphyrin **13** was functionalized with the spacer (Figure 132), then coupled with fluorescein precursor **20**.

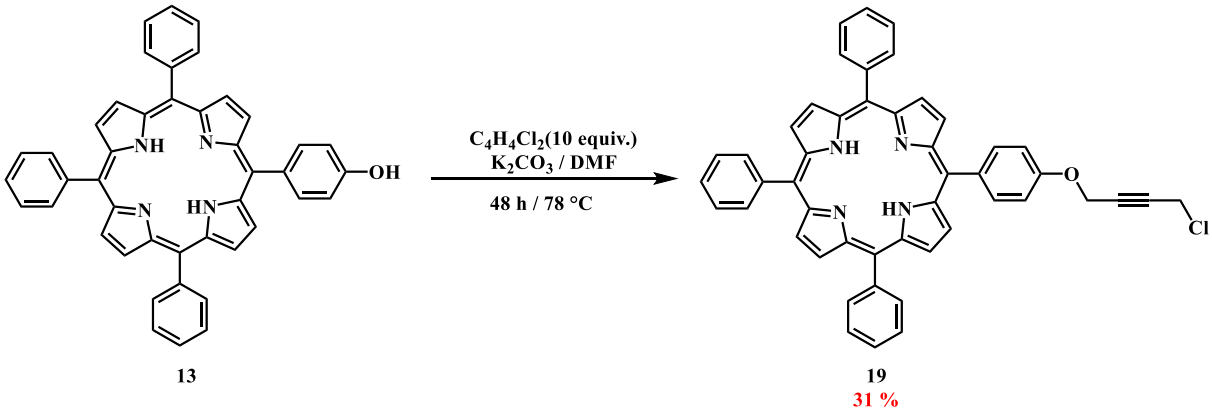

13

19

31 %

Figure 132: Synthesis of porphyrin precursor **19**.

In order to compare dyads, the zinc metallated analog was achieved (Figure 134). In order to obtain precursor **19**, compound **13** was dissolved in DMF with an excess of 1,4-dichloro-2-butyn (Figure 132). Then reaction is stirred during 48 hours at 70 °C, and after salt removing and purification on chromatographic column **19** is obtained with 31 % yields. As for synthesis of modified fluorescein **22** and porphyrin **18**, yields were decreased by the formation of dimers (18-24 %). As for **18** several variables have been changed to increase yields (Table 23).

Table 23: Some conditions used to optimize **19** synthesis.

Entry	Equiv. $C_3H_6Br_2$	Equiv. K_2CO_3	Time (h)	Temperature	Yields (%)
1	5 / 10 / 20	20	48	r.t.	-
2	10	20	48	30 °C	22
3	10	20	48	70 °C	31
4	20	20	48	70 °C	15
5	4	10	48	70 °C	10
6	4	4	48	70 °C	7
7	10	10	4*5 min	200 W / 120 °C	26
8	10	20	4*5 min	200 W / 120 °C	22

Contrary to compound **18** synthesis, reaction must be heated (Entries 1-2). However, modify operating conditions as reactants equivalents (K_2CO_3 and 1,4-dichloro-2-butyn) or type of activation did not lead to a significant improvement in yields (Entries 4-8). In addition, 1,4-dichloro-2-butyn seems to be particularly unstable (even under inert atmosphere, hydrochloric acid formation occurred and a dark coloration appeared) which could explain partially low yields obtained. Thus, when the reagent was added to the porphyrin **13** solution, a green coloration of the porphyrin (phenomenon of protonation) due to HCl appeared for a few moments until DMF addition. To remedy this problem, we proposed to replace chlorine atom by a better leaving group. For this, we started from 1,4-dihydroxy-2-butyn (which is commercial) with *p*-toluenesulfonyl chloride. Unfortunately, first attempts according to Ouchi *et al*. protocol[441] have not led to the desired product. A second approach was chosen (also according to literature) and will be tested soon. It consists in coupling the diol with triflic anhydride in presence of 2,6-lutidine, then reacting the product so formed with porphyrin (Figure 133).[442]

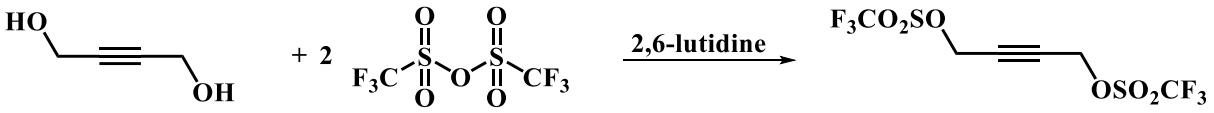

Figure 133: General procedure with triflic anhydride.

Then, as for dyad **25**, coupling with fluorescein precursor **20** is made by nucleophilic substitution in DMF, during 72 hours and at room temperature to avoid alkyne arm degradation (Figure 134). Dyad **27** is obtained with low yields (30 %), however reaction conditions have also not been optimized yet.

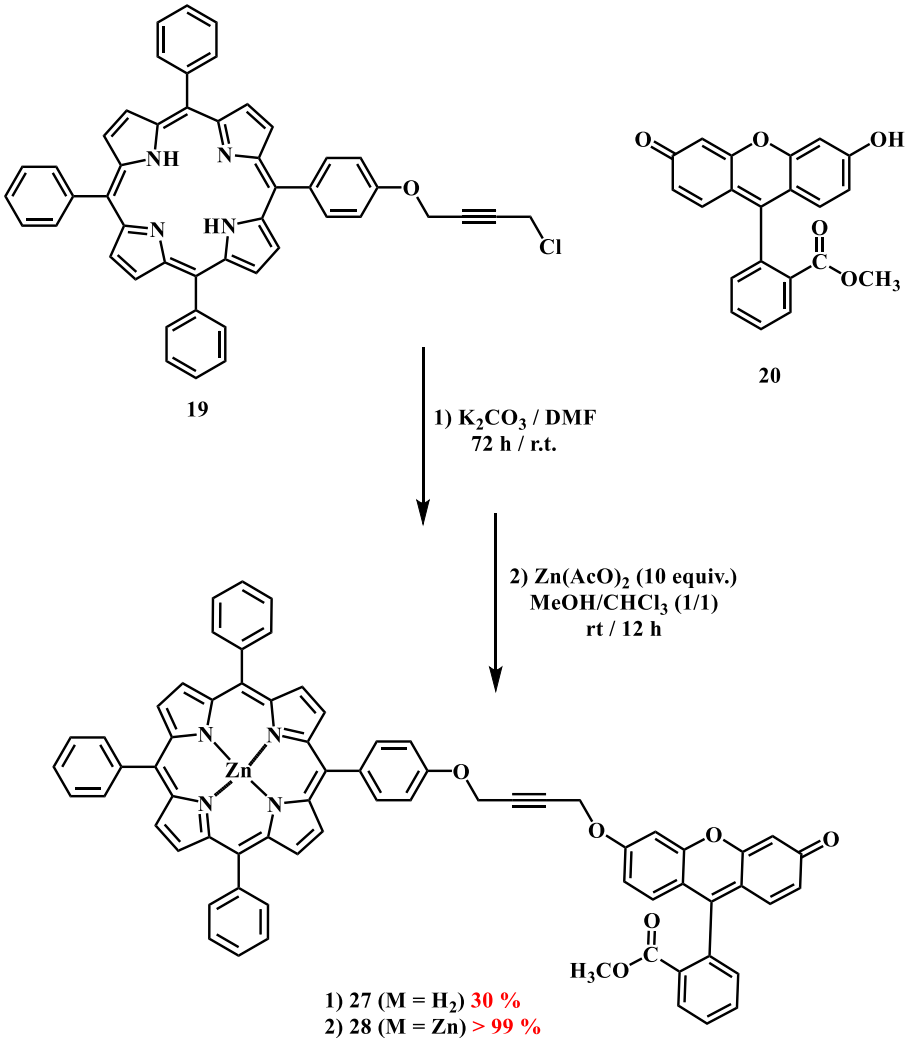

Figure 134: Synthesis of dyads **27** and **28**.

Finally, zinc metallated compound **28** is synthesized in quantitative yields (> 99 %) by using an excess of zinc acetate in a mixture of methanol and chloroform, during 12 hours at room temperature. Monitoring was carried out by UV-Vis absorption spectroscopy.

4.5.2. NMR characterizations

All NMR spectra (^{1}H and ^{13}C) were performed in $CDCl_3$ with TMS as internal reference. As for dyads **24-26**, interpretation of ^{1}H-NMR of dyads **27** and **28** are described separately for the two patterns. ^{1}H-NMR are summarized in Table 24 and Table 25.

- Porphyrin moieties (**19**, **27** and **28**)

Table 24: ^{1}H-NMR of compounds **5**, **15** and **16** in $CDCl_3$. δ are in ppm.

H	**19**	**27** (porphyrin part)	**28** (porphyrin part)
β-pyrrolic	8.87 d (4.7 Hz) (2H) 8.84 d (4.8 Hz) (6H)	8.84 d (4.8 Hz) (2H) 8.82 d (4.1 Hz) (6H)	8.84 d (4.8 Hz) (2H) 8.82 d (4.1 Hz) (6H)
2,6-phenyl	8.21 d (7.7 Hz) (6H)	8.20 d (7.1 Hz) (6H)	8.20 d (7.1 Hz) (6H)
2,6-aryl	8.13 d (8.6 Hz) (2H)	8.05 d (8.5 Hz) (2H)	8.05 d (8.6 Hz) (2H)
3,4,5-phenyl	7.76 m (9H)	7.76 m (9H)	7.76 m (9H)
3,5-aryl	7.33 d (8.6 Hz) (2H)	7.29 d (8.5 Hz) (2H)	7.28 d (8.6 Hz) (2H)
NH_{int}	-2.76 s (2H)	-2.75 s (2H)	--
O-CH_2	5.02 t (1.8 Hz) (2H)	5.02 s_{el} (2H)	5.02 t (1.5 Hz) (2H)
CH_2-Cl	4.29 t (1.8 Hz) (2H)	--	--
CH_2-O	--	4.95 s_{el} (2H)	4.94 t (1.5 Hz) (2H)

- Fluorescein moieties (**27-28**)

Table 25: ^{1}H-NMR of compounds **27-28** in $CDCl_3$. δ are in ppm.

H	**27** (fluorescein part)	**28** (fluorescein part)
13	8.22 m (1H)	8.22 dd (7.9 / 1.1 Hz) (1H)
17	7.77 dt (7.5 / 1.4 Hz) (1H)	7.77 dt (7.5 / 1.4 Hz) (1H)
19	7.71 dt (7.6 /1.3 Hz) (1H)	7.71 dt (7.6 /1.3 Hz) (1H)
18	7.30 dd (7.6 / 0.9 Hz) (1H)	7.30 dd (7.6 / 0.9 Hz) (1H)
11	7.10 d (2.7 Hz) (1H)	7.10 d (2.7 Hz) (1H)
14	6.93 d (8.6 Hz) (1H)	6.93 d (8.6 Hz) (1H)
10	6.91 d (9.7 Hz) (1H)	6.91 d (9.7 Hz) (1H)
9	6.84 dd (8.9 / 2.4 Hz) (1H)	6.84 dd (8.9 / 2.4 Hz) (1H)
20	6.55 dd (9.7 / 1.9) (1H)	6.55 dd (9.7 / 1.9) (1H)
7	6.48 d (2.0 Hz) (1H)	6.48 d (2.0 Hz) (1H)
25	3.52 s (3H)	3.52 s (3H)

^{1}H-NMR spectra confirmed grafting of the chloro-2-butyn arm to the porphyrin. As for **25**, the difference on protons chemical shifts between O-CH_2 (5.02 ppm) and CH_2-Cl (4.29 ppm) comes from the electronegativity gap between oxygen and chloride atoms. In dyad **27,** this gap decreases because the two groups have the same environment (O-CH_2). Disappearance of the signal at -2.76 ppm confirms the complete metalation of **28**. Moreover, ^{13}C-NMR analysis confirms structures.

4.5.3. Mass spectra

Structural analysis of compounds **19**, **27** and **28** was pursued by studying their mass spectrum (Table 26). All compounds exhibited the molecular peak $[M+H]^+$.

Table 26: m/z values of [M+H]+ ions for compounds **19, 27** and **28**; obtained by HRMS.

Compounds	Chemical formula	Monoisotopic mass	$[M+H]^+$
19	$C_{48}H_{33}N_4OCl$	716.23	717.3211
27	$C_{69}H_{46}N_4O_6$	1026.34	1027.3490
28	$C_{69}H_{44}N_4O_6Zn$	1088.26	1089.3128

As for NMR, HRMS analysis confirmed that the structures were well those expected.

5. Conformational analysis

Conformational features of both porphyrin and fluorescein moieties have been extensively described, mainly stressing planarity as being responsible for their photophysical properties.[123] Distortion from planarity has been described for porphyrins depending on the central metal, substituents and environmental conditions.[443,444] In fluorescein, only the xanthen-3-one moiety is fully planar, whereas the phenyl ring is almost perpendicular to the former. In the dyad, both nature and length of the linker are key elements, determining conformation and thus electronic interactions between both chromophores, which should have a pronounced effect especially on energy transfer between the porphyrin and fluorescein moieties.

5.1. Dyad **24**

As seen above, for compound **24**, the linker is particularly flexible. As often observed in such dyad systems bearing two separate chromophores, folding is likely to occur,[445–447] providing two types of conformers. To experimentally investigate the presence of folded *vs*. linear conformations, we conducted temperature dependent ^{1}H-NMR studies of **24** in $CDCl_3$ between 233 K and 333 K in collaboration with the PIAM platform of the University of Angers (B. SIEGLER) (Figure 135).

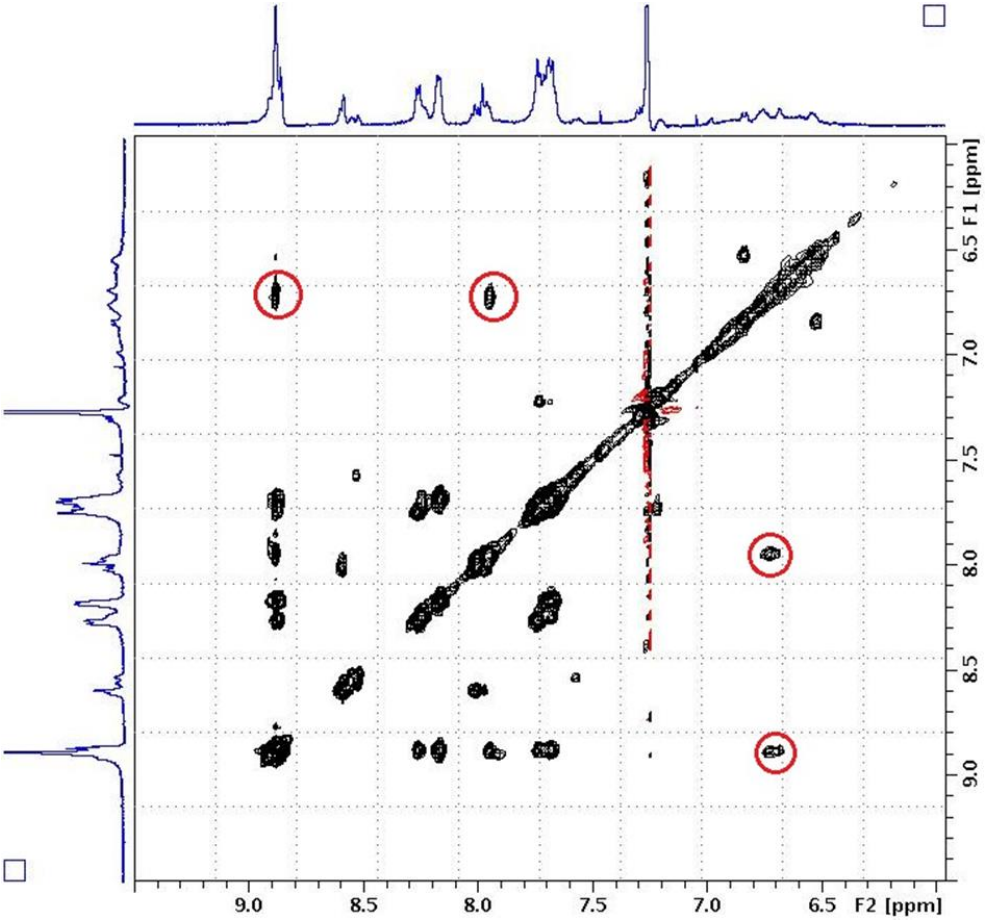

Figure 135: Aromatic region of the NOESY spectrum of **24** at 253 K. The fluorescein-porphyrin correlations are circled in red.

Porphyrin hydrogen peaks were seen as broad signals at high temperature, which sharpened and split as temperature was lowered, possibly revealing the presence of different conformers undergoing fast exchange at high temperature. NOESY spectra were therefore performed at 253 K and 323 K in order to see possible spatial proximity between both the porphyrin and the fluorescein moieties. The NOESY spectrum obtained at low-temperature showed correlation spots between some protons of xanthen-3-one moiety of fluorescein (at 6.7 ppm) and of porphyrin (at 7.9 ppm and 8.9 ppm), revealing a folded geometry of the dyad

(Figure 135). Those correlation spots were absent in the high-temperature spectrum (323 K), probably due to fast exchanges between the conformers.

To support these experimental evidences and to clearly describe conformers, a DFT-based conformational analysis was conducted. This was assessed by using both the standard B3LYP (that does not include dispersion) and the ωB97XD (that includes both dispersion and long-range corrections) exchange-correlation (XC) functionals.[448,449] Full geometry optimizations were performed in the gas phase, as well as in chloroform, DMSO and water by considering implicit solvent (PCM). A systematic conformational exploration revealed a few potential conformations either roughly linear or folded. In a first instance, and in order to simplify the preliminary study, only the most stable conformer, which is folded, was considered throughout this study. An unfolded geometry, which corresponded to the local minimum being almost linear (Figure 136), was also considered in this study for that sake of comparison. This latter geometry avoided, as much as possible, contacts between both chromophores. All properties of both geometries were evaluated after full optimization (absence of any imaginary frequency).

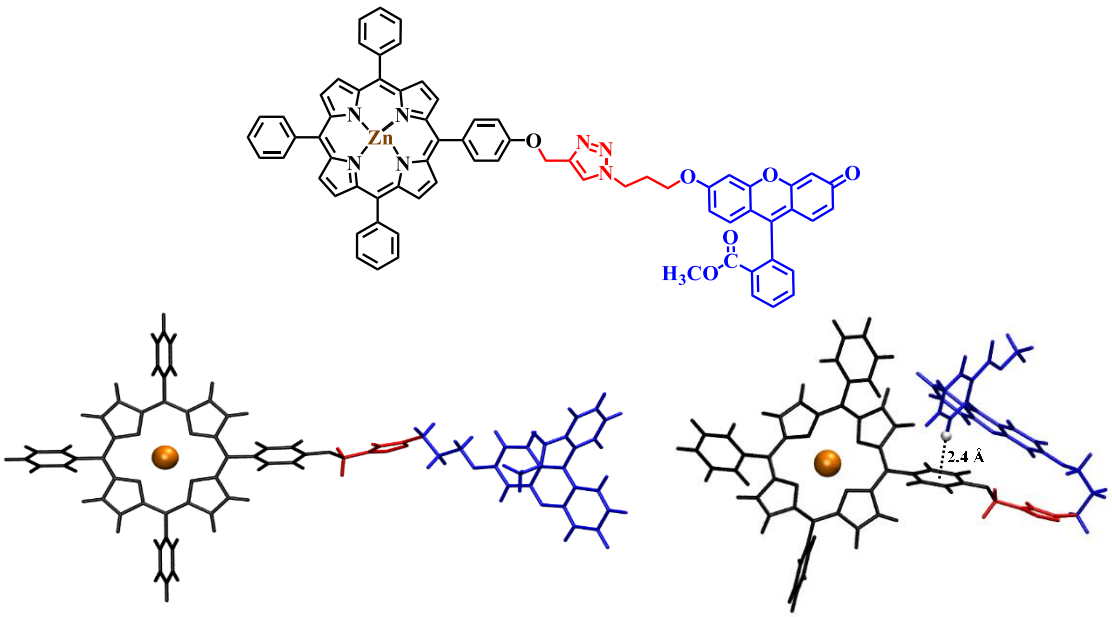

Figure 136: Linear and folded form of **24** according to conformational analysis (ωB97XD).

The folded-type geometry is stabilized against the linear one even at the B3LYP level (relative Gibbs energy of 16.4, 75.4, 85.5 and 98.8 kJ·mol^{-1} in the gas phase, chloroform, DMSO and water, respectively in favor of the folded conformers; Table 27). These results indicate significant electrostatic contributions in stabilization. At the ωB97XD level, the folded forms are additionally stabilized through dispersion interactions (*i.e.* relative Gibbs energy of 78.6, 104.7, 136.6 and 152.7 kJ·mol^{-1} in the gas phase, chloroform, DMSO and water, respectively;

Table 27). The folded conformer highlights in particular an attractive interaction, known as CH-π interaction,[450] between the hydrogen of the benzoate group of fluorescein and the π-system of the phenyl-substituent of porphyrin, with a distance of *ca*. 2.4 Å (lowest inter- fragment distance), as seen in Figure 136. Such interactions are known to be described by a strong dispersion contribution,[451,452] therefore requiring correct description of such interaction, as obtained with the dispersion-corrected ωB97XD functional but not with B3LYP for which the lowest distance between the two moieties is *ca.* 5.8 Å (Table 28). Solvent nature is expected to influence ratio between linear and folded form, especially promoting folded form when polarity increases. Indeed, the calculations assessed with PCM show that stabilization of the folded structure *vs*. the linear one is stronger in water (relative Gibbs energy of 152.7 kJ.mol^{-1} at the ωB97XD level, Table 27) than in chloroform (relative Gibbs energy of 104.7 kJ.mol^{-1}, Table 27).

Table 27: Energy gap between linear and fold form in dyad **24** in different solvents using PCM method.

	Gas phase	Chloroform	DMSO	Water	Gas phase	Chloroform	DMSO	Water
	ΔE (linear-folded) in Hartrees				**ΔE (linear-folded) in kJ.mol^{-1}**			
B3LYP	0.01	0.03	0.03	0.04	16.4	75.4	85.4	98.8
ωB97XD	0.03	0.04	0.05	0.06	78.6	104.7	136.6	152.7
	ΔE (linear-folded) in eV				**ΔE (linear-folded) in kcal.mol^{-1}**			
B3LYP	0.17	0.78	0.89	1.02	3.9	18.0	20.4	23.6
ωB97XD	0.81	1.08	1.42	1.58	18.8	25.0	32.6	36.5

Because the explicit description of solvent molecules is missing with PCM, one can imagine that the absolute values of stabilizing Gibbs energy between folded and linear forms are overestimated. Indeed in our methodology of calculation, the entropic contribution is only partially and indirectly described, and could hardly be accessible at a reasonable computational cost. This ensures a solid comparative description *i.e.*, accuracy of the relative Gibbs energies, but it possibly produces inaccurate absolute energy values. This may explains why the calculations perfectly agree with the NOESY experiments at low-temperature, but not high-temperature. When increasing temperature, the entropic contributions become most probably crucial, which should rationalize fast exchanges between conformers suggested from experimental evidences. To stress the effect of folding on optical properties, a folded and a linear conformer were considered for the theoretical analysis.

Table 28: Distances between the two different patterns (porphyrin and fluorescein) into **24**.

	B3LYP		ωB97XD	
	Lowest inter-fragment distance (Å)	Center to center (Å)*	Lowest inter-fragment distance (Å)	Center to center (Å)*
Linear form	9.5	21.13	10.8	21.15
Folded form	5.8	10.2	2.4	8.4

*Distance between the center of the metal of porphyrin moiety and the center of the xanthen-3-one moiety

5.2. Dyads **26** and **28**

Due to the rigidity of the alkyne linker, as expected, compound **28** did not exhibit folding and only one linear geometry (Figure 137) was obtained with both functionals (B3LYP and ωB97XD), regardless solvent nature (chloroform or DMSO). The higher flexibility of the 3-carbon-alkane linker of compound **26** allows slight bending of the structure, however not sufficient to allow folding and close contact between the two porphyrin and fluorescein moieties (Figure 138).

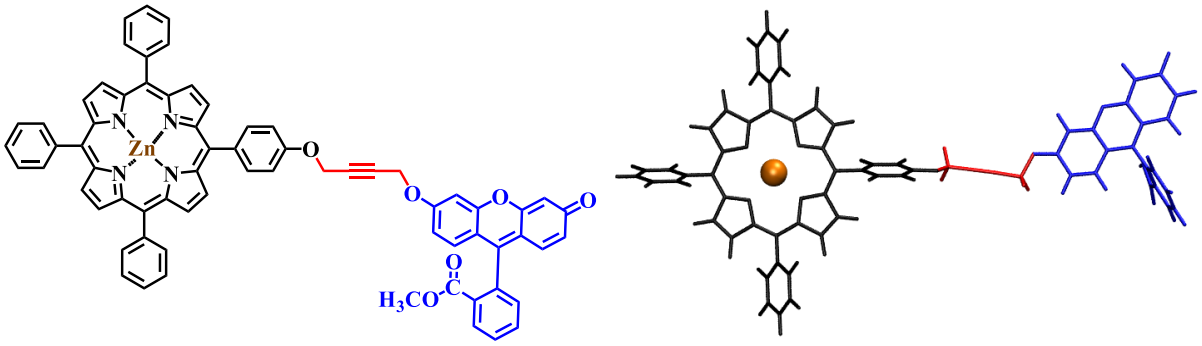

Figure 137: Structure of **28** according to conformational analysis (ωB97XD).

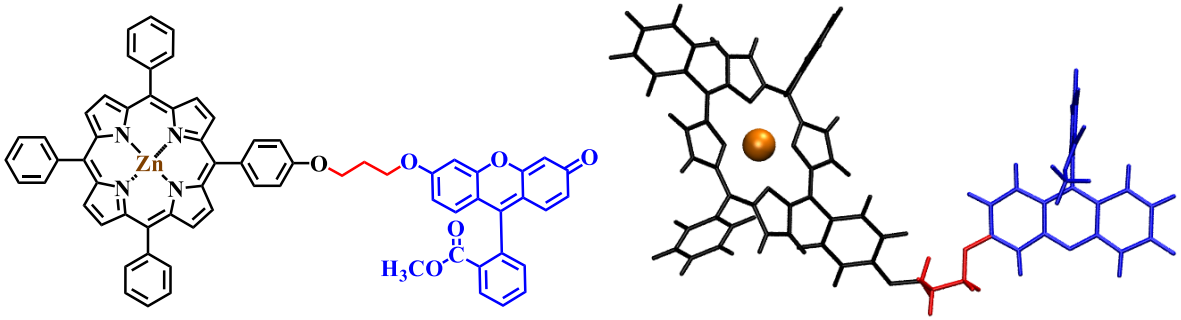

Figure 138: Structure of **26** according to conformational analysis (ωB97XD.

6. Photophysical properties

The absorption and fluorescence emission properties of free-base (**25** and **27**) or zinc-metallated (**24, 26** and **28**) derivatives were performed both in chloroform and in DMSO. All compounds were purified just before all spectral analyses. Moreover, because no oxygen effect was observed on spectra, spectral evaluations were achieved in non-degassed solutions. All compounds were stored under argon between each experiment.

6.1. Experimental and calculated optical properties

All experimental UV-Vis absorption spectra were performed in chloroform and DMSO at room temperature (concentration ca. 2.10^{-6} mol.L^{-1}). All presented results are the averaged of at least three independent experiments.

6.1.1. Optical properties of metallated dyads.

- Reference compounds **15** and **21**

The UV-Vis absorption spectrum of porphyrin **15** in chloroform (Figure 140, Table 29) is characteristic of metallated porphyrins, *i.e.*, with an intense Soret band (424 nm) and the Q-band at lower energy with vibrational structure (two peaks observed at 552 and 595 nm). This classic absorption features are well described by Gouterman's 'four orbital model',[123,124] which bases the analysis on transitions between HOMO (highest occupied molecular orbital, H) and H-1 to LUMO (lowest unoccupied molecular orbital, L) and L+1 (Figure 143 - porphyrin). Similar molecular orbital (MO) schemes were obtained with both functionals (Figure 143 and Figure 144 for B3LYP and ωB97XD, respectively; 6-31+g(d,p) was used as basis set), confirming the classical 'four orbital model'. As extensively described in the literature, the Q-band of the metallated porphyrins corresponds to a degenerated excited state (ES); *i.e.* singlet transitions to S_1, S_2.[127] As expected, the presence of the propyloxy groups slightly breaks the MO symmetry but not sufficiently to significantly break degeneracy (Figure 143 and Figure 144).

The fluorescein derivative **21** exhibits the typical absorption features of fluorescein. The absorption peaks at 439, 463 and 492 nm are assigned to apparent vibronic sub-bands of the first ES,[453] which is mainly described by the H→L electronic transition, as seen with both functionals (Figure 139). Both H and L are fully delocalized over the entire xanthen-3-one moiety. Thus, almost no modification were observed compare to fluorescein, the chemical

modifications being not involved in the π-conjugated system, hence not affecting in the π→π* electronic transition.

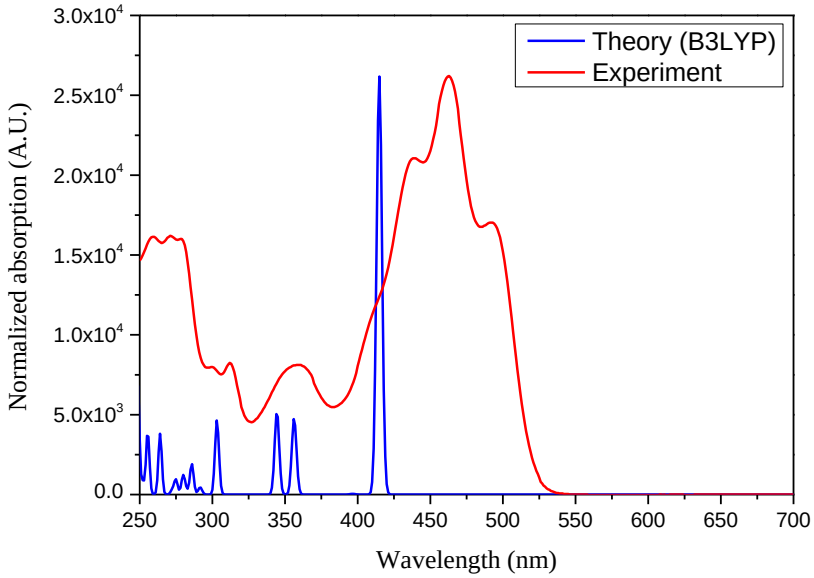

Figure 139: UV-Vis spectra of **21** in $CHCl_3$, obtained both with theoretical calculations (B3LYP/6-31+g(d,p)) and experiments.

➢ Metallated dyads **24**, **26** and **28:**

As seen in Figure 140, the experimental UV-Vis absorption spectrum of **24** in chloroform (Table 29) matches the profile obtained by the superimposition of both spectra of **15** and **21** (dashed lines, Figure 140), indicating the absence of any significant interaction in the ground state.

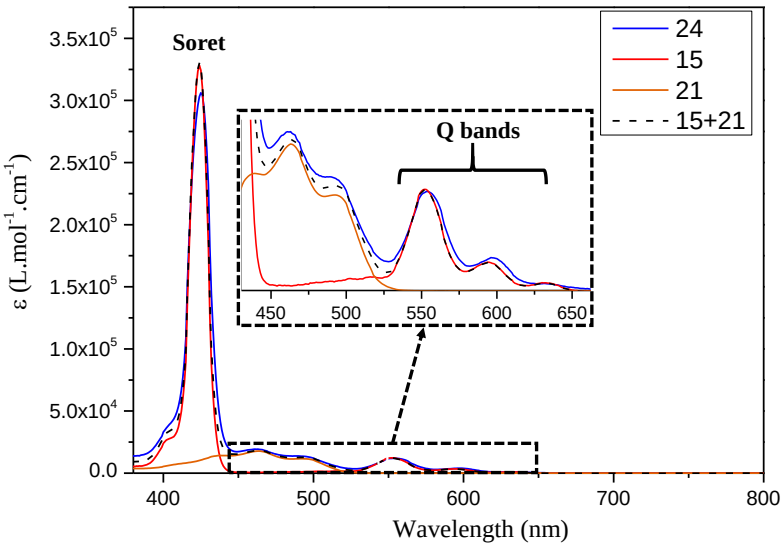

Figure 140: UV-Vis absorption spectra of metalled dyad **24**. For comparison, spectra of reference compounds **15** and **21** are also reported ($CHCl_3$, 298 K).

However, the theoretical analysis is somewhat complex arising from the question of possible charge-transfer (CT) contributions within the ES manifold. The time dependent (TD)-DFT analysis will depend on the dyad conformation (linear *vs*. folded) and on the inclusion of long-range interactions in the DFT functional (*i.e*. B3LYP *vs*. ωB97XD). Although the standard B3LYP functional is widely used to evaluate optical and electronic properties of derivatives of porphyrins,[454–456] it is known to poorly described CT ES.[457] For the most stable, folded geometry of dyad **24**, B3LYP suggests a CT state of very low oscillator strength (0.01) to be the lowest ES ($S_0 \rightarrow S_1$), being somewhat below (0.04 eV) the Q-band formed by S_2, S_3, and essentially described by a H→L excitation (Figure 143 and Appendices). The reason for the occurrence of this low-lying CT state is readily seen in the MO correlation diagram (Figure 143). Indeed, the L of **21** is calculated to be 0.53 eV below that of **15**, so that after formation of **24** (where the frontier MOs of fluorescein become destabilized) L is still formed by the fluorescein moiety, whereas H is entirely located on the porphyrin moiety. The $S_0 \rightarrow S_4$ transition again exhibits (complex) CT character (Figure 143). In the linear conformation the low-lying CT state is absent due to the large spatial separation between the moieties.

In order to decide whether CT contributions are present in the folded dyad, we performed ωB97XD and CAM-B3LYP calculations since those long-range separated XC functionals are known to better behave at describing CT states. Only the ωB97XD results are shown here (Figure 144), as CAM-B3LYP provides similar results. No ICT character was observed in any ES. The first two, nearly degenerated transitions to S_1 and S_2 were assigned to the Q-bands of the porphyrin moiety, as described by the Gouterman's 'four orbital model'. The absence of the low lying CT state is due to the small energy difference (0.19 eV) between L of **15** and L of **21** which leads to greater mixing of MOs of both fragments. So after formation of **24** the L is that of porphyrin (Figure 144), conversely to what was observed with B3LYP. The different behavior observed with both functionals most probably reflects the trend of B3LYP to overestimate π-delocalization, therefore over-stabilizing MO energy levels (*e.g.* here fluorescein), which may artificially generate CT states. On the contrary, inclusion of long-range corrections within the ωB97XD functional prevents it. CT contributions are negligible in the higher ES, which are essentially described by mixtures of fluorescein- and porphyrin-based electronic transitions. In the linear arrangement, the occurrence of CT states becomes even more unlikely due to the spatial separation between the moieties, which is in fact reproduced by ωB97XD calculations (Figure 144).

To tackle the question of CT contributions in the Q-band of **24** from the experimental side, all spectra were also recorded in DMSO as a more polar solvent that should favor the folded conformer and therefore the occurrence of an ICT if it occurs. A solvatochromic study, on a wider solvent polarity range was prevented by solubility limitations (Table 29). Only slight bathochromic shifts were experimentally observed from chloroform to DMSO for the dyad as well as for **15** and **21**. But no new band was observed. Thus, no experimental evidence of the occurrence of an ICT was found. This confirms the lack of CT contributions as suggested by the ωB97XD functional. In summary, both experimental and theoretical results revealed negligible CT contributions in the ES manifold even in the folded conformer. This agrees with the rather large center-to-center distances between the moieties (8-10 Å, Table 28), as well as the non-parallel arrangements between the π-conjugated chromophores observed in the folded conformer (Figure 136).

As observed for **24**, UV-Vis absorption spectra of compounds **26** and **28** are also characteristic of metallated porphyrin (Soret bands observed at 424 and 428 nm and Q bands at 553, 569 and 561, 600 nm for **26** and **28** respectively) associated to a fluorescein moiety (absorption bands recorded at 461 (**26)**, 464 (**28**) and 492 for both **26** and **28**) (Figure 141).

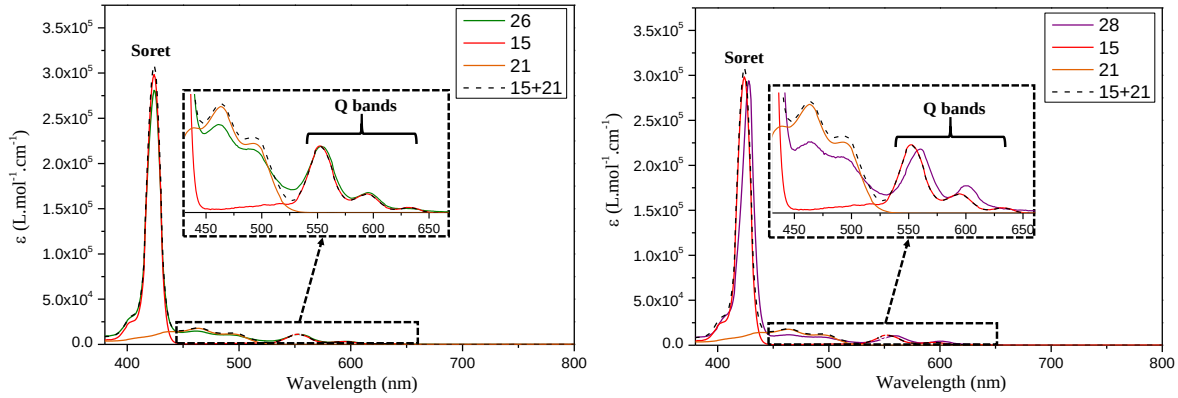

Figure 141: UV-Vis absorption spectra of metalled dyads **26** (left) and **28** (right). For comparison, spectra of reference compounds **15** and **21** are also reported ($CHCl_3$, 298 K).

However, conversely to **24**, the mathematical sum of **15** and **21** (dashed lines) does not strictly match with the spectral profiles of **26** or **28**. For **26**, hypochromic effect on the Soret band is observed in the dyad with respect to reference porphyrin **15**, while for **28** a slight red-shift (5 to 9 nm) of the Q bands is observed. This may suggest weak intramolecular interaction between moieties as no variation of these effects were observed by varying the concentration in the 2-5 µM range. Moreover, in the case of **28**, the slight red-shift could be explained by the use of a different solvent batches (VWR, RPE grade, stabilized with ethanol *vs* Alfa Aesar, Spectrophotometric grade, non-stabilized). This hypothesis is confirmed by the UV-Vis

absorption spectra recorded in DMSO. Indeed, for this solvent, the same absorption wavelengths were observed for dyads **24**, **26** and **28** as well as for reference compounds **15** and **21**. Moreover, it is worth noting that these compounds are weakly soluble in DMSO, especially **28**, requiring up to 5 min of magnetic stirring and heating to obtain homogenous solution (Table 29). Therefore, experiments were performed from 3 to 7 times in order to obtain similar spectra and enable proper calculation of ε. In addition, these spectral features of dyads **26** and **28** in DMSO give further evidence of the lack of ICT in dyad **24**, since the red-shift is not specific to this compound, being the only one for which the folded geometry is likely. Indeed, the other compounds are roughly linear in shape, which should prevent ICT occurrence. This structural difference and the rigidity of **26** and **28**, compared to **24** could also explain their different solubility in DMSO compound **24** being perfectly soluble in DMSO. Indeed, such a weak solubility is most probably attributed to the rigidity of these two compounds, which favor linear geometry and subsequently intermolecular stacking and aggregation. We believe that predominance of the folded geometry for **24** prevents such stacking thus dramatically enhancing solubility.

Table 29: UV-Vis data for dyads **24**, **26** and **28**, and references **15** and **21** in chloroform and DMSO (conc. ca 2.10^{-6} mol.L-1, 298 K). Results are obtained from 3 to 5 independents experiments.

	$CHCl_3$		DMSO	
Compounds	λ (nm	ε (10^{-3} L.mol^{-1}.cm^{-1})	λ (nm	ε (10^{-3} L.mol^{-1}.cm^{-1})
15	424 552 595	325 12 3	429 562 602	176.5 5.9 3.3
21	439 463 492	14 17.7 11.5	435 460 490	21 25 16.3
24	427 463 492 556 598	310 19 14 12 4.5	429 460 491 562 601	402 17.6 11.7 12.5 6.3
26	424 461 492 553 569	281 14.7 10.6 11 3.3	429 460 492 561 601	328 15.2 10.8 12.3 4.1
28	428 464 492 561 600	294 11.6 9.1 10.4 4.4	429 461 491 562 602	315 13.4 9.9 11.4 5.7

Concerning the theoretical analysis, as no folding was observed for compounds **26** and **28**, the MO interpretation was based on linear structures. As expected, similar interpretation than for the linear form of **24** is highlighted from the MO diagrams. Namely, no MO mixtures were observed between both moieties. With the ωB97XD functional, the H-1, H, L and L+1 allow description in terms of Gouterman's 'four orbital model whereas H-2 and L+2 were assigned to the fluorescein moiety (Figure 146 and Figure 148). B3LYP induced a MO inversion of the virtual MO, L being assigned to the fluorescein moiety (Figure 145 and Figure 147). In any event, no specific spectral modifications were predicted.

6.1.2. Optical properties of free-base dyads.

UV-Vis spectra of non-metallated compounds **14**, **25** and **27** exhibit the characteristics of free-base porphyrins (Figure 142, Table 30). A strong absorption band is observed around 419 nm, and other four less intense bands lie in the 510 - 640 nm range, which correspond to the Q bands. A clear *etio-type* profile is observed for compounds **25** and **27**, whereas it appears less clear for **14**, for which the difference in ε of Q between bands I and II is very weak. As for metallated compounds, **25** and **27** exhibit two of the three fluorescein bands, the third one at 439 nm being hidden by the Soret band intensity. In addition, the experimental UV-Vis absorption spectra of **25** and **27** match the profile obtained by the mathematical sum of both spectra of **14** and **21** (dashed lines), indicating the absence of any significant interaction in the ground state. As for metallated compounds, a solvatochromic study in DMSO was performed. As expected, same trend as for compounds **26** and **28** was observed, with a very weak solubility in DMSO requiring stirring and heating.

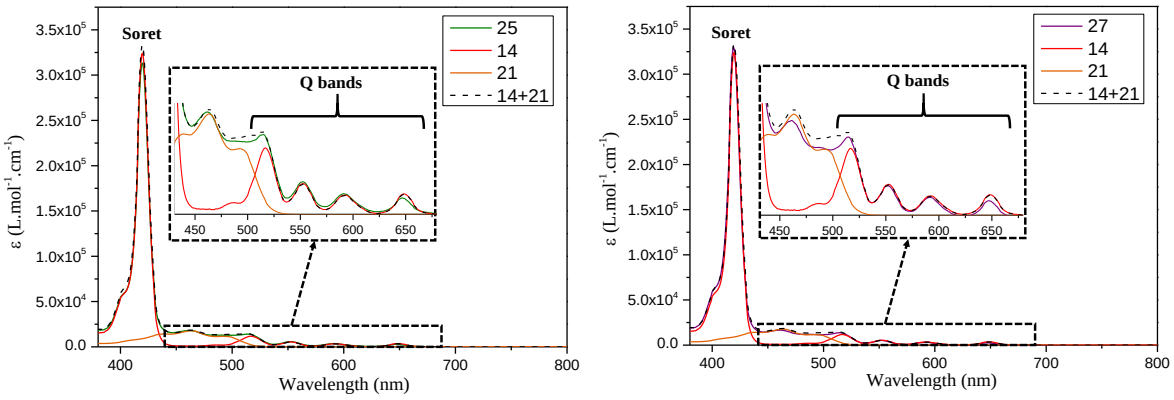

Figure 142: UV-Vis absorption spectra of free-base dyads **25** (left) and **27** (right). For comparison, spectra of reference compounds **14** and **21** are also reported ($CHCl_3$, 298 K).

Table 30: UV-Vis data for dyads **25** and **27**, and reference **14** and **21** in chloroform and DMSO (conc. ca 2.10^{-6} mol.L-1, 298 K). Results are obtained from 3 to 5 independents experiments.

	$CHCl_3$		DMSO	
Compounds	λ (nm	ε (10^{-3} L.mol^{-1}.cm^{-1})	λ (nm	ε (10^{-3} L.mol^{-1}.cm^{-1})
14	420 517 552 593 648	310 11 5.6 3.3 3.6	420 516 552 592 647	342 16 9.5 6 6.4
21	439 463 492	14 17.7 11.5	435 460 490	21 25 16.3
25	419 462 490 515 552 591 647	310 18 13 14 5.7 3.6 2.9	420 460 492 514 551 591 647	403 23 16 18 8 5 4.4
27	419 461 490 515 551 591 647	330 16.6 12 14 5 3 2.5	420 458 490 515 551 592 647	358 21 15.6 16.8 9 6 5

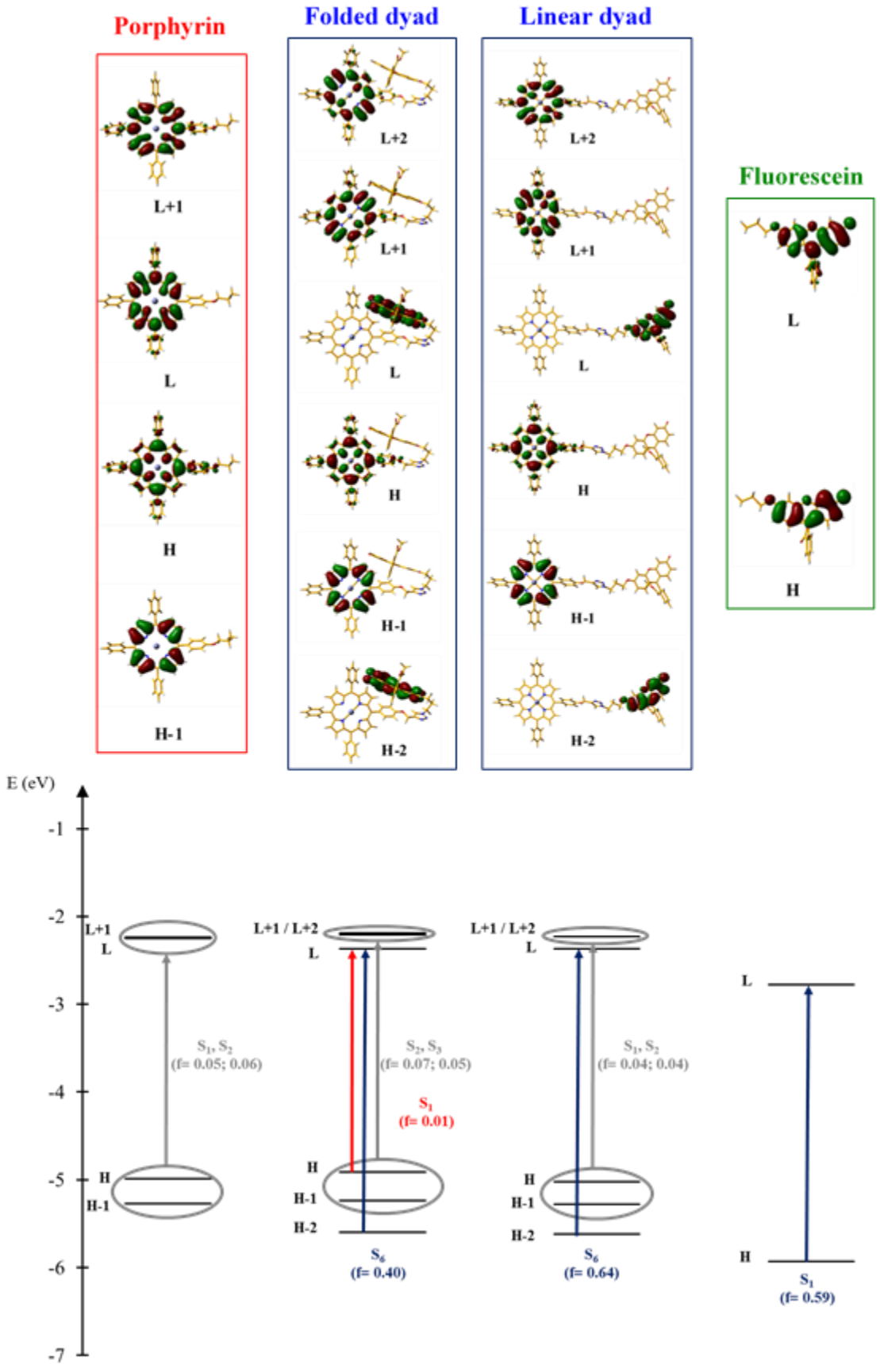

Figure 143: MO diagram of **24** (folded and linear form) and reference compounds **15** and **21** using B3LYP functional. Grey: porphyrin-porphyrin transitions; blue: fluorescein-fluorescein transitions and red: ICT.

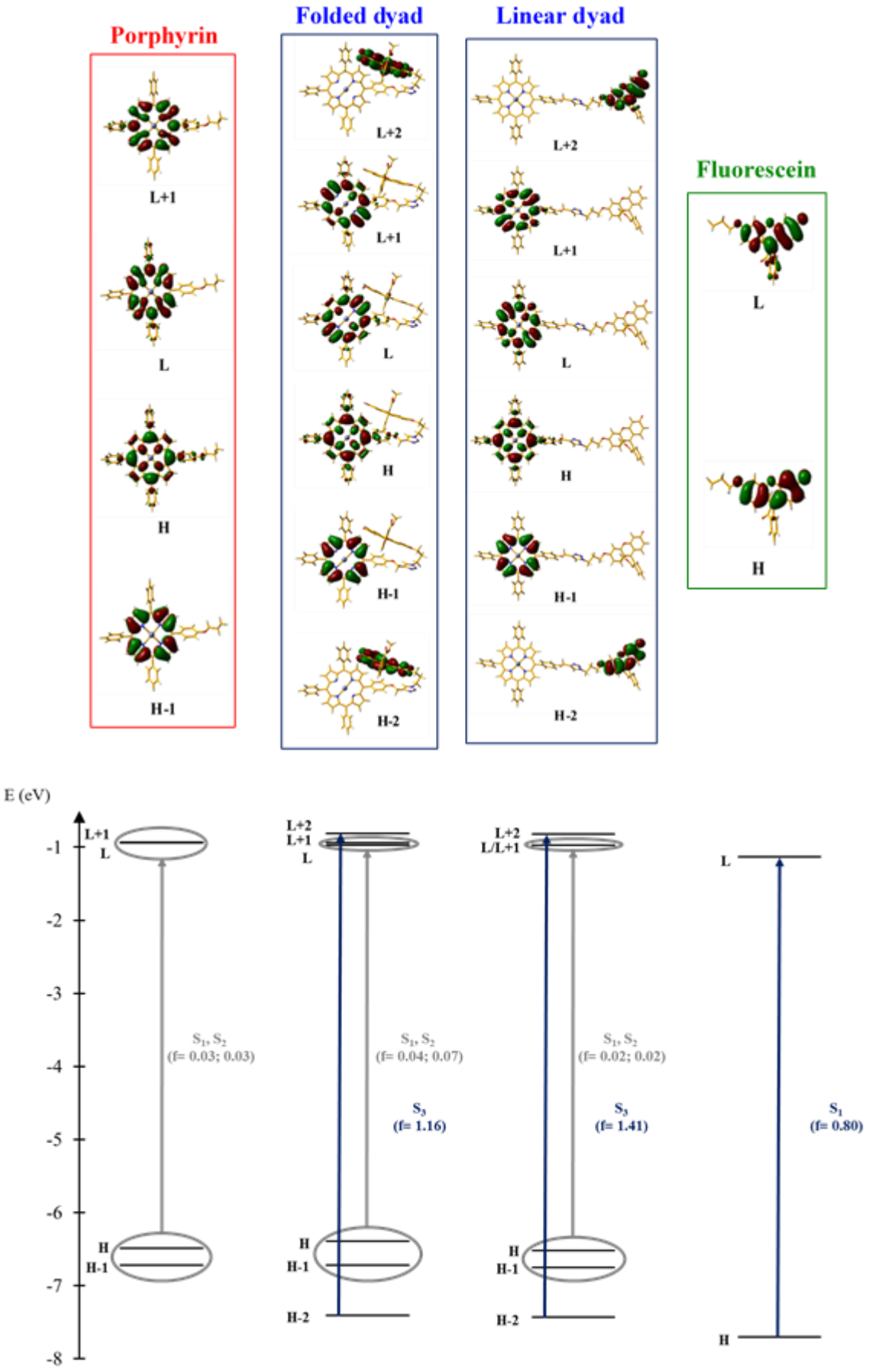

Figure 144: MO diagram of **24** (folded and linear form) and reference compounds **15** and **21** using ωB97XD functional. Grey: porphyrin-porphyrin transitions; blue: fluorescein-fluorescein transitions.

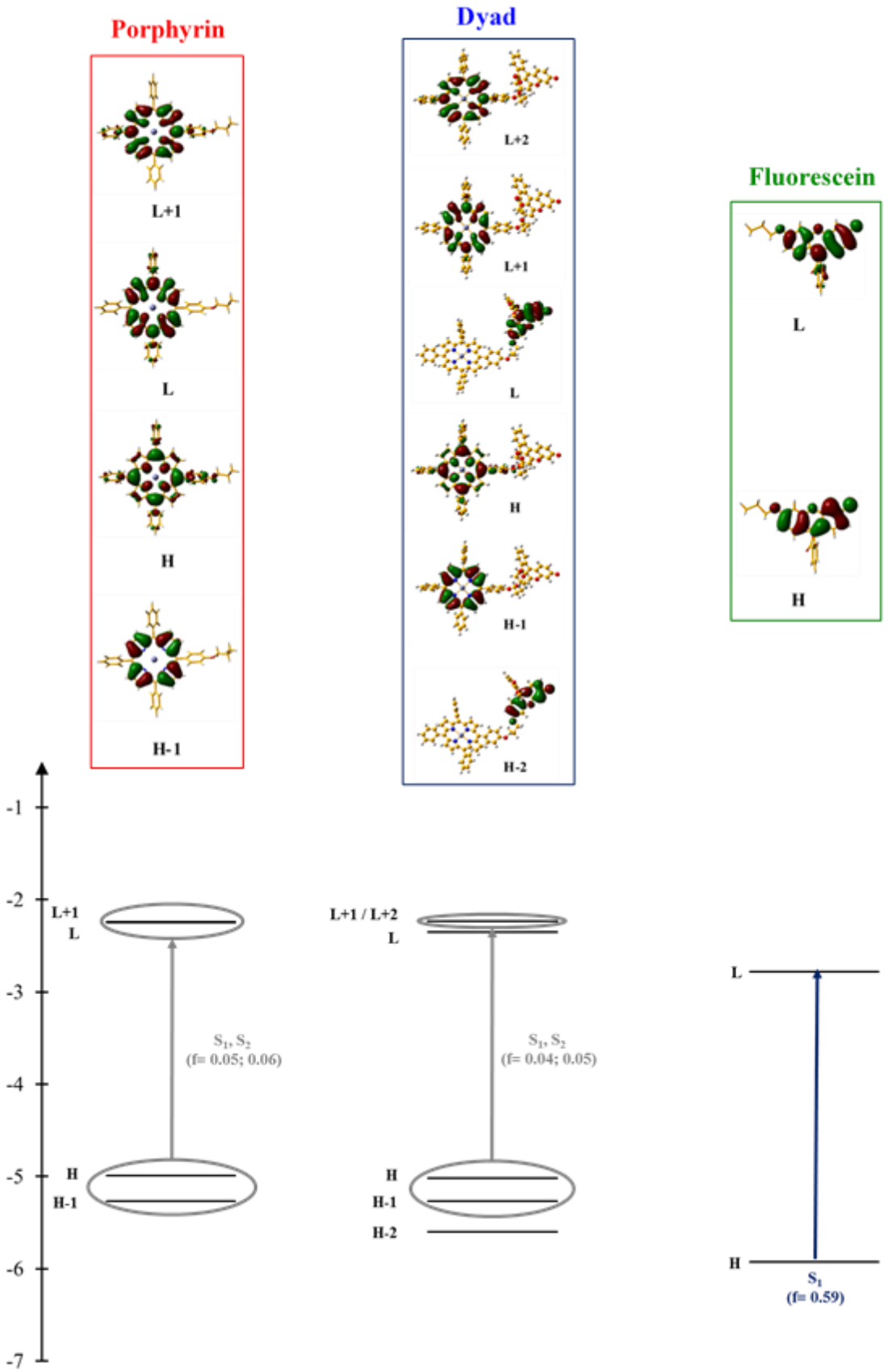

Figure 145: MO diagram of **26** and reference compounds **15** and **21** using B3LYP functional. Grey: porphyrin-porphyrin transitions; blue: fluorescein-fluorescein transitions.

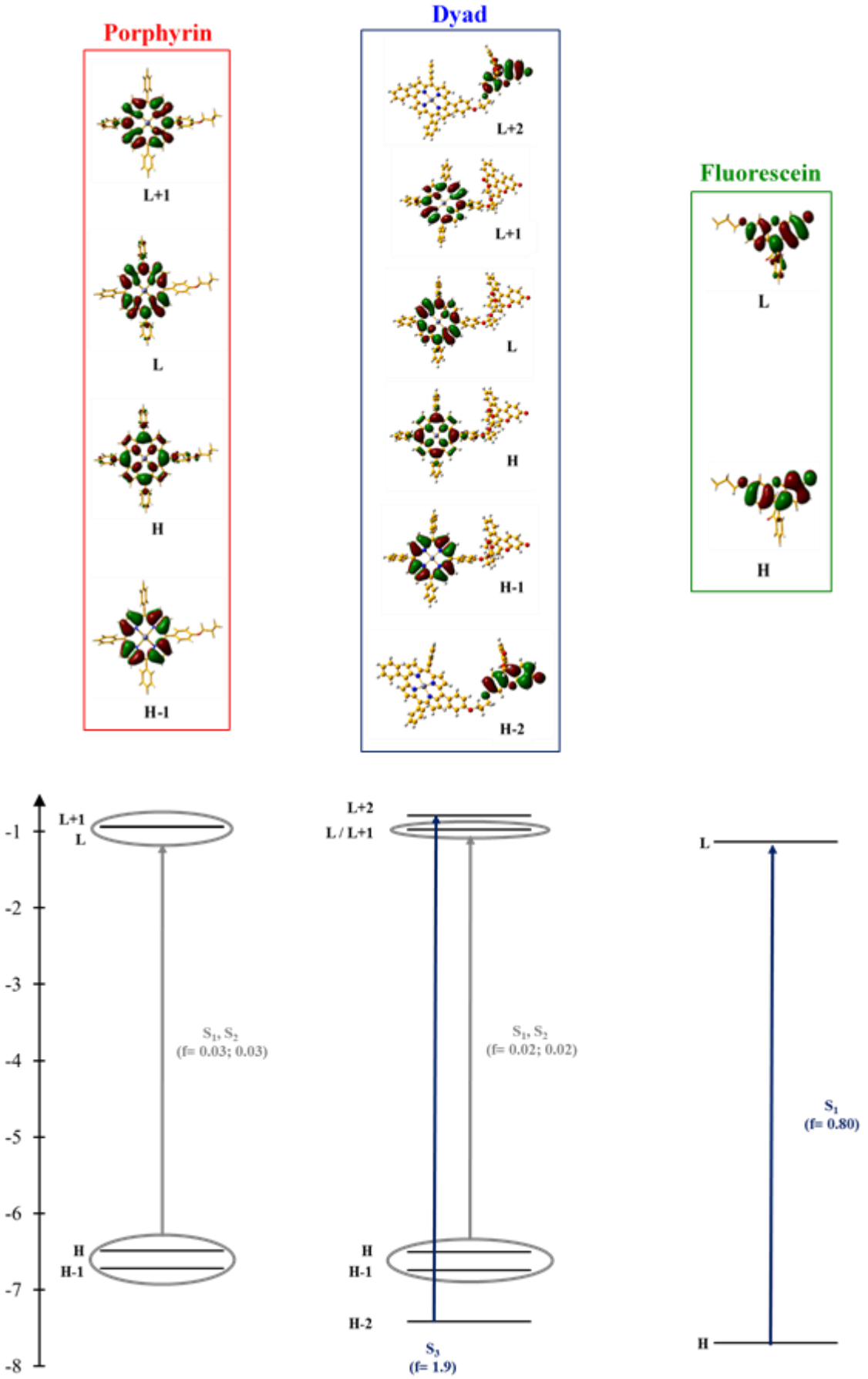

Figure 146: MO diagram of **26** and reference compounds **15** and **21** using ωB9XD functional. Grey: porphyrin-porphyrin transitions; Blue: fluorescein-fluorescein transitions.

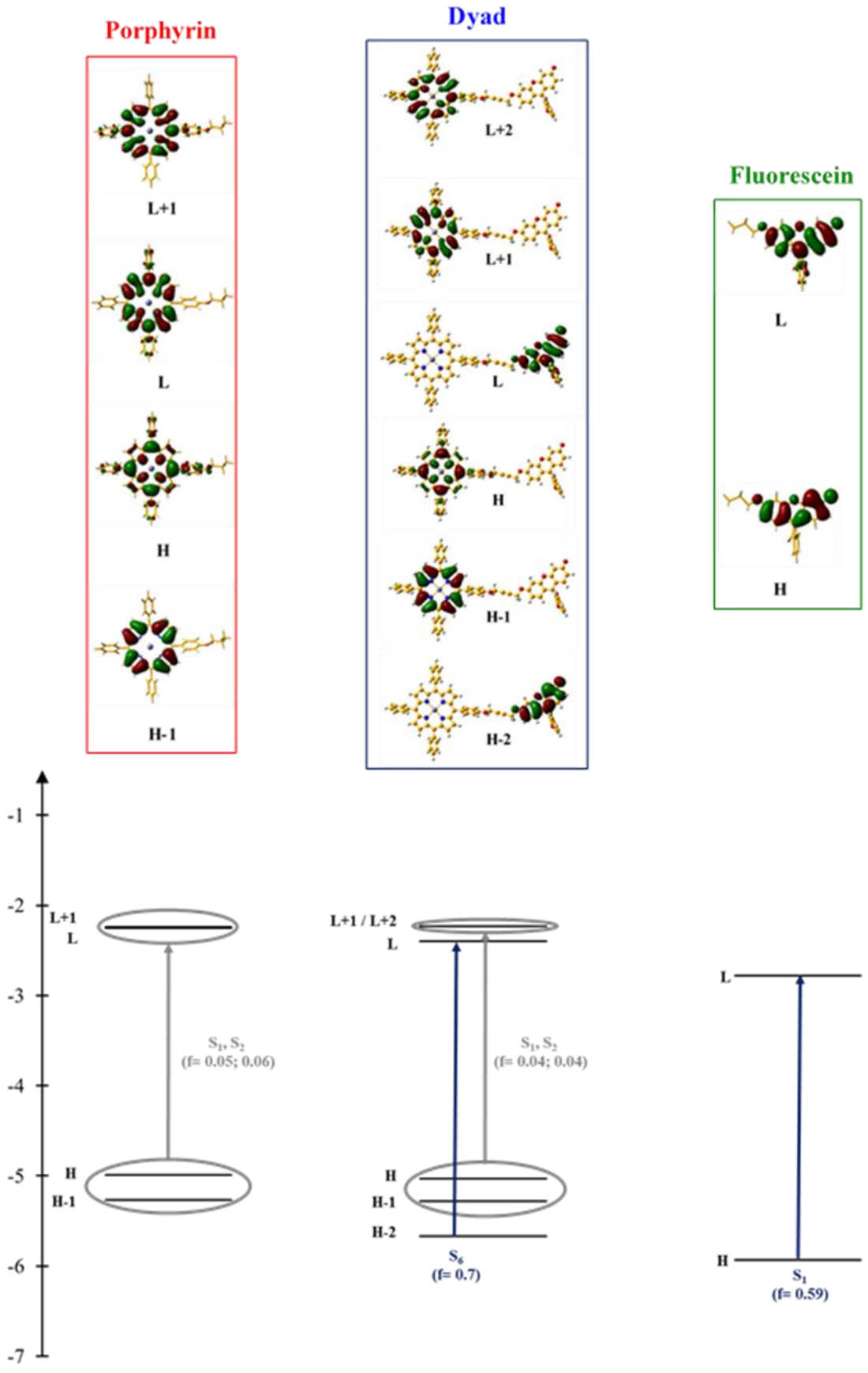

Figure 147: MO diagram of **28** and reference compounds **15** and **21** using B3LYP functional. Grey: porphyrin-porphyrin transitions; blue: fluorescein-fluorescein transitions.

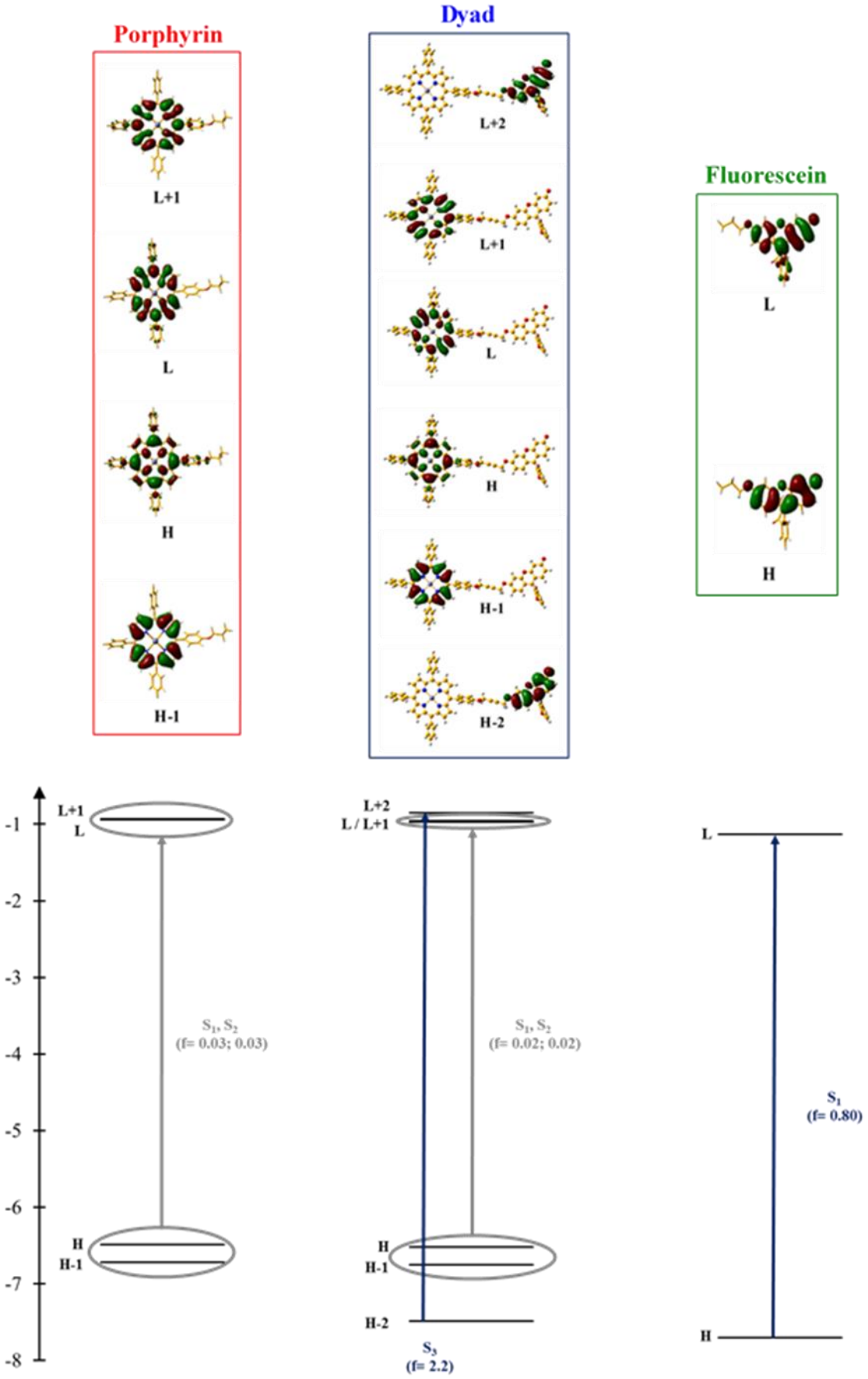

Figure 148: MO diagram of **28** and reference compounds **15** and **21** using ωB9XD functional. Grey: porphyrin-porphyrin transitions; blue: fluorescein-fluorescein transitions.

6.2. Fluorescence emission properties

Corrected emission spectra of dyads **24-28** and references **14-15** and **21** were performed both in chloroform and DMSO, at room temperature and at a concentration of 2.10^{-6} M, in non-degassed solution. Additionally, in order to check compound purity, excitation spectra were recorded and similar profiles than UV-Vis absorption spectra were observed, over the whole wavelength range. Fluorescence emission spectra presented below were recorded either at λ_{exc} = 490 nm for compounds **21** and **24-28**, and at λ_{exc} = Soret band maximum for the reference porphyrins **14** and **15**. The 490 nm wavelength was selected in order to excite as selectively as possible the fluorescein moiety, and so to investigate the occurrence and, if appropriate, the efficiency of energy transfer between the fluorescein and porphyrin moieties.

6.2.1. Free-base dyads

Normalized emission spectra of the free-base dyads **25** and **27**, and their references (**14** and **21**) are presented in Figure 149 while fluorescence date are presented in Table 31.

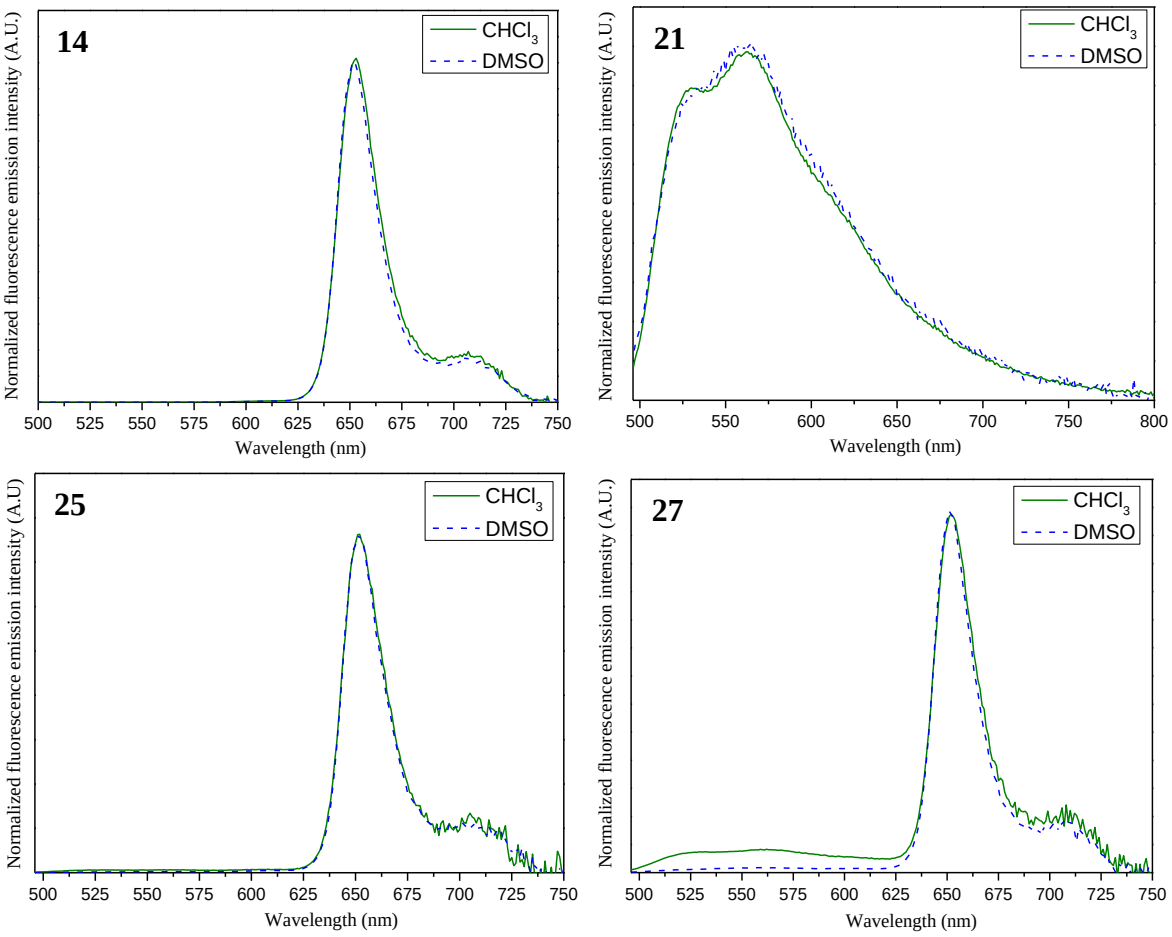

Figure 149: Normalized emission spectra at 298 K for compounds **14**, **21**, **25** and **27** (conc. 2.10^{-6} M). Spectra were recorded at λ_{exc} = Soret (**14**) and at λ_{exc} = 490 nm **(21, 25** and **27**).

Table 31: Spectroscopic characteristics of compounds **14**, **21**, **25** and **27** in chloroform and DMSO. Fluorescence quantum yields (Φ_f) are obtained from three independent experiments.

Compounds	λ_{max} (emission) (nm)		Φ_f [a,b]	
	$CHCl_3$	DMSO	$CHCl_3$	DMSO
14	653 / 707	652 / 708	0.13 (± 0.01)	0.17 (± 0.01)
21	531 / 564	532 /562	0.17 (± 0.01)	0.18 (± 0.01)
25	652 / 707	652 / 708	0.11 (± 0.01)	0.16 (± 0.01)
27	530 / 564 652 / 708	560 652 / 708	0.10 (± 0.01)	0.12 (± 0.01)

[a]: **14**, **25** and **27**: λ_{exc} = 555 nm, at room temperature. H_2TPP in chloroform was chosen as standard (Φ_f = 0.11).[356] [b]: **21**: λ_{exc} = 490 nm, at room temperature. Fluoresceine in NaOH 0.1 M was chosen as standard (Φ_f = 0.92).[458,459]

As expected, the reference compound **14** presents the characteristic profile of free-base porphyrin with an emission band above 600 nm, while **21** emits at around 530 nm, as quinoid form of fluorescein. Moreover, quantum yields of **21** (0.17 and 0.18) are weak compared to the native fluorescein, but in agreement with the literature.[434] Indeed, native fluorescein quantum yields are solvent dependent and the highest values are obtained for the dianionic form (F^{2-}) in NaOH (1 M), and in our case native fluorescein completely disappeared, transformed in compound **21**.[459] For dyads **25** and **27**, emission spectra reflect photo-induced singlet-singlet energy transfer from fluorescein* to porphyrin. Indeed, at 490 nm, according to UV-Vis absorption spectra (Table 30), 78 % of light is absorbed by fluorescein and thus fluorescein emission should be preponderant. Thus, the presence of characteristic emission peaks of porphyrin moiety evidences the occurrence of such a photo-induced energy transfer. In addition, characteristic bands of fluorescein (λ = 460 nm and λ = 490 nm) were observed on the excitation spectra recorded at λ_{obs} = 708 nm, where only the porphyrin moiety emits. This is also confirmed by the strong decrease of fluorescein emission observed in **27**, for which fluorescence is even totally quenched in **25**. In DMSO, the fluorescein emission in **27** is totally quenched, this evidencing that the photo-induced energy transfer must be more efficient in polar solvent (DMSO) than in chloroform (Figure 149).

This effect can be rationalized by the important overlap between fluorescein emission and porphyrin absorption. Indeed, the fluorescein moiety absorbs in the 430-490 nm range (Table 30), while it emits in the 530-560 nm range (Table 31) where lie the absorption of Q bands of porphyrin (Table 30) (see paragraph 6.1).

Fluorescence quantum yields were assessed for all compounds both in chloroform and DMSO (Table 31). However, due to energy transfer occurrence, fluorescein emission spectrum cannot be recorded without the overlapping contribution of porphyrin emission in dyads, and thus prevents determination of fluorescein's fluorescence quantum yields in dyads. Thus, only the values related to the porphyrin pattern (λ_{exc} = 555nm in order to record only the porphyrin emission) were determined. As expected, fluorescence quantum yields of porphyrin moieties in dyads are similar to the one of **14**, all values being around 0,10-0,13 in chloroform and 0,12-0,17 in DMSO, in agreement with the literature.[356]

6.2.2. Metallated dyads

For the metallated compounds **15**, **24**, **26** and **28** (Table 32 and Figure 150), similar experimental conditions were used *i.e.* λ_{exc} = Soret for reference porphyrin **15** and 490 nm for dyads **24**, **26** and **28**.

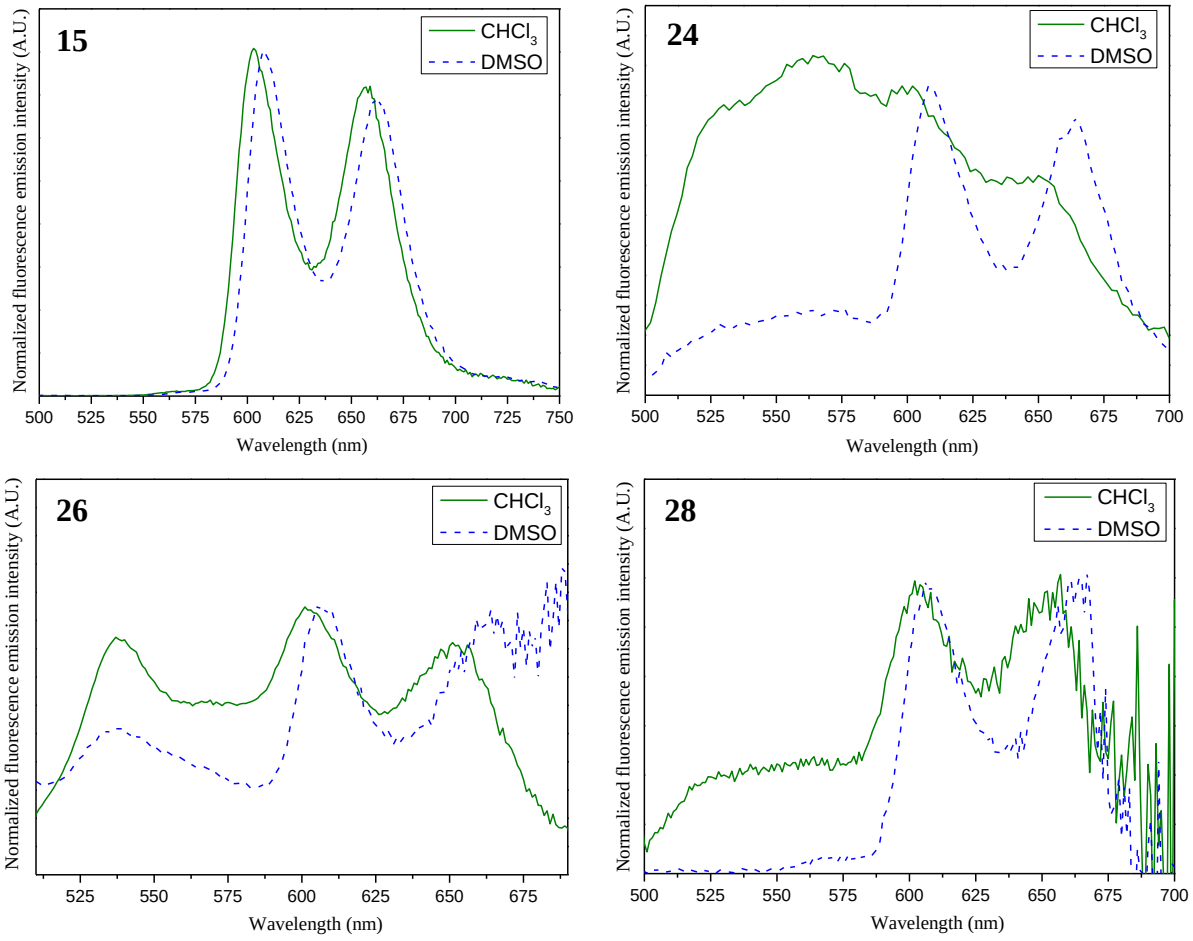

Figure 150: Normalized emission spectra (relative to porphyrin emission maximum) at 298 K for compounds **15, 24**, **26** and **28** (conc. 2.10^{-6} M). Spectra were recorded at λ_{exc} = Soret (**15**) and at λ_{exc} = 490 nm (**24**, **26** and **28**).

As expected, the reference porphyrin **15** exhibits the characteristic fluorescence emission spectrum of metallated porphyrins (Figure 150), with blue-shifted peaks and increase in intensity for the second peak (654 nm), as compared to the free-base derivatives (Table 32).[133] Moreover, for **15** and metallated dyads, spectra recorded in DMSO exhibited a slight red-shift (± 5 nm) of the porphyrin peaks (Table 32), the excited state of the metallated porphyrins being more polar than those of free-base because of the presence of the metallic atom.[460] As for compounds **25** and **27**, a photo-induced singlet-singlet energy transfer from fluorescein* to porphyrin is observed for the three metallated dyads (**24**, **26** and **28**), disregarding the nature of the linker (Figure 150). Moreover, as for the free-base dyads, its efficiency increases with respect to solvent polarity. Whatever, the efficiency of the photo-induced energy transfer is less effective in metallated than in free-base dyads. This perfectly agrees with a decrease in spectral overlap between fluorescein emission and porphyrin absorption, as metallated compounds exhibit only two Q bands in the red side of the absorption spectrum (550-600 nm) *vs.* four (in the 500-650 nm range), respectively (Table 29 and Table 30).

Table 32: Spectroscopic characteristics of compounds **15**, **21**, **24**, **26** and **28** in chloroform and DMSO. Fluorescence quantum yields are obtained from three independent experiments.

Compounds	λ_{max} (emission) (nm)		Φ_f [a,b]	
	$CHCl_3$	DMSO	$CHCl_3$	DMSO
15	602 / 654	608 / 664	0.05 (± 0.01)	0.09 (± 0.01)
21	531 / 564	532 /562	0.17 (± 0.01)	0.18 (± 0.01)
24	530 / 564 604 / 648	532 / 564 608 / 662	0.04 (± 0.01)	0.07 (± 0.01)
26	537 / 567 604 / 654	533 / (-) 607 / 660	0.06 (± 0.01)	0.09 (± 0.01)
28	532 / 561 602 / 652	(-) / (-) 606 / 662	0.03 (± 0.01)	0.07 (± 0.01)

[a]: **15**, **24**, **26** and **28**: λ_{exc} = 555 nm, at room temperature. H_2TPP in chloroform was chosen as standard (Φ_f = 0.11).[356] **[b]**: **21**: λ_{exc} = 490 nm, at room temperature. Fluoresceine in NaOH 0.1 M was chosen as standard (Φ_f = 0.92).[458,459] (-): peaks are too weak to be recorded.

As expected for zinc-porphyrins, all compounds have weaker fluorescence quantum yields than those of the free-base compounds (Table 32)[133] and a slight increase of fluorescence

quantum yields was observed between chloroform and DMSO, as those observed for **14**, **25** and **27** (Table 31).

After having clearly highlighted a photo-induced energy transfer in all dyads, its inter- and/or intra-molecular character has been studied. In that purpose, fluorescence emission spectra were recorded for solution of fluorescein **21**, **24** as dyad reference, and an equimolar mixture of reference compounds **15** and **21**, all solutions being prepared with the same concentration in fluorescein and porphyrin moieties. In the case of inter-molecular interaction, a fluorescence emission decrease of fluorescein **21**, in the mixture, after excitation at λ_{exc} = 490 nm, is expected. This experiment was performed three times in chloroform, at room temperature, and at a concentration of 2.10^{-6} M, and the results are collected in Figure 151.

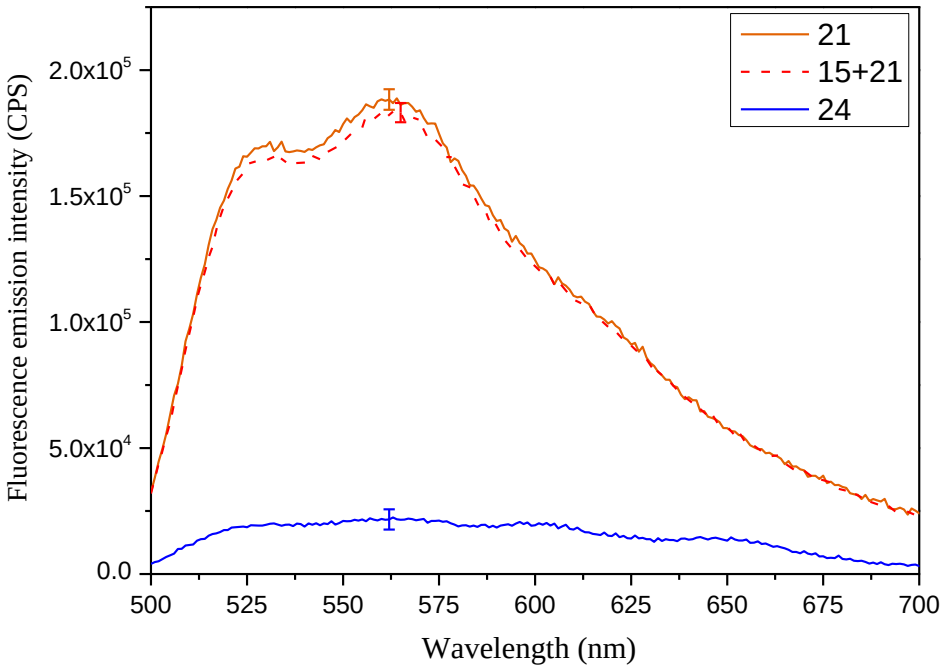

Figure 151 : Fluorescence emission spectra of reference compound **21**, dyad **24**, and an equimolar mixture of compounds **15** and **21**, at λ_{exc} = 490 nm. Emission maxima values represent the mean ± 2% obtained from 3 independent experiments.

At λ_{exc} = 490 nm, the solution of fluorescein **21** showed the same level of fluorescence emission than that recorded for the **15** and **21** solution (Figure 151, orange line), the difference between the two emission spectra being not significant when considering standard deviations. On the contrary, extinction of fluorescence emission into dyad **24** (Figure 151, blue line) is observed. Therefore, the photo-induced energy transfer takes place only into dyad when porphyrin and fluorescein are linked and thus should be an intramolecular process for a concentration of 2.10^{-6} M. Moreover, the same trend is observed with dyads **26** and **28**. However, existence of inter-molecular energy transfer may not be ruled out by this experiment,

at higher concentration inner filter effect can then occur. Whatever, the choice of 2.10^{-6} M was not fortuitous as it was in agreement with biological assays.

6.3. Photo-induced energy transfer efficiency

As outlined before, after excitation at λ_{exc} = 490 nm, a photo-induced energy transfer occurs for all dyads **24-28**. Taking the non-conjugated nature of the spacers into account, this process may be of Förster-type. Thus, to calculate its efficiency (Φ_{ET}), Equation 14, in the absence of acceptor (porphyrin moiety) absorbance, can be used:[461]

$$\Phi_{ET} = \left(1 + \frac{\Phi_A}{\Phi_D} \cdot \frac{I_D}{I_A}\right)^{-1}$$

Equation 14: Energy transfer efficiency in the absence of acceptor absorbance.

Where:

- Φ_D and Φ_A are the fluorescence quantum yields of D and A, respectively;
- I_D/I_A is the relative fluorescence intensity of D and A in the dyad.

In our case, even at λ_{exc} = 490 nm, the acceptor absorbs and thus the prompt fluorescence $I_{P,A}$ of the acceptor has to be taking into account. Φ_{ET} is then calculated by Equation 15:

$$\Phi_{ET} = \left(1 + \frac{\Phi_A}{\Phi_D} \cdot \frac{I_D}{I_A - I_{P,A}}\right)^{-1}$$

Equation 15: Energy transfer efficiency in case of acceptor absorbance.

Where:

- $I_{P,A} = I_D \cdot \frac{\Phi_A}{\Phi_D} \cdot \frac{A_A}{A_D}$; with $A=1-10^{-E}$
- E = Absorbance due to donor or acceptor moiety into dyad.

This leads to Equation 16:

$$\Phi_{ET} = \left(1 + \frac{\Phi_A}{\Phi_D} \cdot \frac{1}{I_A / I_D - (\Phi_A / \Phi_D) \cdot (A_A / A_D)}\right)^{-1}$$

Equation 16: Energy transfer efficiency.

To investigate effects of solvent polarity on energy transfer efficiencies, they were calculated both in chloroform and DMSO using Equation 16 (Table 33).

Table 33: Φ_{ET} calculated. For compound **24-28**, results are obtained from 1 or 2 independents experiments.

Solvent	Φ_{ET}				
	Metallated dyads			**Free-base dyads**	
	24	**26**	**28**	**25**	**27**
$CHCl_3$	0.42 (± 0.08)	0.61 (± 0.03)	0.58	0.96	0.82
DMSO	0.75	0.73 (± 0.06)	0.96	0.98	0.91

The same hierarchy is observed between dyads in both solvents. Indeed, the free-base compounds **25** and **27** have the highest Φ_{ET} (> 0.8 both in chloroform and DMSO, Table 33), which is in agreement with a wider overlap between fluorescein emission and porphyrin absorption due to the presence of the four Q bands (Table 30 and Table 31). Moreover, fluorescein is almost completely quenched in compound **25** and, as expected, energy transfer is quasi quantitative.

Zinc metallation led to UV-Vis spectrum modifications (Figure 140), therefore there is a lower overlap between fluorescein emission and porphyrin absorption (Table 29 and Table 32). This leads to a decrease in energy transfer efficiency. Interestingly, Φ_{ET} are dramatically increased from chloroform to DMSO for dyad **24**, this may be another clue to support the occurrence of both folded and linear conformers, their equilibrium depending on solvent polarity. In chloroform, the three metallated dyads are perfectly soluble and exhibit closed Φ_{ET} (0.42, 0.61 and 0.58), which mean either that the three compounds are in linear geometry or that the folding geometry has no real influence on the efficiency of energy transfer. As a conclusion, the nature of linkage does not significantly impact on energy transfer efficiency.

In DMSO, Φ_{ET} for dyads **24** and **26** are also much closed (0.75 and 0.73, respectively), and in compound **28** it is very close to free-base compounds (0.96). Although Φ_{ET} could be calculated, the value obtained with **28** must be considered with care. Indeed, due to weak solubility, it could have been overestimated. Thus, magnetic stirring and heating may favor new intermolecular interactions, for example *via* π-stacking. However, this last hypothesis is impossible to confirm due to the large solubility disparity between references fluorescein **21** and porphyrin **15** in DMSO (the former is degraded by heat while the latter need heat to be solubilized in DMSO), which prevent any test of equimolar mixtures as done in chloroform (Figure 151). A solution could be to perform temperature-dependent NMR analysis in DMSO. Indeed, in agreement with molecular modeling, visualization of fluorescein-porphyrin moieties

interactions in **26** and **28** must be due to intermolecular interactions, intramolecular ones being prevented by the rigidity of linkage.

Transfer efficiency is also accessible experimentally from time-resolved measurements (Equation 17):

$$\Phi_{ET} = 1 - \tau_{D,A} / \tau_D$$

Equation 17: Transfer efficiency calculation via time-resolved measurements.

Where:

- τ_D is the fluorescence lifetime of the donor molecule (**21**)
- $\tau_{D,A}$ is the fluorescence lifetime of the donor in the dyad

Unfortunately, this was only performed for compound **24** in $CHCl_3$, but Φ_{ET} found using Equation 17 equals 0.33, which is relatively close to values obtained from Equation 16 (Table 33).

6.4. Singlet oxygen production

Conversely to anionic porphyrins, the dyads studied here are not water-soluble and thus EPR study is prevented to quantify singlet oxygen and superoxide anion production. Therefore, photo-oxidation of 9,10-dimethylanthracene (DMA) was used. Indeed, this reaction, occurring in presence of singlet oxygen, is extensively studied in the literature to evaluate singlet oxygen production quantum yield thanks to monitoring of DMA absorption spectrum change. In presence of singlet oxygen, DMA is oxidized into a less conjugated endoperoxide (Figure 152), which does not absorb in the same wavelength region than DMA.[356]

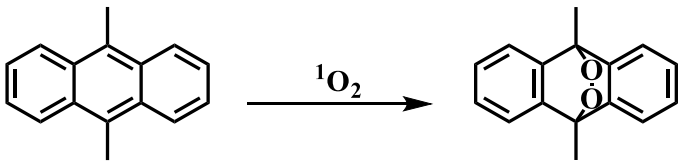

Figure 152: DMA oxidation by singlet oxygen.

Thus, in presence of singlet oxygen a decrease of the three DMA peaks (λ = 360 nm, 380 nm and 401 nm) is observed (Figure 153). Because DMA oxidation reaction follows one-order kinetic (relative to DMA concentration),[356] it is possible to use it to quantify singlet oxygen produced amount as a time function and so production efficiency. Thus, kinetic studies of DMA degradation in presence of dyads **24-28** and H_2TPP (tetraphenylporphyrin) as standard were performed in DMF (Figure 154), by dissolving porphyrin (*ca*. 10^{-6} M) and DMA (10^{-4} M) in DMF. Solution was stirred and saturated with oxygen. Absorbance of solution was recorded

every 5 minutes (Figure 153), no interaction between DMA peak at 401 nm and Soret band being considered. Control reactions without photosensitizer or light were also performed, but no DMA degradation was observed (Figure 153).

For each molecule, plots of experimental values $\ln(A_0/A)$ give a straight line (Figure 154), which confirms that dyads **24** to **28**, as standards, are capable to produce singlet oxygen continuously and without photobleaching or photodegradation over a short period (at least 25 minutes). Then, singlet oxygen quantum yields (Φ_Δ) were calculated for each compound (Table 34), using H_2TPP as a standard[462] (Φ_Δ = 0.64 in DMF) (see experimental part 1.3.9 for equation details).

Table 34: Main data of singlet oxygen production evaluation using DMA. K_{obs} represents DMA photo-oxidation constant. Φ_Δ were calculated using H_2TPP as standard.[462]

Compounds	K_{obs} (s^{-1})	Φ_Δ
H_2TPP	$2.8801.10^{-5}$	0.64
24	$3.7350.10^{-5}$	0.80
26	$1.8563.10^{-5}$	0.40
28	$1.2030.10^{-5}$	0.37
25	$3.9955.10^{-5}$	0.75
27	$2.9094.10^{-5}$	0.64

As presented in Table 34, free-base compounds **25** and **27** produce more singlet oxygen than their metallated analogues **26** and **28** (0.75 and 0.64 *vs* 0.40 and 0.37, respectively), in agreement with the literature.[153] On the contrary, triazole compound **24** appears as the most efficient producer with a yield of 0.80 (Table 34). For **24**, this result can be explained by a higher absorption especially in more polar solvent (Table 29) coupled to a very weak fluorescence quantum yield (Table 32). Therefore, this molecule follows other de-excitation processes than fluorescence, for example intersystem crossing, and ROS production.

For **26** and **28**, zinc-metallation has led to a decrease in singlet oxygen production compared to their free-base analogues **25** and **27**. Thus, it is likely that the free-base analogue of **24** produces more singlet oxygen and so demetallation process on **24** may be interesting.

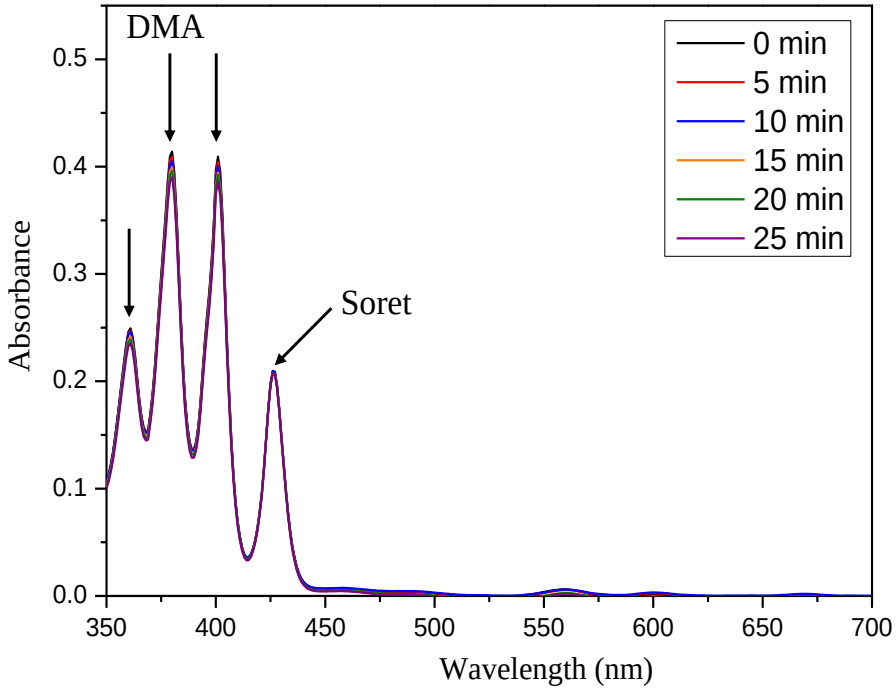

Figure 153: DMA photooxidation in DMF due to singlet oxygen produced by compound **24**.

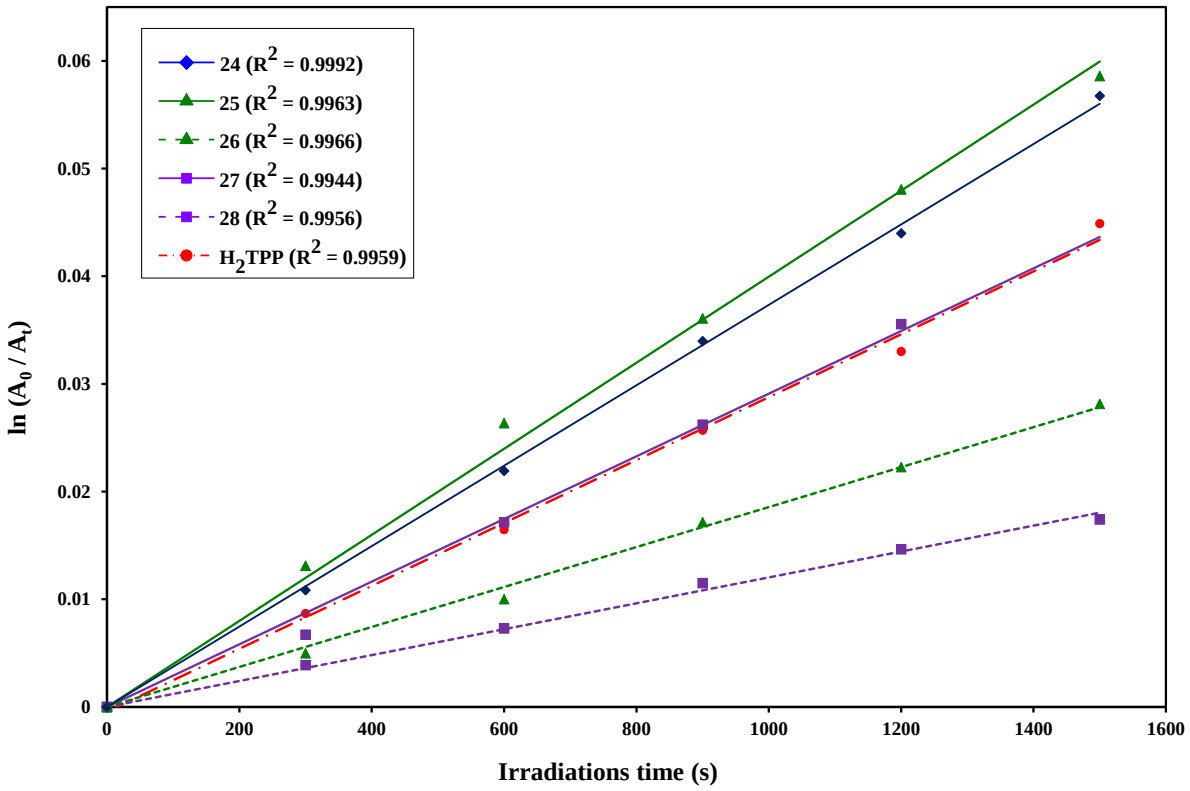

Figure 154 : Linearization of the disappearance of the band at 401 nm depending of irradiations times; for dyads **24-28** and H_2TPP reference.

7. Conclusion

In order to understand mechanisms of action involved in cell death, a series of new dyads containing porphyrins was achieved. Fluorescein was chosen due to its specific properties and its non-toxicity to plants. After having selected the most promising linkers, synthesis, conformational analysis and photophysical properties were achieved. Conformations and optical property issues were performed both theoretically and experimentally. This work has highlighted energy transfer both in free-base and zinc-metallated compounds, due to overlap between fluorescein emission and porphyrin absorption. It revealed that linkage nature and thus rigidity do not prevent energy transfer, contrary that what was expected. To experimentally confirm the Φ_{ET} evaluated thanks to spectral data, measurements of fluorescein moieties lifetimes in dyads are currently in progress for compounds **25-28**. Solubility problems were observed in DMSO, most likely associated to rigidity of these compounds, which impact on (intra or inter) interactions evaluation. To do confirm our hypotheses, another polar solvent (DMF) will be studied soon.

Triazole compound **24** appears as a good candidate for further studies, due to its ability to fold, which allowed better solubility in polar solvent. The folded geometry does not drastically change photophysical properties compared to the linear geometry. Moreover, folded geometries prevent or limit intermolecular interaction, so aggregate formation, which may favor cell penetration. Moreover, in **24**, energy transfer is not total and fluorescein moiety properties (UV-Vis absorption and wavelength of fluorescence emission) do not change (Table 29 and Table 32). Even if fluorescence quantum yield decreases, it remains sufficient to expect tracking the dyad in plants, and thus porphyrin as well as potential degradation events; contrary to non-metallated compounds.

Some differences were observed between theoretical predictions and experimental data for dyads. It may be explained by the solvent description, which is crucial with this kind of compounds due to importance of inter and intramolecular interactions. Indeed, in quantum chemistry, solvent is mimic by a homogeneous dielectric continuum. Moreover, due to size of studied dyads, we are rapidly reaching the limits of quantum chemistry calculations. An elegant alternative could be using QM/MM (Quantum Mechanics / Molecular Mechanism) calculations to improve explicit interactions with any solvent. With QM/MM one can expect treating several dyads simultaneously to establish structure activity relationship.

Conclusion and prospects

The aim of this work was to study the potentiality of using porphyrins as photo-activable herbicides. In that purpose, a series of commercial and synthesized free-base anionic porphyrins were studied first. Both physicochemical properties and biological activities were evaluated in order to rationalize structure-activity relationships. In the case of tetra-substituted porphyrins, this work underlined that both the nature of grafted anionic functions and the linker change drastically physicochemical properties and thus porphyrin capacity to cause cell death. Compound **4**, which has four donor subtituents in *para* position of the *meso*-phenyls, presents a protonation of its internal nitrogen at high pH (up to 7.5), which leads to J-aggregate formation and thus incapacity to penetrate cells. Compound **5,** with four phosphonic acid functions, is subjected to photodegradation phenomena in TBY-2 growth medium, while **1** with sulfonate functions is stable and significantly induces cell death, however it is trapped into cell walls. Compound **2** (a carboxylic porphyrin) is the most promising as ROS producer. Indeed, it does not form aggregates and stays stable in biological medium. Moreover, its capacity to penetrate both into cell wall and nucleus may explain its high efficacy at inducing cell death. Two compounds with eight functions in *meta*, namely **11** (carboxylic acid) and **12** (phosphonic acid), were chosen to assess relationships between the number of charged functions and cell death. Preliminary study of photophysical properties of the former in water seems to rule out aggregate formation, even at the excited state contrary to **4**; and thus this allows expecting a different behavior from its tetra-substituted analogue. Moreover, the *meta* substitution pattern should drastically decrease influence of the mesomeric donor properties of the O-CH_2 linker, especially on protonation properties. The synthesis of the latter is currently under progress and should afford, with respect to **7**, a quantitative comparison between carboxylate and phosphonate derivatives. This study is a real proof of concept of using water-soluble porphyrins as potential photo-activable herbicide.

A better understanding of mechanisms of action involved in cell death has appeared mandatory to enhance biological activities. However porphyrin emission is both too weak and hidden by cell auto-fluorescence, especially because of some endogenous molecules (*e.g.* chlorophyll). To avoid this drawback, new dyads containing porphyrin and fluorescein (as fluorescent tag) moieties were achieved (**24-28**). As energy transfer (ET) from fluorescein to porphyrin could occur, the design of a spacer between the two functional units has deserved much attention. According to conformational analysis, three spacers with different degree of flexibility were selected: 1) a triazole linkage, exhibiting different (up to 8) remarkable conformers, including folded geometries; 2) an alkane with three carbon-chain, with a relatively low flexibility; and 3) an alkyne spacer that was the most rigid among the three. The

corresponding dyads were synthesized and they were both theoretically and experimentally studied. Photophysical investigations highlighted ET in all compounds, no matter the spacers. Not surprisingly, this ET was more efficient in free-base molecules due to a higher overlap between fluorescein emission and porphyrin absorption (Q bands). In the case of metallated systems, unlike what we might have expected, **24** has appeared as the most promising candidate for further study, thanks to its flexibility. Indeed, this compound is more soluble in polar solvent than the other dyads, probably because of its structural properties. Moreover, although fluorescein quantum yields decreased, its properties (absorption and emission) were maintained and even if quantum yield was lowered, fluorescein emission is different from that of chlorophyll. Therefore we can reasonably expect to be able to localize molecules into plants.

Encouraged by these initial results on both aspects of the project, the multidisciplinary work initiated during this thesis will be prosecuted in our laboratory. After their synthesis and / or their characterization will be completed (G. Marchand, PhD student), compounds **7**, **11** and **12** will be tested on TBY-2 cells by biologists (M. Issawi, PhD student and C. Riou, MC). Then anionic porphyrins will be tested directly on plants, interactions into plant cells and plants being different (*e.g.* intercellular interactions).

Dyads are not water-soluble yet and our initial strategy (post-sulfonation of porphyrin moiety) may appear more complex than expected. Indeed, a great degree of purity is required for both photophysical investigations and biological assays. For such assays, a great amount of compound is necessary, which may be difficult to obtain according to reaction yields. Moreover, based on knowledge and expertise acquired in the anionic porphyrins study, direct sulfonation of the dyads may drastically change their properties. Thus, an elegant solution would consist in encapsulation procedures. Different possibilities are now well known such as encapsulation in micelles, organic nanoparticles…[463–465] Based on the expertise of our laboratory, a next project will consist in making dyads water-soluble by encapsulation into lignin nanoparticles. This work has already started with a new PhD project (G. Marchand, October 2015). In addition, this encapsulation project may be a part of an ANR project (deposed in October 2015 and coordinated by LCSN), based on the collaboration between biologists, biochemists, spectroscopists and organic chemists from different universities (Limoges, Marseille and Angers). However, the goal is henceforth to preferentially kill plant pathogens without affecting plant cells.

Moreover, QM/MM study could be performed to describe properly solvent effects and evaluate influence on geometries. QM calculations of optical properties (single point) are likely to be performed on each snapshot of a MD trajectory, which allow better sampling the influence

of conformational flexibility on spectral characteristic. Finally, simulation of compounds **26** and **28** should be envisaged to confirm our hypothesis on existence of intermolecular interactions in DMSO (and thus explain lack of solubility observed).

Experimental part

1. Material

1.1. Reagents and solvents

The origin of the reagents and solvents used in this work is shown in tables below (Table 35 and Table 36). In the case of the reactants, liquids were kept under argon and solids in a desiccator or in an oven. The specified minimum purity is guaranteed by the supplier.

Table 35: Origin and purity of solvents used.

Solvents	**Empirical formula**	**CAS number**	**Provider**
Acetonitrile	C_2H_3N	75-05-8	Carlo Erba
Chloroform 99.9 %	$CHCl_3$	67-66-3	Carlo Erba
Chloroform (NMR) + 0.03 % TMS 99.8 %	$CDCl_3$	865-49-6	Eurisotop
Chloroform RPE grade 99.5 % stabilized with ethanol	$CHCl_3$	67-66-3	VWR
Chloroform spectrophotometric grade 99.9 %	$CHCl_3$	67-66-3	Carlo Erba
Dichloromethane 99.9 %	CH_2Cl_2	75-09-2	Carlo Erba
Diethyl ether 99.8 %	$C_4H_{10}O$	60-29-7	VWR
Distillated water	H_2O	7732-18-5	-
DMF anhydrous 99.8 %	C_3H_7NO	68-12-2	Acros Organics
DMF spectrophotometric grade 99.7 %	C_3H_7ON	68-12-2	Alfa Aesar
DMSO spectrophotometric grade 99.8 %	C_2H_6SO	67-68-5	Alfa Aesar
DMSO-d6 (NMR) + 0.03 % TMS 99.8 %	C_2D_6SO	2206-27-1	Eurisotop
Ethanol absolute 99.5 %	C_2H_6O	64-17-5	VWR
Ethanol anhydrous spectrophotometric grade 90 %	C_2H_6O	64-17-5	Alfa Aesar
Hydrochloric acid 37 %	HCl	7647-01-0	Carlo Erba
Methanol 99.0 %	CH_4O	67-56-1	VWR
Petroleum spirit 99.9 %	-	64742-49-0	VWR
Propionic acid 99 %	$C_3H_6O_2$	79-09-4	Alfa Aesar
Sulfuric acid 96 %	H_2SO_4	7664-93-9	Carlo Erba

TFA 99.5 %	C_2HOF_3	76-05-1	Alfa Aesar
THF 99.9 %	C_4H_8O	109-99-9	VWR
THF spectrophotometric grade 99.9 %	C_4H_8O	109-99-9	Carlo Erba

Table 36: Origin and purity of reagents used.

Products	**Empirical formula**	**CAS number**	**Provider**
1,3-dibromopropane 98 %	$C_3H_6Br_2$	109-9-8	Alfa Aesar
1,4-dichloro-2-butyne 99 %	$C_4H_4Cl_2$	821-10-3	Acros Organics
1-bromopropane 99 %	C_3H_7Br	106-94-5	Alfa Aesar
2,2,6,6-Tetramethyl-4-piperidone 95 %	$C_9H_{17}NO$	826-36-8	Sigma-Aldrich
3,5-dimethoxybenzaldehyde	$C_9H_{10}O_3$	7311-34-4	TCI Chemicals
4-hydroxybenzaldehyde 99 %	$C_7H_6O_2$	123-08-0	Alfa Aesar
5,10,15,20-Tetraphenyl-21H, 23H-porphine-p,p′,p″,p‴-tetrasulfonic acid tetrasodium hydrate	$C_{44}H_{26}N_4Na_4O_{12}S_4$	652154-11-5	Sigma-Aldrich
5,10,15,20-(tetra-4-phosphonatophenyl)-porphyrin 98 %	$C_{44}H_{30}N_4O_4$	51094-17-8	Porphychem
5,10,15,20-(tetra-4-hydroxyphenyl)-porphyrin > 95 %	$C_{44}H_{34}N_4O_{12}P_4$	143969-69-1	Porphychem
9,10-Dimethylanthracene 99 %	$C_{16}H_{14}$	781-43-1	Sigma-Aldrich
Benzaldehyde 98 %	C_7H_6O	100-52-7	Alfa Aesar
Boron tribromide 1 M solution in methylene chloride	BBr_3	10294-33-4	Acros Organics
Bromotrimethylsilane 97 %	C_3H_9SiBr	2857-97-8	Alfa Aesar
Copper (II) acetate 98 %	$C_4H_6O_4Cu$	142-71-2	Sigma-Aldrich
Diethyliodomethylphosphonate 98 %	$C_5H_{12}IO_3P$	10419-77-9	Alfa Aesar
DMPO 97 %	$C_6H_{11}NO$	3317-61-1	Sigma-Aldrich
9,10-dimethylanthracene 99 %	$C_{16}H_{14}$	781-43-1	Sigma-Aldrich
Florisil (60-100 mesh)	SiO_2	1343-88-0	VWR
Fluorescein	$C_{20}H_{12}O_5$	2321-07-5	Sigma-Aldrich
Magnesium sulfate	$MgSO_4$	7487-88-9	Carlo Erba
meso-tetra(4-carboxyphenylporphine ≥ 97 %	$C_{48}H_{30}N_4O_8$	14609-54-2	Frontier Scientific
meso-tetra(N-methyl-4-pyridyl) porphine tetrachloride	$C_{44}H_{38}Cl_4N_8$	92739-63-4	Frontier Scientific

meso-tetraphenylporphyrin ≥ 99 %	$C_{44}H_{30}N_4$	917-23-7	Sigma-Aldrich
Potassium bromide	KBr	7758-02-3	Acros Organics
Potassium carbonate 99 %	K_2CO_3	584-08-7	Alfa Aesar
Propargyl bromide 80 %	C_3H_3Br	106-96-7	Acros Organics
Pyrrole 98 %	C_4H_5N	109-97-7	Alfa Aesar
Silica Gel 60 (0.015-0.040 mm)	SiO_2	7631-86-9	Merck
Sodium ascorbate	$C_6H_7NaO_6$	134-03-2	Sigma-Aldrich
Sodium azide	NaN_3	26628-22-8	Sigma-Aldrich
Sodium chloride	NaCl	7647-14-5	Sigma-Aldrich
Sodium hydroxide	NaOH	1310-73-2	Sigma-Aldrich
Tert-butylbromoacetate 98 %	$C_6H_{11}O_2Br$	5292-43-3	Alfa Aesar
Triethylamine 99 %	$C_6H_{15}NO_3$	121-44-8	Acros Organics
Zinc (II) acetate dihydrate 98 %	$C_4H_6O_4Zn$, $2H_2O$	5970-45-6	Acros Organics
Zn(II) *meso*-tetra(N-methyl-4-pyridyl) Porphine Tetrachloride	$C_{44}H_{36}Cl_4N_8Zn$	28850-44-4	Frontier Scientific

1.2. Chromatography

1.2.1. Analytical thin layer chromatography (TLC)

Silica plates (Kieselger 60 F254, thickness 0.2 mm, Merck) are used for thin layer chromatography. Plates revelation is done by direct observation for colored compounds or under ultraviolet light (λ = 254 nm or λ = 365 nm) for conjugated compounds.

The various eluents used are specified in the synthesis chapter after each experimental protocol. The ratio indicated are by volume.

1.2.2. Preparative thin layer chromatography

A uniform layer of silica, thick 2 mm (Kieselger 60 PF254, Merck) is deposited on glass plates (20 x 20 cm). After drying for 15 hours in the air, plates are finally activated 2 hours at 100 ° C before use.

1.2.3. Column chromatography

Purifications were performed with columns from 2 to 5 centimeters in diameter, packed on 20 to 40 centimeters tall with silica (Silica Gel 60, granulometry 0.015 to 0.040 mm, Merck) dispersed in the eluent mixture selected. In order to be purified, all crude products are dissolved in a minimum of starting eluent or fixed on Florisil (60-100 mesh, VWR) and deposited in the column heading.

1.2.4. Automated flash chromatography

Combiflash Rf 100® used is from "Teledyne Isco" brand. It allows to use solvents with rates ranging from 5 to 100 mL/min (± 5 %), and with a maximum pressure of 3.45 bars. The use of Combiflash Rf 100® allows regulation in real time of the proportion for each solvent.

This device also allows instant UV detection and separation of the products based on their absorbance. In this case, a wavelength of 254 nm (± 5) was used. The stationary phase consists of silica (35 – 70 µm), preconditioned in column from 4 to 80 g. In order to be purified, all crude products are dissolved in a minimum of starting eluent or fixed on Florisil (60-100 mesh, VWR) and deposited in the column heading.

1.3. Physico-chemical analysis

1.3.1. UV-Vis absorption spectroscopy

UV-Vis spectra were acquired on a double beam spectrophotometer "AnalytikaJena SPECORD 210". They were carried out in high precision quartz cells with an optical path of 10 mm from "Hellma Analytics".

All spectra were performed at concentration *ca.* 2.10^{-6} M in suitable solvent. The corresponding wavelength for maximum absorption are expressed in nanometers (nm). Molar absorption coefficients ε are expressed in $L.mol^{-1}.cm^{-1}$, and were determined using three independent measurements.

1.3.2. Fluorescence emission spectroscopy

Steady-state photoluminescence spectra were recorded on:

1) a spectrofluorimeter QM-4/QuantaMaster (PTI) equipped with a xenon short arc lamp. Detection was made in the 300-800 nm range using a R1527P Hamamatsu photomultiplier.

2) a FLS980 spectrometer from Edinburgh Instruments (UK) equipped with a 450 W xenon lamp (platform PLATINOM of XLim institute, Limoges). Detection was made in the 300–800 nm range using a cooled R928P Hamamatsu photomultiplier (dark count 50 cps). All emission spectra were corrected for the excitation.

Quantum yields were measured on both experimental set-up using tetraphenylporphyrin (H_2TPP)[356] in toluene and commercial fluorescein (spectroscopic quality)[458,459] in aqueous 0.1 M NaOH as standards, by three or more independents experiments.

Time-resolved spectroscopy measurements were performed on a FLS980 spectrometer from Edinburgh Instruments (UK) equipped with a picosecond diode laser at 509.2 nm as excitation source (temporal width of 150 ps, repetition frequency from 20 kHz to 20 MHz) and using time correlated single photon counting (TCSPC) method. The instrument response function was measured using a diffusive reference sample (LUDOX ® from Sigma-Aldrich).

All measurements were performed using high precision quartz cells with an optical path of 10 mm from "Hellma Analytics", and at concentration *ca*. 2.10^{-6} M in suitable solvent, in aerated conditions, as this parameter has no influence on recorded spectra.

1.3.3. Infrared spectroscopy

IR spectra were performed on a Perkin-Elmer FT-IR spectrometer SPECTRUM 1000, on samples conditioned in potassium bromide pellet (1-2 wt%). The wave numbers are given in cm^{-1}.

1.3.4. Melting point

Melting point (MP) are determined using an electro-thermal melting point apparatus (IA9100 series).

1.3.5. NMR spectroscopy

^{1}H and ^{13}C nuclear magnetic resonance (^{1}H-NMR and ^{13}C-NMR) spectra were recorded in deuterated solvents ($CDCl_3$ and DMSO-d_6), on Brüker DPX 400 and 500 spectrometers at the SCRABL platform from GEIST Institute (Limoges University).

^{31}P nuclear magnetic resonance spectra were recorded in deuterated solvents (DMSO-d_6 and D_2O) on a Brüker DPX 500 spectrometer at the SCRABL platform from GEIST Institute (Limoges University).

^{1}H and NOESY spectra for compound **24** at variable temperature were recorded in $CDCl_3$, on a Bruker DRX 500 spectrometer with a BVT3000 variable temperature unit, at the PIAM platform (Angers University).

Chemical shifts are reported as δ (parts per million), downfield from internal tetramethylsilane (TMS), and coupling constants J are given in Hertz (Hz). Abbreviations used for naming the figures are: s (singlet), d (doublet), dd (double doublet) t (triplet), q (quartet) quint (quintuplet) and m (multiplet). Extended figure include "el" acronym in index.

Symbol * means that signals correspond to the expected compound, but an analogy with starting reactants failed to differentiate.

1.3.6. High Resolution Mass Spectrometry

Maldi-TOF mass spectra were recorded on a 4800 MALDI TOF/TOF™ Analyzer from AB SCIEX at the SCRABL platform from GEIST Institute (Limoges University).

High resolution electrospray ionization mass spectra (HR ESI-MS) were performed on a Bruker Q-TOF maXis mass spectrometer, coupled to an Ultimate 3000 RSLC chain (Dionex); by the ICOA/CBM (FR2708) platform (Orleans University).

1.3.7. pH-metric analysis

pH measurements were performed using a Mettler Toledo Five Easy^{TM} FE20 apparatus, equipped with a pH probe LE409 and thermometer. The device has previously been calibrated with two buffer solutions of pH 4 and 7 respectively.

All solutions were prepared using volumetric flasks and masses weighed using a Radwag MYA 5.3Y Microbalance from Grosseron (with Internal Automatic Calibration).

All UV-Vis measurements were performed as described in 1.3.1.

1.3.8. ROS production evaluation by Electron Paramagnetic Resonance

Evaluation of ROS production (singlet oxygen and superoxide anion) by water soluble compounds (**1-2**, **4-5**, **CP** and **CP-Zn**) were performed by EPR under visible irradiations (white light) provided by a 20 W halogen lamp. The intensity of illumination was measured by a luxmeter (Digital Lux Tester YF-1065). EPR spectra were recorded with a Bruker Model

ESP300E spectrometer operating at room temperature. TEMP (2,2,6,6-Tetramethyl-4-piperidone) and DMPO (5,5-Dimethyl-1-pyrroline *N*-oxide) were used as radicals trap.

- Singlet oxygen ($^1O_2$) detection:

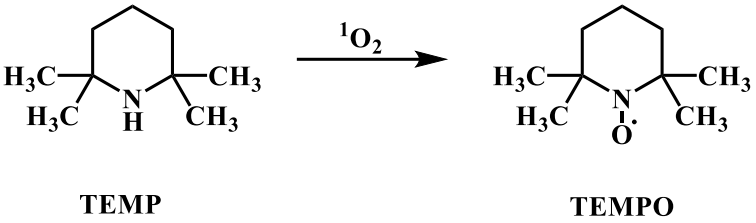

Figure 155: Singlet oxygen detection using TEMP.

To 50 µL of fresh TEMP solution (25 mM in 0.01 M phosphate buffer, pH 7.4) were added 50 µL of fresh porphyrin solution (80 µM in 1,5 % aqueous NaOH). The solution obtained was then immediately transferred into quartz capillaries (100 µL) and placed at 21 cm from the source of illumination with a light intensity of 20.10^3 lm.m^{-2}. EPR spectra were performed under the following conditions: modulation frequency: 100 kHz; microwave frequency: 9.78 GHz; microwave power: 0.51 mW; modulation amplitude: 0.987 G; time constant: 10.24 ms; scans number 2.

- Superoxide anion ($O_2^{\bullet -}$) detection:

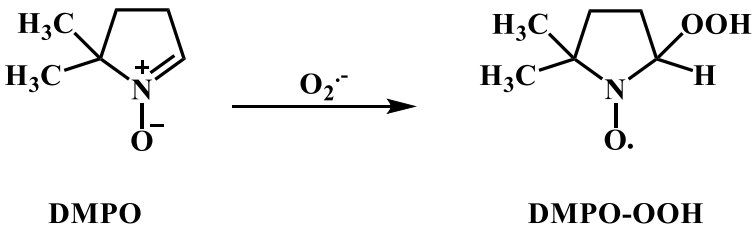

Figure 156: Superoxide anion detection using DMPO.

To 50 µL of fresh DMPO solution (450 mM in DMSO) were added 50 µL of fresh porphyrin solution (100 µM in DMSO - water 90-10 v/v solution). The solution obtained was then immediately transferred into quartz capillaries (100 µL) and placed at 39.5 cm from the source of illumination with light intensity of 5.10^3 lm.m^{-2}. The EPR conditions were the same as above except: microwave power 20 mW.

1.3.9. Singlet oxygen production quantum yield determination by UV-Vis absorption spectroscopy

Singlet oxygen production of compounds **24** to **28** were evaluated by monitoring 9,10-Dimethylanthracene (DMA) photo-oxidation (Figure 152) by UV-Vis absorption spectroscopy.

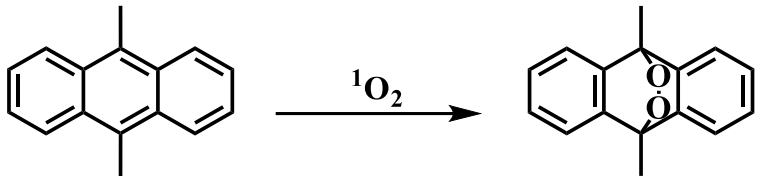

Figure 157: DMA oxidation by singlet oxygen.

1.5 mL of a fresh DMA solution (DMF, 10^{-4} M) were mixed with 1.5 mL of dyad (DMF, 10^{-6} M) in a 1 centimeter quartz cell equipped with a magnetic stirrer and under air flux. A 92 W – 1200 Lumen halogen lamp was used in order to produce white light. Samples were placed at 22 cm from the source of illumination with light intensity of $2.5.10^3$ $lm.m^{-2}$; and an optical filter (Asahi Spectra shortpass, optical window between 400 and 700 nm) was placed between the sample and the lamp. The absorption spectrum of the mixture was recorded every five minutes and the decrease of absorption at 401 nm recorded in order to study the kinetic of DMA photo-oxidation. Dark control and experiment without compounds **24-28** were also performed and no effect recorded. K_{obs}, the DMA photo-oxidation rate constant, could be determined using following formula: $\ln (A_0/A_t) = K_{obs} * t$.

Singlet oxygen quantum yields were then determined by comparison with same experimental set-up applied to TPP (as reference compound) according to:[356]

$$\Phi_{\Delta \text{ compound}} = \frac{\mathbf{K}_{\text{obs compound}} \text{ x } \mathbf{I}_{400\text{-}700 \textbf{ ref}}}{\mathbf{K}_{\text{obs }\textbf{ref}} \text{ x } \mathbf{I}_{400\text{-}700 \text{ compound}}}$$

Where:

- Φ_Δ is the singlet oxygen quantum yield.
- K_{obs} is the rate constant of DMA photo-oxidation by singlet oxygen.
- $I_{400\text{-}700}$ is the intensity (I) sum of absorbed light by the compound between 400 and 700 nanometers: $I = I_0 \text{ x } (1 - e^{2.3A})$.

1.4. Ultrasonic and microwave devices

1.4.1. Ultrasonic bath

Dissolution of the reagents in suitable solvents was performed using an ELMA-ONE ultrasonic bath with a frequency of 35 kHz and a power of 30 W. They are all carried out in a flask, immersed in the tank filled with water.

1.4.2. Microwave oven

Microwave irradiations were performed by means of a laboratory microwave (Milestone, Ethos 1600Microsynth). Temperature is measured using an optical fiber thermometer (ATC-FO)/Ethos. Duration, power, and temperature of irradiation can be adjusted by means of a computer using control software (Milestone GmBH easy control / MWD-640).

1.5. Molecular modeling

Quantum chemistry calculations based on DFT were performed to investigate the conformational space of reference compounds **15** and **21** as well as dyads **24**, **26** and **28**. Because of the structure of **24**, non-covalent interactions between the porphyrin and fluorescein moieties were expected. In particular, a proper description of dispersive forces appeared mandatory. The use of the ωB97XD XC functional has been recommended to properly describe non-covalent interactions (π-π stacking and H-bonding).[448,449] The conformational analysis was assessed by a systematic exploration of the potential energy surface of the linkage. The most stable conformers were confirmed by the absence of any imaginary frequency. The Pople-type double-ζ basis set 6-31+G(d,p) was used as being an adapted compromise between accuracy and computational cost. Triple ζ basis sets did not significantly enhance description. Adding diffuse function (+) is mandatory to better evaluate electron distribution on these highly π-conjugated systems, however it is known to dramatically slower optimization procedures. The size of the porphyrin derivatives has indeed prevented easy optimization, therefore all geometries and frequency analyses were optimized with 6-31G(d,p) and single points were further achieved with 6-31+G(d,p). When necessary, the extensively recommended LANL2DZ basis set, using core pseudo potentials, was used for the transition metal Zn.[466] Solvent effects were taken into account implicitly using the IEFPCM (Integral Equation Formalism Polarizable Continuum Model). In PCM models, the substrate is embedded into a shape-adapted cavity surrounded by a dielectric continuum characterized by its dielectric constant (ε = 4.71, 46.83

and 78.35 in chloroform, DMSO and water, respectively). Optical properties (*i.e.*, UV-Vis absorption, MO transitions and ES description) were predicted by using TD(Time Dependent)-DFT calculations. Three different functionals were used, namely B3LYP as classically used for porphyrins and dyads and the long-range separated functionals, namely ωB97XD and CAM-B3LYP, due to their capacity to properly describe CT in ES. However, only the ωB97XD results are provided because CAM-B3LYP give similar results. All calculations were performed with Gaussian09[467], using the CALI (CAlcul en LImousin) cluster.

2. Synthesis

Sodium 4,4',4",4"'-(porphyrin-5,10,15,20-tetrayl)tetrabenzenesulfonate (**1**)

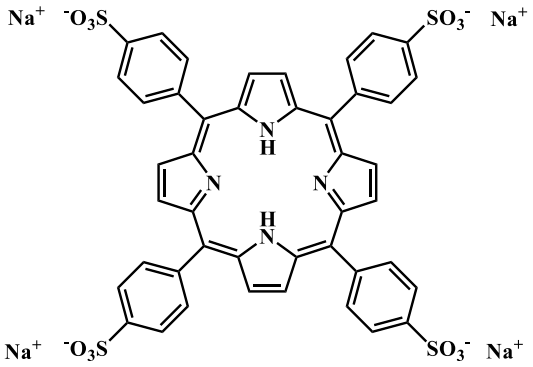

Commercial compound.

^{1}H NMR (DMSO-d6, 400.13 MHz) δ_{ppm}: 8.84 (s_{el}, 8H, $\mathbf{H}_{\beta\text{-pyrrolic}}$); 8.16 (d, 8H, J = 8.0 Hz, $\mathbf{H}_{2,6\text{-aryl}}$); 8.03 (d, 8H, J = 8.0 Hz, $\mathbf{H}_{3,5\text{-aryl}}$); -2.94 (s, 2H, $\mathbf{H}_{NHint}$).

UV-Vis ($CHCl_3$) λ_{max} nm (ε, 10^{-3} L.mol^{-1}.cm^{-1}): 414 (219), 516 (7.3), 553 (3.7), 582 (4.1), 636 (3.9).

4,4',4",4"'-(porphyrin-5,10,15,20-tetrayl)tetrabenzoic acid (**2**)

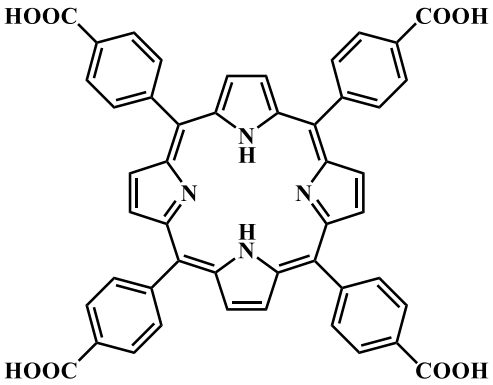

Commercial compound.

^{1}H NMR (DMSO-d6, 500.15 MHz) δ_{ppm}: 8.86 (s_{el}, 8H, $\mathbf{H}_{\beta\text{-pyrrolic}}$); 8.38 (d, 8H, J = 8.0 Hz, $\mathbf{H}_{3,5\text{-aryl}}$); 8.32 (d, 8H, J = 8.0 Hz, $\mathbf{H}_{2,6\text{-aryl}}$); -2.91 (s, 2H, $\mathbf{H}_{NHint}$).

^{13}C NMR (DMSO-d6, 500.15 MHz) δ_{ppm}: 167.5 (C acid); 145.1 (C-4 aryl); 134.3 (C-1 and C-3,5 aryl) ; 131.1 (Cβ pyrrole); 127.8 (C-1 and C-2,6 aryl); 119.3; (C*meso*).

MS (ESI-Q3): m/z = 791.3527 $[M+H]^{+}$.

UV-Vis ($CHCl_3$) λ_{max} nm (ε, 10^{-3} $L.mol^{-1}.cm^{-1}$): 416 (413), 518 (13.7), 556 (7.8), 583 (7), 638 (7.3).

Tetra-tert-butyl 2,2',2",2'"-((porphyrin-5,10,15,20-tetrayltetrakis(benzene-4,1-diyl))tetrakis(oxy))tetraacetate **3)**

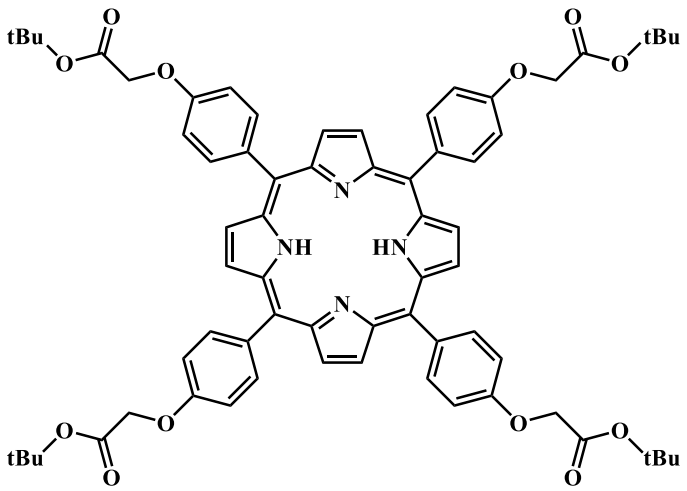

5,10,15,20-(tetra-4-hydroxyphenyl)porphyrin (1 equiv., 150 mg, 0.22 mmol), tert-butylbromoacetate (10 equiv., 324 µL, 2.2 mmol), K_2CO_3 (20 equiv., 611 mg, 4.4 mmol) were dissolved in dry DMF (20 mL). The solution was stirred in the dark for 24 h under argon and at 70 °C. After solvent removing, the crude product was dissolved in DCM, washed with distillated water (3x25 mL) and dried over $MgSO_4$. After filtration and evaporation, the residue was purified by chromatographic column (solid phase: silica gel, eluent: petroleum ether with a DCM gradient ranging from 80 to 100 %) to give compound **3** as a purple solid (205 mg, 82 %).

Rf = 0.8 ($CHCl_3$).

^{1}H NMR (DMSO-d6, 500.15 MHz) δ_{ppm}: 8.84 (s_{el}, 8H, $\mathbf{H}_{\beta\text{-pyrrolic}}$); 8.12 (d, 8H, J = 8.5 Hz, $\mathbf{H}_{2,6\text{-aryl}}$); 7.35 (d, 8H, J = 8.5 Hz, $\mathbf{H}_{3,5\text{-aryl}}$); 4.96 (s, 8H, $\mathbf{H}_{O\text{-}CH2}$); 1.55 (s, 36H, $\mathbf{H}_{tBu}$); -2.90 (s, 2H, $\mathbf{H}_{NHint}$).

^{13}C NMR (DMSO-d6, 500.15 MHz) δ_{ppm}: 167.9 (C ester); 157.6 (C-4 aryl); 135.2 (C-1 aryl); 133.9 (C-2,6 aryl; 119.5; (C*meso*); 113.0 (C-3,5 aryl); 81.5 (C quaternary tBu); 65.3 (O-CH_2); 27.5 (CH_3).

MS (ESI-Q3): m/z = 1135.7179 $[M+H]^+$.

UV-Vis ($CHCl_3$) λ_{max} nm (ε, 10^{-3} L.mol^{-1}.cm^{-1}): 422 (311), 518 (11), 555 (7), 595 (3.5), 649 (3).

2,2',2",2"'-((porphyrin-5,10,15,20-tetrayltetrakis(benzene-4,1-diyl))tetrakis(oxy))tetraacetic acid **(4)**

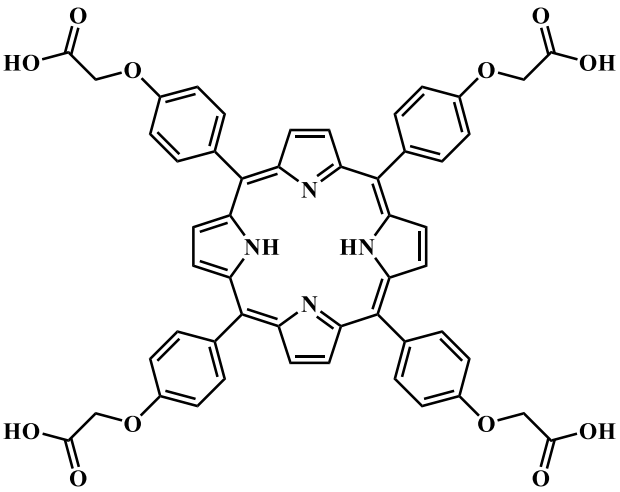

Compound **3** (1 equiv., 288 mg, 0.42 mmol) was dissolved in TFA (2 mL). The solution was stirred in the dark for one night at room temperature. After TFA removing, the crude product was washed twice with diethyl ether to eliminate acid residues. Compound **4** was obtained as a green solid (378 mg, > 99%).
Rf = 0.4 ($CHCl_3$/EtOH 5/5).

^{1}H NMR (DMSO-d6, 500.15 MHz) δ_{ppm}: 13.18 (s_{el}, 4H, $\mathbf{H}_{carboxylic\ acid}$); 8.85 ($s_{el}$, 8H, $\mathbf{H}_{\beta\text{-pyrrolic}}$); 8.13 (d, 8H, J = 8.1 Hz, $\mathbf{H}_{2,6\text{-aryl}}$); 7.36 (d, 8H, J = 8.2 Hz, $\mathbf{H}_{3,5\text{-aryl}}$); 4.99 ($s_{el}$, 8H, $\mathbf{H}_{O\text{-}CH2}$); -2.90 ($s_{el}$, 2H, $\mathbf{H}_{NHint}$).

^{13}C NMR (DMSO-d6, 500.15 MHz) δ_{ppm}: 170.2 (C acid); 157.7 (C-4 aryl); 135.2 (C-1 aryl); 133.9 (C-2,6 aryl; 131.3 (β-pyrrolic); 119.5; (C*meso*); 113.0 (C-3,5 aryl); 64.8 (O-CH_2).

MS (ESI-Q3): m/z = 911.3003 $[M+H]^+$.

UV-Vis (H_2O) λ_{max} nm (ε, 10^{-3} $L.mol^{-1}.cm^{-1}$): 418 (210), 522 (6), 562 (5), 585 (3), 641 (2.8).

(4-(10,15,20-tris(4-phosphonophenyl)porphyrin-5-yl)phenyl)phosphonic acid (**5**)

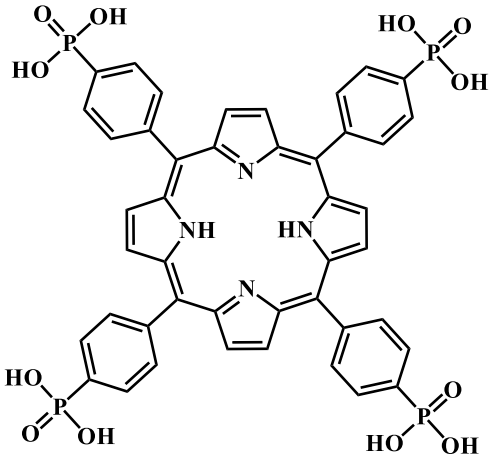

Commercial compound.

^{31}P NMR (DMSO-d6, 500.15 MHz) δ_{ppm}: 11.4.

UV-Vis ($CHCl_3$) λ_{max} nm (ε, 10^{-3} L.mol^{-1}.cm^{-1}): 418 (183), 522 (8.5), 558 (3.9), 583 (3.5), 640 (2.8).

Diethyl ((4-(10,15,20-tris(4-((diethoxyphosphoryl)methoxy)phenyl)porphyrin-5-yl)phenoxy)methyl)phosphonate **(6)**

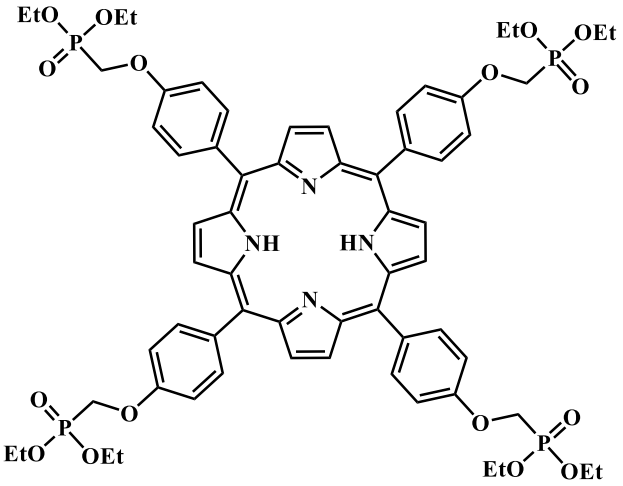

5,10,15,20-(tetra-hydroxyphenyl)porphyrin (1 equiv., 150 mg, 0.22 mmol), diethyl-iodo-methylphosphonate (10 equiv., 367 µL, 2.2 mmol), K_2CO_3 (20 equiv., 611 mg, 4.4 mmol) were dissolved in dry DMF (15 mL). The solution was stirred in the dark for 24 h under argon and at 70 °C. After solvent removing, the crude product was dissolved in DCM, washed with distillated water (3x25 mL) and dried over $MgSO_4$. After filtration and evaporation, the residue was purified by chromatographic column (solid phase: silica gel, eluent: $CHCl_3$) to give compound **6** as a purple solid (68 mg, 24 %).
Rf = 0.6 ($CHCl_3$).

^{1}H NMR (DMSO-d6, 500.15 MHz) δ_{ppm}: 8.85 (s, 8H, $\mathbf{H}_{\beta\text{-pyrrolic}}$); 8.14 (d, 8H, J = 9.00 Hz, $\mathbf{H}_{2,6\text{-aryl}}$); 7.48 (d, 8H, J = 8.5 Hz, $\mathbf{H}_{3,5\text{-aryl}}$); 4.74 (d, 8H, J = 10.0 Hz; $\mathbf{H}_{O\text{-}CH2}$); 4.26 (m, 16H, $\mathbf{H}_{ethyl}$); 1.50 (t, 24H, Hz, J = 7.0 Hz, $\mathbf{H}_{CH3}$); -2.89 (s, 2H, $\mathbf{H}_{NHint}$).

^{31}P NMR (DMSO-d6, 500.15 MHz) δ_{ppm}: 19.9.

^{13}C NMR (DMSO-d6, 500.15 MHz) δ_{ppm}: 158.4 (C-4 aryl); 135.3 (C-1 aryl); 134.4 (C-2,6 aryl); 131.5 (C_β pyrrole); 119.5; (C*meso*); 113.1 (C-3,5 aryl); 62.3 (CH_2-ethyl 27.5 (CH_3-ethyl).

MS (ESI-Q3): m/z = 1280.3453 $[M+H]^+$.

UV-Vis ($CHCl_3$) λ_{max} nm (ε, 10^{-3} L.mol^{-1}.cm^{-1}): 417, 521, 558 584, 648.

((4-(10,15,20-tris(4-(phosphonomethoxy)phenyl)porphyrin-5-yl)phenoxy)methyl)phosphonic acid **(7)**

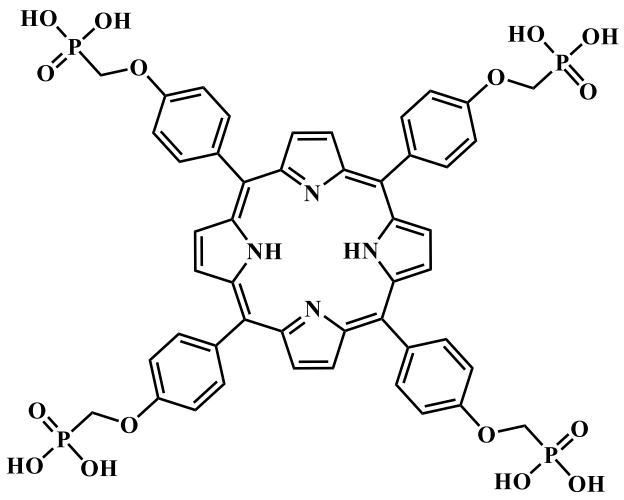

Compound **6** (1 equiv., 40 mg, 0.03 mmol), was dissolved in acetonitrile (10 mL). The solution was stirred in the dark for 10 minutes under argon, then bromotrimethylsilane was added slowly (24 equiv., 98.2 µL, 0.74 mmol). The mixture was stirred in the dark for 24 h then distillated water (5 mL) was added. After 2 h, the reaction was evaporated to dryness. Compound **7** was obtained as a green solid (30.1 mg, > 95 %).

Rf = 0.1 ($CHCl_3$ / EtOH 5/5).

^{31}P NMR (-d6, 500.15 MHz) δ_{ppm}: 13.1.

5,10,15,20-tetrakis(3,5-dimethoxyphenyl)porphyrin **(8)**

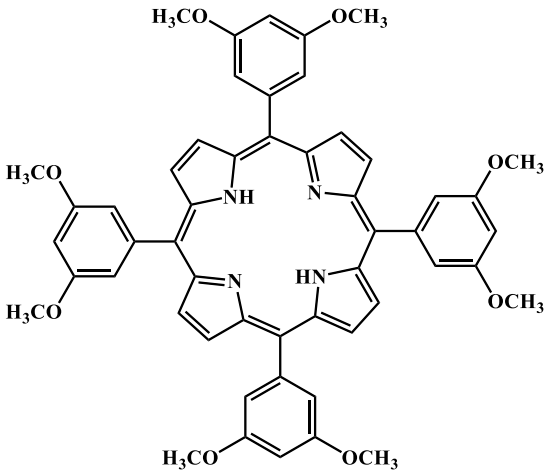

3,5-dimethoxybenzaldehyde (1 equiv., 2.5 g, 15 mmol) were dissolved in 100 mL of propionic acid. The solution was heated at 120 °C under reflux with vigorous stirring for 1 h, then freshly distilled pyrrole (1 equiv., 1.05 mL, 15 mmol) were added. After 1 h, the mixture was stored at -20 °C during 24 h. Then, compound **8** was obtained by simple filtration and washed with methanol (2 x 15 mL) to give a purple solid (1.17 g, 36 %).
Rf = 0.7 ($CHCl_3$).

^{1}H NMR (DMSO-d6, 500.15 MHz) δ_{ppm}: 8.91 (s_{el}, 8H, $\mathbf{H}_{\beta\text{-pyrrolic}}$); 7.37 (d, 8H, J = 2.5 Hz, $\mathbf{H}_{2,6\text{-aryl}}$); 6.98 (t, 4H, J = 2.5 Hz, $\mathbf{H}_{4\text{-aryl}}$); 3.93 ($s_{el}$, 24H, $\mathbf{H}_{methyl}$); -2.99 (s_{el}, 2H, $\mathbf{H}_{NHint}$).

^{13}C NMR (DMSO-d6, 500.15 MHz) δ_{ppm}: 158.6 (C-3,5 aryl); 147.3 (Cα pyrrole); 142.5 (C-1 aryl); 119.5 (C *meso*); 113.5 (C-2,6 aryl); 99.9 (C-4 aryl); 55.4 (CH_3).

MS (MALDI-TOF): m/z = 855.3385 $[M+H]^+$.

UV-Vis ($CHCl_3$) λ_{max} nm (ε, 10^{-3} $L.mol^{-1}.cm^{-1}$): 421 (314), 516 (13), 550 (3.7), 589 (4), 646 (2).

5,5',5",5"'-(porphyrin-5,10,15,20-tetrayl)tetrakis(benzene-1,3-diol) **(9)**

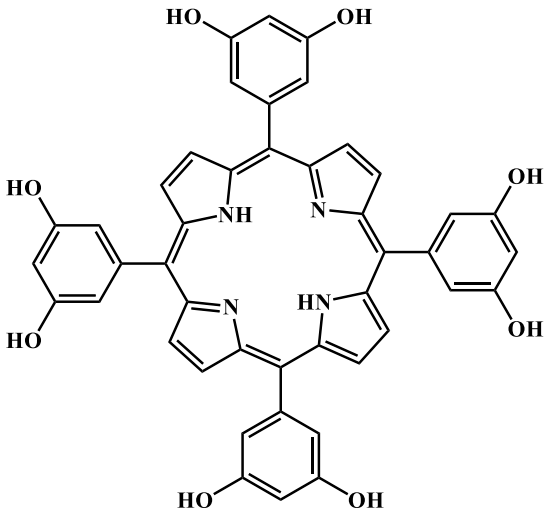

Compound **8** (1 equiv., 1.98 g, 2.32 mmol) was dissolved in dry DCM (100 mL), then boron tribromide (20 equiv.; 10.8 mL; 46.4 mmol) was slowly added. The green mixture was stirring at room temperature in the dark, and under argon during 24 h. Then 50 mL of distillated water were added, and the solution was stirring for 2 h. After solvent evaporation, the crude product was dissolved in EtOH/Et_3N 9/1 to neutralize acidity due to boron tribromide then dried to give compound **9** as a purple solid. Presence of boron salts prevented to obtain yield, but NMR and mass analysis show quantitative yield (> 99%).
Rf = 0.2 ($CHCl_3$/EtOH 5/5).

^{1}H NMR (DMSO-d6, 500.15 MHz) δ_{ppm}: 9.30 (s_{el}, 8H, $\mathbf{H}_{hydroxyl}$); 8.94 (s_{el}, 8H, $\mathbf{H}_{\beta\text{-pyrrolic}}$); 7.06 (d, 8H, J = 2.2 Hz, $\mathbf{H}_{2,6\text{-aryl}}$); 6.70 (t, 4H, J = 2.2 Hz, $\mathbf{H}_{4\text{-aryl}}$); -3.02 ($s_{el}$, 2H, $\mathbf{H}_{NHint}$).

^{13}C NMR (DMSO-d6, 500.15 MHz) δ_{ppm}: 158.6 (C-3,5 aryl); 147.3 (Cα pyrrole); 142.7 (C-1 aryl); 131.2 (C_β pyrrole); 119.4 (C *meso*); 113.4 (C-2,6 aryl); 101.5 (C-4 aryl).

MS (MALDI-TOF): m/z = 743.2129 $[M+H]^+$.

UV-Vis (EtOH) λ_{max} nm (ε, 10^{-3} $L.mol^{-1}.cm^{-1}$): 418 (228), 514 (12), 549 (5), 589 (4.5), 646 (2).

Octa-tert-butyl 2,2',2",2''',2'''',2''''',2''''''-((porphyrin-5,10,15,20-tetrayltetrakis(benzene-5,1,3-triyl))octakis(oxy))octaacetate **(10)**

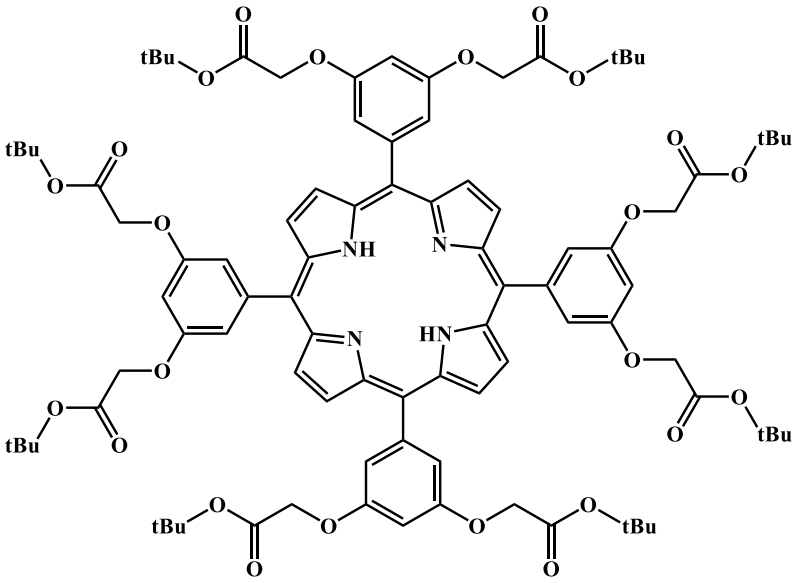

Compound **9** (1 equiv., 250 mg, 0.34 mmol), tert-butylbromoacetate (20 equiv., 995 µL, 6.74 mmol), K_2CO_3 (32 equiv., 1.49 g, 10.8 mmol) were dissolved in dry DMF (20 mL). The solution was stirred in the dark for 48 h under argon and at 70 °C. After solvent removing, the crude product was dissolved in DCM, then washed with distillated water (4x20 mL) and brine if necessary. Then crude product was dried over $MgSO_4$, filtered, evaporated then purified by chromatographic column (solid phase: silica gel, eluent: petroleum ether with a DCM gradient ranging from 80 to 100 %) to give compound **10** as a purple solid (412 mg, 73 %).

Rf = 0.7 ($CHCl_3$).

^{1}H NMR (DMSO-d6, 500.15 MHz) δ_{ppm}: 8.90 (s_{el}, 8H, $\mathbf{H}_{\beta\text{-pyrrolic}}$); 7.37 (d, 8H, J = 2.1 Hz, $\mathbf{H}_{2,6\text{-aryl}}$); 6.98 (t, 4H, J = 2.1 Hz, $\mathbf{H}_{4\text{-aryl}}$); 4.87 (s, 16H, $\mathbf{H}_{O\text{-}CH2}$); 1.41 ($s_{el}$, 72H, $\mathbf{H}_{methyl}$); -2.99 (s_{el}, 2H, $\mathbf{H}_{NHint}$).

^{13}C NMR (DMSO-d6, 500.15 MHz) δ_{ppm}: 166.2-167.4-168.7 (C ester); 157.0 (C-3,5 aryl); 142.7 (Cα pyrrole); 134.1 (C-1 aryl); 131.2 (Cβ pyrrole); 119.4 (C *meso*); 114.6 (C-2,6 aryl); 101.5 (C-4 aryl); 80.6 (Cquaternary tBu); 65.2 (O-CH_2); 27.7 (CH_3).

MS (MALDI-TOF): m/z = 1655.7662 $[M+H]^+$.

UV-Vis ($CHCl_3$) λ_{max} nm (ε, 10^{-3} L.mol^{-1}.cm^{-1}): 421 (263), 516 (11), 550 (2.3), 590 (3), 646 (1).

2,2',2",2'",2"",2""",2""",2"""""-((porphyrin-5,10,15,20-tetrayltetrakis(benzene-5,1,3-triyl))octakis(oxy))octaacetic acid **(11)**

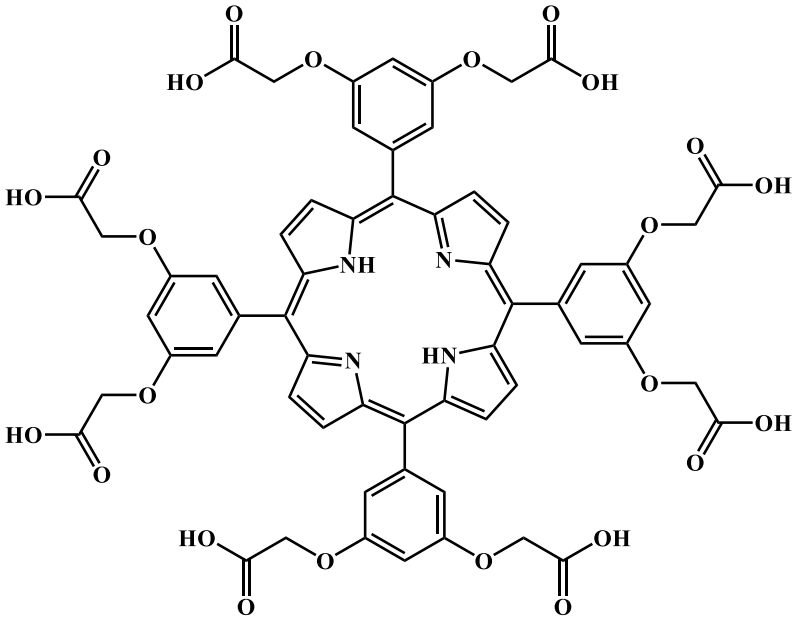

Compound **10** (1 equiv., 205 mg, 0.12 mmol) was dissolved in TFA (3 mL). The solution was stirred in the dark for one night at room temperature. After TFA removing, the crude product was washed twice with diethyl ether to eliminate acid residues and dried to give compound **11** as a green solid (148.6 mg, > 99%).
Rf = 0.3 ($CHCl_3$/EtOH 5/5).

^{1}H NMR (DMSO-d6, 500.15 MHz) δ_{ppm}: 12.87 (s_{el}, 8H, $H_{carboxylic\ acid}$); 8.94 (s_{el}, 8H, $\mathbf{H}_{\beta\text{-pyrrolic}}$); 7.39 (d, 8H, J = 2.1 Hz, $\mathbf{H}_{2,6\text{-aryl}}$); 6.98 (t, 4H, J = 2.1 Hz, $\mathbf{H}_{4\text{-aryl}}$); 4.88 (s, 16H, $\mathbf{H}_{O\text{-}CH2}$); -3.00 ($s_{el}$, 2H, $\mathbf{H}_{NHint}$).

^{13}C NMR (DMSO-d6, 500.15 MHz) δ_{ppm}: 170.8-171.0-171.1 (C acid); 157.1 (C-3,5 aryl); 142.8 (Cα pyrrole); 131.4 (Cβ pyrrole); 119.3 (C *meso*); 114.3 (C-2,6 aryl); 101.5 (C-4 aryl); 63.4 (O-CH_2).

MS (ESI-Q3): m/z = 1208.3457 $[M+H]^+$.

UV-Vis (H_2O) λ_{max} nm (ε, 10^{-3} $L.mol^{-1}.cm^{-1}$): 417 (227) / 517 (8.6) / 554 (2.6) / 580 (3.4) / 635 (1.4).

5-(4-hydroxyphenyl)-10,15,20-triphenylporphyrin **(13)**

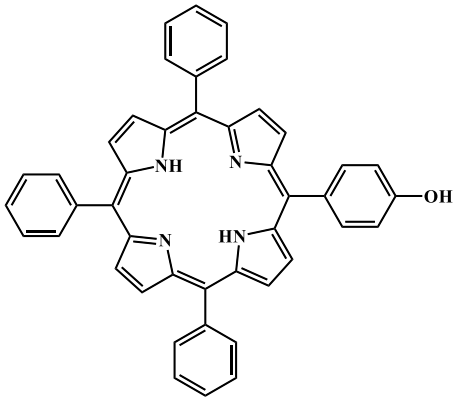

4-hydroxybenzaldehyde (1 equiv., 1.22 g, 10 mmol) and benzaldehyde (3 equiv., 3.1 mL, 30 mmol) were dissolved in 200 mL of propionic acid. The solution was heated at 120 °C under reflux with vigorous stirring for 1 h, then freshly distilled pyrrole (4 equiv., 2.8 mL, 40 mmol) were added. After 1 h, the mixture was cooled and the solvent was evaporated to dryness. The crude product was purified by chromatographic column (stationary phase: silica gel) using petroleum ether with a $CHCl_3$ gradient ranging from 70 to 100 % as eluent. Compound **13** was obtained as a purple solid (435 mg, 7 %).
Rf = 0.3 ($CHCl_3$).

^{1}H NMR ($CDCl_3$, 400.13 MHz) δ_{ppm}: 8.87 (d, 2H, J = 4.8Hz, $\mathbf{H}_{\beta pyrrolic}$); 8.83 ($s_{el}$, 6H, $\mathbf{H}_{\beta pyrrolic}$); 8.21 (d, 6H, J = 7.6 Hz, $\mathbf{H}_{2,6\text{-phenyl}}$); 8.04 (d, 2H, J = 8.3 Hz, $\mathbf{H}_{2,6\text{-aryl}}$); 7.75 (d, 9H, 7.4 Hz, $\mathbf{H}_{3,4,5\text{-phenyl}}$); 7.16 (d, 2H, J = 8.2 Hz, $\mathbf{H}_{3,5\text{-aryl}}$); -2.74 (s, 2H, $\mathbf{H}_{NHint}$).

^{13}C NMR ($CDCl_3$, 400.13 MHz) δ_{ppm}: 155.5 (C-4 aryl); 142.2 (Cα pyrrole); 135.7 (C-1 aryl); 134.6 (C-2,6 aryl); 131.2-132.3 (Cβ pyrrole); 126.7 to 129.1 (C phenyl); 119.9-120.1 (C*meso*); 113.7 (C-3,5 aryl).

MS (MALDI-TOF): m/z = 631.5248 $[M+H]^+$.

UV-Vis ($CHCl_3$) λ_{max} nm (ε, 10^{-3} $L.mol^{-1}.cm^{-1}$): 419 (563), 518 (11), 556 (9), 598 (3), 647 (1).

5-(4-propoxyphenyl)-10,15,20-triphenylporphyrin **(14)**

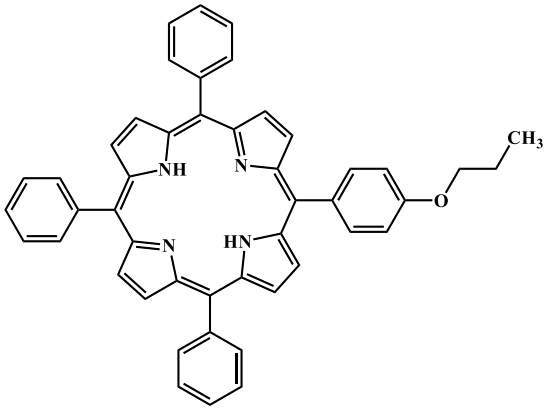

Compound **13** (1 equiv., 59 mg, 0.09 mmol), 1-bromopropane (5 equiv., 41 µL, 0.45 mmol) and K_2CO_3 (10 equiv., 124.4 mg, 0.9 mmol) were dissolved in dry DMF (10 mL). The reaction was activated twice by micro-waves irradiations (5'/ 200 W/ 120 °C). After solvent evaporation, the crude product was dissolved in DCM, washed with distillated water (2x25 mL) then dried over $MgSO_4$. After filtration and evaporation, the residue was purified on column (stationary phase: silica gel, eluent $CHCl_3$) to give compound **14** as a purple solid (47.3 mg, 78 %).
Rf = 0.8 ($CHCl_3$).

^{1}H NMR ($CDCl_3$, 400.13 MHz) δ_{ppm}: 8.86 (d, 2H, J = 4.8Hz, $\mathbf{H}_{\beta pyrrolic}$); 8.82 ($s_{el}$, 6H, $\mathbf{H}_{\beta pyrrolic}$); 8.21 (d, 6H, J = 7.6 Hz, $\mathbf{H}_{2,6\text{-phenyl}}$); 8.06 (d, 2H, J = 8.3 Hz, $\mathbf{H}_{2,6\text{-aryl}}$); 7.75 (d, 9H, 7.4 Hz, $\mathbf{H}_{3,4,5\text{-phenyl}}$); 7.15 (d, 2H, J = 8.2 Hz, $\mathbf{H}_{3,5\text{-aryl}}$); 4.32 (t, 2H, J = 6.8 Hz, $\mathbf{H}_{O\text{-}CH2}$); 1.84 (m, 2H, $\mathbf{H}_{CH2}$); 1.04 (t, 3H, J = 7.3 Hz, $\mathbf{H}_{CH3}$); -2.74 (s, 2H, $\mathbf{H}_{NHint}$).

^{13}C NMR ($CDCl_3$, 400.13 MHz) δ_{ppm}: 159.0 (C-4 aryl); 142.2 (Cα pyrrole); 135.6 (C-1 aryl); 134.4 (C-2,6 aryl); 130.9 (Cβ pyrrole); 126.7-127.7 (C phenyl); 120.1 (C*meso*); 112.8 (C-3,5 aryl); 69.8 (O-CH_2); 22.8 (CH_2); 10.7 (CH_3).

MS (MALDI-TOF): m/z = 673.3217 $[M+H]^+$.

UV-Vis ($CHCl_3$) λ_{max} nm (ε, 10^{-3} L.mol^{-1}.cm^{-1}): 420 (310), 517 (11), 552 (5.6), 593 (3.3), 648 (3.6).

Zinc(II) 5-(4-propoxyphenyl)-10,15,20-triphenylporphyrin **(15)**

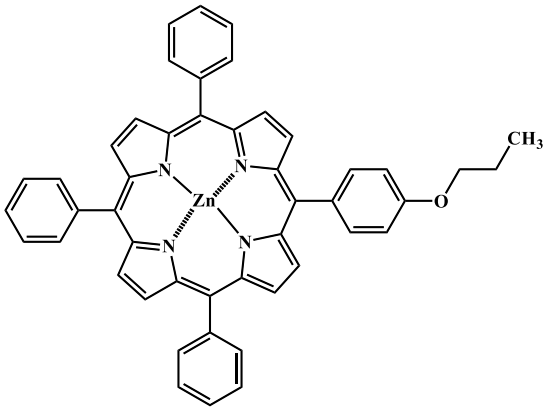

Compound **14** (1 equiv., 26.1 mg, 0.04 mmol) and zinc (II) acetate (10 equiv., 85.6 mg, 0.4 mmol) were dissolved in a solution of $CHCl_3$/MeOH (1/1, v/v). The mixture was stirred during one night at room temperature. After solvent evaporation, the product was dissolved in DCM and washed with distillated water (2x15 mL), then dried over $MgSO_4$. After filtration and evaporation steps, compound **15** was obtained as a purple solid (26.7 mg, > 99 %).
Rf = 0.7 ($CHCl_3$).

^{1}H NMR ($CDCl_3$, 400.13 MHz) δ_{ppm}: 8.87 (d, 2H, J = 4.8Hz, $\mathbf{H}_{\beta\text{-pyrrolic}}$); 8.82 ($s_{el}$, 6H, $\mathbf{H}_{\beta\text{-pyrrolic}}$); 8.21 (d, 6H, J = 7.6 Hz, $\mathbf{H}_{2,6\text{-phenyl}}$); 8.06 (d, 2H, J = 8.3 Hz, $\mathbf{H}_{2,6\text{-aryl}}$); 7.75 (d, 9H, 7.4 Hz, $\mathbf{H}_{3,4,5\text{-phenyl}}$); 7.15 (d, 2H, J = 8.2 Hz, $\mathbf{H}_{3,5\text{-aryl}}$); 4.32 (t, 2H, J = 6.8 Hz, $\mathbf{H}_{O\text{-}CH2}$); 1.84 (m, 2H, $\mathbf{H}_{CH2}$); 1.04 (t, 3H, J = 7.3 Hz, $\mathbf{H}_{CH3}$).

^{13}C NMR ($CDCl_3$, 400.13 MHz) δ_{ppm}: 159.0 (C-4 aryl); 142.2 (Cα pyrrole); 135.6 (C-1 aryl); 134.4 (C-2,6 aryl); 130.9 (Cβ pyrrole); 126.7-127.7 (C phenyl); 120.1 (C*meso*); 112.8 (C-3,5 aryl); 69.8 (O-CH_2); 22.8 (CH_2); 10.9 (CH_3).

MS (MALDI-TOF): m/z = 735.2439 $[M+H]^+$.

UV-Vis ($CHCl_3$) λ_{max} nm (ε, 10^{-3} $L.mol^{-1}.cm^{-1}$): 424 (325), 552 (12), 595 (3).

5-(4-propargyloxyphenyl)-10,15,20-triphenylporphyrin **(16)**

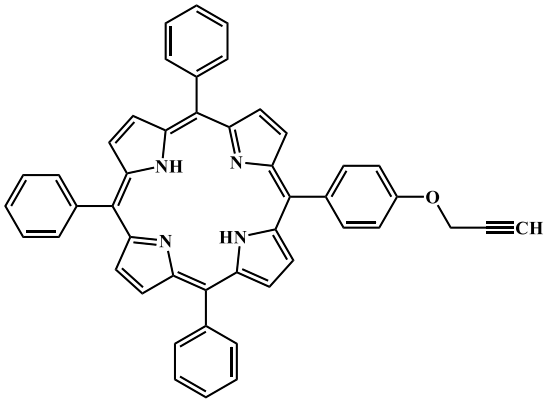

5-(4-hydroxyphenyl)-10,15,20-triphenylporphyrine **13** (1 equiv., 140 mg, 0.22 mmol), propargyl bromide (20 equiv., 0.93 mL, 4.4 mmol), K_2CO_3 (20 equiv., 605 mg, 4.4 mmol) were dissolved in dry DMF (30 mL). The solution was stirred in the dark for 24 h under argon and at room temperature. After solvent removing, the crude product was dissolved in DCM, washed with distillated water (2x25 mL) and dried over $MgSO_4$. After filtration, the solvent was evaporated to dryness. The residue was purified by chromatographic column (stationary phase: silica gel, eluent: $CHCl_3$) to give compound **16** as a purple solid (116 mg, 79 %).
Rf = 0.8 ($CHCl_3$).

^{1}H NMR ($CDCl_3$, 400.13 MHz) δ_{ppm}: 8.87 (d, 2H, J = 4.8Hz, $\mathbf{H}_{\beta pyrrolic}$); 8.83 ($s_{el}$, 6H, $\mathbf{H}_{\beta pyrrolic}$); 8.21 (d, 6H, J = 7.6 Hz, $\mathbf{H}_{2,6\text{-phenyl}}$); 8.04 (d, 2H, J = 8.3 Hz, $\mathbf{H}_{2,6\text{-aryl}}$); 7.75 (d, 9H, 7.4 Hz, $\mathbf{H}_{3,4,5\text{-phenyl}}$); 7.16 (d, 2H, J = 8.2 Hz, $\mathbf{H}_{3,5\text{-aryl}}$); 4.98 (d, 2H, J = 2.3 Hz, $\mathbf{H}_{O\text{-bound}}$); 2.69 (t, 1H, J = 2.3 Hz, $\mathbf{H}_{propargyl}$); -2.74 (s, 2H, $\mathbf{H}_{NHint}$).

^{13}C NMR ($CDCl_3$, 400.13 MHz) δ_{ppm}: 157.4 (C-4 aryl); 137.3 to 139.3 (Cα pyrrole); 135.5 (C-1 aryl); 134.5 (C-2,6 aryl); 131.0-131.1 (Cβ pyrrole); 127.4 to 129.3 (C phenyl); 119.4-120.1 (C*meso*); 113.1 (C-3,5 aryl); 78.7 (C propargyl); 75.8 (CH propargyl); 56.2 (O-CH_2).

MS (MALDI-TOF): m/z = 669.2367 $[M+H]^+$.

UV-Vis ($CHCl_3$) λ_{max} nm (ε, 10^{-3} L.mol^{-1}.cm^{-1}): 419 (337), 518 (13), 556 (6), 598 (3), 647 (1).

IR υ (cm^{-1}), KBr: 2120 (C≡C); 3282 (C-H).

Zinc(II) 5-(4-propargyloxyphenyl)-10,15,20-triphenylporphyrin **(17)**

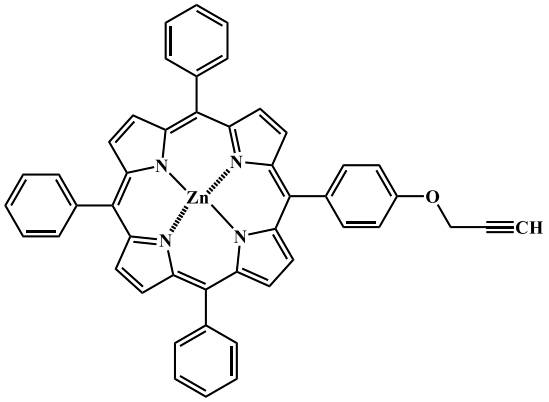

5-(4-propargyloxyphenyl)-10,15,20-triphenylporphyrine **16** (1 equiv., 115.8 mg, 0.17 mmol) and zinc (II) acetate (10 equiv., 311 mg, 1.7 mmol) were dissolved in a solution of $CHCl_3$/MeOH (1/1, v/v). The mixture was stirred during one night at room temperature. After solvent evaporation, the product was dissolved in DCM and washed with distillated water (2x25 mL), then dried over $MgSO_4$. After filtration and evaporation compound **17** was obtained as a purple solid (123.5 mg, > 99 %).
Rf = 0.75 ($CHCl_3$).

^{1}H NMR ($CDCl_3$, 400.13 MHz) δ_{ppm}: 8.88 (d, 2H, J = 4.7Hz, $\mathbf{H}_{\beta pyrrolic}$); 8.84 ($s_{el}$, 6H, $\mathbf{H}_{\beta pyrrolic}$); 8.21 (d, 6H, J = 7.4 Hz, $\mathbf{H}_{2,6\text{-phenyl}}$); 8.14 (d, 2H, J = 8.4 Hz, $\mathbf{H}_{2,6\text{-aryl}}$); 7.75 (d, 9H, 7.4 Hz, $\mathbf{H}_{3,4,5\text{-phenyl}}$); 7.36 (d, 2H, J = 8.5 Hz, $\mathbf{H}_{3,5\text{-aryl}}$); 4.99 (d, 2H, J = 2.4 Hz, $\mathbf{H}_{O\text{-}CH2}$); 2.69 (t, 1H, J = 2.3 Hz, $\mathbf{H}_{propargyl}$).

^{13}C NMR ($CDCl_3$, 400.13 MHz) δ_{ppm}: 157.4 (C-4 aryl); 137.3 to 139.3 (Cα pyrrole); 135.6 (C-1 aryl); 134.5 (C-2,6 aryl); 131.0-132.1 (Cβ pyrrole); 127.4 to 129.3 (C phenyl); 119.4-120.1 (C*meso*); 113.1 (C-3,5 aryl); 78.7 (C propargyl); 75.9 (CH propargyl); 56.2 (O-CH_2).

MS (MALDI-TOF): m/z = 731.1529 $[M+H]^+$.

UV-Vis ($CHCl_3$) λ_{max} nm (ε, 10^{-3} L.mol^{-1}.cm^{-1}): 426 (301), 556 (12), 598 (3.7).

IR υ (cm^{-1}), KBr: 2120 (C≡C); 3282 (C-H).

5-(4-(3-bromopropoxy)phenyl)-10,15,20-triphenylporphyrin **(18)**

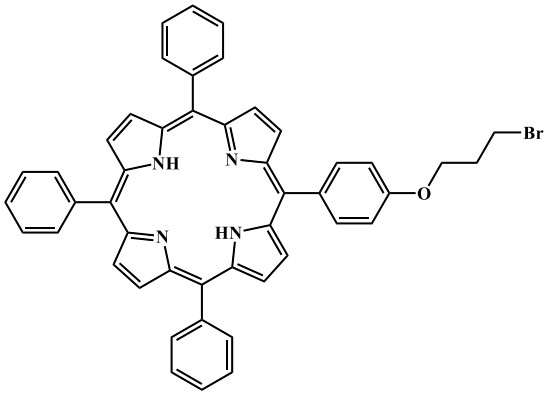

Compound **13** (1 equiv., 200 mg, 0.32 mmol), 1,3-dibromopropane (4 equiv., 128 µL, 1.28 mmol) and K_2CO_3 (4 equiv., 0.87 g, 6.3 mmol) were dissolved in dry DMF (15 mL). The solution was stirring for 48 h in the dark, at room temperature and under argon. After solvent evaporation, the crude product was dissolved in DCM, washed with distillated water (2x25 mL) then dried over $MgSO_4$. After filtration and evaporation, the residue was purified by chromatographic column (stationary phase: silica gel, eluent: petroleum spirit with a DCM gradient ranging from 50 to 100 %) to give compound **18** as a purple solid (213.8 mg, 61 %).
Rf = 0.85 ($CHCl_3$).

^{1}H NMR ($CDCl_3$, 500.15 MHz) δ_{ppm}: 8.87 (d, 2H, J = 4.7Hz, $\mathbf{H}_{\beta\text{-pyrrolic}}$); 8.84 ($s_{el}$, 6H, $\mathbf{H}_{\beta\text{-pyrrolic}}$); 8.21 (d, 6H, J = 7.8 Hz, $\mathbf{H}_{2,6\text{-phenyl}}$); 8.10 (d, 2H, J = 8.3 Hz, $\mathbf{H}_{2,6\text{-aryl}}$); 7.76 (d, 9H, 7.4 Hz, $\mathbf{H}_{3,4,5\text{-phenyl}}$); 7.26 (d, 2H, J = 8.6 Hz, $\mathbf{H}_{3,5\text{-aryl}}$); 4.55 (t, 2H, J = 6.3 Hz, $\mathbf{H}_{O\text{-}CH2}$); 4.35 (t, 2H, J = 6.0 Hz, $\mathbf{H}_{Br\text{-}CH2}$); 2.35 (q, 2H, J = 6.2 Hz, $\mathbf{H}_{CH2}$) ; -2.76 (s, 2H, $\mathbf{H}_{NHint}$).

^{13}C NMR ($CDCl_3$, 500.15 MHz) δ_{ppm}: 158.1 (C-4 aryl); 142.2 (Cα pyrrole); 135.6 (C-1 aryl); 134.4 (C-2,6 aryl); 130.9 (Cβ pyrrole); 126.4-127.5 (C phenyl); 120.1 (C*meso*); 113.0 (C-3,5 aryl); 67.7 (O-CH_2); 32.8 (CH_2-Br); 29.1 (CH_2).

MS (ESI-Q3): m/z = 753.2053 $[M+H]^+$.

UV-Vis ($CHCl_3$) λ_{max} nm (ε, 10^{-3} L.mol^{-1}.cm^{-1}): 420 (310), 517 (11), 552 (6), 593 (3), 648 (4).

5-(4-((4-chlorobut-2-yn-1-yl)oxy)phenyl)-10,15,20-triphenylporphyrin **(19)**

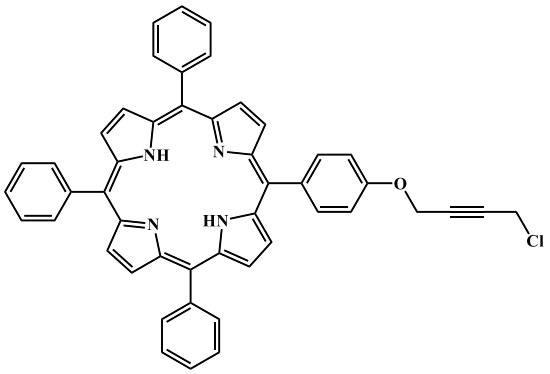

Compound **13** (1 equiv., 161 mg, 0.26 mmol), 1,4-dichloro-2-butyn (10 equiv., 137 µL, 2.57 mmol) and K_2CO_3 (20 equiv., 710 mg, 5.14 mmol) were dissolved in dry DMF (25 mL). The solution was stirring and heating at 70 °C for 48 h in the dark, under argon. After solvent evaporation, the crude product was dissolved in DCM, washed with distillated water (2x25 mL) then dried over $MgSO_4$. After filtration and evaporation steps, the residue was purified by chromatographic column (stationary phase: silica gel, eluent: petroleum spirit with a DCM ranging from 80 to 100 %) to give compound **19** as a purple solid (56.9 mg, 31 %).
Rf = 0.8 ($CHCl_3$/EP 80/20).

^{1}H NMR ($CDCl_3$, 500.15 MHz) δ_{ppm}: 8.87 (d, 2H, J = 4.7Hz, $\mathbf{H}_{\beta\text{-pyrrolic}}$); 8.84 (d, 6H, J = 4.8Hz, $\mathbf{H}_{\beta\text{-pyrrolic}}$); 8.21 (d, 6H, J = 7.7 Hz, $\mathbf{H}_{2,6\text{-phenyl}}$); 8.13 (d, 2H, J = 8.6 Hz, $\mathbf{H}_{2,6\text{-aryl}}$); 7.76 (m, 9H, $\mathbf{H}_{3,4,5\text{-phenyl}}$); 7.33 (d, 2H, J = 8.6 Hz, $\mathbf{H}_{3,5\text{-aryl}}$); 5.02 (t, 2H, J = 1.8 Hz, $\mathbf{H}_{O\text{-}CH2}$); 4.29 (t, 2H, J = 1.8 Hz, $\mathbf{H}_{Cl\text{-}CH2}$); -2.76 (s, 2H, $\mathbf{H}_{NHint}$).

IR υ (cm^{-1}), KBr: 2238 (C≡C).

^{13}C NMR ($CDCl_3$, 500.15 MHz) δ_{ppm}: 157.4 (C-4 aryl); 142.2 (Cα pyrrole); 135.6 (C-1 aryl); 134.6 (C-2,6 aryl); 130.9 (Cβ pyrrole); 126.9- 127.7 (C phenyl); 119.7-120.1 (C*meso*); 113.1 (C-3,5 aryl); 82.4 (C alkyne); 81.4 (C alkyne); 56.3 (O-CH_2); 30.3 (CH_2-Cl)

MS (MALDI-TOF): m/z = 717.3211 $[M+H]^+$.

UV-Vis ($CHCl_3$) λ_{max} nm (ε, 10^{-3} $L.mol^{-1}.cm^{-1}$): 419 (165), 516 (6), 552 (4), 591 (2.5), 647 (2).

Methyl 2-(6-hydroxy-3-oxo-3H-xanthen-9-yl)benzoate **(20)**

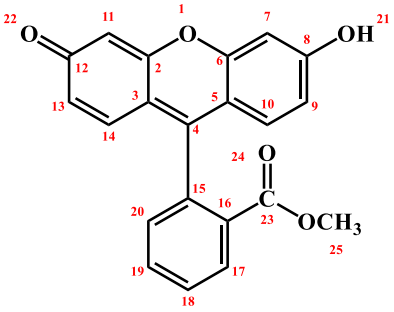

Fluorescein (1 equiv., 2.76 g, 8.3 mmol) was dissolved in freshly distillated MeOH (200 mL). Fuming sulfuric acid (1 mL) was added dropwise, then the mixture was stirring in the dark for 18 h. The reaction was stopped by addition of cooled water, then the solution was filtered and dried to give compound **20** as an orange solid (2.8 g, 98 %).
Rf = 0.45 ($CHCl_3$/EtOH; 90/10).

Tf: 228°C (*literature* 228-230 °C).

^{1}H NMR ($CDCl_3$, 400.13 MHz) δ_{ppm}: 8.25 (dd, 1H, ^{3}J = 7.8 Hz, ^{4}J = 1.2 Hz, **H**$_{13}$); 7.74 (dt, 1H, ^{3}J = 7.5 Hz, ^{4}J = 1.4 Hz, **H**$_{17}$); 7.66 (dt, 1H, ^{3}J = 7.6 Hz, ^{4}J = 1.4 Hz, **H**$_{19}$); 7.30 (dd, 1H, ^{3}J = 7.5 Hz, ^{4}J = 1 Hz, **H**$_{18}$); 6.96 (d, 1H, J = 2.4 Hz, **H**$_{11}$); 6.89 (d, 1H, J = 8.8 Hz, **H**$_{14}$); 6.85 (d, 1H, J = 9.7 Hz, **H**$_{10}$); 6.74 (dd, 1H, ^{3}J = 8.9 Hz, ^{4}J = 2.4 Hz, **H**$_9$); 6.55 (dd, 1H, ^{3}J = 9.7 Hz, ^{4}J = 1.7 Hz, **H**$_{20}$); 6.47 (d, 1H, J = 1.6 Hz, **H**$_7$); 3.64 (s, 3H, **H**$_{25}$).

^{13}C NMR ($CDCl_3$, 400.13 MHz) δ_{ppm} : 185.7 (C_8 and C_{12}); 165.6 (C_{23}); 159.0 (C_4); 150.0 (C_2 and C_6); 134.6 (C_{15}); 132.7 (C_{10} and C_{14}); 130.6 (C_9); 130.5 (C_{13}); 130.4 (C_{17} and C_{18}); 130.3 (C_{20}); 130.2 (C_{19}); 129.6 (C_{16}); 114.7 (C_3 and C_5); 105.8 (C_7 and C_{11}); 52.4 (C_{25}).

MS (ESI-Q3): m/z = 347.0913 $[M+H]^+$.

UV-Vis ($CHCl_3$) λ_{max} nm (ε, 10^{-3} L.mol^{-1}.cm^{-1}) : 438 (12), 462 (15), 491 (10).

Methyl 2-(3-oxo-6-propoxy-3H-xanthen-9-yl)benzoate **(21)**

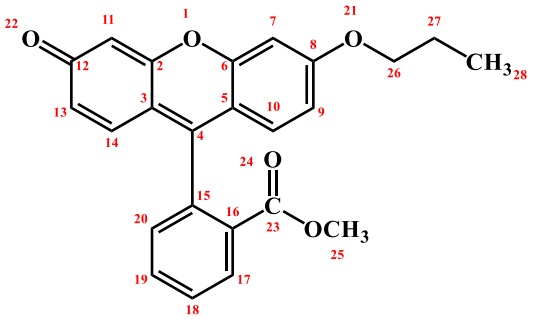

Compound **20** (1 equiv., 173.2 mg, 0.5 mmol), 1-bromopropane (3 equiv., 136.4 µL, 1.5 mmol) and K_2CO_3 (20 equiv., 1.38 g, 10 mmol) were dissolved in dry DMF (20 mL). The solution was stirring for 18 h in the dark, at room temperature and under argon. After solvent evaporation, the residue was dissolved in DCM and washed twice with distillated water (2x25 mL), then dried over $MgSO_4$. After filtration and evaporation steps, the product was purified on column (stationary phase: silica gel, eluent DCM) to give compound **21** as an orange solid (172.8 mg, 89 %).

Rf = 0.7 ($CHCl_3$/EtOH; 90/10).

Tf: 232-234 °C

^{1}H NMR ($CDCl_3$, 400.13 MHz) δ_{ppm}: 8.24 (dd, 1H, ^{3}J = 7.2 Hz, ^{4}J = 1.2 Hz, **H**$_{13}$); 7.73 (dt, 1H, ^{3}J = 7.4 Hz, ^{4}J = 0.9 Hz, **H**$_{17}$); 7.66 (dt, 1H, ^{3}J = 7.6 Hz, ^{4}J = 0.9 Hz, **H**$_{19}$); 7.31 (dd, 1H, ^{3}J = 7.2 Hz, ^{4}J = 1 Hz, **H**$_{18}$); 6.94 (d, 1H, J = 2.3 Hz, **H**$_{11}$); 6.87 (d, 1H, J = 8.9 Hz, **H**$_{14}$); 6.84 (d, 1H, J = 9.7 Hz, **H**$_{10}$); 6.73 (dd, 1H, ^{3}J = 8.9 Hz, ^{4}J = 2.3 Hz, **H**$_9$); 6.54 (dd, 1H, ^{3}J = 9.7 Hz, ^{4}J = 1.8 Hz, **H**$_{20}$); 6.45 (d, 1H, J = 1.8 Hz, **H**$_7$); 4.02 (t, 2H, J = 6.5 Hz, **H**$_{26}$); 3.63 (s, 3H, **H**$_{25}$); 1.86 (m, 2H, **H**$_{27}$); 1.06 (t, 3H, J = 7.4 Hz, **H**$_{28}$).

^{13}C NMR ($CDCl_3$, 400.13 MHz) δ_{ppm}: 185.7 (C_8 and C_{12}); 165.6 (C_{23}); 159.0 (C_4); 150.1 (C_2 and C_6); 134.7 (C_{15}); 132.7 (C_{10} and C_{14}); 130.6 (C_9); 130.5 (C_{13}); 130.4 (C_{17} and C_{18}); 130.3 (C_{20}); 130.2 (C_{19}); 129.9 (C_{16}); 114.7 (C_3 and C_5); 105.8 (C_7 and C_{11}); 70.4 (C_{26}); 52.4 (C_{25}); 22.3 (C_{27}); 10.4 (C_{28}).

MS (ESI-Q3): m/z = 389.1381 $[M+H]^+$.

UV-Vis ($CHCl_3$) λ_{max} nm (ε, 10^{-3} L.mol^{-1}.cm^{-1}): 439 (14), 463 (17.7), 492 (11.5).

Methyl 2-(6-(3-bromopropoxy)-3-oxo-3H-xanthen-9-yl)benzoate **(22)**

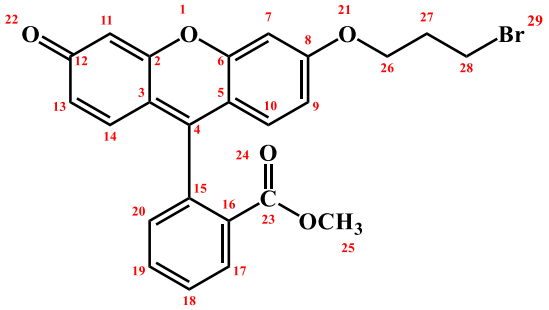

Methyl 2-(6-hydroxy-3-oxo-3H-xanthen-9-yl)benzoate **20** (1 equiv., 330 mg, 0.95 mmol), 1,3-dibromopropane (3 equiv., 290 µL, 2.85 mmol) and K_2CO_3 (10 equiv., 1.3 g, 9.5 mmol) were dissolved in dry DMF (25 mL). The solution was stirring at room temperature, in the dark and under argon for 20 h. After solvent evaporation, the residue was dissolved in $CHCl_3$ and washed with distillated water (3x25 mL) then dried over $MgSO_4$. After filtration and evaporation steps, the crude product was purified by column (stationary phase: silica gel, eluent $CHCl_3$) to give compound **22** as an orange oil (285.7 mg, 64 %).
Rf = 0.5 ($CHCl_3$/EtOH; 90/10).

^{1}H NMR ($CDCl_3$, 400.13 MHz) δ_{ppm}: 8.25 (dd, 1H, ^3J = 7.8 Hz, ^4J = 1.2 Hz, $\mathbf{H}_{13}$); 7.74 (dt, 1H, ^3J = 7.5 Hz, ^4J = 1.4 Hz, $\mathbf{H}_{17}$); 7.66 (dt, 1H, ^3J = 7.6 Hz, ^4J = 1.4 Hz, $\mathbf{H}_{19}$); 7.30 (dd, 1H, ^3J = 7.5 Hz, ^4J = 1 Hz, $\mathbf{H}_{18}$); 6.96 (d, 1H, J = 2.4 Hz, $\mathbf{H}_{11}$); 6.89 (d, 1H, J = 8.8 Hz, $\mathbf{H}_{14}$); 6.85 (d, 1H, J = 9.7 Hz, $\mathbf{H}_{10}$); 6.74 (dd, 1H, ^3J = 8.9 Hz, ^4J = 2.4 Hz, $\mathbf{H}_9$); 6.55 (dd, 1H, ^3J = 9.7 Hz, ^4J = 1.7 Hz, $\mathbf{H}_{20}$); 6.47 (d, 1H, J = 1.6 Hz, $\mathbf{H}_7$); 4.24 (t, 2H, J = 5.8 Hz, $\mathbf{H}_{26}$); 3.64 (s, 3H, $\mathbf{H}_{25}$); 3.60 (t, 2H, J = 6.3 Hz, $\mathbf{H}_{28}$); 2.37 (quint, 2H, J = 6.1 Hz, $\mathbf{H}_{27}$).

^{13}C NMR ($CDCl_3$, 400.13 MHz) δ_{ppm}: 185.7 (C_8 and C_{12}); 165.6 (C_{23}); 159.0 (C_4); 150.4 (C_2 and C_6); 134.7 (C_{15}); 132.7 (C_{10} and C_{14}); 130.6 (C_9); 130.5 (C_{13}); 130.4 (C_{17} and C_{18}); 130.2 (C_{20}); 130.1 (C_{19}); 129.6 (C_{16}); 114.8 (C_3 and C_5); 105.8 (C_7 and C_{11}); 70.4 (C_{26}); 52.4 (C_{25}); 33.9 (C_{28}); 27.3 (C_{27}).

MS (ESI-Q3): m/z = 467.0918 $[M+H]^+$.

UV-Vis ($CHCl_3$) λ_{max} nm (ε, 10^{-3} L.mol^{-1}.cm^{-1}): 438 (12), 461 (16), 491 (10).

Methyl 2-(6-(3-azidopropoxy)-3-oxo-3H-xanthen-9-yl)benzoate **(23)**

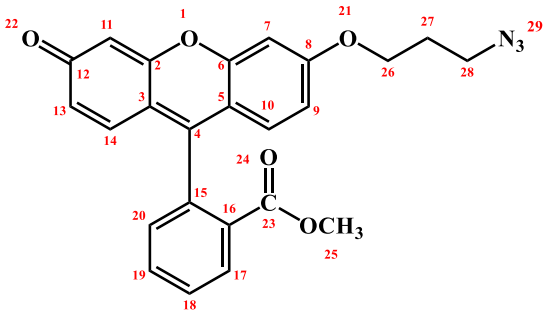

Methyl 2-(6-(3-bromopropoxy)-3-oxo-3H-xanthen-9-yl)benzoate **22** (1 equiv., 286 mg, 0.61 mmol) and sodium azide (4 equiv., 158.6 mg, 2.44 mmol) were dissolved in dry DMF (15 mL). The solution was stirring in the dark for 24 h, at room temperature and under argon. After solvent evaporation, the crude product was dissolved in DCM and washed twice with distillated water (2x25 mL), then dried over $MgSO_4$. After filtration, solvent was evaporated to dryness and compound **23** was obtained as an orange oil (261.8 mg, > 99 %).
Rf = 0.8 ($CHCl_3$/EtOH; 90/10).

^{1}H NMR ($CDCl_3$, 400.13 MHz) δ_{ppm}: 8.24 (dd, 1H, ^{3}J = 7.6 Hz, ^{4}J = 1.2 Hz, **H**$_{13}$); 7.74 (dt, 1H, ^{3}J = 7.5 Hz, ^{4}J = 1.4 Hz, **H**$_{17}$); 7.67 (dt, 1H, ^{3}J = 7.6 Hz, ^{4}J = 1.4 Hz, **H**$_{19}$); 7.30 (dd, 1H, ^{3}J = 7.5 Hz, ^{4}J = 1 Hz, **H**$_{18}$); 6.96 (d, 1H, J = 2.4 Hz, **H**$_{11}$); 6.90 (d, 1H, J = 8.9 Hz, **H**$_{14}$); 6.85 (d, 1H, J = 9.7 Hz, **H**$_{10}$); 6.74 (dd, 1H, ^{3}J = 8.9 Hz, ^{4}J = 2.4 Hz, **H**$_9$); 6.55 (dd, 1H, ^{3}J = 9.7 Hz, ^{4}J = 1.5 Hz, **H**$_{20}$); 6.47 (d, 1H, J = 1.6 Hz, **H**$_7$); 4.17 (t, 2H, J = 5.7 Hz, **H**$_{26}$); 3.63 (s, 3H, **H**$_{25}$); 3.53 (t, 2H, J = 6.5 Hz, **H**$_{28}$); 2.10 (quint, 2H, J = 6.4 Hz, **H**$_{27}$).

^{13}C NMR ($CDCl_3$, 400.13 MHz) δ_{ppm}: 185.8 (C_8 and C_{12}); 165.6 (C_{23}); 159.1 (C_4); 150.5 (C_2 and C_6); 134.6 (C_{15}); 132.7 (C_{10} and C_{14}); 130.6 (C_9); 130.3 (C_{13}); 130.2 (C_{17} and C_{18}); 130.0 (C_{20}); 129.9 (C_{19}); 129.7 (C_{16}); 115.0 (C_3 and C_5); 105.8 (C_7 and C_{11}); 65.4 (C_{26}); 52.4 (C_{25}); 48.0 (C_{28}); 28.6 (C_{27}).

UV-Vis ($CHCl_3$) λ_{max} nm (ε, 10^{-3} L.mol^{-1}.cm^{-1}): 439 (11), 463 (15), 492 (9).

IR υ (cm^{-1}), KBr: 2099 (N_3).

Zn(II) Triazole dyad **(24)**

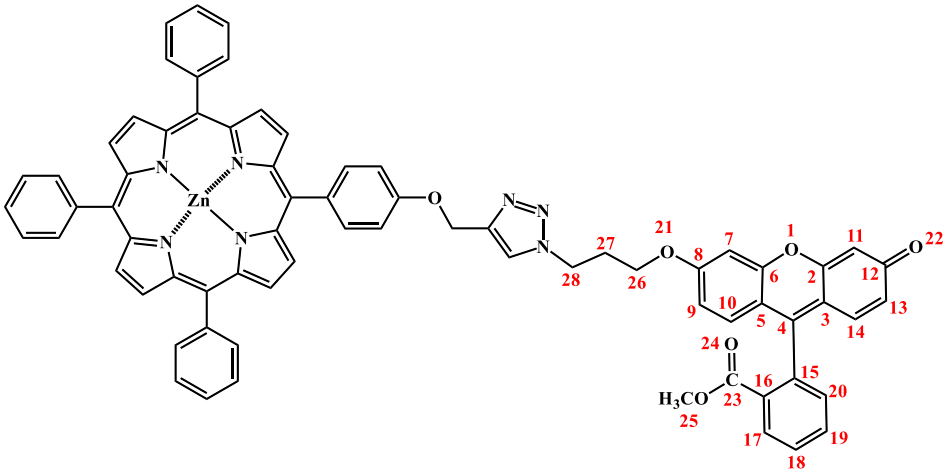

Compound **17** (1 equiv., 276.7 mg, 0.38 mmol) and compound **23** (1.5 equiv., 250.8 mg, 0.57 mmol) were dissolved in THF (45 mL). Copper (II) acetate (2.7 equiv., 187 mg, 1.03 mmol) and sodium ascorbate (7 equiv., 527 mg, 2.66 mmol) in solution in distillated water (4 mL) were added. The mixture was stirring for 24 h, in the dark and at room temperature. After solvent evaporation, the crude product was dissolved in DCM and washed with distillated water (2x25 mL), then dried over $MgSO_4$ and filtered. Finally the dry residue was purified by chromatographic column (solid phase: silica gel, eluent: DCM with an EtOH gradient ranging from 0 to 10%) to give compound **24** as a red-orange solid (403.5 mg, 91 %).
Rf = 0.6 ($CHCl_3$/EtOH; 9/1).

^{1}H NMR ($CDCl_3$, 400.13 MHz)
Porphyrin moiety: δ_{ppm}: 8.98 (d, 2H, J = 4.7Hz, $\mathbf{H}_{\beta\text{-pyrrolic}}$); 8.94 ($s_{el}$, 6H, $\mathbf{H}_{\beta\text{-pyrrolic}}$); 8.14 (d, 6H, J = 7.7 Hz, $\mathbf{H}_{2,6\text{-phenyl}}$); 8.03 (d, 2H, J = 8.3 Hz, $\mathbf{H}_{2,6\text{-aryl}}$); 7.73 (m, 9H, $\mathbf{H}_{3,4,5\text{-phenyl}}$); 7.36 (d, 2H, J = 8.5 Hz, $\mathbf{H}_{3,5\text{-aryl}}$); 5.53 (d, 2H, J = 2.4 Hz, $\mathbf{H}_{O\text{-}CH2}$).

Fluorescein moiety: δ_{ppm}: 8.24 (dd, 1H, ^{3}J = 7.5 Hz, ^{4}J = 1.2 Hz, $\mathbf{H}_{13}$); 7.74 (dt, 1H, ^{3}J = 7.5 Hz, ^{4}J = 1.3 Hz, $\mathbf{H}_{17}$); 7.67 (dt, 1H, ^{3}J = 7.6 Hz, ^{4}J = 1.4 Hz, $\mathbf{H}_{19}$); 7.30 (dd, 1H, ^{3}J = 7.5 Hz, ^{4}J = 1 Hz, $\mathbf{H}_{18}$); 6.95 (d, 1H, J = 2.4 Hz, $\mathbf{H}_{11}$); 6.90 (d, 1H, J = 8.9 Hz, $\mathbf{H}_{14}$); 6.80 (d, 1H, J = 8.9 Hz, $\mathbf{H}_{10}$); 6.73 (dd, 1H, ^{3}J = 8.9 Hz, ^{4}J = 2.4 Hz, $\mathbf{H}_9$); 6.61 (dd, 1H, ^{3}J = 8.8 Hz, ^{4}J = 2.1 Hz, $\mathbf{H}_{20}$); 6.42 (d, 1H, J = 1.6 Hz, $\mathbf{H}_7$); 4.14 (t, 2H, J = 5.9 Hz, $\mathbf{H}_{26}$); 3.63 (s, 3H, $\mathbf{H}_{25}$); 3.54 (s_{el}, 2H, $\mathbf{H}_{28}$); 2.10 (m, 2H, $\mathbf{H}_{27}$).

Triazole moiety: δ_{ppm}: 8.07 (s, 1H, $\mathbf{H}_{triazole}$).

^{13}C NMR ($CDCl_3$, 400.13 MHz)

Porphyrin moiety: δ_{ppm}: 157.4 (C-4 aryl); 143.5 (Cα pyrrole); 135.8 (C-1 aryl); 134.4-134.8 (C-2,6 aryl); 131.0 (Cβ pyrrole); 127.3-128.9-129.6 (C phenyl); 120.1 (C*meso*); 113.5 (C-3,5 aryl); 76.6 ($O-CH_2$).

Fluorescein moiety: δ_{ppm}: 184.6 (C_8 and C_{12}); 165.6 (C_{23}); 158.3 (C_4); 150.1 (C_2 or C_6); 134.8 (C_{15}); 132.7 (C_{10} or C_{14}); 130.6 (C_9); 130.4 (C_{13}); 130.2 (C_{17} or C_{18}); 129.8 (C_{20}); 129.6 (C_{19}); 128.9 (C_{16}); 115.0 (C_3 or C_5); 105.0 (C_7 or C_{11}); 100.7 (C_7 or C_{11}); 65.4 (C_{26}); 52.4 (C_{25}); 47.9 (C_{28}); 22.6 (C_{27}).

Triazole moiety: δ_{ppm}: 143.3; 129.1.

Undifferentiated signals*: δ_{ppm}: 150.4; 150.2; 150.0; 132.6; 131.8; 131.7; 131.6; 131.5; 130.1; 127.2; 126.5; 126.4; 126.3; 121.9; 120.9; 120.8; 112.8; 112.7.

MS (ESI-Q3): m/z = 1160.3102 $[M+H]^+$.

UV-Vis ($CHCl_3$) λ_{max} nm (ε, 10^{-3} $L.mol^{-1}.cm^{-1}$): 427 (310), 463 (19), 492 (14), 556 (12), 598 (4.5).

IR υ (cm^{-1}), KBr: 2102 (C-N).

Methyl 2-(3-oxo-6-(3-(4-(10,15,20-triphenylporphyrin-5-yl)phenoxy)propoxy)-3H-xanthen-9-yl)benzoate **(25)**

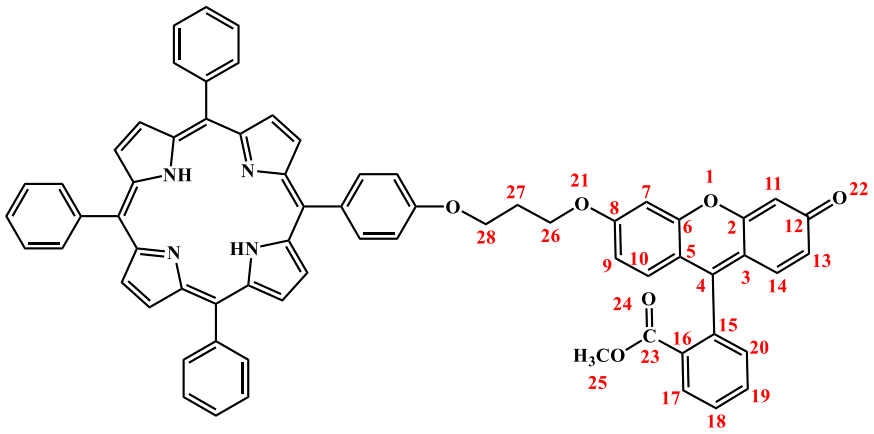

Compound **18** (1 equiv., 201 mg, 0.27 mmol), compound **20** (1 equiv., 92.5 mg, 0.27 mmol) and K_2CO_3 (20 equiv., 738 mg, 5.34 mmol) were dissolved in dry DMF (20 mL). The solution was stirring for 72 h in the dark, at room temperature and under argon. After solvent evaporation, the crude product was dissolved in DCM, washed with distillated water (3x25 mL) then dried over $MgSO_4$. After filtration and evaporation steps, the residue was purified on preparative plates (solid phase: silica gel, eluent: DCM/EtOH 9/1) to give compound **25** as a red-orange solid (55.5 mg, 20 %).

Rf = 0.7 ($CHCl_3$).

^{1}H NMR ($CDCl_3$, 500.15 MHz)

Porphyrin moiety : δ_{ppm}: 8.85 (d, 2H, J = 4.7Hz, $\mathbf{H}_{\beta\text{-pyrrolic}}$); 8.82 (d, 6H, J = 6.4Hz, $\mathbf{H}_{\beta\text{-pyrrolic}}$); 8.21 (d, 6H, J = 7.5 Hz, $\mathbf{H}_{2,6\text{-phenyl}}$); 8.11 (d, 2H, J = 8.5 Hz, $\mathbf{H}_{2,6\text{-aryl}}$); 7.74 (m, 9H, $\mathbf{H}_{3,4,5\text{-phenyl}}$); 7.27 (d, 2H, J = 8.6 Hz, $\mathbf{H}_{3,5\text{-aryl}}$); 4.10 (t, 4H, J = 6.2 Hz, $\mathbf{H}_{26\text{-}28}$) ; 2.49 (q, J = 6.1 Hz, $\mathbf{H}_{27}$); -2.76 (s, 2H, $\mathbf{H}_{NHint}$).

Fluorescein moiety : δ_{ppm}: 8.24 (dd, 1H, ^{3}J = 7.9 Hz, ^{4}J = 1.1 Hz, $\mathbf{H}_{13}$); 7.74 (dt, 1H, ^{3}J = 7.5 Hz, ^{4}J = 1.4 Hz, $\mathbf{H}_{17}$); 7.66 (dt, 1H, ^{3}J = 7.8 Hz, ^{4}J = 1.1 Hz, $\mathbf{H}_{19}$); 7.31 (dd, 1H, ^{3}J = 7.6 Hz, ^{4}J = 1.0 Hz, $\mathbf{H}_{18}$); 7.08 (d, 1H, J = 2.4 Hz, $\mathbf{H}_{11}$); 6.92 (d, 1H, J = 8.9 Hz, $\mathbf{H}_{14}$); 6.85 (d, 1H, J = 9.7 Hz, $\mathbf{H}_{10}$); 6.82 (dd, 1H, J = 2.4 Hz, $\mathbf{H}_{9}$); 6.54 (dd, 1H, ^{3}J = 9.7 Hz, ^{4}J = 1.9 Hz, $\mathbf{H}_{20}$); 6.48 (d, 1H, J = 1.9 Hz, $\mathbf{H}_{7}$); 3.64 (s, 3H, $\mathbf{H}_{25}$).

^{13}C NMR ($CDCl_3$, 500.15 MHz)

Porphyrin moiety: δ_{ppm}: 158.5 (C-4 aryl); 142.2 (Cα pyrrole); 135.6 (C-1 aryl); 134.5 (C-2,6 aryl); 130.9-131.1 (Cβ pyrrole); 126.7-127.7 (C phenyl); 119.8-120.1 (C*meso*); 113.7 (C-3,5 aryl); 65.5 ($O-CH_2$); 64.3 ($O-CH_2$); 29.7 (CH_2).

Fluorescein moiety: δ_{ppm}: 185.7 (C_8 and C_{12}); 165.6 (C_{23}); 158.9 (C_4); 149.9 (C_2 and C_6); 134.7 (C_{15}); 132.7 (C_{10} and C_{14}); 130.6 (C_9 and $_{13}$); 130.4 (C_{17} or $_{18}$); 130.2 (C_{19} or C_{20}); 129.6 (C_{16}); 112.7 (C_3 or C_5); 105.9 (C_7 or C_{11}); 52.4 (C_{25}).

Undifferentiated signals*: δ_{ppm}: 120.09; 120.02; 115.0.

MS (ESI-Q3): m/z = 1017.3702 $[M+H]^+$.

UV-Vis ($CHCl_3$) λ_{max} nm (ε, 10^{-3} $L.mol^{-1}.cm^{-1}$): 419 (310), 462 (18), 490 (13), 515 (14), 552 (5.7), 591 (3.6), 647 (2.9).

Zn(II) Methyl 2-(3-oxo-6-(3-(4-(10,15,20-triphenylporphyrin-5-yl)phenoxy)propoxy)-3H-xanthen-9-yl)benzoate **(26)**

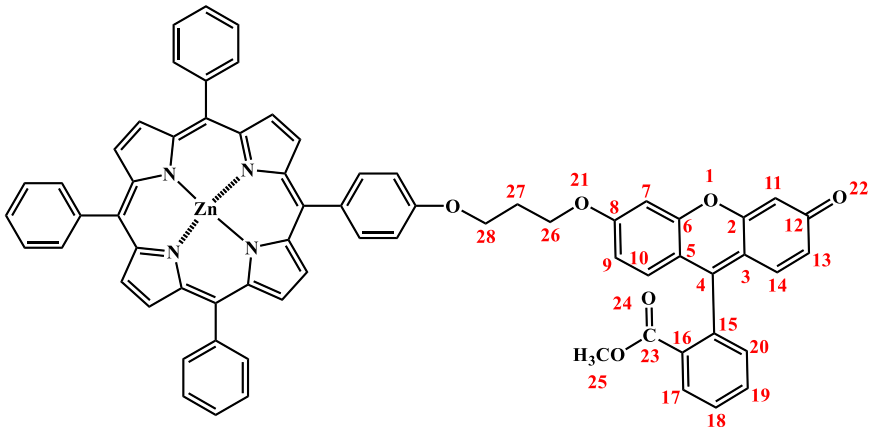

Compound **25** (1 equiv., 55.5 mg, 0.055 mmol) and zinc (II) acetate (10 equiv., 121 mg, 0.55 mmol) were dissolved in a solution of $CHCl_3$/MeOH (1/1, v/v). The mixture was stirred during one night at room temperature. After solvent evaporation, the product was dissolved in DCM and washed with distillated water (2x20 mL), then dried over $MgSO_4$. After filtration, the solvent was evaporated to dryness and compound **26** was obtained as a red-orange solid (59.2 mg, > 99 %).

Rf = 0.7 ($CHCl_3$).

^{1}H NMR ($CDCl_3$, 500.15 MHz)

Porphyrin moiety: δ_{ppm}: 8.85 (d, 2H, J = 4.7Hz, $\mathbf{H}_{\beta\text{-pyrrolic}}$); 8.82 (d, 6H, J = 6.4Hz, $\mathbf{H}_{\beta\text{-pyrrolic}}$); 8.21 (d, 6H, J = 7.5 Hz, $\mathbf{H}_{2,6\text{-phenyl}}$); 8.11 (d, 2H, J = 8.5 Hz, $\mathbf{H}_{2,6\text{-aryl}}$); 7.74 (m, 9H, $\mathbf{H}_{3,4,5\text{-phenyl}}$); 7.27 (d, 2H, J = 8.6 Hz, $\mathbf{H}_{3,5\text{-aryl}}$); 4.10 (t, 4H, J = 6.2 Hz, $\mathbf{H}_{26\text{-}28}$) ; 2.49 (q, J = 6.1 Hz, $\mathbf{H}_{27}$).

Fluorescein moiety: δ_{ppm}: 8.24 (dd, 1H, ^{3}J = 7.9 Hz, ^{4}J = 1.1 Hz, $\mathbf{H}_{13}$); 7.74 (dt, 1H, ^{3}J = 7.5 Hz, ^{4}J = 1.4 Hz, $\mathbf{H}_{17}$); 7.66 (dt, 1H, ^{3}J = 7.8 Hz, ^{4}J = 1.1 Hz, $\mathbf{H}_{19}$); 7.31 (dd, 1H, ^{3}J = 7.6 Hz, ^{4}J = 1.0 Hz, $\mathbf{H}_{18}$); 7.08 (d, 1H, J = 2.4 Hz, $\mathbf{H}_{11}$); 6.92 (d, 1H, J = 8.9 Hz, $\mathbf{H}_{14}$); 6.85 (d, 1H, J = 9.7 Hz, $\mathbf{H}_{10}$); 6.82 (dd, 1H, J = 2.4 Hz, $\mathbf{H}_{9}$); 6.54 (dd, 1H, ^{3}J = 9.7 Hz, ^{4}J = 1.9 Hz, $\mathbf{H}_{20}$); 6.48 (d, 1H, J = 1.9 Hz, $\mathbf{H}_{7}$); 3.64 (s, 3H, $\mathbf{H}_{25}$).

^{13}C NMR ($CDCl_3$, 500.15 MHz)

Porphyrin moiety: δ_{ppm}: 158.5 (C-4 aryl); 142.2 (Cα pyrrole); 135.6 (C-1 aryl); 134.5 (C-2,6 aryl); 130.9-131.1 (Cβ pyrrole); 126.7-127.7 (C phenyl); 119.8-120.1 (C*meso*); 113.7 (C-3,5 aryl); 65.5 (O-CH_2); 64.3 (O-CH_2); 29.7 (CH_2)..

Fluorescein moiety: δ_{ppm}: 185.7 (C_8 and C_{12}); 165.6 (C_{23}); 158.9 (C_4); 149.9 (C_2 and C_6); 134.7 (C_{15}); 132.7 (C_{10} and C_{14}); 130.6 (C_9 and $_{13}$); 130.4 (C_{17} or $_{18}$); 130.2 (C_{19} or C_{20}); 129.6 (C_{16}); 112.7 (C_3 or C_5); 105.9 (C_7 or C_{11}); 52.4 (C_{25}).

Undifferentiated signals*: δ_{ppm} : 120.3; 120.2; 115.6; 114.3.

MS (ESI-Q3): m/z = 1017.2247 $[M+H]^+$.

UV-Vis ($CHCl_3$) λ_{max} nm (ε, 10^{-3} $L.mol^{-1}.cm^{-1}$): 424 (281), 461 (14.7), 492 (10.6), 553 (11), 596 (3.3).

Methyl 2-(3-oxo-6-((4-(4-(10,15,20-triphenylporphyrin-5-yl)phenoxy)but-2-yn-1-yl)oxy)-3H-xanthen-9-yl)benzoate **(27)**

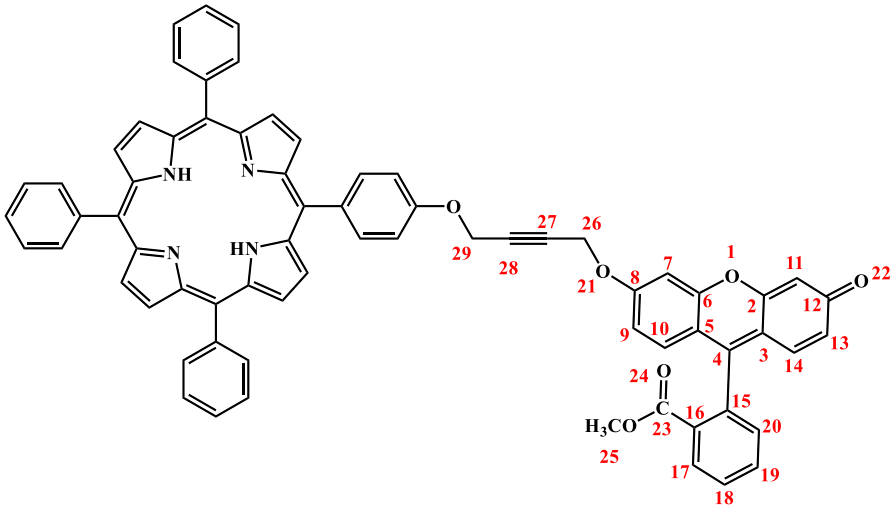

Compound **19** (1 equiv., 88 mg, 0.12 mmol), compound **20** (4 equiv., 170 mg, 0.49 mmol) and K_2CO_3 (20 equiv., 337 mg, 2.44 mmol) were dissolved in dry DMF (10 mL). The solution was stirring for 72 h in the dark, at room temperature and under argon. After solvent evaporation, the crude product was dissolved in DCM, washed with distillated water (2x25 mL) then dried over $MgSO_4$. After filtration and evaporation, the residue was purified on preparative plates (solid phase: silica gel, eluent: DCM/EtOH 95/5) to give compound **27** as a red-orange solid (37.4 mg, 30 %).

Rf = 0.8 ($CHCl_3$).

^{1}H NMR ($CDCl_3$, 500.15 MHz)

Porphyrin moiety: δ_{ppm}: 8.84 (d, 2H, J = 4.8Hz, $\mathbf{H}_{\beta\text{-pyrrolic}}$); 8.82 (d, 6H, J = 4.1Hz, $\mathbf{H}_{\beta\text{-pyrrolic}}$); 8.20 (d, 6H, J = 7.1 Hz, $\mathbf{H}_{2,6\text{-phenyl}}$); 8.05 (d, 2H, J = 8.5 Hz, $\mathbf{H}_{2,6\text{-aryl}}$); 7.76 (m, 9H, $\mathbf{H}_{3,4,5\text{-phenyl}}$); 7.29 (d, 2H, J = 8.5 Hz, $\mathbf{H}_{3,5\text{-aryl}}$); 5.02 ($s_{el}$, 2H, $\mathbf{H}_{26\text{-}29}$); 4.95 ($s_{el}$, 2H , $\mathbf{H}_{26\text{-}29}$); -2.75 (s, 2H, $\mathbf{H}_{NHint}$).

Fluorescein moiety: δ_{ppm}: 8.22 (m, 1H, $\mathbf{H}_{13}$); 7.77 (dt, 1H, ^{3}J = 7.5 Hz, ^{4}J = 1.4 Hz, $\mathbf{H}_{17}$); 7.71 (dt, 1H, ^{3}J = 7.6 Hz, ^{4}J = 1.3 Hz, $\mathbf{H}_{19}$); 7.30 (dd, 1H, ^{3}J = 7.6 Hz, ^{4}J = 0.9 Hz, $\mathbf{H}_{18}$); 7.10 (d, 1H, J = 2.7 Hz, $\mathbf{H}_{11}$); 6.93 (d, 1H, J = 8.6 Hz, $\mathbf{H}_{14}$); 6.91 (d, 1H, J = 9.7 Hz, $\mathbf{H}_{10}$); 6.84 (dd, 1H, ^{3}J = 8.9 Hz, ^{4}J = 2.4 Hz, $\mathbf{H}_{9}$); 6.55 (dd, 1H, ^{3}J = 9.7 Hz, ^{4}J = 1.9 Hz, $\mathbf{H}_{20}$); 6.48 (d, 1H, J = 2.0 Hz, $\mathbf{H}_{7}$); 3.52 (s, 3H, $\mathbf{H}_{25}$).

^{13}C NMR ($CDCl_3$, 500.15 MHz)

Porphyrin moiety: δ_{ppm}: 158.8 (C-4 aryl); 142.2 (Cα pyrrole); 135.6 (C-1 aryl); 134.6 (C-2,6 aryl); 131.1 (Cβ pyrrole); 126.7- 127.7 (C phenyl); 119.5-120.1 (C*meso*); 113.7 (C-3,5 aryl); 83.7 (C alkyne); 81.3 (C alkyne); 56.6 (O-CH_2); 56.2 (O-CH_2)

Fluorescein moiety: δ_{ppm}: 185.7 (C_8 and C_{12}); 165.4 (C_{23}); 157.3 (C_4); 149.6 (C_2 and C_6); 134.7 (C_{15}); 132.7 (C_{10} or $_{14}$); 130.6 (C_9); 130.5 (C_{13}); 130.4 (C_{17} or C_{18}); 130.2 (C_{19} or C_{20}); 129.6 (C_{16}); 115.5 (C_3 or C_5); 105.9 (C_7 or C_{11}); 101.9 (C_7 or C_{11}); 52.3 (C_{25}).

Undifferentiated signals*: δ_{ppm}: 132.2; 131.2; 131.1; 131.0; 130.0; 129.2; 129.0; 127.7; 126.7; 120.1; 113.3; 113.2.

MS (ESI-Q3): m/z = 1027.3490 $[M+H]^+$.

UV-Vis ($CHCl_3$) λ_{max} nm (ε, 10^{-3} $L.mol^{-1}.cm^{-1}$): 419 (330), 461 (16.6), 490 (12), 515 (14), 551 (5), 591 (3), 647 (2.5).

Zn(II) Methyl 2-(3-oxo-6-((4-(4-(10,15,20-triphenylporphyrin-5-yl)phenoxy)but-2-yn-1-yl)oxy)-3H-xanthen-9-yl)benzoate **(28)**

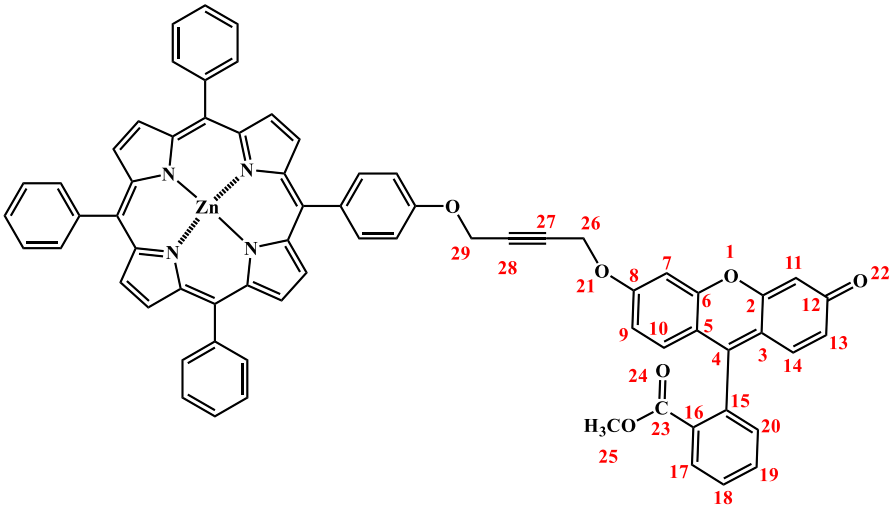

Compound **27** (1 equiv., 37.4 mg, 0.036 mmol) and zinc (II) acetate (10 equiv., 80 mg, 0.36 mmol) were dissolved in a solution of $CHCl_3$/MeOH (1/1, v/v). The mixture was stirred during one night at room temperature. After solvent evaporation, the product was dissolved in DCM and washed with distillated water (2x20 mL), then dried over $MgSO_4$. After filtration and evaporation steps, compound **28** was obtained as a red-orange solid (39.2 mg, > 99 %).
Rf = 0.8 ($CHCl_3$).

^{1}H NMR ($CDCl_3$, 500.15 MHz)
Porphyrin moiety: δ_{ppm}: 8.84 (d, 2H, J = 4.8Hz, $\mathbf{H}_{\beta\text{-pyrrolic}}$); 8.82 (d, 6H, J = 4.1Hz, $\mathbf{H}_{\beta\text{-pyrrolic}}$); 8.20 (d, 6H, J = 7.1 Hz, $\mathbf{H}_{2,6\text{-phenyl}}$); 8.05 (d, 2H, J = 8.6 Hz, $\mathbf{H}_{2,6\text{-aryl}}$); 7.76 (m, 9H, $\mathbf{H}_{3,4,5\text{-phenyl}}$); 7.28 (d, 2H, J = 8.6 Hz, $\mathbf{H}_{3,5\text{-aryl}}$); 5.02 (t, 2H, J = 1.5 Hz, $\mathbf{H}_{26\text{-}29}$); 4.94 (t, 2H, J = 1.5 Hz, $\mathbf{H}_{26\text{-}29}$).

Fluorescein moiety: δ_{ppm}: 8.22 (dd, 1H, ^{3}J = 7.9 Hz, ^{4}J = 1.1 Hz) (1H) $\mathbf{H}_{13}$); 7.77 (dt, 1H, ^{3}J = 7.5 Hz, ^{4}J = 1.4 Hz, $\mathbf{H}_{17}$); 7.71 (dt, 1H, ^{3}J = 7.6 Hz, ^{4}J = 1.3 Hz, $\mathbf{H}_{19}$); 7.30 (dd, 1H, ^{3}J = 7.6 Hz, ^{4}J = 0.9 Hz, $\mathbf{H}_{18}$); 7.10 (d, 1H, J = 2.7 Hz, $\mathbf{H}_{11}$); 6.93 (d, 1H, J = 8.6 Hz, $\mathbf{H}_{14}$); 6.91 (d, 1H, J = 9.7 Hz, $\mathbf{H}_{10}$); 6.84 (dd, 1H, ^{3}J = 7.6 Hz, ^{4}J = 2.4 Hz, $\mathbf{H}_9$); 6.55 (dd, 1H, ^{3}J = 9.7 Hz, ^{4}J = 1.9 Hz, $\mathbf{H}_{20}$); 6.48 (d, 1H, J = 2.0 Hz, $\mathbf{H}_7$); 3.52 (s, 3H, $\mathbf{H}_{25}$).

^{13}C NMR ($CDCl_3$, 500.15 MHz)

Porphyrin moiety: δ_{ppm}: 158.8 (C-4 aryl); 142.2 (Cα pyrrole); 135.4 (C-1 aryl); 134.5 (C-2,6 aryl); 131.2 (Cβ pyrrole); 126.7- 127.7 (C phenyl); 119.5-120.1 (C*meso*); 113.7 (C-3,5 aryl); 83.7 (C alkyne); 81.3 (C alkyne); 56.6 (O-CH_2); 56.2 (O-CH_2).

Fluorescein moiety: δ_{ppm}: 185.7 (C_8 and C_{12}); 165.4 (C_{23}); 157.3 (C_4); 149.6 (C_2 and C_6); 134.7 (C_{15}); 132.7 (C_{10} or $_{14}$); 130.6 (C_9); 130.5 (C_{13}); 130.4 (C_{17} or C_{18}); 130.2 (C_{19} or C_{20}); 129.2 (C_{16}); 115.5 (C_3 or C_5); 105.9 (C_7 or C_{11}); 101.9 (C_7 or C_{11}); 52.3 (C_{25}).

Undifferentiated signals*: δ_{ppm}: 132.2; 131.2; 131.1; 131; 130.9; 130.8; 130.7; 130.6; 130.0; 129.0; 127.7; 126.7; 120.1; 113.3; 113.2.

MS (ESI-Q3): m/z = 1089.3128 $[M+H]^+$.

UV-Vis ($CHCl_3$) λ_{max} nm (ε, 10^{-3} $L.mol^{-1}.cm^{-1}$): 428 (294), 464 (11.6), 492 (9.1), 561 (10.4), 600 (4.4).

Bibliography

(1) Kadish, K. M. *The porphyrin handbook*; Elsevier, **1999**.
(2) Caughey, W. S.; Smythe, G. A.; O'Keeffe, D. H.; Maskasky, J. E.; Smith, M. I. *J. Biol. Chem.* **1975**, *250* (19), 7602–7622.
(3) Luzgina, V. N.; Filippovich, E. I.; Evstigneeva, R. P. *Pharm. Chem. J.* **1977**, *11* (5), 613–620.
(4) Mauzerall, D. In *Photosynthesis I*; Trebst, P. D. A., Avron, P. D. M., Eds.; Encyclopedia of Plant Physiology; Springer Berlin Heidelberg, **1977**; pp 117–124.
(5) Scott, J. M.; Molloy, A. M. *Ann. Nutr. Metab.* **2012**, *61* (3), 239–245.
(6) Kadish, K. M.; Smith, K. M.; Guilard, R. *Handbook of Porphyrin Science: With Applications to Chemistry, Physics, Materials Science, Engineering, Biology and Medicine*; World Scientific, **2011**.
(7) Thudichum, J. L. W. *Rep. Med Privy Counc.* **1867**, *10*, 152.
(8) Drabkin, D. L. Philadelphia Oxford Press, London, England, **1958**.
(9) Wolstenholme, G. E. W.; Millar, E. C. *Ciba Foundation symposium: Porphyrin Biosynthesis and Metabolism*; Little, Brown, **1956**.
(10) Kalisch, W. W.; Senge, M. O. *Angew. Chem. Int. Ed.* **1998**, *37* (8), 1107–1109.
(11) Kadish, K. M.; Smith, K. M.; Guilard, R. *The Porphyrin Handbook: Inorganic, organometallic and coordination chemistry*; Elsevier, **2000**.
(12) Vicente, M. da G. H.; Smith, K. M. *Curr. Org. Synth.* **2014**, *11* (1), 3–28.
(13) Xu, H.; Chen, R.; Sun, Q.; Lai, W.; Su, Q.; Huang, W.; Liu, X. *Chem. Soc. Rev.* **2014**, *43* (10), 3259.
(14) Knör, G. *Coord. Chem. Rev.* **2015**, *304-305*, 102–108.
(15) Figueira, F.; M.R. Pereira, P.; Silva, S.; A.S. Cavaleiro, J.; P.C. Tome, J. *Curr. Org. Synth.* **2014**, *11* (1), 110–126.
(16) Alves, E.; Faustino, M. A. F.; Neves, M. G. P. M. S.; Cunha, Â.; Nadais, H.; Almeida, A. *J. Photochem. Photobiol. C Photochem. Rev.* **2015**, *22*, 34–57.
(17) Lu, H.; Zhang, X. P. *Chem. Soc. Rev.* **2011**, *40* (4), 1899–1909.
(18) Vogel, E.; Köcher, M.; Schmickler, H.; Lex, J. *Angew. Chem. Int. Ed. Engl.* **1986**, *25* (3), 257–259.
(19) Gale, P. A.; Sessler, J. L.; Král, V. *Chem. Commun.* **1998**, No. 1, 1–8.
(20) Jasat, A.; Dolphin, D. *Chem. Rev.* **1997**, *97* (6), 2267–2340.
(21) Sessler, J. L.; Camiolo, S.; Gale, P. A. *Coord. Chem. Rev.* **2003**, *240* (1-2), 17–55.
(22) Saito, S.; Osuka, A. *Angew. Chem. Int. Ed.* **2011**, *50* (19), 4342–4373.
(23) Chmielewski, P. J.; Latos-Grażyński, L. *Coord. Chem. Rev.* **2005**, *249* (21–22), 2510–2533.
(24) Chmielewski, P. J.; Latos-Grażyński, L.; Rachlewicz, K.; Glowiak, T. *Angew. Chem. Int. Ed. Engl.* **1994**, *33* (7), 779–781.
(25) Furuta, H.; Asano, T.; Ogawa, T. *J. Am. Chem. Soc.* **1994**, *116* (2), 767–768.
(26) Pacholska, E.; Latos-Grazynski, L.; Szterenberg, L.; Ciunik, Z. *J. Org. Chem.* **2000**, *65* (24), 8188–8196.
(27) Saegusa, Y.; Ishizuka, T.; Komamura, K.; Shimizu, S.; Kotani, H.; Kobayashi, N.; Kojima, T. *Phys. Chem. Chem. Phys.* **2015**, *17* (22), 15001–15011.
(28) Luck, R. L. *Mater. Manuf. Process.* **1999**, *14* (3), 450–451.
(29) Jiang, J.; Bekaroğlu, Ö. *Functional Phthalocyanine Molecular Materials*; Springer Science & Business Media, **2010**.
(30) Braun, A.; Tcherniac, J. *Berichte Dtsch. Chem. Ges.* **1907**, *40* (2), 2709–2714.
(31) de Diesbach, H.; von der Weid, E. *Helv. Chim. Acta* **1927**, *10* (1), 886–888.
(32) Sheldon, R. A. *Metalloporphyrins in Catalytic Oxidations*; CRC Press, **1994**.
(33) J.E. Merritt; Loening, K. L. *Pure Appl. Chem.* **1979**, *51*, 2251–2304.

(34) Kadish, K. M.; Smith, K. M.; Guilard, R. *The Porphyrin Handbook: Applications of phthalocyanines*; Elsevier, **2003**.
(35) Okada, S.; Segawa, H. *J. Am. Chem. Soc.* **2003**, *125* (9), 2792–2796.
(36) Brothers, P. J. *Chem. Commun.* **2008**, No. 18, 2090.
(37) Lavallee, D. K. *Synth. React. Inorg. Met.-Org. Chem.* **1982**, *12* (3), 323–324.
(38) Lash, T. D.; Jones, S. A.; Ferrence, G. M. *J. Am. Chem. Soc.* **2010**, *132* (37), 12786–12787.
(39) Osuka, A.; Saito, S. *Chem. Commun.* **2011**, *47* (15), 4330.
(40) Gest, H.; Blankenship, R. E. *Photosynth. Res.* **2004**, *80* (1-3), 59–70.
(41) Bryant, D. A.; Costas, A. M. G.; Maresca, J. A.; Chew, A. G. M.; Klatt, C. G.; Bateson, M. M.; Tallon, L. J.; Hostetler, J.; Nelson, W. C.; Heidelberg, J. F.; Ward, D. M. *Science* **2007**, *317* (5837), 523–526.
(42) Montforts, F.-P.; Glasenapp-Breiling, M. In *Progress in Heterocyclic Chemistry*; Gilchrist, G. W. G. and T. L., Ed.; A critical review of the 1997 literature preceded by two chapters on current heterocyclic topics; Elsevier, **1998**; Vol. 10, pp 1–24.
(43) de la Torre, G.; Claessens, C. G.; Torres, T. *Eur. J. Org. Chem.* **2000**, *2000* (16), 2821–2830.
(44) Baulin, V. E.; Ovsyannikova, E. V.; Kalashnikova, I. P.; Girina, G. P.; Andreev, V. N.; Alpatova, N. M.; Tsivadze, A. Y. *Prot. Met. Phys. Chem. Surf.* **2013**, *49* (1), 5–31.
(45) Fischer, H. *Org. Synth.* **1941**, *21*, 53.
(46) Labbe, R. F.; Nishida, G. *Biochim. Biophys. Acta* **1957**, *26* (2), 437.
(47) Rothemund, P. *J. Am. Chem. Soc.* **1935**, *57* (10), 2010–2011.
(48) Rothemund, P.; Menotti, A. R. *J. Am. Chem. Soc.* **1941**, *63* (1), 267–270.
(49) Adler, A. D.; Longo, F. R.; Shergalis, W. *J. Am. Chem. Soc.* **1964**, *86* (15), 3145–3149.
(50) Adler, A. D.; Longo, F. R.; Finarelli, J. D.; Goldmacher, J.; Assour, J.; Korsakoff, L. *J. Org. Chem.* **1967**, *32* (2), 476–476.
(51) Little, R. G.; Anton, J. A.; Loach, P. A.; Ibers, J. A. *J. Heterocycl. Chem.* **1975**, *12* (2), 343–349.
(52) Lindsey, J. S. In *Metalloporphyrins Catalyzed Oxidations*; Springer, **1994**; pp 49–86.
(53) Carter, F. L.; Siatkowski, R. E. *Molecular Electronic Devices: Proceedings of the 3rd International Symposium on Molecular Electronic Devices, Arlington, Virginia, 6-8 October 1986*; North-Holland, **1988**.
(54) Taniguchi, M.; Du, H.; Lindsey, J. S. *J. Chem. Inf. Model.* **2011**, *51* (9), 2233–2247.
(55) Lindsey, J. S.; Schreiman, I. C.; Hsu, H. C.; Kearney, P. C.; Marguerettaz, A. M. *J. Org. Chem.* **1987**, *52* (5), 827–836.
(56) Kadish, K. M. *The Porphyrin Handbook: Synthesis and organic chemistry*; Elsevier, **2000**.
(57) Leznoff, C. C.; Svirskaya, P. I. *Angew. Chem. Int. Ed. Engl.* **1978**, *17* (12), 947–947.
(58) Yaseen, M.; Ali, M.; NajeebUllah, M.; Ali Munawar, M.; Khokhar, I. *J. Heterocycl. Chem.* **2009**, *46* (2), 251–255.
(59) Nascimento, B. F. O.; Pineiro, M.; Rocha Gonsalves, A. M. d'A.; Ramos Silva, M.; Matos Beja, A.; Paixão, J. A. *J. Porphyr. Phthalocyanines* **2007**, *11* (02), 77–84.
(60) Nascimento, B. F. O.; Rocha Gonsalves, A. M. d'A.; Pineiro, M. *Inorg. Chem. Commun.* **2010**, *13* (3), 395–398.
(61) Lucas, R.; Vergnaud, J.; Teste, K.; Zerrouki, R.; Sol, V.; Krausz, P. *Tetrahedron Lett.* **2008**, *49* (38), 5537–5539.
(62) Boëns, B.; Faugeras, P.-A.; Vergnaud, J.; Lucas, R.; Teste, K.; Zerrouki, R. *Tetrahedron* **2010**, *66* (11), 1994–1996.
(63) Vignaud, Y.; Granet, R.; Krausz, P. *J. Porphyr. Phthalocyanines* **2006**, *10* (07), 937–941.

(64) Yu, L.; Muthukumaran, K.; Sazanovich, I. V.; Kirmaier, C.; Hindin, E.; Diers, J. R.; Boyle, P. D.; Bocian, D. F.; Holten, D.; Lindsey, J. S. *Inorg. Chem.* **2003**, *42* (21), 6629–6647.
(65) Littler, B. J.; Ciringh, Y.; Lindsey, J. S. *J. Org. Chem.* **1999**, *64* (8), 2864–2872.
(66) Rao, P. D.; Dhanalekshmi, S.; Littler, B. J.; Lindsey, J. S. *J. Org. Chem.* **2000**, *65* (22), 7323–7344.
(67) Laha, J. K.; Dhanalekshmi, S.; Taniguchi, M.; Ambroise, A.; Lindsey, J. S. *Org. Process Res. Dev.* **2003**, *7* (6), 799–812.
(68) Wiehe, A.; Ryppa, C.; Senge, M. O. *Org. Lett.* **2002**, *4* (22), 3807–3809.
(69) Peters, M. V.; Goddard, R.; Hecht, S. *J. Org. Chem.* **2006**, *71* (20), 7846–7849.
(70) Jiblaoui, A.; Leroy-Lhez, S.; Ouk, T.-S.; Grenier, K.; Sol, V. *Bioorg. Med. Chem. Lett.* **2015**, *25* (2), 355–362.
(71) Arsenault, G. P.; Bullock, E.; MacDonald, S. F. *J. Am. Chem. Soc.* **1960**, *82* (16), 4384–4389.
(72) Woodward, R. B.; Ayer, W. A.; Beaton, J. M.; Bickelhaupt, F.; Bonnett, R.; Buchschacher, P.; Closs, G. L.; Dutler, H.; Hannah, J.; Hauck, F. P.; Itô, S.; Langemann, A.; Le Goff, E.; Leimgruber, W.; Lwowski, W.; Sauer, J.; Valenta, Z.; Volz, H. *J. Am. Chem. Soc.* **1960**, *82* (14), 3800–3802.
(73) Ogoshi, H.; Sugimoto, H.; Nishiguchi, T.; Watanabe, T.; Matsuda, Y.; Yoshida, Z. *Chem. Lett.* **1978**, *7* (1), 29–32.
(74) Manka, J. S.; Lawrence, D. S. *Tetrahedron Lett.* **1989**, *30* (50), 6989–6992.
(75) Montierth, J. M.; Duran, A. G.; Leung, S. H.; Smith, K. M.; Schore, N. E. *Tetrahedron Lett.* **2000**, *41* (39), 7423–7426.
(76) Naik, R.; Joshi, P.; Kaiwar (nee Vakil), S. P.; Deshpande, R. K. *Tetrahedron* **2003**, *59* (13), 2207–2213.
(77) Temelli, B.; Unaleroglu, C. *Tetrahedron* **2009**, *65* (10), 2043–2050.
(78) Milcent, R. *Chimie organique hétérocyclique : Structures fondamentales, chimie et biochimie des principaux composés naturels*; EDP Sciences, **2003**.
(79) Evstigneeva, R. P. *Pure Appl. Chem.* **1981**, *53* (6), 1129–1140.
(80) Ongayi, C. O. Synthesis of Symmetric and Asymmetric Water-Soluble Porphyrin Derivatives, Faculty of the Louisiana State University and Agricultural and Mechanical College in partial fulfillment of the requirements for the degree of Doctor of Philosophy in The Department of Chemistry by Caroline Owendi Ongayi BS, University of Nairobi, Kenya 1999, **2005**.
(81) Paine, J. B.; Chang, C. K.; Dolphin, D. *Heterocycles* **1977**, *7*, 831–838.
(82) John B. Paine, J. H. *J. Org. Chem. - J ORG CHEM* **1988**, *53* (12), 2796–2802.
(83) Saltsman, I.; Goldberg, I.; Balasz, Y.; Gross, Z. *Tetrahedron Lett.* **2007**, *48* (2), 239–244.
(84) Gałęzowski, M.; Jaźwiński, J.; Lewtak, J. P.; Gryko, D. T. *J. Org. Chem.* **2009**, *74* (15), 5610–5613.
(85) Joule, J. A.; Mills, K. *Heterocyclic chemistry*, 5th ed.; Wiley: Hoboken, N.J, **2009**.
(86) Sabine Hatscher, M. O. S. *Tetrahedron Lett.* **2003**, *44* (1), 157–160.
(87) Saltsman, I.; Gross, Z. *Tetrahedron Lett.* **2008**, *49* (2), 247–249.
(88) Dilek Kiper Dogutan, S. H. H. Z. *J. Org. Chem.* **2007**, *72* (20), 7701–7714.
(89) Lindsey, J. S. *Acc. Chem. Res.* **2010**, *43* (2), 300–311.
(90) Senge, M. O.; Shaker, Y. M.; Pintea, M.; Ryppa, C.; Hatscher, S. S.; Ryan, A.; Sergeeva, Y. *Eur. J. Org. Chem.* **2010**, *2010* (2), 237–258.
(91) Senge, M. O. *Chem. Commun.* **2011**, *47* (7), 1943.
(92) Dolphin, D. *The Porphyrins. Volume II. Structure and Synthesis, Part B*, 1st edition.; Academic Press, **1978**.
(93) Schlesinger, W.; Corwin, A. H.; Sargent, L. J. *J. Am. Chem. Soc.* **1950**, *72* (7), 2867–2871.

(94) Eisner, U. *J. Chem. Soc. Resumed* **1957**, No. 0, 3461–3469.
(95) Whitlock, H. W.; Hanauer, R.; Oester, M. Y.; Bower, B. K. *J. Am. Chem. Soc.* **1969**, *91* (26), 7485–7489.
(96) Varamo, M.; Loock, B.; Maillard, P.; Grierson, D. S. *Org. Lett.* **2007**, *9* (23), 4689–4692.
(97) Shea, K. M.; Jaquinod, L.; Smith, K. M. *J. Org. Chem.* **1998**, *63* (20), 7013–7021.
(98) de Souza, J. M.; de Assis, F. F.; Carvalho, C. M. B.; Cavaleiro, J. A. S.; Brocksom, T. J.; de Oliveira, K. T. *Tetrahedron Lett.* **2014**, *55* (8), 1491–1495.
(99) Bonnett, R.; Dimsdale, M. J.; Stephenson, G. F. *J. Chem. Soc. C Org.* **1969**, No. 4, 564–570.
(100) Callot, H. J. *Tetrahedron Lett.* **1972**, *13* (11), 1011–1014.
(101) Bonnett, R.; Nizhnik, A. N.; White, S. G.; Berenbaum, M. C. *J. Photochem. Photobiol. B* **1990**, *6* (1-2), 29–37.
(102) Pineiro, M. *Curr. Org. Synth.* **2014**, *11* (1), 89–109.
(103) Jacobi, P. A.; Lanz, S.; Ghosh, I.; Leung, S. H.; Löwer, F.; Pippin, D. *Org. Lett.* **2001**, *3* (6), 831–834.
(104) Snow, R. J.; Fookes, C. J. R.; Battersby, A. R. *J. Chem. Soc. Chem. Commun.* **1981**, No. 11, 524–526.
(105) Battersby, A. R.; Reiter, L. A. *J. Chem. Soc. [Perkin 1]* **1984**, No. 0, 2743–2749.
(106) Battersby, A. R.; Block, M. H.; Fookes, C. J. R.; Harrison, P. J.; Henderson, G. B.; Leeper, F. J. *J. Chem. Soc. [Perkin 1]* **1992**, No. 17, 2175–2187.
(107) Strachan, J.-P.; O'Shea, D. F.; Balasubramanian, T.; Lindsey, J. S. *J. Org. Chem.* **2000**, *65* (10), 3160–3172.
(108) Drogat, N.; Barrière, M.; Granet, R.; Sol, V.; Krausz, P. *Dyes Pigments* **2011**, *88* (1), 125–127.
(109) Drogat, N.; Gady, C.; Granet, R.; Sol, V. *Dyes Pigments* **2013**, *98* (3), 609–614.
(110) Linstead, R. P. *J. Chem. Soc. Resumed* **1934**, No. 0, 1016–1017.
(111) Ongarora, B. G. Syntheses and Characterization of Water-Soluble Phthalocyanines for Diagnosis and Treatment of Cancer, Faculty of the Louisiana State University and Agricultural and Mechanical College in partial fulfillment of the requirement for the degree of Doctor of Philosophy in The Department of Chemistry by Benson Getenga Ongarora B. Sc., Moi University, **2012**.
(112) Leznoff, C. C.; Marcuccio, S. M.; Greenberg, S.; Lever, A. B. P.; Tomer, K. B. *Can. J. Chem.* **1985**, *63* (3), 623–631.
(113) Sommerauer, M.; Rager, C.; Hanack, M. *J. Am. Chem. Soc.* **1996**, *118* (42), 10085–10093.
(114) Oliver, S. W.; Smith, T. D. *J. Chem. Soc. Perkin Trans. 2* **1987**, No. 11, 1579–1582.
(115) Chen, J.; Chen, N.; Huang, J.; Wang, J.; Huang, M. *Inorg. Chem. Commun.* **2006**, *9* (3), 313–315.
(116) Leznoff, C. C.; Hall, T. W. *Tetrahedron Lett.* **1982**, *23* (30), 3023–3026.
(117) Wöhrle, D.; Krawczyk, G. *Polym. Bull.* **1986**, *15* (3), 193–200.
(118) Erdem, S. S.; Nesterova, I. V.; Soper, S. A.; Hammer, R. P. *J. Org. Chem.* **2008**, *73* (13), 5003–5007.
(119) Dumoulin, F.; Durmuş, M.; Ahsen, V.; Nyokong, T. *Coord. Chem. Rev.* **2010**, *254* (23–24), 2792–2847.
(120) Makhseed, S.; Machacek, M.; Alfadly, W.; Tuhl, A.; Vinodh, M.; Simunek, T.; Novakova, V.; Kubat, P.; Rudolf, E.; Zimcik, P. *Chem. Commun.* **2013**, *49* (95), 11149.
(121) Hanack, M.; Crucius, G.; J.F. Calvete, M.; Ziegler, T. *Curr. Org. Synth.* **2014**, *11* (1), 59–66.

(122) Ptaszek, M. In *Progress in Molecular Biology and Translational Science*; Morris, M. C., Ed.; Fluorescence-Based BiosensorsFrom Concepts to Applications; Academic Press, **2013**; Vol. 113, pp 59–108.
(123) Gouterman, M. *J. Mol. Spectrosc.* **1961**, *6*, 138–163.
(124) Gouterman, M.; Wagnière, G. H.; Snyder, L. C. *J. Mol. Spectrosc.* **1963**, *11* (1–6), 108–127.
(125) Wohrle, D. *Adv. Mater.* **1997**, *9* (15), 1191–1192.
(126) Grahn, M. F.; McGuinness, A.; Benzie, R.; Boyle, R.; de Jode, M. L.; Dilkes, M. G.; Abbas, B.; Williams, N. S. *J. Photochem. Photobiol. B* **1997**, *37* (3), 261–266.
(127) Marsh, D.; Mink, L. *J. Chem. Educ.* **1996**, *73* (12), 1188.
(128) Milgrom, L. R. *The Colours of Life: An Introduction to the Chemistry of Porphyrins and Related Compounds*; OUP Oxford: Oxford ; New York, **1997**.
(129) Jablonski, A. *Nature* **1933**, *131*, 839–840.
(130) Pauli, W. *Exclusion principle and quantum mechanics*; Springer, **1946**.
(131) Baskin, J. S.; Yu, H.-Z.; Zewail, A. H. *J. Phys. Chem. A* **2002**, *106* (42), 9837–9844.
(132) Turro, N. J. *Modern Molecular Photochemistry*; University Science Books, **1991**.
(133) Seybold, P. G.; Gouterman, M. *J. Mol. Spectrosc.* **1969**, *31* (1–13), 1–13.
(134) Fukuzumi, S.; Ohkubo, K.; Chen, Y.; Pandey, R. K.; Zhan, R.; Shao, J.; Kadish, K. M. *J. Phys. Chem. A* **2002**, *106* (20), 5105–5113.
(135) Ogunsipe, A.; Nyokong, T. *J. Mol. Struct.* **2004**, *689* (1–2), 89–97.
(136) Singh, S.; Aggarwal, A.; Thompson, S.; Tomé, J. P. C.; Zhu, X.; Samaroo, D.; Vinodu, M.; Gao, R.; Drain, C. M. *Bioconjug. Chem.* **2010**, *21* (11), 2136–2146.
(137) George, R. D.; Snow, A. W.; Shirk, J. S.; Barger, W. R. *J. Porphyr. Phthalocyanines* **1998**, *2* (1), 1–7.
(138) Adachi, K.; Chayama, K.; Watarai, H. *Langmuir* **2006**, *22* (4), 1630–1639.
(139) Brouwer, A. M. *Pure Appl. Chem.* **2011**, *83* (12).
(140) Gentemann, S.; Medforth, C. J.; Forsyth, T. P.; Nurco, D. J.; Smith, K. M.; Fajer, J.; Holten, D. *J. Am. Chem. Soc.* **1994**, *116* (16), 7363–7368.
(141) Figueiredo, T. L.; Johnstone, R. A.; Sørensen, A. M.; Burget, D.; Jacques, P. *Photochem. Photobiol.* **1999**, *69* (5), 517–528.
(142) Ogunsipe, A.; Maree, D.; Nyokong, T. *J. Mol. Struct.* **2003**, *650* (1–3), 131–140.
(143) Zenkevich, E.; Sagun, E.; Knyukshto, V.; Shulga, A.; Mironov, A.; Efremova, O.; Bonnett, R.; Songca, S. P.; Kassem, M. *J. Photochem. Photobiol. B* **1996**, *33* (2), 171–180.
(144) Brune, D. C.; Blankenship, R. E.; Seely, G. R. *Photochem. Photobiol.* **1988**, *47* (5), 759–763.
(145) Nyokong, T. *Coord. Chem. Rev.* **2007**, *251* (13-14), 1707–1722.
(146) Röder, B.; Büchner, M.; Rückmann, I.; Senge, M. O. *Photochem. Photobiol. Sci.* **2010**, *9* (8), 1152–1158.
(147) Costa, L.; Faustino, M. A. F.; Neves, M. G. P. M. S.; Cunha, Â.; Almeida, A. *Viruses* **2012**, *4* (12), 1034–1074.
(148) Kehrer, J. P. *Toxicology* **2000**, *149* (1), 43–50.
(149) Halliwell, B. *Free Radic. Res.* **1999**, *31* (4), 261–272.
(150) Winterbourn, C. C.; Kettle, A. J. *Biochem. Biophys. Res. Commun.* **2003**, *305* (3), 729–736.
(151) DeRosa, M. C.; Crutchley, R. J. *Coord. Chem. Rev.* **2002**, *233*, 351–371.
(152) Schweitzer, C.; Schmidt, R. *Chem. Rev.* **2003**, *103* (5), 1685–1758.
(153) Mathai, S.; Smith, T. A.; Ghiggino, K. P. *Photochem. Photobiol. Sci.* **2007**, *6* (9), 995.
(154) Kuznetsova, N. A.; Gretsova, N. S.; Derkacheva, V. M.; Kaliya, O. L.; Lukyanets, E. A. *J. Porphyr. Phthalocyanines* **2003**, *07* (03), 147–154.

(155) Bonkovsky, H. L.; Guo, J.-T.; Hou, W.; Li, T.; Narang, T.; Thapar, M. In *Comprehensive Physiology*; Terjung, R., Ed.; John Wiley & Sons, Inc.: Hoboken, NJ, USA, **2013**.
(156) Wittenberg, J. B.; Wittenberg, B. A. *Annu. Rev. Biophys. Biophys. Chem.* **1990**, *19* (1), 217–241.
(157) Hohmann-Marriott, M. F.; Blankenship, R. E. *Annu. Rev. Plant Biol.* **2011**, *62* (1), 515–548.
(158) Thackray, S. J.; Mowat, C. G.; Chapman, S. K. *Biochem. Soc. Trans.* **2008**, *36* (Pt 6), 1120–1123.
(159) Basran, J.; Efimov, I.; Chauhan, N.; Thackray, S. J.; Krupa, J. L.; Eaton, G.; Griffith, G. A.; Mowat, C. G.; Handa, S.; Raven, E. L. *J. Am. Chem. Soc.* **2011**, *133* (40), 16251–16257.
(160) Rendic, S.; Guengerich, F. P. *Chem. Res. Toxicol.* **2015**, *28* (1), 38–42.
(161) Rogers, S. *The Guardian*. March 18, **2011**.
(162) Mandalia, H. C.; Jain, V. K.; Pattanaik, B. N. *Res. J. Chem. Sci. ISSN* **2012**, *2231*, 606X.
(163) Braga, A. F. B.; Moreira, S. P.; Zampieri, P. R.; Bacchin, J. M. G.; Mei, P. R. *Sol. Energy Mater. Sol. Cells* **2008**, *92* (4), 418–424.
(164) Badawy, W. A. *J. Adv. Res.* **2015**, *6* (2), 123–132.
(165) Walter, M. G.; Rudine, A. B.; Wamser, C. C. *J. Porphyr. Phthalocyanines* **2010**, *14* (09), 759–792.
(166) Li, L.-L.; Diau, E. W.-G. *Chem Soc Rev* **2013**, *42* (1), 291–304.
(167) Nikolaou, V.; Angaridis, P. A.; Charalambidis, G.; Sharma, G. D.; Coutsolelos, A. G. *Dalton Trans* **2015**, *44* (4), 1734–1747.
(168) Han, M.; Zhang, X.; Zhang, X.; Liao, C.; Zhu, B.; Li, Q. *Polyhedron* **2015**, *85*, 864–873.
(169) Mathew, S.; Yella, A.; Gao, P.; Humphry-Baker, R.; Curchod, B. F. E.; Ashari-Astani, N.; Tavernelli, I.; Rothlisberger, U.; Nazeeruddin, M. K.; Grätzel, M. *Nat. Chem.* **2014**, *6* (3), 242–247.
(170) Chandrasekharam, M.; Rajkumar, G.; Rao, C. S.; Suresh, T.; Reddy, P. Y.; Soujanya, Y. *J. Chem. Sci.* **2011**, *123* (5), 555–565.
(171) Hardin, B. E.; Snaith, H. J.; McGehee, M. D. *Nat. Photonics* **2012**, *6* (3), 162–169.
(172) Lin, C.-F.; Zhang, M.; Liu, S.-W.; Chiu, T.-L.; Lee, J.-H. *Int. J. Mol. Sci.* **2011**, *12* (1), 476–505.
(173) Park, W. J.; Chae, S. H.; Shin, J.; Choi, D. H.; Lee, S. J. *Synth. Met.* **2015**, *205*, 206–211.
(174) Nakamura, Y.; Aratani, N.; Osuka, A. *Chem. Soc. Rev.* **2007**, *36* (6), 831.
(175) Gust, D.; Moore, T. A.; Moore, A. L. *Acc. Chem. Res.* **2009**, *42* (12), 1890–1898.
(176) Fukuzumi, S.; Ohkubo, K.; Suenobu, T. *Acc. Chem. Res.* **2014**, *47* (5), 1455–1464.
(177) Berardi, S.; Drouet, S.; Francàs, L.; Gimbert-Suriñach, C.; Guttentag, M.; Richmond, C.; Stoll, T.; Llobet, A. *Chem. Soc. Rev.* **2014**, *43* (22), 7501–7519.
(178) Lim, G. N.; Maligaspe, E.; Zandler, M. E.; D'Souza, F. *Chem. - Eur. J.* **2014**, *20* (51), 17089–17099.
(179) Nath, K.; Najafpour, M. M.; Voloshin, R. A.; Balaghi, S. E.; Tyystjärvi, E.; Timilsina, R.; Eaton-Rye, J. J.; Tomo, T.; Nam, H. G.; Nishihara, H.; Ramakrishna, S.; Shen, J.-R.; Allakhverdiev, S. I. *Photosynth. Res.* **2015**.
(180) Tanaka, T.; Osuka, A. *Chem. Soc. Rev.* **2015**, *44* (4), 943–969.
(181) Guldi, D. M.; Nishihara, H.; Venkataraman, L. *Chem. Soc. Rev.* **2015**, *44* (4), 842–844.
(182) Lee, C. W.; Kim, O. Y.; Lee, J. Y. *J. Ind. Eng. Chem.* **2014**, *20* (4), 1198–1208.
(183) Golmar, F.; Stoliar, P.; Monton, C.; Valmianski, I.; Schuller, I. K.; Hueso, L. E.; Casanova, F. *Phys. Status Solidi A* **2015**, *212* (3), 607–611.

(184) Hohnholz, D.; Steinbrecher, S.; Hanack, M. *J. Mol. Struct.* **2000**, *521* (1-3), 231–237.
(185) Bae, Y. J.; Lee, N. J.; Kim, T. H.; Cho, H.; Lee, C.; Fleet, L.; Hirohata, A. *Nanoscale Res. Lett.* **2012**, *7* (1), 1–6.
(186) Warner, M.; Din, S.; Tupitsyn, I. S.; Morley, G. W.; Stoneham, A. M.; Gardener, J. A.; Wu, Z.; Fisher, A. J.; Heutz, S.; Kay, C. W. M.; Aeppli, G. *Nature* **2013**, *503* (7477), 504–508.
(187) Melville, O. A.; Lessard, B. H.; Bender, T. P. *ACS Appl. Mater. Interfaces* **2015**, *7* (24), 13105–13118.
(188) Chen, J.; Che, C.-M. *Angew. Chem. Int. Ed Engl.* **2004**, *43* (37), 4950–4954.
(189) Rosenthal, J.; Luckett, T. D.; Hodgkiss, J. M.; Nocera, D. G. *J. Am. Chem. Soc.* **2006**, *128* (20), 6546–6547.
(190) Elouarzaki, K.; Le Goff, A.; Holzinger, M.; Thery, J.; Cosnier, S. *J. Am. Chem. Soc.* **2012**, *134* (34), 14078–14085.
(191) Groves, J. T.; Myers, R. S. *J. Am. Chem. Soc.* **1983**, *105* (18), 5791–5796.
(192) Sorokin, A. B. *Chem. Rev.* **2013**, *113* (10), 8152–8191.
(193) Perng, Y.-S.; Oloman, C. W.; Watson, P. A.; James, B. R. *Tappi J.* **1994**, *77* (11), 119–125.
(194) Löbbert, G. In *Ullmann's Encyclopedia of Industrial Chemistry*; Wiley-VCH Verlag GmbH & Co. KGaA, **2000**.
(195) Gregory, P. *J. Porphyr. Phthalocyanines* **2000**, *04* (04), 432–437.
(196) Wöhrle, D.; Schnurpfeil, G.; Makarov, S. G.; Kazarin, A.; Suvorova, O. N. *Macroheterocycles* **2012**, *5* (3), 191–202.
(197) Hunger, K. *Industrial Dyes: Chemistry, Properties, Applications*; John Wiley & Sons, **2007**.
(198) Liao, G.; He, C.; Hu, N.; Sun, Y.; Li, Y.; Tai, X.; Cao, X.; Ren, H.; Cai, Y.; Xiao, T.; Niu, J. Q. Phthalocyanine Dye Used for Color Filter of Lcd. WO/2015/010331, January 30, **2015**.
(199) Biesaga, M.; Pyrzyńska, K.; Trojanowicz, M. *Talanta* **2000**, *51* (2), 209–224.
(200) van Staden, J. (Koos) F. *Talanta* **2015**, *139*, 75–88.
(201) Wei, C.; Jia, G.; Yuan, J.; Feng, Z.; Li, C. *Biochemistry (Mosc.)* **2006**, *45* (21), 6681–6691.
(202) Rubio-Magnieto, J.; Di Meo, F.; Lo, M.; Delcourt, C.; Clément, S.; Norman, P.; Richeter, S.; Linares, M.; Surin, M. *Org Biomol Chem* **2015**, *13* (8), 2453–2463.
(203) Li, Y.; Lin, T.; Luo, Y.; Liu, Q.; Xiao, W.; Guo, W.; Lac, D.; Zhang, H.; Feng, C.; Wachsmann-Hogiu, S.; Walton, J. H.; Cherry, S. R.; Rowland, D. J.; Kukis, D.; Pan, C.; Lam, K. S. *Nat. Commun.* **2014**, *5*.
(204) Huang, H.; Song, W.; Rieffel, J.; Lovell, J. F. *Biomed. Phys.* **2015**, *3*, 23.
(205) Huynh, E.; Lovell, J. F.; Helfield, B. L.; Jeon, M.; Kim, C.; Goertz, D. E.; Wilson, B. C.; Zheng, G. *J. Am. Chem. Soc.* **2012**, *134* (40), 16464–16467.
(206) Abuteen, A.; Zanganeh, S.; Akhigbe, J.; Samankumara, L. P.; Aguirre, A.; Biswal, N.; Braune, M.; Vollertsen, A.; Röder, B.; Brückner, C.; Zhu, Q. *Phys. Chem. Chem. Phys.* **2013**, *15* (42), 18502–18509.
(207) Liu, T. W.; MacDonald, T. D.; Jin, C. S.; Gold, J. M.; Bristow, R. G.; Wilson, B. C.; Zheng, G. *ACS Nano* **2013**, *7* (5), 4221–4232.
(208) Shi, J.; Liu, T. W. B.; Chen, J.; Green, D.; Jaffray, D.; Wilson, B. C.; Wang, F.; Zheng, G. *Theranostics* **2011**, *1*, 363–370.
(209) J.F. Calvete, M.; V.C. Simoes, A.; A. Henriques, C.; M.A. Pinto, S.; M. Pereira, M. *Curr. Org. Synth.* **2014**, *11* (1), 127–140.

(210) Mouraviev, V.; Venkatraman, T. N.; Tovmasyan, A.; Kimura, M.; Tsivian, M.; Mouravieva, V.; Polascik, T. J.; Wang, H.; Amrhein, T. J.; Batinic-Haberle, I.; Lascola, C. *J. Endourol.* **2012**, *26* (11), 1420–1424.
(211) Photodynamic Therapy for Cancer http://www.cancer.gov/about-cancer/treatment/types/surgery/photodynamic-fact-sheet (accessed Oct 1, 2015).
(212) Group, V. I. P. T. S. *Am. J. Ophthalmol.* **2001**, *131* (5), 541–560.
(213) Dai, T.; Huang, Y.-Y.; Hamblin, M. R. *Photodiagnosis Photodyn. Ther.* **2009**, *6* (3-4), 170–188.
(214) Arnaut, L. G. In *Advances in Inorganic Chemistry*; Stochel, R. van E. and G., Ed.; Inorganic Photochemistry; Academic Press, 2011; Vol. 63, pp 187–233.
(215) Bechet, D.; Mordon, S. R.; Guillemin, F.; Barberi-Heyob, M. A. *Cancer Treat. Rev.* **2014**, *40* (2), 229–241.
(216) Kawczyk-Krupka, A.; Bugaj, A. M.; Latos, W.; Zaremba, K.; Wawrzyniec, K.; Kucharzewski, M.; Sieroń, A. *Photodiagnosis Photodyn. Ther.* **2014**.
(217) Quirk, B. J.; Brandal, G.; Donlon, S.; Vera, J. C.; Mang, T. S.; Foy, A. B.; Lew, S. M.; Girotti, A. W.; Jogal, S.; LaViolette, P. S.; Connelly, J. M.; Whelan, H. T. *Photodiagnosis Photodyn. Ther.* **2015**.
(218) Stallivieri, A.; Guern, F. L.; Vanderesse, R.; Meledje, D.; Jori, G.; Frochot, C.; Acherar, S. *Photochem. Photobiol. Sci.* **2015**.
(219) Banerjee, S.; Das, T.; Samuel, G.; Sarma, H. D.; Venkatesh, M.; Pillai, M. R. *Nucl. Med. Commun.* **2001**, *22* (10), 1101–1107.
(220) Sarma, H. D.; Das, T.; Banerjee, S.; Venkatesh, M.; Vidyasagar, P. B.; Mishra, K. P. *Curr. Radiopharm.* **2011**, *4* (2), 150–160.
(221) Peng, J.; Zhao, L.; Zhu, X.; Sun, Y.; Feng, W.; Gao, Y.; Wang, L.; Li, F. *Biomaterials* **2013**, *34* (32), 7905–7912.
(222) Carpenter, B. L.; Feese, E.; Sadeghifar, H.; Argyropoulos, D. S.; Ghiladi, R. A. *Photochem. Photobiol.* **2012**, *88* (3), 527–536.
(223) Sperandio, F. F.; Huang, Y.-Y.; Hamblin, M. R. *Recent Patents Anti-Infect. Drug Disc.* **2013**, *8* (2), 108.
(224) Fu, X.; Fang, Y.; Yao, M. *BioMed Res. Int.* **2013**, *2013*, 1–9.
(225) A Almeida, A. C. **2013**.
(226) Liu, K.; Liu, Y.; Yao, Y.; Yuan, H.; Wang, S.; Wang, Z.; Zhang, X. *Angew. Chem.* **2013**, *125* (32), 8443–8447.
(227) Thomas, M.; Craik, J. D.; Tovmasyan, A.; Batinic-Haberle, I.; Benov, L. T. *Future Microbiol.* **2015**, *10* (5), 709–724.
(228) Rosseti, I. B.; Chagas, L. R.; Costa, M. S. *Lasers Med. Sci.* **2014**, *29* (3), 1059–1064.
(229) Panhóca, V. H.; Geralde, M. C.; Corrêa, T. Q.; Carvalho, M. T.; Souza, C.; Bagnato, V. S. *J Phys Sci Applic* **2014**, *4*, 107–114.
(230) Ringot, C.; Sol, V.; Granet, R.; Krausz, P. *Mater. Lett.* **2009**, *63* (21), 1889–1891.
(231) Ringot, C.; Sol, V.; Barrière, M.; Saad, N.; Bressollier, P.; Granet, R.; Couleaud, P.; Frochot, C.; Krausz, P. *Biomacromolecules* **2011**, *12* (5), 1716–1723.
(232) Merchán, M.; Ouk, T. S.; Kubát, P.; Lang, K.; Coelho, C.; Verney, V.; Commereuc, S.; Leroux, F.; Sol, V.; Taviot-Guého, C. *J. Mater. Chem. B* **2013**, *1* (16), 2139–2146.
(233) Noimark, S.; Dunnill, C. W.; Parkin, I. P. *Adv. Drug Deliv. Rev.* **2013**, *65* (4), 570–580.
(234) Amor, T. B.; Bortolotto, L.; Jori, G. *Photochem. Photobiol.* **1998**, *68* (3), 314–318.
(235) Amor, T. B.; Jori, G. *Insect Biochem. Mol. Biol.* **2000**, *30* (10), 915–925.
(236) Rebeiz, C. A.; Gut, L. J.; Lee, K.; Juvik, J. A.; Rebeiz, C. C.; Bouton, C. E.; Towers, G. H. N. *Crit. Rev. Plant Sci.* **1995**, *14* (4), 329–366.
(237) Kassab, K.; Dei, D.; Roncucci, G.; Jori, G.; Coppellotti, O. *Photochem. Photobiol. Sci.* **2003**, *2* (6), 668–672.

(238) Lucantoni, L.; Magaraggia, M.; Lupidi, G.; Ouedraogo, R. K.; Coppellotti, O.; Esposito, F.; Fabris, C.; Jori, G.; Habluetzel, A. *PLoS Negl Trop Dis* **2011**, *5* (12), e1434.
(239) Fabris, C.; Ouédraogo, R. K.; Coppellotti, O.; Dabiré, R. K.; Diabaté, A.; Di Martino, P.; Guidolin, L.; Jori, G.; Lucantoni, L.; Lupidi, G.; Martena, V.; Sawadogo, S. P.; Soncin, M.; Habluetzel, A. *Acta Trop.* **2012**, *123* (3), 239–243.
(240) Rebeiz, C. A.; Montazer-Zouhoor, A.; Hopen, H. J.; Wu, S. M. *Enzyme Microb. Technol.* **1984**, *6* (9), 390–396.
(241) Carré, V.; Gaud, O.; Sylvain, I.; Bourdon, O.; Spiro, M.; Biais, J.; Granet, R.; Krausz, P.; Guilloton, M. *J. Photochem. Photobiol. B* **1999**, *48* (1), 57–62.
(242) Jori, G.; Brown, S. B. *Photochem. Photobiol. Sci. Off. J. Eur. Photochem. Assoc. Eur. Soc. Photobiol.* **2004**, *3* (5), 403–405.
(243) Viana, O. S.; Ribeiro, M. S.; Rodas, A. C. D.; Rebouças, J. S.; Fontes, A.; Santos, B. S. *Molecules* **2015**, *20* (5), 8893–8912.
(244) Dessaisaix, R. *J Agr Prat* **1925**, *43*, 334–336.
(245) AYRES, P. G. *Mycologist* **2004**, *18* (1), 23–26.
(246) Dixon, B. *Lancet Infect. Dis.* **2004**, *4* (9), 594.
(247) Vilcoq, A. *La Nat. 1368* **1909**, 171-172.
(248) Aslander, A. *J Agr Res.* **1927**, *34*, 1065.
(249) Timmons, F. L. *Weed Sci.* **1970**, *18* (2), 294–307.
(250) Chauvel, B.; Guillemin, J.-P.; Gasquez, J.; Gauvrit, C. *Crop Prot.* **2012**, *42*, 320–326.
(251) Cobb, A.; Reade, J. P. H. *Herbicides and plant physiology*, 2nd ed.; Wiley-Blackwell: Chichester, West Sussex ; Ames, Iowa, **2010**.
(252) Pokorny, R. *J. Am. Chem. Soc.* **1941**, *63* (6), 1768–1768.
(253) Yemets, A.; Stelmakh, O.; Blume, Y. B. *Cell Biol. Int.* **2008**, *32* (6), 623–629.
(254) LeBaron, H. M.; McFarland, J. E.; Burnside, O. *The triazine herbicides: 50 years revolutionizing agriculture*; Elsevier Science Ltd, **2008**.
(255) Johal, G. S.; Huber, D. M. *Eur. J. Agron.* **2009**, *31* (3), 144–152.
(256) Bi, Y. F.; Miao, S. S.; Lu, Y. C.; Qiu, C. B.; Zhou, Y.; Yang, H. *J. Hazard. Mater.* **2012**, *243*, 242–249.
(257) Hussain, S.; Arshad, M.; Springael, D.; SøRensen, S. R.; Bending, G. D.; Devers-Lamrani, M.; Maqbool, Z.; Martin-Laurent, F. *Crit. Rev. Environ. Sci. Technol.* **2015**, *45* (18), 1947–1998.
(258) UIPP. *La qualité de l'eau et assainissement en France (annexes) Annexe 45 - DONNÉES STATISTIQUES SUR LES PESTICIDES*; Rapports d'office parlementaire; Sénat, **2012**.
(259) Use of herbicides across Europe — European Environment Agency (EEA) http://www.eea.europa.eu/data-and-maps/figures/use-of-herbicides-across-europe (accessed Aug 5, **2015**).
(260) EUR-Lex - 31991L0414 - FR http://eur-lex.europa.eu/LexUriServ/LexUriServ.do?uri=CELEX:31991L0414:FR:HTML (accessed Aug 5, **2015**).
(261) Zucconi, S.; Volpato, C.; Adinolfi, F.; Gandini, E.; Gentile, E.; Loi, A.; Fioriti, L. *Extern. Sci. Rep. Eur. Food Saf. Auth.* **2013**.
(262) Menne, H.; Köcher, H. *Mod. Crop Prot. Compd.* **2007**, 5–26.
(263) *Atlas of Plant Cell Structure*; Noguchi, T., Kawano, S., Tsukaya, H., Matsunaga, S., Sakai, A., Karahara, I., Hayashi, Y., Eds.; Springer Japan: Tokyo, **2014**.
(264) Phillips, R. *Physical biology of the cell*, Second edition.; Garland Science: London : New York, NY, **2013**.
(265) *The plant cell wall*; Rose, J. K. C., Ed.; Annual plant reviews; Blackwell [u.a.]: Oxford, **2003**.

(266) Keegstra, K. *Plant Physiol.* **2010**, *154* (2), 483–486.
(267) Lerouxel, O.; Cavalier, D. M.; Liepman, A. H.; Keegstra, K. *Curr. Opin. Plant Biol.* **2006**, *9* (6), 621–630.
(268) Benson, A. A. *Annu. Rev. Plant Physiol.* **1964**, *15* (1), 1–16.
(269) *Plasmodesmata*; Oparka, K. J., Ed.; Annual plant reviews; Blackwell Pub: Oxford, UK ; Ames, Iowa, USA, **2005**.
(270) *Plasmodesmata*; Heinlein, M., Ed.; Methods in Molecular Biology; Springer New York: New York, NY, **2015**; Vol. 1217.
(271) Raven, P. H.; Evert, R. F.; Eichhorn, S. E. *Biologie végétale*; De Boeck Supérieur, **2000**.
(272) Burström, H. *Growth and Growth Substances / Wachstum und Wuchsstoffe*; Springer Berlin Heidelberg : Imprint : Springer: Berlin, Heidelberg, **1961**.
(273) Duke, S. O.; Dayan, F. E. In *Comprehensive Biotechnology (Second Edition)*; Moo-Young, M., Ed.; Academic Press: Burlington, **2011**; pp 23–35.
(274) Grossmann, K. *Plant Signal. Behav.* **2007**, *2* (5), 421–423.
(275) Katekar, G. F.; Geissler, A. E. *Plant Physiol.* **1980**, *66* (6), 1190–1195.
(276) Lomax, T. L.; Muday, G. K.; Rubery, P. H. In *Plant Hormones*; Davies, P. J., Ed.; Springer Netherlands, **1995**; pp 509–530.
(277) Gest, H. *Photosynth. Res.* **2002**, *73* (1-3), 7–10.
(278) Govindjee. *Discoveries in Photosynthesis*; Springer Science & Business Media, **2006**.
(279) Staehelin, L. A. *Photosynth. Res.* **2003**, *76* (1-3), 185–196.
(280) Shen, J.-R. *Annu. Rev. Plant Biol.* **2015**, *66* (1), 23–48.
(281) Heap, I. In *Integrated Pest Management*; Pimentel, D., Peshin, R., Eds.; Springer Netherlands: Dordrecht, **2014**; pp 281–301.
(282) Büchel, K. H. *Pestic. Sci.* **1972**, *3* (1), 89–110.
(283) Moreland, D. E. *Annu. Rev. Plant Physiol.* **1980**, *31* (1), 597–638.
(284) Bai, X.; Sun, C.; Xie, J.; Song, H.; Zhu, Q.; Su, Y.; Qian, H.; Fu, Z. *Environ. Sci. Pollut. Res.* **2015**, 1–9.
(285) Summers, L. A. **1980**, 450 pp.
(286) Witkowski, D. A.; Halling, B. P. *Plant Physiol.* **1989**, *90* (4), 1239–1242.
(287) Duke, S. O.; Lydon, J.; Becerril, J. M.; Sherman, T. D.; Lehnen, L. P., Jr.; Matsumoto, H. *Weed Sci.* **1991**, *39* (3), 465–473.
(288) Bartels, P. G.; Watson, C. W. *Weed Sci.* **1978**, *26* (2), 198–203.
(289) Kirkwood, R. *Target Sites for Herbicide Action*; Springer Science & Business Media, **2013**.
(290) Nitschke, L.; Schüssler, W. *Chemosphere* **1998**, *36* (1), 35–41.
(291) Glozier, N. E.; Struger, J.; Cessna, A. J.; Gledhill, M.; Rondeau, M.; Ernst, W. R.; Sekela, M. A.; Cagampan, S. J.; Sverko, E.; Murphy, C.; Murray, J. L.; Donald, D. B. *Environ. Sci. Pollut. Res.* **2011**, *19* (3), 821–834.
(292) Bono-Blay, F.; Guart, A.; Fuente, B. de la; Pedemonte, M.; Pastor, M. C.; Borrell, A.; Lacorte, S. *Environ. Sci. Pollut. Res.* **2012**, *19* (8), 3339–3349.
(293) Hermosin, M. C.; Calderon, M. J.; Real, M.; Cornejo, J. *Agric. Ecosyst. Environ.* **2013**, *164*, 229–243.
(294) *Le Monde.fr*. July 24, **2013**.
(295) Valo, M. *Le Monde.fr*. September 25, **2014**.
(296) Upchurch, R. P. In *Residue Reviews / Rückstands-Berichte*; Gunther, F. A., Ed.; Residue Reviews / Rückstands-Berichte; Springer New York, **1966**; pp 46–85.
(297) Jie, C.; Jing-zhang, C.; Man-zhi, T.; Zi-tong, G. *J. Geogr. Sci.* **2002**, *12* (2), 243–252.
(298) Seeger, M.; Hernández, M.; Méndez, V.; Ponce, B.; Córdova, M.; González, M. *J. Soil Sci. Plant Nutr.* **2010**, *10* (3), 320–332.

(299) Mamy, L. Comparaison des impacts environnementaux des herbicides à large spectre et des herbicides sélectifs: Caractérisation de leur devenir dans le sol et modélisation. phdthesis, INAPG (AgroParisTech), **2004**.
(300) Service, O. S. U. E.; Anderson, N. P.; Hart, J. M. (John M.; Sullivan, D. M. (Dan M.; Hulting, A. G.; Horneck, D. A.; Christensen, N. W. *Soil acidity in Oregon : understanding and using concepts for crop production*; Technical Report; Corvallis, Or. : Extension Service, Oregon State University, **2013**.
(301) MELLANBY, K. **1967**, 221 pp.
(302) Grover, R.; Cessna, A. *Environmental Chemistry of Herbicides*; CRC Press, **1990**.
(303) Conway, G. R.; Pretty, J. N. *Unwelcome Harvest: Agriculture and Pollution*; Routledge, **2013**.
(304) Bertazzi, P. A.; Bernucci, I.; Brambilla, G.; Consonni, D.; Pesatori, A. C. *Environ. Health Perspect.* **1998**, *106* (Suppl 2), 625–633.
(305) Broughton, E. *Environ. Health* **2005**, *4*, 6.
(306) Young, A. L.; Calcagni, J. A.; Thalken, C. E.; Tremblay, J. W. *The toxicology, environmental fate, and human risk of herbicide orange and its associated dioxin*; DTIC Document, **1978**.
(307) Schecter, A.; Päpke, O.; Prange, J.; Constable, J. D.; Matsuda, M.; Thao, V. D.; Piskac, A. L.; others. *J. Occup. Environ. Med.* **2001**, *43* (5), 435–443.
(308) Manh, H. D.; Kido, T.; Okamoto, R.; XianLiang, S.; Anh, L. T.; Supratman, S.; Maruzeni, S.; Nishijo, M.; Nakagawa, H.; Honma, S.; Nakano, T.; Takasuga, T.; Nhu, D. D.; Hung, N. N.; Son, L. K. *Environ. Sci. Technol.* **2014**, *48* (6), 3496–3503.
(309) Gasnier, C.; Dumont, C.; Benachour, N.; Clair, E.; Chagnon, M.-C.; Séralini, G.-E. *Toxicology* **2009**, *262* (3), 184–191.
(310) Carrasco, A. *GMLS 2012* **2013**, 24.
(311) Gress, S.; Lemoine, S.; Séralini, G.-E.; Puddu, P. E. *Cardiovasc. Toxicol.* **2014**, *15* (2), 117–126.
(312) Owen, M. D.; Zelaya, I. A. *Pest Manag. Sci.* **2005**, *61* (3), 301–311.
(313) Délye, C.; Jasieniuk, M.; Le Corre, V. *Trends Genet.* **2013**, *29* (11), 649–658.
(314) Beckie, H. J.; Tardif, F. J. *Crop Prot.* **2012**, *35*, 15–28.
(315) How Weeds Become Resistant. *Take Action*.
(316) HRAC - Herbicide Resistance Action Committee http://www.hracglobal.com/ (accessed Jul 23, **2015**).
(317) Report Says GMO Crop Contamination Cannot Be Stopped http://naturalsociety.com/gmo-crop-contamination-cannot-be-stopped/ (accessed Sep 25, **2015**).
(318) GMO Crops Mean More Herbicide, Not Less http://www.forbes.com/sites/bethhoffman/2013/07/02/gmo-crops-mean-more-herbicide-not-less/ (accessed Sep 24, **2015**).
(319) Benbrook, C. M. *Environ. Sci. Eur.* **2012**, *24* (1), 24.
(320) Price, B.; Cotter, J. *Int. J. Food Contam.* **2014**, *1* (1), 5.
(321) Zimdahl, R. L. *A History of Weed Science in the United States*; Elsevier, **2010**.
(322) *The Guardian*. February 10, **2008**.
(323) Martini, E. A. *Proving Grounds: Militarized Landscapes, Weapons Testing, and the Environmental Impact of U.S. Bases*; University of Washington Press, **2015**.
(324) Walsh, E. *The Washington Post*. February 1, **2003**.
(325) Guitton, M. Interdiction du paraquat : et après ? http://www.ladepeche.pf/Interdiction-du-paraquat-et-apres_a7141.html (accessed Aug 11, **2015**).
(326) Ujjana B. Nandihalli; Stephen O. Duke. In *Pest Control with Enhanced Environmental Safety*; ACS Symposium Series; American Chemical Society, **1993**; Vol. 524, pp 62–78.

(327) Rebeiz, C. A.; Reddy, K. N.; Nandihalli, U. B.; Velu, J. *Photochem. Photobiol.* **1990**, *52* (6), 1099–1117.
(328) Stephen O. Duke; Jose M. Becerril; Timothy D. Sherman; Hiroshi Matsumoto. In *Naturally Occurring Pest Bioregulators*; ACS Symposium Series; American Chemical Society, **1991**; Vol. 449, pp 371–386.
(329) Kouji, H.; Masuda, T.; Matsunaka, S. *Pestic. Biochem. Physiol.* **1989**, *33* (3), 230–238.
(330) Villanueva, A.; Hazen, M. J.; Stockert, J. C. *Experientia* **1986**, *42* (11-12), 1269–1271.
(331) Villanueva, A.; Cañete, M.; Hazen, M. J. *Mutagenesis* **1989**, *4* (2), 157–159.
(332) Burke Hurt, S. S.; Smith, J. M.; Wallace Hayes, A. *Toxicology* **1983**, *29* (1–2), 1–37.
(333) Lau, C.; Cameron, A. M.; Irsula, O.; Robinson, K. S. *Toxicol. Appl. Pharmacol.* **1986**, *86* (1), 22–32.
(334) Rio, B.; Parent-Massin, D.; Lautraite, S.; Hoellinger, H. *Hum. Exp. Toxicol.* **1997**, *16* (2), 115–122.
(335) Kojima, H.; Iida, M.; Katsura, E.; Kanetoshi, A.; Hori, Y.; Kobayashi, K. *Environ. Health Perspect.* **2003**, *111* (4), 497–502.
(336) Gupta, P. K. In *Biomarkers in Toxicology*; Gupta, R. C., Ed.; Academic Press: Boston, **2014**; pp 409–431.
(337) Riou, C.; Calliste, C. A.; Da Silva, A.; Guillaumot, D.; Rezazgui, O.; Sol, V.; Leroy-Lhez, S. *Photochem. Photobiol. Sci.* **2014**, *13* (4), 621.
(338) Barbat, A.; Gloaguen, V.; Sol, V.; Krausz, P. *Bioresour. Technol.* **2010**, *101* (16), 6538–6544.
(339) Bonnett, R.; Djelal, B. D.; Hamilton, P. A.; Martinez, G.; Wierrani, F. *J. Photochem. Photobiol. B* **1999**, *53* (1–3), 136–143.
(340) Tekrony, A. D.; Kelly, N. M.; Fage, B. A.; Cramb, D. T. *Photochem. Photobiol.* **2011**, *87* (4), 853–861.
(341) Nagata, T.; Nemoto, Y.; Hasezawa, S. In *International Review of Cytology*; Elsevier, **1992**; Vol. 132, pp 1–30.
(342) Cherrington, C. A.; Hinton, M.; Mead, G. C.; Chopra, I. In *Advances in Microbial Physiology*; Tempest, A. H. R. and D. W., Ed.; Academic Press, **1991**; Vol. 32, pp 87–108.
(343) Demmer, C. S.; Krogsgaard-Larsen, N.; Bunch, L. *Chem. Rev.* **2011**, *111* (12), 7981–8006.
(344) Wilson, J. R. H.; Sullivan, A. C.; Man, S. P.; Robson, L. Substituted phosphonate fluorescent sensors and use thereof. WO2004101579 A2, November 25, **2004**.
(345) Gutierrez, A. J.; Prisbe, E. J.; Rohloff, J. C. *Nucleosides Nucleotides Nucleic Acids* **2001**, *20* (4-7), 1299–1302.
(346) Marshall Gates, G. T. *J. Am. Chem. Soc. - J AM CHEM SOC* **1956**, *124* (42).
(347) Rice, K. C. *J. Med. Chem.* **1977**, *20* (1), 164–165.
(348) Liang, G.; Xu, Y.; Seiple, I. B.; Trauner, D. *J. Am. Chem. Soc.* **2006**, *128* (34), 11022–11023.
(349) Sindt, M.; Stephan, B.; Schneider, M.; Mieloszynski, J. L. *Phosphorus Sulfur Silicon Relat. Elem.* **2001**, *174* (1), 163–175.
(350) Weinkauf, J. R.; Cooper, S. W.; Schweiger, A.; Wamser, C. C. *J. Phys. Chem. A* **2003**, *107* (18), 3486–3496.
(351) Rudine, A. B.; DelFatti, B. D.; Wamser, C. C. *J. Org. Chem.* **2013**, *78* (12), 6040–6049.
(352) Maiti, N. C.; Ravikanth, M.; Mazumdar, S.; Periasamy, N. *J. Phys. Chem.* **1995**, *99* (47), 17192–17197.
(353) Maiti, N. C.; Mazumdar, S.; Periasamy, N. *J. Phys. Chem. B* **1998**, *102* (9), 1528–1538.
(354) Moliton, A.; Nunzi, J.-M. *Polym. Int.* **2006**, *55* (6), 583–600.

(355) Hollingsworth, J. V.; Richard, A. J.; Vicente, M. G. H.; Russo, P. S. *Biomacromolecules* **2012**, *13* (1), 60–72.
(356) Ormond, A. B.; Freeman, H. S. *Dyes Pigments* **2013**, *96* (2), 440–448.
(357) Dzwigaj, S.; Pezerat, H. *Free Radic. Res.* **1995**, *23* (2), 103–115.
(358) Clément, J.-L.; Ferré, N.; Siri, D.; Karoui, H.; Rockenbauer, A.; Tordo, P. *J. Org. Chem.* **2005**, *70* (4), 1198–1203.
(359) Ribó, J. M.; Crusats, J.; Farrera, J.-A.; Valero, M. L. *J. Chem. Soc. Chem. Commun.* **1994**, No. 6, 681–682.
(360) Dalla Via, L.; Marciani Magno, S. *Curr. Med. Chem.* **2001**, *8* (12), 1405–1418.
(361) Ghosh, A.; Maity, D. K.; Ravikanth, M. *New J. Chem.* **2012**, *36* (12), 2630–2641.
(362) Reeta, P. S.; Kanaparthi, R. K.; Giribabu, L. *J. Chem. Sci.* **2013**, *125* (2), 259–266.
(363) Yu, Z.; Pancholi, C.; Bhagavathy, G. V.; Kang, H. S.; Nguyen, J. K.; Ptaszek, M. *J. Org. Chem.* **2014**, *79* (17), 7910–7925.
(364) Kozma, E.; Kotowski, D.; Catellani, M.; Luzzati, S.; Cavazzini, M.; Bossi, A.; Orlandi, S.; Bertini, F. *Mater. Chem. Phys.* **2015**, *163*, 152–160.
(365) Whited, M. T.; Patel, N. M.; Roberts, S. T.; Allen, K.; Djurovich, P. I.; Bradforth, S. E.; Thompson, M. E. *Chem Commun* **2012**, *48* (2), 284–286.
(366) Wenger, O. S. *Coord. Chem. Rev.* **2015**, *282–283*, 150–158.
(367) D'Souza, F.; Ito, O. *Chem. Soc. Rev.* **2011**, *41* (1), 86–96.
(368) D'Souza, F.; Chitta, R.; Ohkubo, K.; Tasior, M.; Subbaiyan, N. K.; Zandler, M. E.; Rogacki, M. K.; Gryko, D. T.; Fukuzumi, S. *J. Am. Chem. Soc.* **2008**, *130* (43), 14263–14272.
(369) Zhao, H.; Liu, Z.; Zhang, X.; Tian, J.; Chen, C.; Zhu, Y.; Zheng, J. *Chin. J. Chem.* **2012**, *30* (8), 1766–1770.
(370) Das, S. K.; Song, B.; Mahler, A.; Nesterov, V. N.; Wilson, A. K.; Ito, O.; D'Souza, F. *J. Phys. Chem. C* **2014**, *118* (8), 3994–4006.
(371) Yamamoto, M.; Takano, Y.; Matano, Y.; Stranius, K.; Tkachenko, N. V.; Lemmetyinen, H.; Imahori, H. *Meet. Abstr.* **2014**, *MA2014-01* (32), 1238–1238.
(372) Liu, J.-Y.; El-Khouly, M. E.; Fukuzumi, S.; Ng, D. K. P. *ChemPhysChem* **2012**, *13* (8), 2030–2036.
(373) Maligaspe, E.; Hauwiller, M. R.; Zatsikha, Y. V.; Hinke, J. A.; Solntsev, P. V.; Blank, D. A.; Nemykin, V. N. *Inorg. Chem.* **2014**, *53* (17), 9336–9347.
(374) Wu, X.; Wu, W.; Cui, X.; Zhao, J.; Wu, M. *J. Mater. Chem. C* **2015**.
(375) Brizet, B.; Desbois, N.; Bonnot, A.; Langlois, A.; Dubois, A.; Barbe, J.-M.; Gros, C. P.; Goze, C.; Denat, F.; Harvey, P. D. *Inorg. Chem.* **2014**, *53* (7), 3392–3403.
(376) Baffreau, J.; Leroy-Lhez, S.; Vân Anh, N.; Williams, R. M.; Hudhomme, P. *Chem. – Eur. J.* **2008**, *14* (16), 4974–4992.
(377) Kölle, P.; Pugliesi, I.; Langhals, H.; Wilcken, R.; Esterbauer, A. J.; Vivie-Riedle, R. de; Riedle, E. *Phys. Chem. Chem. Phys.* **2015**, *17* (38), 25061–25072.
(378) Sánchez, R. S.; Gras-Charles, R.; Bourdelande, J. L.; Guirado, G.; Hernando, J. *J. Phys. Chem. C* **2012**, *116* (12), 7164–7172.
(379) Pu, S.; Ding, H.; Liu, G.; Zheng, C.; Xu, H. *J. Phys. Chem. C* **2014**, *118* (13), 7010–7017.
(380) Abad, S.; Kluciar, M.; Miranda, M. A.; Pischel, U. *J. Org. Chem.* **2005**, *70* (25), 10565–10568.
(381) Kwon, M. S.; Gierschner, J.; Seo, J.; Park, S. Y. *J. Mater. Chem. C* **2014**, *2* (14), 2552–2557.
(382) Swamy P, C. A.; Mukherjee, S.; Thilagar, P. *Inorg. Chem.* **2014**, *53* (10), 4813–4823.
(383) de Silva, A. P.; Fox, D. B.; Moody, T. S.; Weir, S. M. *Trends Biotechnol.* **2001**, *19* (1), 29–34.

(384) Dou, C.; Han, L.; Zhao, S.; Zhang, H.; Wang, Y. *J. Phys. Chem. Lett.* **2011**, *2* (6), 666–670.
(385) Crivat, G.; Taraska, J. W. *Trends Biotechnol.* **2012**, *30* (1), 8–16.
(386) Middleton, R. J.; Kellam, B. *Curr. Opin. Chem. Biol.* **2005**, *9* (5), 517–525.
(387) Ngen, E. J.; Xiao, L.; Rajaputra, P.; Yan, X.; You, Y. *Photochem. Photobiol.* **2013**, *89* (4), 841–848.
(388) Roquet, S.; Cravino, A.; Leriche, P.; Alévêque, O.; Frère, P.; Roncali, J. *J. Am. Chem. Soc.* **2006**, *128* (10), 3459–3466.
(389) Miranda, Y. C.; Pereira, L. L. A. L.; Barbosa, J. H. P.; Brito, H. F.; Felinto, M. C. F. C.; Malta, O. L.; Faustino, W. M.; Teotonio, E. E. S. *Eur. J. Inorg. Chem.* **2015**, *2015* (18), 3019–3027.
(390) Seneviratne, D. S.; Uddin, M. J.; Swayambunathan, V.; Schlegel, H. B.; Endicott, J. F. *Inorg. Chem.* **2002**, *41* (6), 1502–1517.
(391) Lord, R. L.; Allard, M. M.; Thomas, R. A.; Odongo, O. S.; Schlegel, H. B.; Chen, Y.-J.; Endicott, J. F. *Inorg. Chem.* **2013**, *52* (3), 1185–1198.
(392) Rehm, D.; Weller, A. *Z. Für Phys. Chem.* **1970**, *69* (3_4), 183–200.
(393) Rehm, D.; Weller, A. *Isr. J. Chem.* **1970**, *8* (2), 259–271.
(394) Főrster, T. *Discuss. Faraday Soc.* **1959**, *27* (0), 7–17.
(395) Dexter, D. L. *J. Chem. Phys.* **1953**, *21* (5), 836.
(396) Förster, T. *Z. Für Naturforscher* **1949**, *4a*, 321–327.
(397) Khan, T. K.; Ravikanth, M. *Tetrahedron* **2012**, *68* (3), 830–840.
(398) Khan, T. K.; Bröring, M.; Mathur, S.; Ravikanth, M. *Coord. Chem. Rev.* **2013**, *257* (15–16), 2348–2387.
(399) Li, C.-Y.; Zhang, X.-B.; Qiao, L.; Zhao, Y.; He, C.-M.; Huan, S.-Y.; Lu, L.-M.; Jian, L.-X.; Shen, G.-L.; Yu, R.-Q. *Anal. Chem.* **2009**, *81* (24), 9993–10001.
(400) Moura, N. M. M.; Núñez, C.; Faustino, M. A. F.; Cavaleiro, J. A. S.; Neves, M. G. P. M. S.; Capelo, J. L.; Lodeiro, C. *J. Mater. Chem. C* **2014**, *2* (24), 4772–4783.
(401) Lu, J.-Z.; Tan, X.-C.; Huang, J.-W.; Dong, C.-H.; Fu, B.; Yu, H.-C.; Ji, L.-N. *Transit. Met. Chem.* **2005**, *30* (5), 643–649.
(402) Sun, X.; Chen, G.; Zhang, J. *Dyes Pigments* **2008**, *76* (2), 499–501.
(403) Getman, R. B.; Bae, Y.-S.; Wilmer, C. E.; Snurr, R. Q. *Chem. Rev.* **2012**, *112* (2), 703–723.
(404) Gunsteren, W. F. van; Weiner, P. K.; Wilkinson, A. J. *Computer Simulation of Biomolecular Systems: Theoretical and Experimental Applications*; Springer Science & Business Media, **2013**.
(405) Meneksedag-Erol, D.; Tang, T.; Uludağ, H. *Biomaterials* **2014**, *35* (25), 7068–7076.
(406) Leach, A. R. *Molecular Modelling: Principles and Applications*; Pearson Education, **2001**.
(407) Born, M.; Oppenheimer, R. *Ann. Phys.* **1927**, *389* (20), 457–484.
(408) Hehre, W. J. *A guide to molecular mechanics and quantum chemical calculations*; Wavefunction, Inc: Irvine, CA, **2003**.
(409) Jensen, F. *Introduction to computational chemistry*, 2nd ed.; John Wiley & Sons: Chichester, England ; Hoboken, NJ, **2007**.
(410) Alder, B. J.; Wainwright, T. E. *J. Chem. Phys.* **1959**, *31* (2), 459–466.
(411) Gibson, J. B.; Goland, A. N.; Milgram, M.; Vineyard, G. H. *Phys. Rev.* **1960**, *120* (4), 1229–1253.
(412) Rahman, A. *Phys. Rev.* **1964**, *136* (2A), A405–A411.
(413) Schrödinger, E. *Phys. Rev.* **1926**, *28* (6), 1049–1070.
(414) Echenique, P.; Alonso, J. L. *Mol. Phys.* **2007**, *105* (23-24), 3057–3098.

(415) Cramer, C. J. *Essentials of computational chemistry: theories and models*, 2nd ed.; Wiley: Chichester, West Sussex, England ; Hoboken, NJ, **2004**.
(416) Jones, R. O.; Gunnarsson, O. *Rev. Mod. Phys.* **1989**, *61* (3), 689–746.
(417) Kohn, W.; Sham, L. J. *Phys. Rev.* **1965**, *140* (4A), A1133–A1138.
(418) Perdew, J. P.; Burke, K.; Wang, Y. *Phys. Rev. B* **1996**, *54* (23), 16533–16539.
(419) Lee, C.; Yang, W.; Parr, R. G. *Phys. Rev. B* **1988**, *37* (2), 785.
(420) Miehlich, B.; Savin, A.; Stoll, H.; Preuss, H. *Chem. Phys. Lett.* **1989**, *157* (3), 200–206.
(421) Becke, A. D. *J. Chem. Phys.* **1993**, *98* (2), 1372.
(422) *Fundamentals of time-dependent density functional theory*; Marques, M. A. L., Maitra, N. T., Nogueira, F. M. S., Gross, E. K. U., Rubio, A., Eds.; Lecture notes in physics; Springer: Heidelberg, **2012**.
(423) Davidson, E. R.; Feller, D. *Chem. Rev.* **1986**, *86* (4), 681–696.
(424) Ditchfield, R.; Hehre, W. J.; Pople, J. A. *J. Chem. Phys.* **1971**, *54* (2), 724–728.
(425) Hehre, W. J.; Stewart, R. F.; Pople, J. A. *J. Chem. Phys.* **1969**, *51* (6), 2657–2664.
(426) Clark, T.; Chandrasekhar, J.; Spitznagel, G. W.; Schleyer, P. V. R. *J. Comput. Chem.* **1983**, *4* (3), 294–301.
(427) DiLoreto, D. A.; Das, T.; del Cerro, C.; Cox, C.; del Cerro, M. *Curr. Eye Res.* **1997**, *16* (11), 1159–1165.
(428) Koide, K.; Garner, A. L.; Song, F. Hydroxymethyl fluorescein derivatives for use as biological markers and dyes. US8084627 B2, December 27, **2011**.
(429) Mathew, T.; Kundan, S.; Abdulsamad, M. I.; Menon, S.; Dharan, B. S.; Jayakumar, K. *Ann. Thorac. Surg.* **2014**, *97* (1), e27–e28.
(430) Kolb, H. C.; Sharpless, K. B. *Drug Discov. Today* **2003**, *8* (24), 1128–1137.
(431) Tron, G. C.; Pirali, T.; Billington, R. A.; Canonico, P. L.; Sorba, G.; Genazzani, A. A. *Med. Res. Rev.* **2008**, *28* (2), 278–308.
(432) Qiu, S. *Synthèse de porphyrines hydrosolubles à marqueurs fluorescents*; Rapport Master 2; Limoges University, **2012**; p 44.
(433) Endo, I. *Nano/Micro Biotechnology*; Springer Science & Business Media, **2010**.
(434) Pérez Guarin, S. A.; Tsang, D.; Skene, W. G. *New J. Chem.* **2007**, *31* (2), 210.
(435) Punidha, S.; Sinha, J.; Kumar, A.; Ravikanth, M. *J. Org. Chem.* **2008**, *73* (1), 323–326.
(436) Himo, F.; Lovell, T.; Hilgraf, R.; Rostovtsev, V. V.; Noodleman, L.; Sharpless, K. B.; Fokin, V. V. *J. Am. Chem. Soc.* **2005**, *127* (1), 210–216.
(437) Singh, I.; Freeman, C.; Heaney, F. *Eur. J. Org. Chem.* **2011**, *2011* (33), 6739–6746.
(438) Huisgen, R. *Angew. Chem. Int. Ed. Engl.* **1963**, *2* (11), 633–645.
(439) Huisgen, R. *Angew. Chem.* **1963**, *75* (13), 604–637.
(440) Tornøe, C. W.; Christensen, C.; Meldal, M. *J. Org. Chem.* **2002**, *67* (9), 3057–3064.
(441) Ouchi, M.; Inoue, Y.; Liu, Y.; Nagamune, S.; Nakamura, S.; Wada, K.; Hakushi, T. *Bull. Chem. Soc. Jpn.* **1990**, *63* (4), 1260–1262.
(442) Moussodia, R.-O.; Acherar, S.; Bordessa, A.; Vanderesse, R.; Jamart-Grégoire, B. *Tetrahedron* **2012**, *68* (24), 4682–4692.
(443) Bonnett, R.; McGarvey, D. J.; Harriman, A.; Land, E. J.; Truscott, T. G.; Winfield, U.-J. *Photochem. Photobiol.* **1988**, *48* (3), 271–276.
(444) Senge, M. O. *Chem Commun* **2006**, No. 3, 243–256.
(445) Colominas, C.; Eixarch, L.; Fors, P.; Lang, K.; Nonell, S.; Teixidó, J.; Trull, F. R. *J. Chem. Soc. Perkin Trans. 2* **1996**, No. 5, 997–1004.
(446) Kobori, Y.; Shibano, Y.; Endo, T.; Tsuji, H.; Murai, H.; Tamao, K. *J. Am. Chem. Soc.* **2009**, *131* (5), 1624–1625.
(447) Tamiaki, H.; Fukai, K.; Shimazu, H.; Shoji, S. *Photochem. Photobiol.* **2014**, *90* (1), 121–128.
(448) Chai, J.-D.; Head-Gordon, M. *J. Chem. Phys.* **2008**, *128* (8), 084106.

(449) Chai, J.-D.; Head-Gordon, M. *Phys. Chem. Chem. Phys.* **2008**, *10* (44), 6615.
(450) Kodama, Y.; Nishihata, K.; Nishio, M.; Nakagawa, N. *Tetrahedron Lett.* **1977**, *18* (24), 2105–2108.
(451) Shibasaki, K.; Fujii, A.; Mikami, N.; Tsuzuki, S. *J. Phys. Chem. A* **2006**, *110* (13), 4397–4404.
(452) Albertí, M.; Aguilar, A.; Huarte-Larrañaga, F.; Lucas, J. M.; Pirani, F. *J. Phys. Chem. A* **2014**, *118* (9), 1651–1662.
(453) Fabian, W. M.; Schuppler, S.; Wolfbeis, O. S. *J. Chem. Soc. Perkin Trans. 2* **1996**, No. 5, 853–856.
(454) Nguyen, K. A.; Day, P. N.; Pachter, R. *J. Phys. Chem. A* **1999**, *103* (46), 9378–9382.
(455) Dulski, M.; Kempa, M.; Kozub, P.; Wójcik, J.; Rojkiewicz, M.; Kuś, P.; Szurko, A.; Ratuszna, A.; Wrzalik, R. *Spectrochim. Acta. A. Mol. Biomol. Spectrosc.* **2013**, *104*, 315–327.
(456) Zhang, M.-J.; Guo, Y.-R.; Fang, G.-Z.; Pan, Q.-J. *Comput. Theor. Chem.* **2013**, *1019*, 94–100.
(457) Yanai, T.; Tew, D. P.; Handy, N. C. *Chem. Phys. Lett.* **2004**, *393* (1-3), 51–57.
(458) Weber, G.; Teale, F. W. J. *Trans Faraday Soc* **1958**, *54*, 640–648.
(459) Sjöback, R.; Nygren, J.; Kubista, M. *Spectrochim. Acta. A. Mol. Biomol. Spectrosc.* **1995**, *51* (6), L7–L21.
(460) Bajju, G. D.; Devi, G.; Katoch, S.; Bhagat, M.; Deepmala; Ashu; Kundan, S.; Anand, S. K. *Bioinorg. Chem. Appl.* **2013**, *2013*.
(461) Poulsen, L.; Jazdzyk, M.; Communal, J.-E.; Sancho-García, J. C.; Mura, A.; Bongiovanni, G.; Beljonne, D.; Cornil, J.; Hanack, M.; Egelhaaf, H.-J.; Gierschner, J. *J. Am. Chem. Soc.* **2007**, *129* (27), 8585–8593.
(462) Bhaumik, J.; Weissleder, R.; McCarthy, J. R. *J. Org. Chem.* **2009**, *74* (16), 5894–5901.
(463) Mandal, S.; Bhattacharyya, S.; Borovkov, V.; Patra, A. *J. Phys. Chem. C* **2011**, *115* (49), 24029–24036.
(464) Lee, D.-E.; Koo, H.; Sun, I.-C.; Ryu, J. H.; Kim, K.; Kwon, I. C. *Chem Soc Rev* **2012**, *41* (7), 2656–2672.
(465) Ng, K. K.; Zheng, G. *Chem. Rev.* **2015**, *115* (19), 11012–11042.
(466) Yang, Y.; Weaver, M. N.; Merz, K. M. *J. Phys. Chem. A* **2009**, *113* (36), 9843–9851.
(467) Frisch, M. J.; Trucks, G. W.; Schlegel, H. B.; Scuseria, G. E.; Robb, M. A.; Cheeseman, J. R.; Scalmani, G.; Barone, V.; Mennucci, B.; Petersson, G. A.; Nakatsuji, H.; Caricato, M.; Li, X.; Hratchian, H. P.; Izmaylov, A. F.; Bloino, J.; Zheng, G.; Sonnenberg, J. L.; Hada, M.; Ehara, M.; Toyota, K.; Fukuda, R.; Hasegawa, J.; Ishida, M.; Nakajima, T.; Honda, Y.; Kitao, O.; Nakai, H.; Vreven, T.; Montgomery, Jr., J. A.; Peralta, J. E.; Ogliaro, F.; Bearpark, M.; Heyd, J. J.; Brothers, E.; Kudin, K. N.; Staroverov, V. N.; Kobayashi, R.; Normand, J.; Raghavachari, K.; Rendell, A.; Burant, J. C.; Iyengar, S. S.; Tomasi, J.; Cossi, M.; Rega, N.; Millam, N. J.; Klene, M.; Knox, J. E.; Cross, J. B.; Bakken, V.; Adamo, C.; Jaramillo, J.; Gomperts, R.; Stratmann, R. E.; Yazyev, O.; Austin, A. J.; Cammi, R.; Pomelli, C.; Ochterski, J. W.; Martin, R. L.; Morokuma, K.; Zakrzewski, V. G.; Voth, G. A.; Salvador, P.; Dannenberg, J. J.; Dapprich, S.; Daniels, A. D.; Farkas, O.; Foresman, J. B.; Ortiz, J. V.; Cioslowski, J.; Fox, D. J. *Gaussian 09, Revision A.1*; Gaussian, Inc.: Wallingford, CT, 2009.

Appendices

Table A1: Computed optical properties obtained with a) B3LYP and b) ωB97XD (absorption wavelength, vertical transition energies, oscillator strength, configuration interaction (CI) description) for compound **15**.

A) B3LYP

Excited states	λ (nm)	E (eV)	f	MO contribution*
1	555.3	2.23	0.05	H-1→L+1 (40 %) H→L (58 %)
2	554.3	2.24	0.06	H-1→L (-41 %) H→L+1 (58 %)
3	408.8	3.03	1.62	H-2→L+1 (24 %) H-1→L (53 %) H→L+1 (38 %)
4	405.3	3.06	1.45	H-2→L (-15 %) H-1→L+1 (56 %) H→L (-39 %)

B) ωB97XD

Excited states	λ (nm)	E (eV)	f	MO contribution*
1	564.3	2.20	0.03	H→L (54 %) H→L+1 (-45 %)
2	564.1	2.20	0.03	H-1→L (45 %) H→L+1 (54 %)
3	380.0	3.26	1.96	H-1→L (54 %) H→L (10 %) H→L+1 (-45 %)
4	379.0	3.27	1.85	H-1→L+1 (54 %) H→L (45 %) H→L+1 (-10 %)

Table A2: Computed optical properties obtained with a) B3LYP and b) ωB97XD (absorption wavelength, vertical transition energies, oscillator strength, configuration interaction (CI) description) for compound **21**.

A) B3LYP

Excited state	λ (nm)	E (eV)	f	MO contribution*
1	428.8	2.89	0.59	H-2→L (15 %) H→L (68 %)

.

B) ωB97XD

Excited state	λ (nm)	E (eV)	f	MO contribution*
1	387.0	3.20	0.80	H-1→L (-11 %) H→L (69 %)

Table A3: Calculated optical properties (vertical transition wavelengths and energies, oscillator strength, configuration interaction description) as obtained with a) B3LYP and b) ωB97XD functionals for compound **24** (folded form).

A) B3LYP

Excited states	λ (nm)	E (eV)	f	MO contribution*
1	566.9	2.19	0.01	H-1→L+2 (14 %) **H→L (68 %)** H→L+1 (-13 %)
2	555.3	2.23	0.07	H-1→L+1 (35 %) H-1→L+2 (19 %) H→L+1 (-28 %) H→L+2 (50 %)
3	553.9	2.28	0.05	H-1→L+1 (19 %) H-1→L+2 (-32 %) **H→L (19 %)** H→L+1 (50 %) H→L+2 (28 %)
4	492.0	2.52	0.01	**H-1→L (70 %)**
5	422.3	2.94	0.06	H-4→L (63 %) *H-2→L (-25 %)*
6	417.1	2.97	0.40	*H-4→L (26 %)* *H-2→L (54 %)* **H-2→L+1 (-18 %)** H-1→L+1 (19 %) H-1→L+2 (-14 %) H→L+2 (-12 %)
7	407.6	3.04	1.18	**H-2→L+1 (42 %)** **H-2→L+2 (-22 %)** H-1→L+1 (35 %) H-1→L+2 (24 %) H→L+1 (16 %) H→L+2 (-25 %)
8	406.9	3.05	0.38	*H-2→L (13 %)* H-2→L+1 (53 %) H-1→L+1 (-19 %) H-1→L+2 (-30 %) H→L+1 (-20 %) H→L+2 (13 %)
9	402.8	3.08	0.58	*H-2→L (-15 %)* *H-2→L+2 (54 %)* H-1→L+1 (31 %) H-1→L+2 (-14 %) H→L+2 (-22 %) *H→L+3 (12 %)*
10	401.7	3.09	0.78	*H-2→L (-20 %)* H-2→L+2 (-37 %) H-1→L+1 (13 %) H-1→L+2 (-30 %) H→L+1 (-21 %) *H→L+3 (38 %)*
11	400.8	3.09	0.50	*H-2→L (15 %)* **H-2→L+2 (13 %)** H-1→L+1 (-14 %) H-1→L+2 (23 %) H→L+1 (16 %) H→L+3 (58 %)

B) ωB97XD

Excited states	λ (nm)	E (eV)	f	MO contribution*
1	572.8	2.16	0.04	H-1→L+1 (43 %) H→L (54 %)
2	571.6	2.17	0.07	H-1→L (-43 %) H→L+1 (54 %)
3	388.8	3.19	1.16	*H-2→L+2 (44 %)* H-1→L (34 %) H-1→L+1 (25 %) H→L (-19 %) H→L+1 (28 %)
4	384.5	3.22	1.77	H-1→L (-35 %) H-1→L+1 (42 %) H→L (-32 %) H→L+1 (-28 %)
5	377.0	3.29	1.61	H-2→L (-10 %) *H-2→L+2 (50 %)* H-1→L (-24 %) H-1→L+1 (-27 %) H→L (21 %) H→L+1 (-19 %)
8	306.5	4.04	0.12	H-9→L+2 (10 %) H-7→L+2 (-23 %) H-5→L+2 (-14 %) H-4→L (-14 %) *H-4→L+2 (55 %)* *H-2→L+2 (11 %)*

*In black : transfer from porphyrin to porphyrin. In **red** : transfer from fluorescein to porphyrin orbitals. In *blue* : from fluorescein to fluorescein.

Table A4: Calculated optical properties (vertical transition wavelengths and energies, oscillator strength, configuration interaction description) as obtained with a) B3LYP and b) ωB97XD functionals for compound **24** (linear form).

A) B3LYP

Excited states	λ (nm)	E (eV)	f	MO contribution*
1	542.7	2.28	0.04	H-1→L+2 (42 %) H→L+1 (56 %)
2	542.4	2.29	0.04	H-1→L+1 (-42 %) H→L+2 (56 %)
3	491.5	2.52	0.00	H→L (71 %)
4	446.3	2.78	0.00	H-1→L (71 %)
5	426.0	2.91	0.00	H-4→L (70 %)
6	412.1	3.01	0.64	H-5→L (-16 %) *H-2→L (67 %)*
7	399.4	3.10	1.66	H-3→L+2 (16 %) H-1→L+1 (52 %) H-1→L+2 (-15 %) H→L+1 (11 %) H→L+2 (40 %)
8	397.4	3.12	1.59	H-1→L+1 (16 %) H-1→L+2 (54 %) H→L+1 (-40 %) H→L+2 (12 %)

B) ωB97XD

Excited states	λ (nm)	E (eV)	f	MO contribution*
1	561.2	2.21	0.02	H-1→L (-44 %) H-1→L+1 (-11 %) H→L (-13 %) H→L+1 (-52 %)
2	561.1	2.21	0.02	H-1→L (11 %) H-1→L+1 (44 %) H→L (52 %) H→L+1 (13 %)
3	380.0	3.26	1.41	*H-4→L+2 (-10 %)* *H-2→L+2 (64 %)* H-1→L (19 %) H→L+1 (16 %)
4	377.7	3.28	1.28	*H-2→L+2 (-24 %)* H-1→L (47 %) H-1→L+1 (-17 %) H→L (14 %) H→L+1 (40 %)
5	377.3	3.29	1.93	H-1→L (17 %) H-1→L+1 (51 %) H→L (-43 %) H→L+1 (14 %)

*In black : transfer from porphyrin to porphyrin. In *blue* : from fluorescein to fluorescein.

Table A5: Calculated optical properties (vertical transition wavelengths and energies, oscillator strength, configuration interaction description) as obtained with a) B3LYP and b) ωB97XD functionals for compound **26**.

A) B3LYP

Excited states	λ (nm)	E (eV)	f	MO contribution*
1	543.36	2.2818	0.0351	H-1→L+2 (42 %) H→L+1 (56 %)
2	542.87	2.2839	0.0468	H-1→L+1 (42 %) H→L+2 (56 %)
5	420.66	2.9474	0.0014	*H-4→L (70 %)*
6	413.78	2.9963	0.8932	*H-8→L (-14 %)* *H-2→L (67 %)* H-1→L+1 (-11 %)
7	401.83	3.0855	1.2937	H-3→L+2 (-24 %) *H-2→L (14 %)* H-1→L+1 (51 %) H→L+2 (-38 %)
8	399.14	3.1063	1.4061	H-3→L+1 (17 %) H-1→L+2 (54 %) H→L+1 (40 %)
9	390.06	3.1786	0.0087	H-2→L+1 (-32 %) H-2→L+2 (63 %)
10	389.95	3.1795	0.0085	H-2→L+1 (62 %) H-2→L+2 (32 %)

B) ωB97XD

Excited states	λ (nm)	E (eV)	f	MO contribution*
1	561.41	2.2084	0.0233	H-1→L (34 %) H-1→L+1 (-30 %) H→L (35 %) H→L+1 (40 %)
2	561.10	2.2096	0.0180	H-1→L (-30 %) H-1→L+1 (-34 %) H→L (40 %) H→L+1 (-35 %)
3	382.28	3.2433	1.9094	*H-2→L+2 (59 %)* H-1→L (25 %) H-1→L+1 (-13 %) H→L (-11 %) H→L+1 (-20 %)
4	377.54	3.2840	1.7972	H-1→L (35 %) H-1→L+1 (41 %) H→L (34 %) H→L+1 (-30 %)
5	377.04	3.2883	0.8552	*H-2→L+2 (35 %)* H-1→L (-33 %) H-1→L+1 (33 %) H→L (-28 %) H→L+1 (28 %)

*In black : transfer from porphyrin to porphyrin. In **red** : transfer from fluorescein to porphyrin orbitals. In *blue* : from fluorescein to fluorescein.

Table A6: Calculated optical properties (vertical transition wavelengths and energies, oscillator strength, configuration interaction description) as obtained with a) B3LYP and b) ωB97XD functionals for compound **28**.

A) B3LYP

Excited states	λ (nm)	E (eV)	f	MO contribution*
1	542.09	2.2872	0.0356	H-1→L+2 (42 %) H→L+1 (56 %)
2	541.69	2.2889	0.0391	H-1→L+1 (43 %) H→L+2 (56 %)
5	424.71	2.9193	0.0007	*H-4→L (70 %)*
6	412.31	3.0071	0.6943	H-5→L (-16 %) *H-2→L (67 %)*
7	398.84	3.1086	1.6244	H-3→L+2 (14 %) H-1→L+1 (53 %) H-1→L+2 (12 %) H→L+2 (40 %)
8	397.15	3.1218	1.5977	H-1→L+1 (-13 %) H-1→L+2 (54 %) H→L+1 (41 %)

B) ωB97XD

Excited states	λ (nm)	E (eV)	f	MO contribution*
1	560.78	2.2109	0.0196	H-1→L+1 (-45 %) H→L (52 %) H→L+1 (-11 %)
2	560.58	2.2117	0.0193	H-1→L (45 %) H→L (11 %) H→L+1 (52 %)
3	379.15	3.2700	2.2099	*H-2→L+2 (48 %)* H-1→L (38 %) H→L+1 (-32 %)
4	377.29	3.2862	1.8771	H-1→L (-12 %) H-1→L+1 (53 %) H→L (45 %) H→L+1 (10 %)
5	376.61	3.2921	0.5640	*H-2→L+2 (49 %)* H-1→L (-36 %) H→L+1 (31 %)

*In black : transfer from porphyrin to porphyrin. In *blue* : from fluorescein to fluorescein.

Excited States diagrams

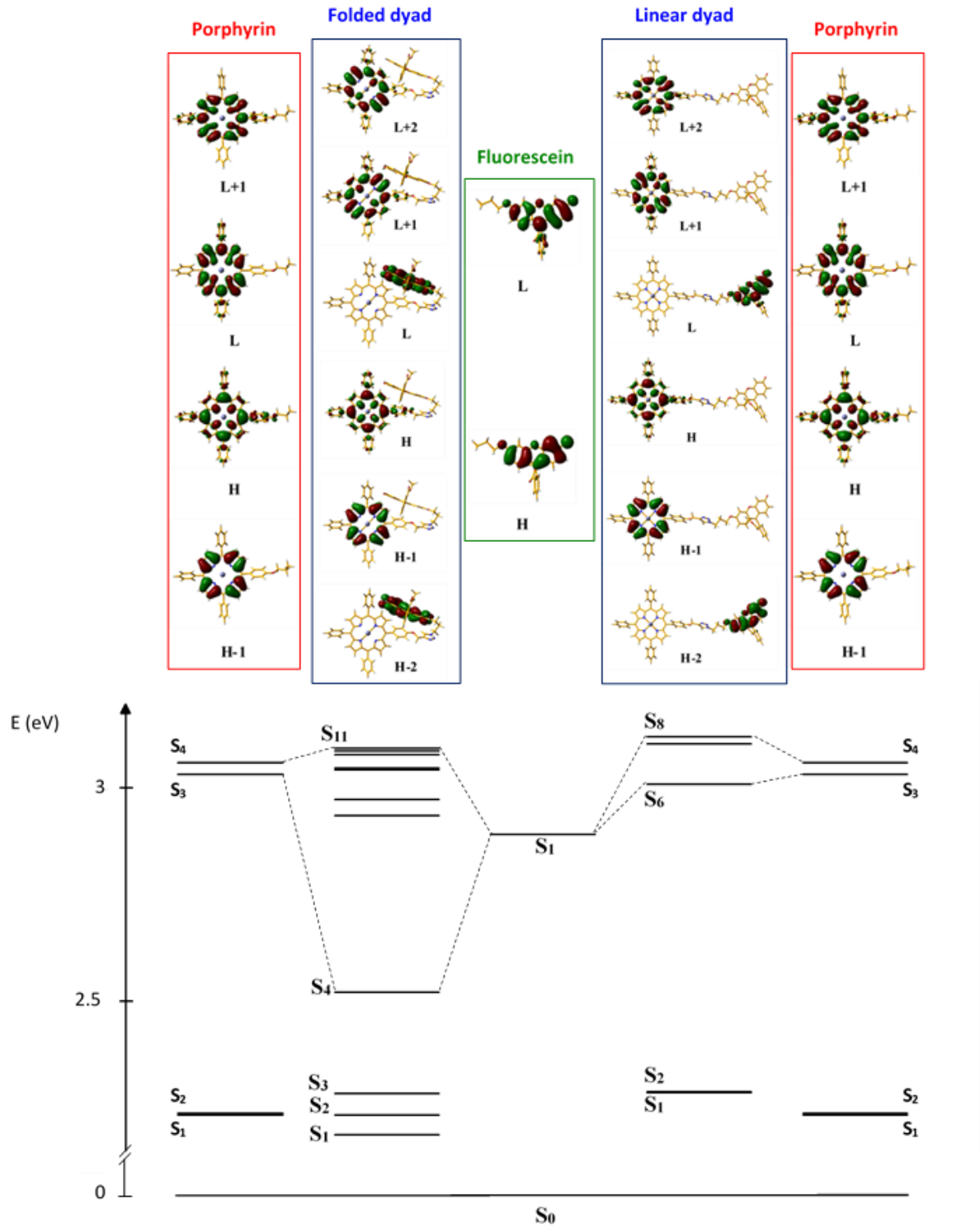

Figure A158: Molecular orbitals and excited states involved in dyad **24** and references **15** and **21** with B3LYP functional.

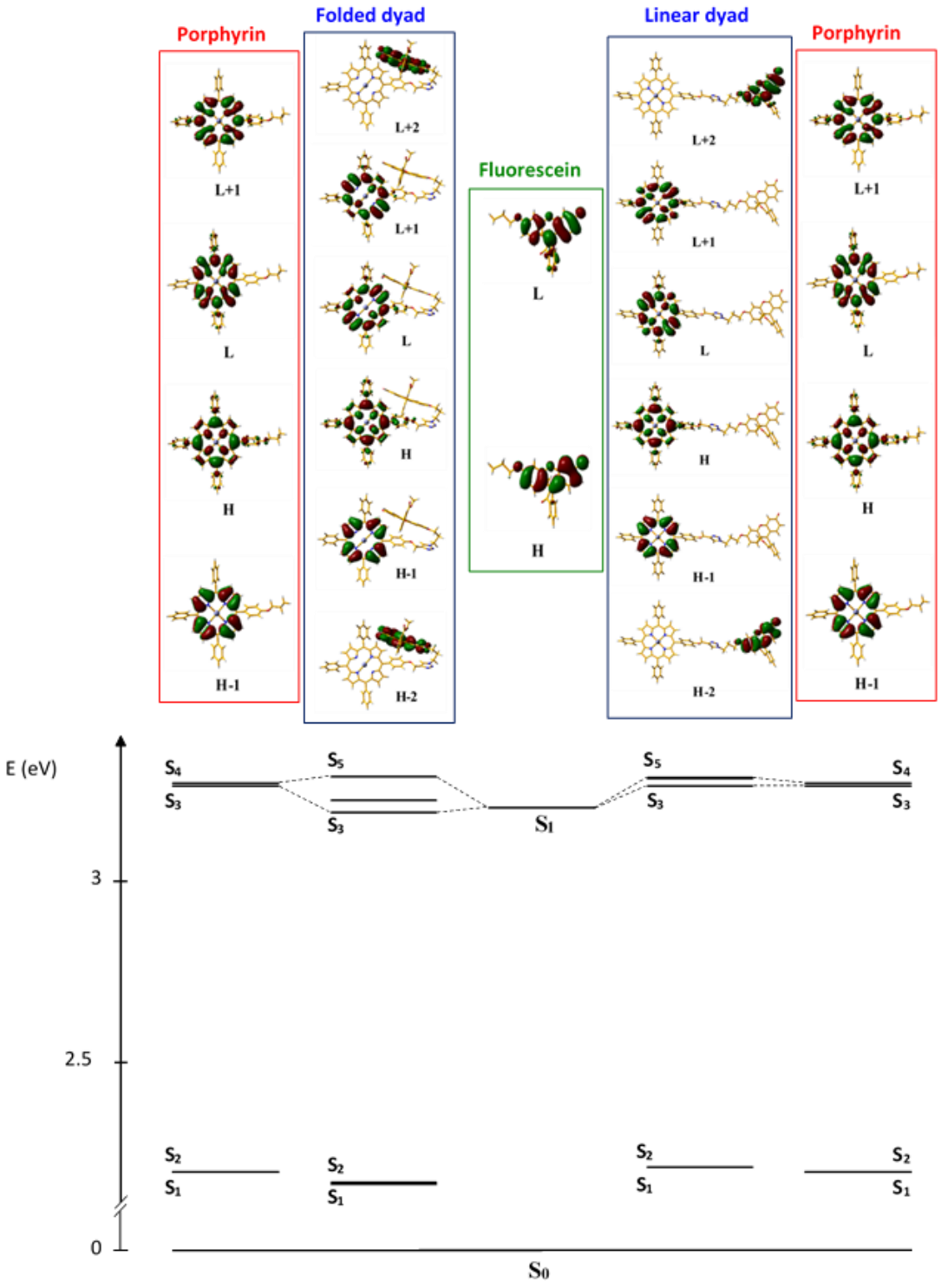

Figure A159: Molecular orbitals and excited states involved in dyad **24** and references **15** and **21** with ωB97XD functional.

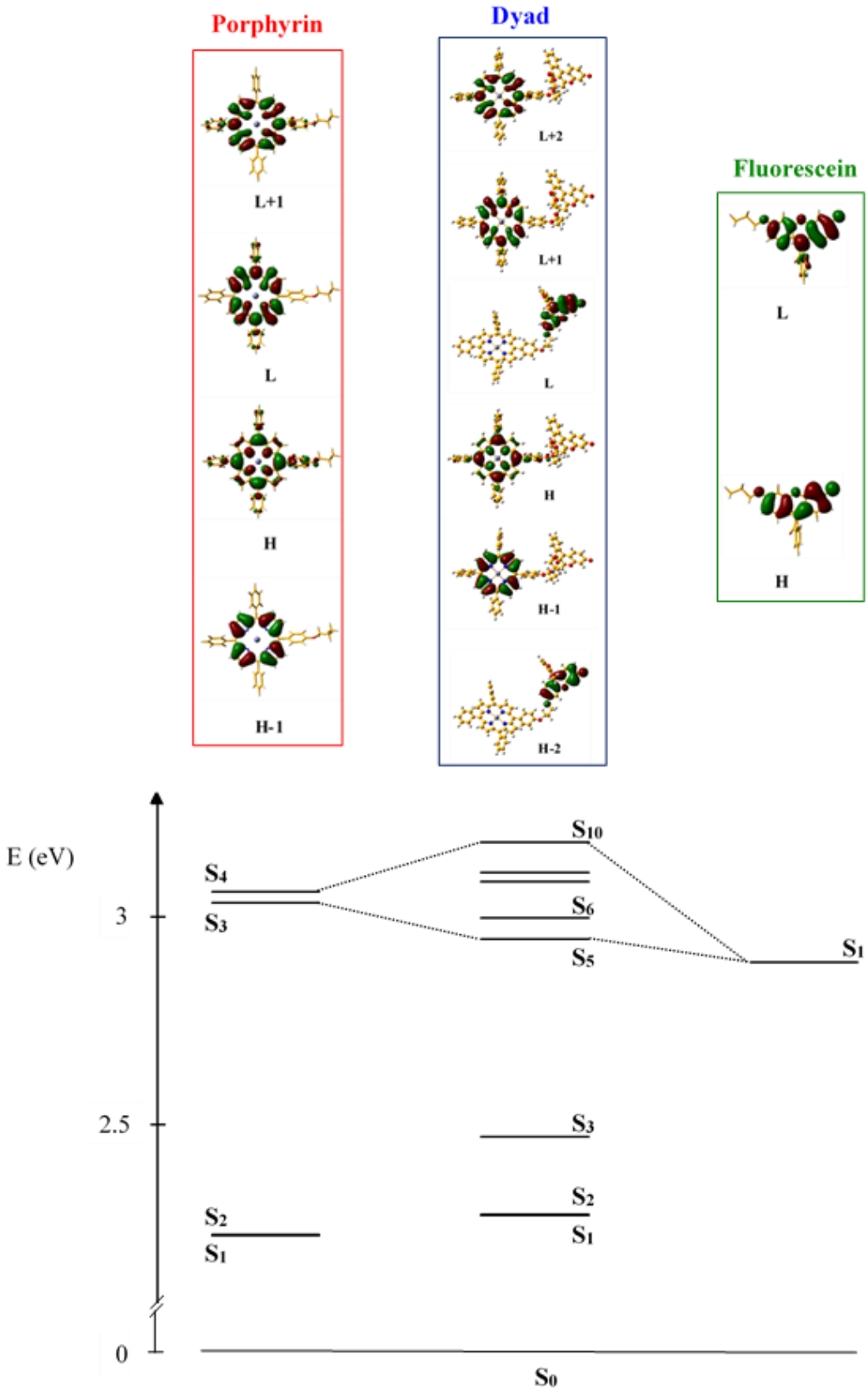

Figure A160: Molecular orbitals and excited states involved in dyad **26** and references **15** and **21** with B3LYP functional.

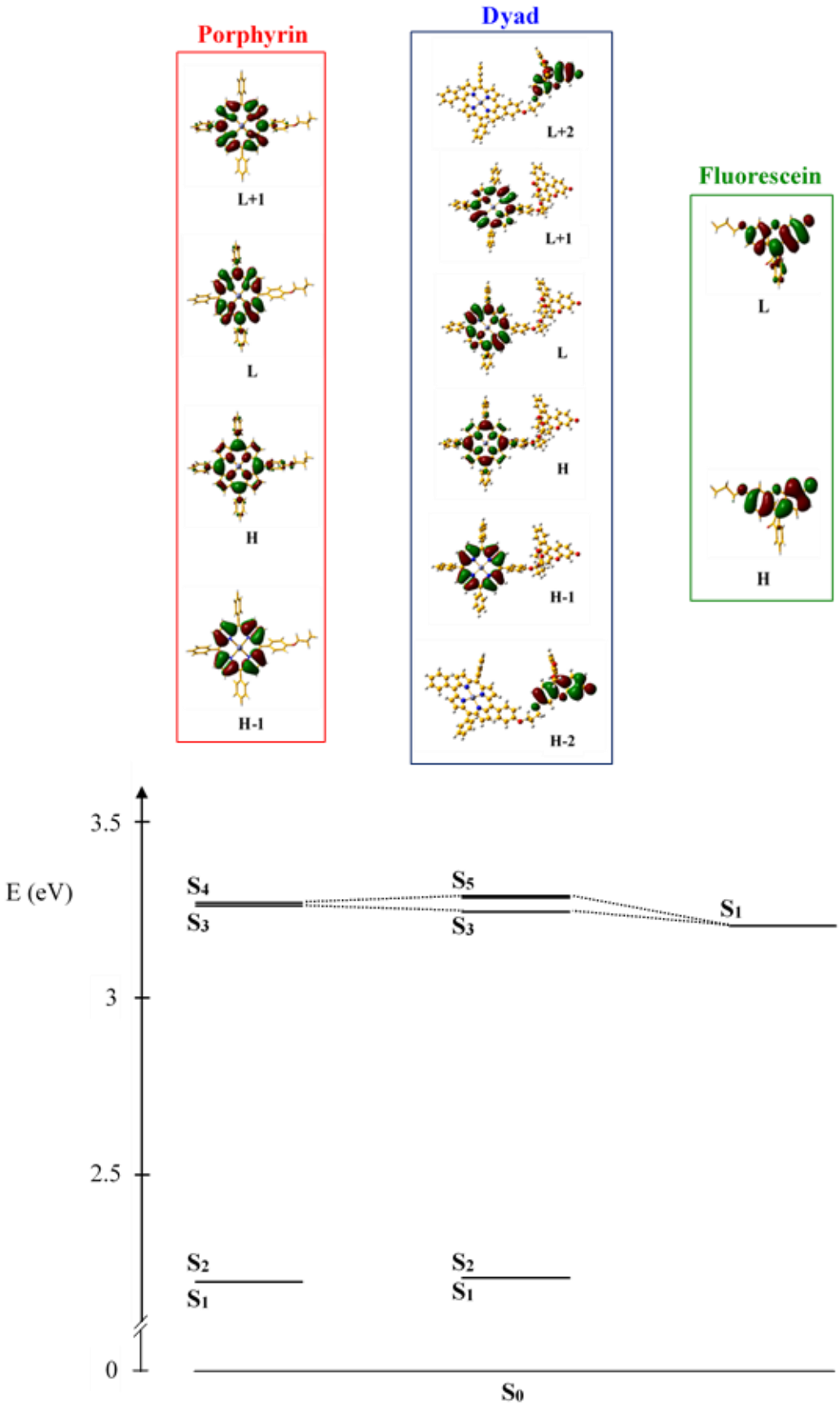

Figure A161: Molecular orbitals and excited states involved in dyad **26** and references **15** and **21** with ωB97XD functional.

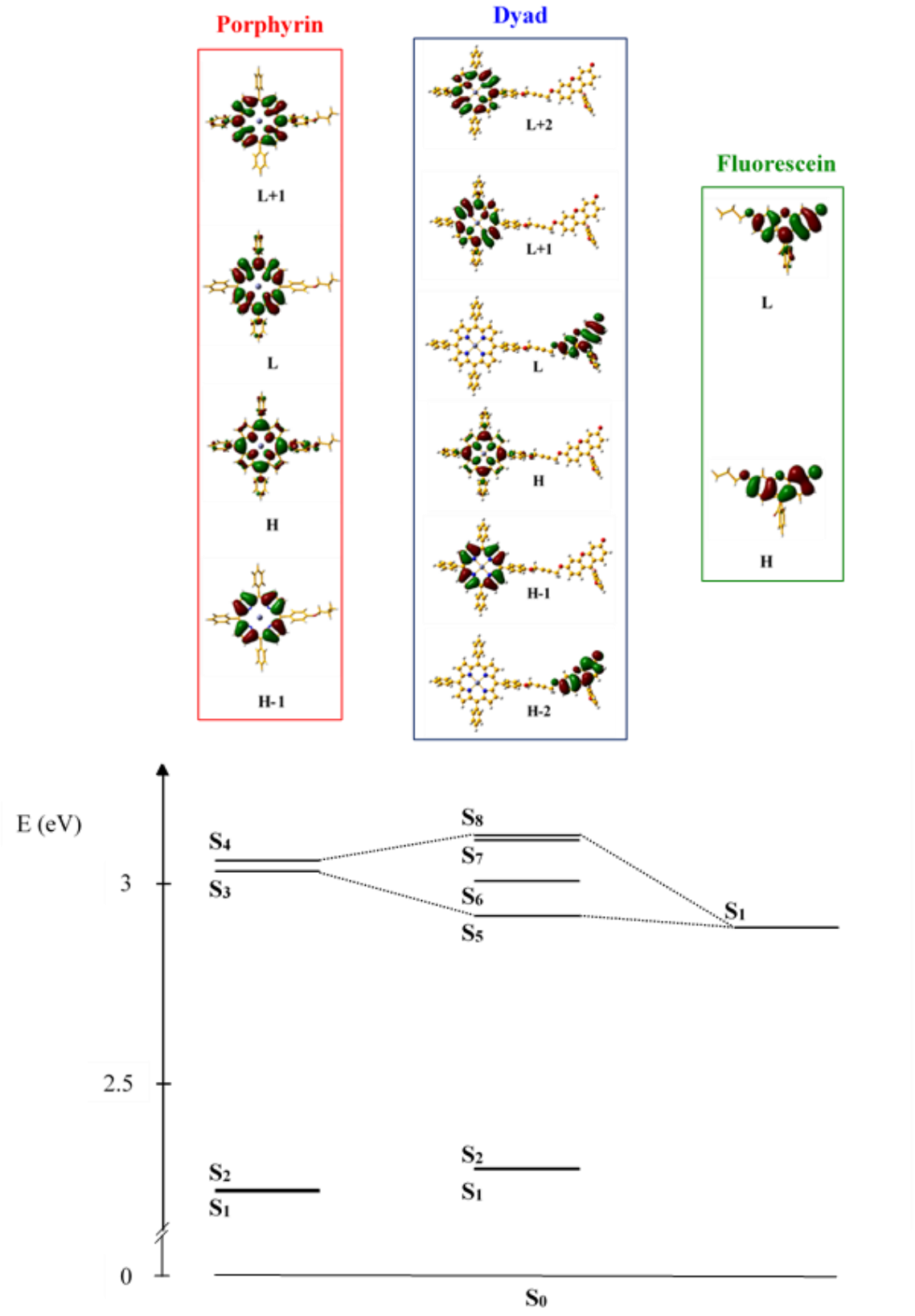

Figure A162: Molecular orbitals and excited states involved in dyad **28** and references **15** and **21** with B3LYP functional.

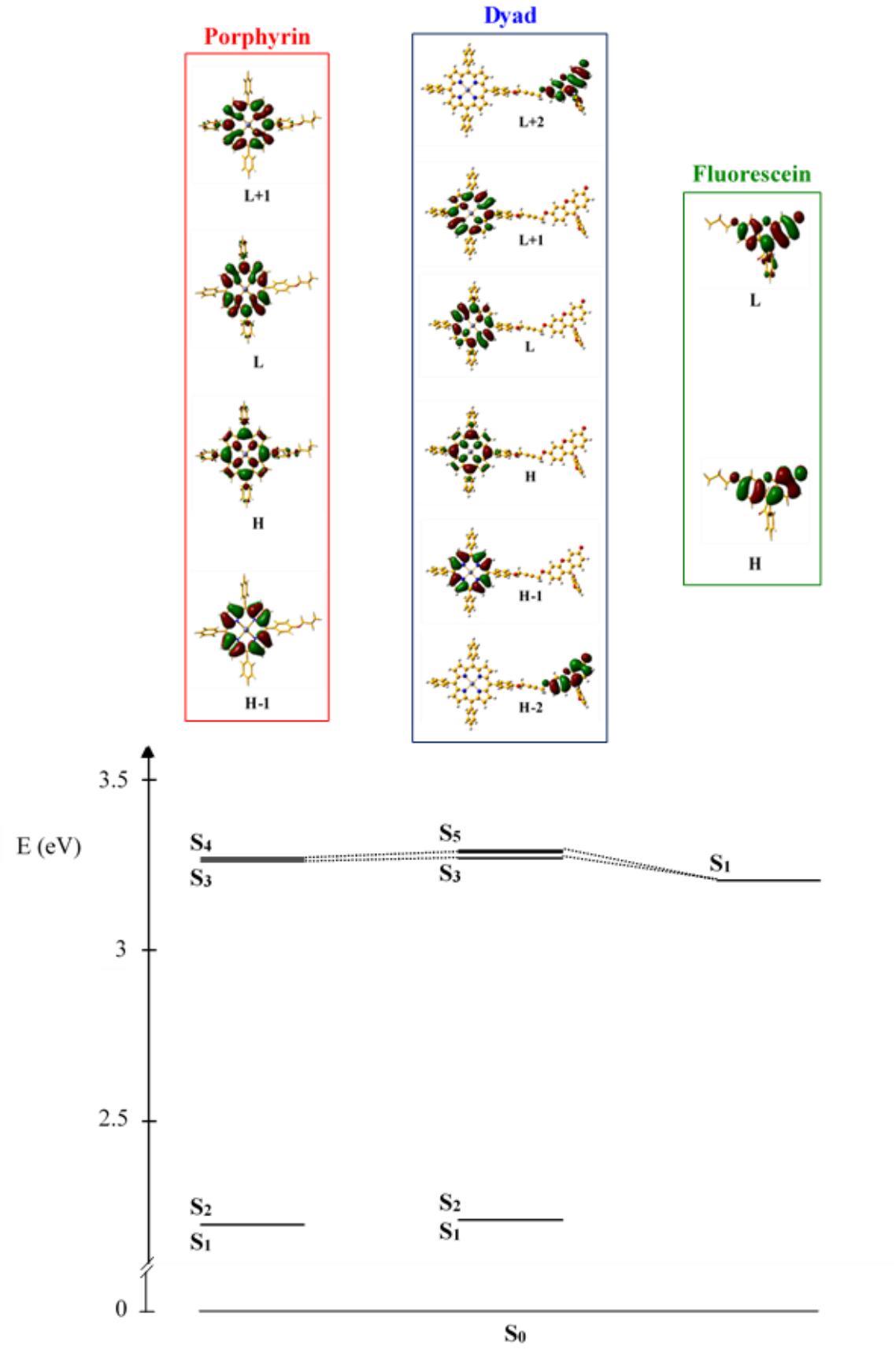

Figure A163: Molecular orbitals and excited states involved in dyad **28** and references **15** and **21** with ωB97XD functional.